Structural Studies of Membrane Transport Proteins

Dissertation

zur Erlangung des Doktorgrades der Naturwissenschaften

vorgelegt beim Fachbereich Biochemie, Chemie und Pharmazie
der Johann Wolfgang Goethe Universität

in Frankfurt am Main

von

Vinothkumar Kutti Ragunath

Aus Madurai, Indien

Frankfurt am Main 2005

vom Fachbereich Biochemie, Chemie und Pharmazie der Johann Wolfgang Goethe Universität als Dissertation angenommen

Dekan:

1. Gutachter:

2. Gutachter:

Datum der Disputation:

TABLE OF CONTENTS

SUMMARY

Membrane proteins consist either of α-helices or β-sheets. The outer membrane of Gram-negative bacteria consists of β-sheet proteins while the inner membrane consists of proteins that have multiple membrane-spanning α-helices. Among these transporters are dynamic and diverse proteins, undergoing a large conformational change and transporting wide range of substrates. Based on their energy source they can be classified into primary and secondary transport systems. Primary transport systems are driven by the use of chemical (ATP) or light energy, while secondary transporters utilize ion gradients to transport substrates. I began my PhD dissertation on secondary transporters by two-dimensional crystallization and electron crystallographic analysis. Since the resolution obtained by electron microscopy (EM) is moderate, at later stage of the thesis my focus has also shifted towards 3D crystallization.

The major part of my thesis deals with two-dimensional crystallization of secondary transporters of prokaryotic origin with homologues in higher eukaryotes with importance to ion homeostasis or disease. I succeeded in obtaining 2D crystals of three different transporters yielding structural information at various resolutions. In addition the higher yield of protein by over-expression allowed initial 3D crystallization trials of these transporters, yielding crystals that diffract x-rays. I studied the following proteins during my thesis:

1) 2D crystallization of MjNhaP1 and pH induced structural change

MjNhaP1 is a pH regulated Na^+/H^+ antiporter that has been implicated in homeostasis of H^+ and Na^+ in *Methanococcus jannaschii*, a hyperthermophilic archaeon that grows optimally at 85°C. MjNhaP1 shows higher sequence homology to human NHE1 than to *E.coli* NhaA, the best characterized sodium/proton antiporter. MjNhaP1 was cloned and expressed in *E. coli*. Two-

dimensional crystals were obtained from purified protein at pH4. Electron cryo-microscopy yielded an 8Å projection map. The map of MjNhaP1 shows elongated densities in the centre of the dimer and a cluster of density peaks on either side of the dimer core, indicative of a bundle of 4-6 membrane-spanning helices. This projection structure of MjNhaP1 differs significantly from the projection structure of *E.coli* NhaA (Williams et al 1999).

The effect of pH on the structure of MjNhaP1was studied *in situ* in 2D crystals revealing a major change in density within the helix bundle relative to the dimer interface. This change occurred at pH6 and above. The position of the difference peaks indicated that the ion translocation pathway is located within the monomer and not at dimer interface, either within the helix bundle or at the bundle-core interface, The two monomers in the dimer appeared to be active independently of one another undergoing the same pH induced conformational change in 2D crystals. The limited extent of this change is consistent with one translocation pathway per monomer. The two conformations at low and high pH most likely represent the closed and open states of the antiporter, respectively. This is the first instance where a conformational change associated with the regulation of a secondary transporter has been mapped structurally.

2) 2D crystallization of proline transporter:

Proline transporter (PutP) from *E.coli* belongs to the sodium-solute symporter family. Sodium and proline are co-transported with a stoichiometry of 1:1 (Jung et al 2001). Purified PutP was reconstituted to yield 2D crystals that were hexagonal in nature. The 2D crystals had a tendency to stack indicating their willingness to form 3D crystals. A projection map of PutP from negatively stained crystals showed a trimeric arrangement of protein. My analysis of the oligomeric state of PutP in detergent by blue native gel electrophoresis indicated a monomer in detergent solution. It is likely that PutP can function as a monomer but in the conditions used for 2D crystallization it tends to form a trimer. The functional relevance of trimer

needs to be studied.

3) Oligomeric state and crystallization of the carnitine transporter from *E.coli:*

E.coli carnitine transporter (CaiT) belongs to the BCCT (betaine, carnitine and choline) superfamily that transports molecules with quaternary amine groups. CaiT is predicted to span the membrane 12 times and acts as a L-carnitine/□-butyrobetaine exchanger. Unlike other members in this transporter family, it does not require an ion gradient and does not respond to osmotic stress. Over-expression of the protein yielded ~2mg of protein/L of culture. The structure and oligomeric state of the protein were analyzed in detergent and lipid bilayers. Blue native gel electrophoresis indicated that CaiT was a trimer in detergent solution. Reconstitution of CaiT into lipid bilayers resulted in 2D crystals. Analysis of negatively stained 2D crystals confirmed that CaiT is a trimer in the membrane. Initial 3D crystallization trials have been successful and currently, the crystals diffract to 6Å and are being improved.

Due to interest in solid state NMR, a bacterial outer membrane □-barrel protein OmpG was studied. OmpG is monomeric and its size (33kDa) places it as a prime candidate for a structural solution, using the recently developed method of solid state NMR (work in collaboration with Prof.Hartmut Oschkinat, FMP, Berlin). A long-term aim would be to study porins as templates for designing nanopores, for DNA sequencing and identification. I have expressed OmpG in inclusion bodies and refolded the protein at an efficiency of >90% into a functional form using detergent. OmpG was then crystallized by 2D crystallization yielding an 8Å projection map whose structure was similar to native protein. In addition, these crystals were used for structure determination by solid state NMR. An initial spectrum of isotopically labeled OmpG has allowed identification of specific amino acid residues including threonine and proline. Additionally, I obtained 3D crystals in detergent that diffract x-rays to 5.5Å and are being improved.

1 INTRODUCTION

1.1 ORIGIN OF MEMBRANE TRANSPORT

All living cells to date are surrounded by a membrane. It is hard to imagine how life could have evolved without a membrane that separates components of vital metabolic processes from the external milieu; hence membranes provide an identity to the cell. The formation of vesicles was probably the first step in the process of evolution towards the generation of life, since it occurs spontaneously as a result of the drive towards thermodynamic equilibrium (Tanford 1978). They do have the right size and shape to fill the role as protocell (Stillwell 1980). As defined by Tanford, “hydrophobic force is a unique organizing force, based on repulsion by the solvent instead of attractive forces at the site of organization “. This indeed is responsible for assembly of membranes and the absence of strong attractive forces makes the membrane fluid and deformable.

Lipid vesicles can trap high molecular weight polymers and the well-defined water-bilayer interface allows for many kinds of surface reactions as well as for reactions between lipid and water-soluble components. The vesicle wall contains a 35Å hydrocarbon core that acts as an effective barrier to many molecules. Small water-soluble electrolytes have been demonstrated to traverse the lipid bilayer with great difficulty. The permeability of these molecules can be increased in two different ways

a) altering the membrane permeability

b) molecules could be modified to increase their lipid solubility.

It is possibly the later process that was chosen in the early stages of evolution.

Permeability across a membrane is largely determined by the nature of the hydrocarbon phase and the ability of a given solute to partition into this phase. Small hydrophobic molecules that dissolve well in organic solvents will cross the cell membranes more efficiently, while hydrophilic and larger

molecules will cross very slowly or not all. In simpler terms the cell membrane acts as a molecular sieve not just based on the size but also based on the hydrophobic nature of the solute. The lipid bilayer is impermeable to various building blocks of the macromolecules such as amino acids, sugars, and nucleotides. Many different organic compounds have been shown to be in the primordial soup (Miller and Urey 1959) and these organic compounds by virtue of their ability to partition in to the lipid bilayer might have acted as carriers in transportation of building blocks (Stillwell 1980). These organic molecules include the aldehydes and ketones that can form Schiff's bases with macromolecules such as proteins and amines that can react with the carbohydrates, thereby mediating their transport. Inorganic ions such as magnesium might have played a major role in the diffusion of macromolecules into the protocell by virtue of their ability to disrupt the bilayer (Stillwell 1980).

It is clear that facilitated diffusion promotes the facile accumulation of water-soluble material into primordial protocells by making the diffusing species more lipid soluble. The sequestration of scarce reagents in the vesicle favors interaction of the molecules to form products in a reasonable time and progressively to form cells. The membranes have proved to be durable, dynamic and functionally complex structures that perform a wide range of physiological tasks besides the delineation of cellular boundaries. The lipid bilayer provides most of the static physical properties of a cell, while the proteins give the membrane its dynamic, biochemical functions. Since a cell depends upon and communicates with the external environment, its membranes must allow the passage of certain molecules while preventing the passage of others. Due to this property of lipid bilayer a charge separation occurs.

1.2 CHARGE SEPERATION AND DONNAN POTENTIAL

Cells contain a large number of ionic species that cannot cross the membranes including the macromolecules and the byproducts of metabolism which in most cases are negatively charged and are called "fixed anions". The

presence of accompanying small cations that complement the charge on these non-diffusible anions causes diffusion potential to be established across the membrane. Whenever a cation diffuses out, a charge separation arises between this cation and non-diffusible anions that charges the membrane, such that interior is negative. The potential arising due to the presence of fixed anions in the lipid vesicle is called the “Donnan potential”.

At equilibrium, the concentrations of an ion at the two faces of the barrier will not be the same if there is a net trans-barrier electrical potential which defines the Nernst equilibrium potential [□□ = RT/ZF ln (S_{II}/S_{I})], the potential difference for which it will be in equilibrium across the barrier if it is at the concentrations S_I and S_{II} of the barrier. The force on the ion brought about by the trans-barrier electrical potential is here just balanced against the diffusive “force” due to the concentration difference of the ion across the barrier. The Nernst and the Donnan potential form the basis of membrane transport.

1.3 OSMOTIC CONSEQUNECES OF FIXED ANIONS WITHIN THE CELL

The presence of non-diffusible ions within the cell results in an increased concentration of osmotically active material in the cell when compared to the extracellular solution, unless non-diffusible material is present there, too. The Donnan distribution adds to the problem because intracellular cation concentrations are increased above those in the extracellular solutions, adding to the osmotic pressure. The higher osmotic pressure within the cell will cause the flow of water into the cell to equalize the internal and external osmolarity. This dilution of the intracellular cation is followed again by entry of cations into the cell due to the Donnan potential that will lead to the entry of water again. Thus the cell constantly faces certain extinction by flooding, unless prevented by other forces. This problem is solved by two ways in living organisms

a) Bacteria and plants have evolved a cell wall which acts as a rigid skeleton

around the cell, holding the cell at the required volume. This means that the interior of the cell is under an enormous hydrostatic pressure, offsetting the osmotic pressure of the non-diffusible cellular constituents. The difference in the pressure between the outside and inside the cell is the 'turgor pressure' that keeps these cells expanded by pressing its plasma membrane outward against the mechanically strong cell wall.

b) Since animal cells lack a cell wall they continually fight against the cell being flooded by pumping out sodium ions as fast as they enter the cell. This ensures that sodium ions are effectively non-diffusible and kept outside the cell. This is a "Double Donnan potential". Holding sodium outside of the cell offsets the Donnan effect of intracellular non-diffusible anions. The animal cell must continually invest metabolic energy to pump out the sodium that enters down its concentration gradient. The ions that are not pumped out of the cell are subject to the Donnan potential brought about by the fixed anions.

The lipid bilayer is highly impermeable to protons and the amount of cations that can diffuse across depends on the saturation of the hydrocarbon chain of lipid molecules and the water shell of the cation. The free energy of transfer in moving a charged body from a region of dielectric strength ε_2 to a region of dielectric strength ε_1 is given by the Born expression, $W_B = q^2/2_r\ (1/\varepsilon_1 - 1/\varepsilon_2)$. With a bulk aqueous dielectric constant $\varepsilon_2 = 80$ and a bulk lipid membrane dielectric constant $\varepsilon_1 = 2$, the Born energy transfer of a charge q = Ze becomes (where r in Å), $W_{Born} \sim 81\ Z^2/r$ kcal/mol. This poses the most significant barrier to ion transport across bilayers and the energy required is called the "Born energy" (Facciotti, Rouhani-Manshadi et al. 2004). Membrane transport proteins have evolved to have a structural design that enables them to overcome the 'Born' energy. Thus the differential functions of membrane proteins ranging from transport to signal transduction accounts for >25% of genes in the sequenced genomes. They can either be embedded in the membrane or anchored via a lipid chain or loosely associated. Membrane embedded proteins belong to two major class based on the secondary

structure.

1.4 MEMBRANE PROTEINS ARE α-HELICAL OR β-SHEETS

Membrane proteins consist of either β-sheets or α-helices. So far they have not been found together in the membrane domain of one protein. The specificity for an either totally alpha helical or beta barrel protein is explained based on their structural design to completely fulfill hydrogen bonding. Membrane proteins expose their hydrophobic surface to the lipid bilayer core and maximize their hydrogen bonding. All donor and acceptor groups could be saturated either intra-segmentally as in α-helices or inter-segmentally as in β-sheets. Can both secondary structures exist together in the membrane? It is possible to think in two possible ways existence of mixed structure. One that would have a β-sheeted scaffold surrounding a bundle of helices (initially thought for acetylcholine receptor – Henderson R personal communication) or a central pore formed of β-sheets covered by trans-membrane helices with highly hydrophobic residues essentially substituting for lipids. However till date only in the structure of NalP, an outer membrane protein of *E.coli* belonging to the family of autotransporters (Oomen, Van Ulsen et al. 2004) such a mixture has been seen. This structure has been modeled to have a single α-helix in the middle of the β-barrel.

The α-helix predominates in membrane protein structures, forming the basic structure in many different classes and families ranging from channels, transporters, receptors, translocases and many more. The well-known β-barrel membrane proteins are mainly found in the outer membrane of Gram-negative bacteria where they are the only means of transport. The amino acid residues in these proteins are connected by main chain hydrogen bonds to form a stable scaffold. The outer membrane functions as a shield against mechanical and chemical stress allowing passage of small solutes. Apart from the outer membranes of the Gram-negative bacteria the β-barrel proteins are found in the membranes of mycobacteria, cyanobacteria and in the outer membranes of mitochondria and the chloroplasts. In addition the pore forming

toxins like □-hemolysin and cytolysin form a □-barrel in the target membrane. Thus different proteins in the cell membranes are the site of a large variety of cellular processes ranging from transport and excitability to intercellular interaction, morphological differentiation, and fusion.

1.5 TRANSPORT OF SOLUTES

Solutes in the membrane can diffuse from one interface to the other from aqueous phase to the cis interface, to the trans face and to the aqueous phase again. All these steps are reversible and have a finite rate. A membrane as a whole is not a perfect barrier, but functions as a semi-permeable barrier that can discriminate between different solutes. The concept of the membrane as a barrier implies that at least some substances can pass across it and the flow of these species is generally related to forces.

There are two ways for transport:
1) A solubility diffusion type mechanism based on partitioning of solutes in the bilayer.
2) Facilitated transport of solutes through a limited number of sites.

1.5.1 DIFFUSION AND PERMEATION

The thermal motion of molecules is the prime moving force. If there is a concentration gradient, molecules from a higher concentration side will be transferred to lower concentration side hence, the average number of displacements is directly proportional to the concentration of the solute. Thus diffusion is a one-sided, spontaneous, and irreversible process, which at equilibrium brings about uniformity of concentration within a homogenous system.

1.5.2 FACILITATED TRANSPORT

In the membrane the transport is mediated by discrete sites, hence the rate of transport shows a maximal rate as a function of solute concentration. Transport sites have a finite affinity for a given solute. Thus the specificity of a

transport system and its selectivity would be determined by the relative affinities of a series of solutes for the transport sites. Since binding is only a prelude to transport, the overall specificity and selectivity for transport will be determined not only by the binding affinity of a solute but also by the ability of the occupied site to translocate solute from one interface to the other and to leave the site. Of the various steps one may be slow (for a poor substrate with reduced transport rate) or blocked (inhibitor). The transport step is coupled generally to another solute, the membrane potential, to a chemical reaction such as ATP hydrolysis or to the gradient of another solute. Facilitated transport systems tend to lower the energy barrier for the transport of solutes. This is achieved by one of the following means:

A carrier mechanism requires a site that binds stoichiometrically to the permeant, and the site is exposed alternatively at the two interfaces. The translocation step may be achieved by free diffusion or by a conformational change. In any event the two compartments separated by the membrane remain osmotically separate during translocation.

A channel or pore implies a fixed opening in the membrane through which a permeant can pass which may or may not involve binding. Some of these proteins in addition could have loops or domains that can act as a gate regulating the entry of the permeant.

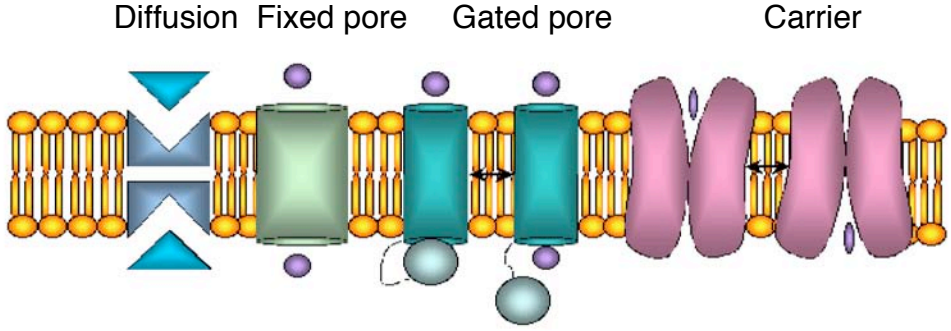

Figure 1.1: Site mediated facilitated transport systems. Different types of translocation are illustrated.

The kinetic steps in different types of transport involve similar steps as described in figure 1.2. Facilitated transport can be divided into passive and active transport based on the requirement of energy. In passive transport the driving force is the concentration difference. Active transport involves the movement against a higher chemical or electrical gradient. To accomplish this, metabolic energy has to be provided (Csaky 1965).

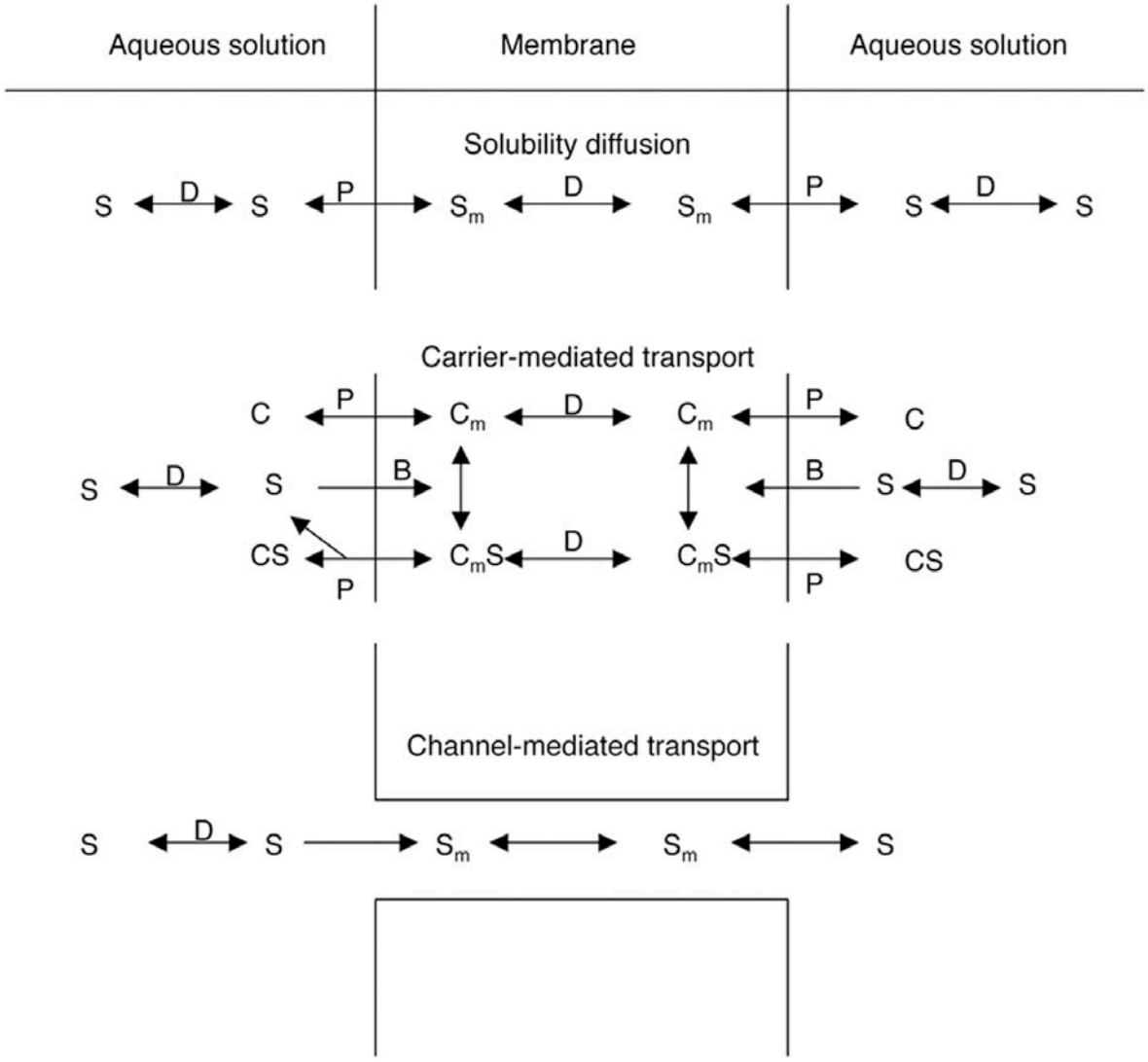

Figure 1.2: The kinetic steps required for translocation of a solute by different types of transport by solubility diffusion, carrier mediated transport and by a channel mediated transport system across a lipid bilayer: B, binding step; S, solute; D, diffusion step; P, partitioning step. S – solute in aqueous solution and S_m-Solute in membrane. The carrier type mechanism depicted here is a representation of ionophores such as valinomycin. Picture redrawn from Jain and Wagner 1980.

1.5.3 HALLMARKS OF FACILITATED TRANSPORT

Specificity and Selectivity: Binding sites are very selective in both carriers and channels. The configuration of the binding site, or the charge distribution at the site, matches that of a distinctive portion of a particular substrate. The binding forces are usually weaker than a covalent bond and allow the release of substrate once it has crossed the membrane. Selectivity of the transport process is inversely related to the transport rate. When the pathway is more selective, interactions with multiple sites may be necessary for positive identification; hence these strong interactions tend to slow down transport.

Saturability: The rate of the facilitated transport approaches an asymptotic value as the substrate concentration difference across the membrane increases. This occurs because there is a maximum rate to the carrier translocation process itself.

1.6 WHY DO WE HAVE CHANNELS AND PUMPS/CARRIERS

Most biological membranes have both channels and pumps/carriers. The channels have evolved to act as charge and size-discriminating filters. They comprise a membrane-spanning pore formed by association of four monomers in the case of ion channels (but they can also be pentameric as in the case of acetylcholine receptor or mechanosensitive channel). They allow fast passage of ions at a rate of 10^7-10^8 per second. These channels often have a gate that can close or open, thereby regulating the passage of the ions. All channels mediate the movement of ions down their respective chemical or electrochemical gradients in passive transport.

By contrast a carrier has a greater ability to bind a specific substrate, preferring one sugar to another or selecting one amino acid from 20 different ones. This specificity is attained at the expense of a slow rate of transport. The rate of transport of a given carrier directly depends on the extent of the conformational changes it undergoes. While a single gate is sufficient to regulate a channel, carriers/pumps tend to have two gates, possibly one on

either side of the membrane, allowing the carrier to prevent the escape of substrate. A pump/carrier never opens both gates at the same time.

The major function of an ion channel is to facilitate, usually for a very short duration, the movements of ions down the electrochemical gradient, previously established across the membrane that causes a transient dissipation of the ionic gradient. This represents a perturbation of cell function and underscores the predominant use of ion channels for rapid signal transduction or information transfer. Carrier-type transporters function to establish and maintain the trans-membrane electrochemical gradients of physiologically significant inorganic cations and anions. Thus, a carrier/pump builds gradients across the membrane while the ion channels dissipate the gradient (Figure 1.3).

A pump could easily become channel-like but not the other way. For example the sodium pump moves ~130 ions per second energetically uphill. If in circumstances both gates were open then it would let in 10^7 ions per second downhill, which would make this pump useless, hence the probability of both gates open is very small. But binding of a toxin to the sodium pump changes its property to a channel like protein (Artigas and Gadsby 2002).

As a common structural feature these proteins possess several membrane-spanning α-helices that create an amino acid-lined pore, which acts as the physical conduit for the ion or solute as it passes from one side of the membrane to the other. The composition of this amino acid-lined pore creates a microenvironment, with suitable electrostatic and polar characteristics, that greatly reduces the energetic constraints, effectively preventing the direct passage of an ion to pass through the lipid bilayer (Dubyak 2004) thereby allowing to overcome the born energy barrier (section 1.3).

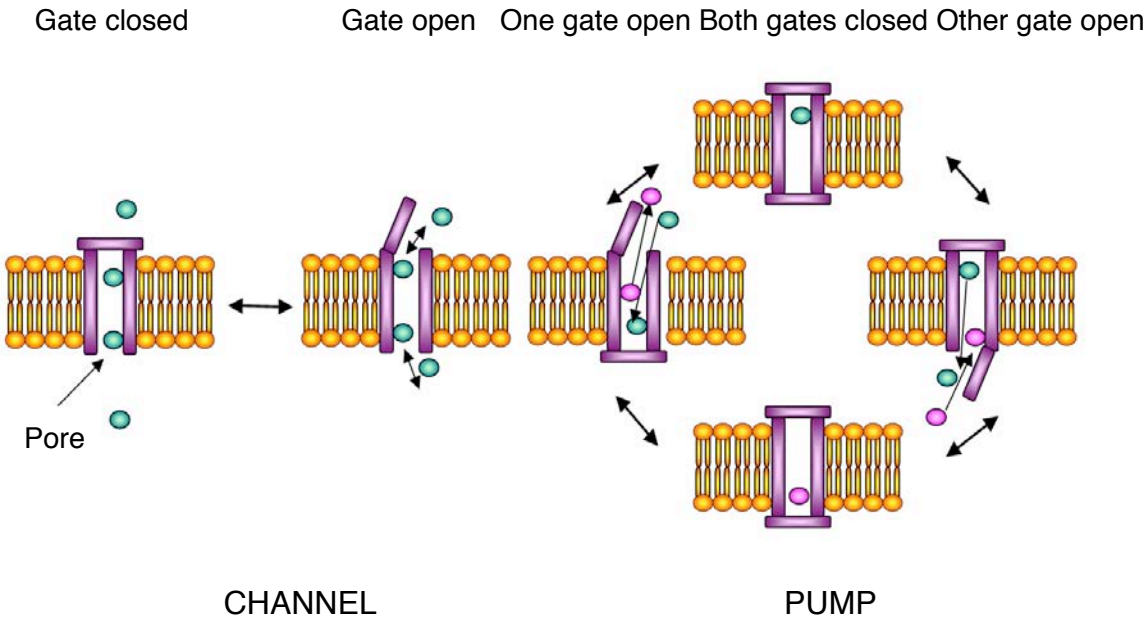

Figure 1.3: Difference between a channel and pump. Ion channels need only one gate, which when open will allow the passage of ions (green). A pump needs two gates, which are never both open. Each gate can open only if the other is closed, to prevent unrestricted flow, and transports two different ions (green and pink). The picture was redrawn from (Gadsby 2004).

1.7 IMPORTANCE OF IONS AND ION GRADIENTS

A large portion of contemporary bioenergetics is centered on carefully controlled pH and ion gradients established by various processes across a non-leaky lipid membrane. The establishment, maintenance and controlled discharge of these gradients are responsible for the synthesis and accumulation of energy-rich biochemical. The chemiosmotic hypothesis was proposed to explain the coupling of respiration to ATP generation (Mitchell 1966; Mitchell 1967). The hypothesis predicted the formation of an electrochemical proton gradient ($\Delta\Delta_{H}^{+}$) across the membrane by harnessing the free energy of oxidation reactions during respiration or light energy during photosynthesis. The proteins involved are membrane localized that couple the

exergonic chemical reaction or the absorption of light to the electrogenic transport of protons across the membrane, thus creating an energized state in the form of Δp_{H^+} that consists of an electrical term ($\Delta\psi$) and the chemical pH gradient (ΔpH). These two parameters are linked by $\Delta p_{H^+}/F = \Delta\psi - (2.3RT/F)\Delta$pH. The hypothesis predicts that Δp_{H^+} is a convertible energy form of the cell that can be used as driving force for endergonic reactions such as the synthesis of ATP. Since then the theory has been extended to many different systems and organisms both aerobic and anaerobic, with not only protons but also sodium playing a crucial role in vectorial metabolism (Harold 1991; Skulachev 1991). Apart from protons and sodium, other inorganic ions like potassium, chloride and bicarbonate are important in maintaining the ion homeostasis of the cell but their role as an energy source is not documented. I would like to add on the importance of inorganic ions leaving out protons since it is well documented.

1.7.1 SODIUM

The importance of the sodium gradient has been known since the discovery of the sodium pump in animal cells (Skou and Zerahn 1959). Many of these proteins were isolated from the alkalotolerant and fermentative organisms (Skulachev 1991). The first such pump was discovered in *Klebsiella pneumoniae*, a decarboxylase (Dimroth 1990). Following this a Na^+ cycle was found operating as an energetic link between the methylmalonly-CoA decarboxylase Na^+ pump and a unique sodium-dependent F_1F_0 ATPase (Hilpert and Dimroth 1984; Dimroth 1997). Since then sodium dependent primary pumps have been found in many different organisms functioning very similar to the proton based systems as postulated by P.Mitchell. Some of the enzymes include an equivalent of complex I that pumps sodium as found in *Vibrio alginolyticus* (Tokuda and Unemoto 1981) and the unique methyltransferase in methanogens (Müller, Blaut et al. 1988). In parallel to the primary sodium pumps, secondary transporters function in coupled transport of sodium to another substrate.

1.7.2 POTASSIUM

A potassium gradient as an energy source is very rare. But it is important for a given cell to maintain the concentration of K^+. The main function of the cellular potassium is to activate a large number of intracellular enzymes and maintaining the osmolarity of the cell. Indeed a wide range of cellular K^+ concentration has been found in organisms living in different environment up to 4M in *Halobacterium* (Christian and Waltho 1962). One of the primary responses of the cell that undergoes an osmotic stress is the influx of potassium followed by the import of osmolytes such as glycine betaine. In eukaryotes, multiple pathways exist that are mediated by primary and secondary transporters including the K^+/H^+ exchanger.

1.7.3 ANIONS

Chloride and bicarbonate are the most common anions used by the cells. However, the studies on anions are very limited but some of the well-characterized systems include the chloride/proton antiporter of *E.coli* which has been implicated in removal of protons during acidic stress (Iyer, Iverson et al. 2002). In eukaryotic red blood cells, chloride/bicarbonate antiporter is the predominant protein in the membrane that is crucial in maintaining the cytoplasmic pH and in removal of carbon dioxide as bicarbonate (Casey and Reithmeier 1998; Strange 2004).

Asymmetric distribution of Na^+ and K^+ across the cell membrane is a common feature of living cells that contain a low concentration of Na^+ and a high K^+ concentration in the cytoplasm than the surrounding medium. This rule holds good for a variety of prokaryotes and eukaryotes that live in different environments. This asymmetry in combination with the transport of anions forms the basis of cell volume regulation which is defined as a process whereby a cell is able to restore volume to normal levels subsequent to an osmotic swelling or shrinkage (Figure 1.4). Volume regulation is a consequence of net solute flux and osmotically obliged water flow. Solute

serving as an osmotic effector must be available in sufficient quantity to effect volume changes of the magnitude necessary to restore normal volume. Additionally the thermodynamic forces must be of sufficient magnitude and in appropriate direction to drive the volume regulatory process. Asymmetry of Na^+/K^+ is responsible for volume regulation subsequent to cell swelling and shrinkage (loss of K^+ or uptake of Na^+). A cell could use the amino acid pool to maintain homeostasis but generally they are small and hence they rely on inorganic ions.

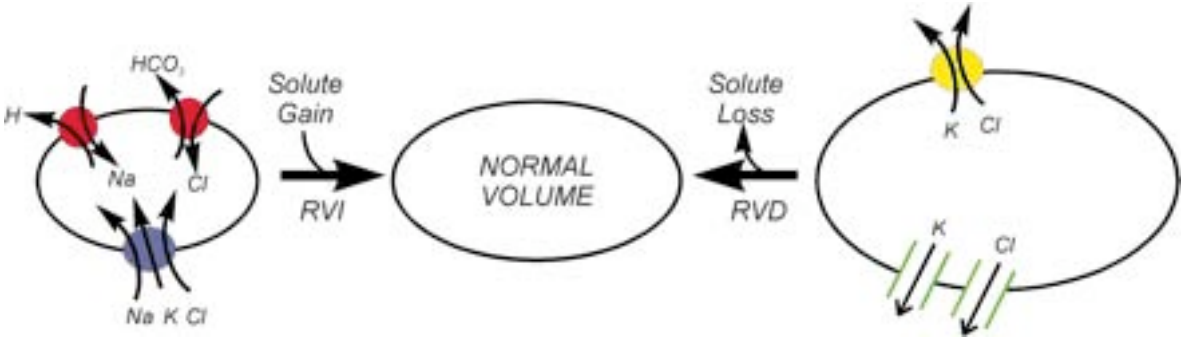

Figure 1.4 Different pathways for the maintenance of cellular homeostasis and cell volume regulation as described in Strange K Adv.Physiol.Educ 2004. Regulated volume increase (RVI) is mediated by electrolyte uptake. Regulated volume decrease (RVD) is mediated by electrolyte and organic osmolyte loss.

Ion asymmetry may be achieved one of the following means:

a) Na^+/K^+ motive pumps – as found in the plasma membrane of the animal cells

b) a sodium pump and a K^+ uniporter

c) a proton pump, Na^+/H^+ antiporter and K^+ uniporter

1.8 ACTIVE TRANSPORT

P. Mitchell (1967) defined two classes of the active transport system as primary and secondary based on their source of energy. Control of coupled reaction sequence in active transport depends on systematic changes in the

properties of the carrier protein as the reaction proceeds. These changes would have to be brought about by specific interactions with the substrate, the binding forces being used to stabilize either,

1) a carrier state with altered properties

2) transition state in a carrier transformation.

The tightness of coupling will at first rise with the increment in binding energy in the altered state but will approach an upper limit when overly strong binding forces retard substrate dissociation in a subsequent step in the coupled reaction sequence. Primary and secondary transport can result in slippage since coupling mechanism necessarily involves intermediates in which substrate is strongly bound.

1.8.1 PRIMARY TRANSPORT

In order to generate a chemical and/or electrical solute gradient, the membrane must be equipped with a primary pump. These are vectorial catalysts that can use chemical energy to perform transport of charged or uncharged molecules against a concentration gradient. The active transport of uncharged molecules gives rise to a chemical gradient only, while the transport of charged molecules in addition leads to the generation of a membrane potential.

1.8.1.1 ATPases

ATPases involved in ion translocation are found in all biological membranes. Three major classes of these enzymes are P type (Phosphorylated), V type (Vacuolar) and the F (F_1F_0) type (Figure 1.5) are found in wide range of organisms (Pedersen and Amzel 1992). In addition, the archaeal type ATPase that resemble closely to V-type ATPase are also found. Many of these ATPase can carry out both ATP generation and hydrolysis with the possible exception of the eukaryotic V-type ATPase.

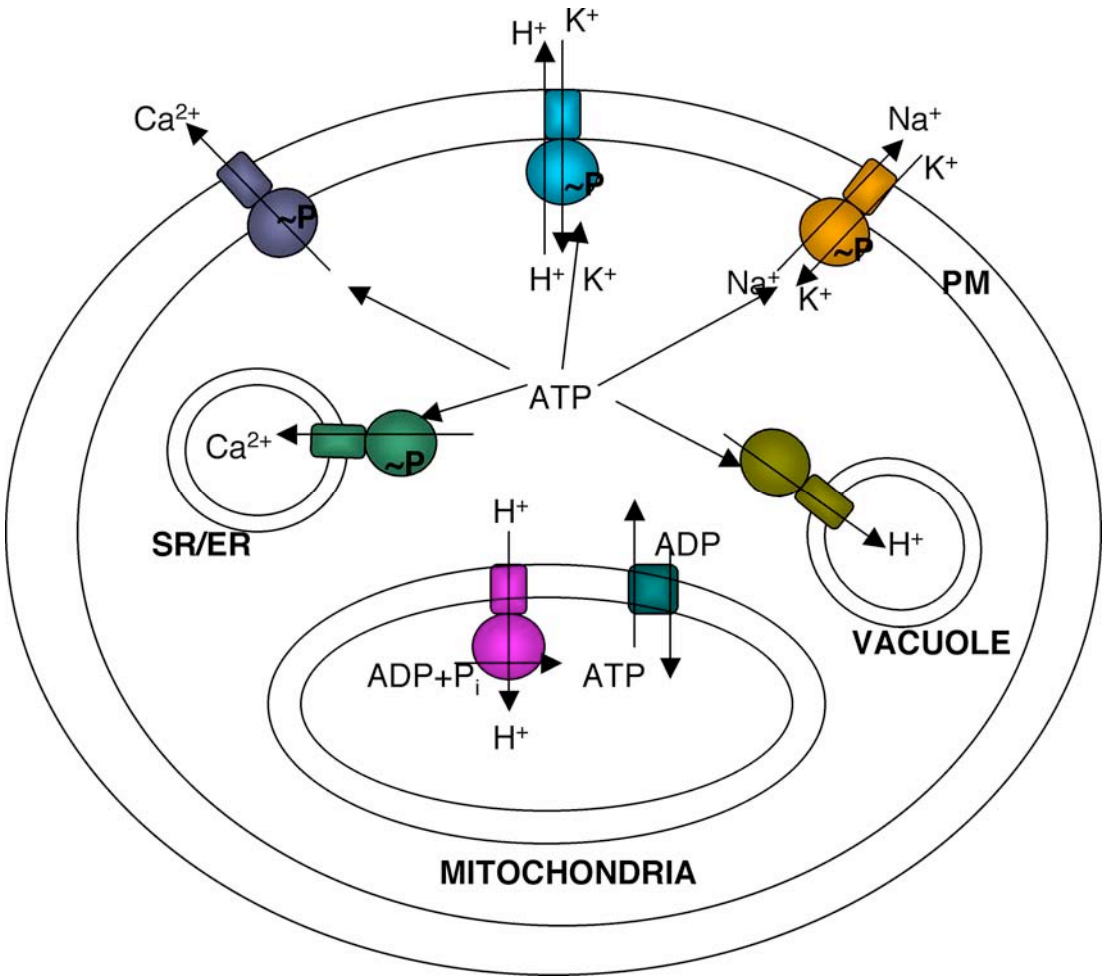

Figure 1.5: Three major types of ATPases as found in the eukaryotic cells. The ATP generating F_1F_0 ATPase in mitochondria, V-ATPase in vacuoles and the superfamily of P-type ATPase found in the plasma membrane and the sarcoplasmic reticulum.

1.8.1.2 GROUP TRANSLOCATION

The transported substrate is chemically modified during translocation. The only known examples are the phosphotransferase (PTS) systems of bacteria. This system imports extracellular glucose into the bacterium by phosphorylation to form glucose-6-phosphate. The energy difference between the high-energy phosphate bond in the substrate (in this case phosphoenolpyruvate) and low energy phosphate bond in the product (glucose-6-phosphate) is used to accumulate sugar inside the cell. The PTS

system solves two problems simultaneously a) it carries out uphill transport of sugar from the medium and b) initiates glycolysis by phosphorylating sugar (Skulachev 1991).

1.8.1.3 BACTERIORHODOPSIN

Bacteriorhodopsin (BR) is a small integral membrane protein (27kDa) belonging to the family of archaeal rhodopsins that includes halorhodopsin and the sensory rhodopsins (Haupts, Tittor et al. 1999). All these proteins possess seven trans-membrane helices, perhaps the most familiar architecture for a membrane protein. BR has a buried retinal chromophore covalently bound to a conserved lysine via Schiff base. Due to its stability and the fact that it is highly enriched in the native membrane, bacteriorhodopsin has served as a prototype for elucidating general features of vectorial ion transport across a cell membrane. An enormous body of biophysical knowledge derived from many different approaches has been built over the years. Starting with the first structure in 1975 (Henderson and Unwin 1975), the 3D structure of BR has been obtained at increasing resolution to 1.55Å till date (Luecke, Schobert et al. 1999) revealing the position of charged residues and a number of water molecules arranged to form the proton translocation pathway that extends across the membrane through the center of heptahelical bundle (Neutze, Pebay-Peyroula et al. 2002). Light induced structural changes cause these residues and water molecules to relay the proton from one group to another in a well-orchestrated sequence of events that has been characterized by detailed spectroscopic and mutational studies. As such structural rearrangements of the protein serve both to define a pathway for proton exchange between charged groups for each step in this process, and to manipulate the pK_a's of the key residues so that the correct proton donor/acceptor relationship is achieved during the photocycle. The essence of vectorial proton transport lies in light induced structural rearrangement that changes the accessibility of the Schiff base, and to reverse its proton donor/acceptor relationship with respect to key charged groups.

1.8.1.4 ABC TRANSPORTERS

The other major class of primary transporter is the ABC transporter family. These carry out the influx and efflux of nutrients and drugs using the energy obtained from the hydrolysis of ATP. They play no role in energy transduction but serve the cells directly. ABC transporters have higher binding affinities (K_d <1 μM) that are required to scavenge substrates available at low concentrations in the environment. ABC transporters have four core domains; two trans-membrane domains (TMD) each with 6 helices, forming the pathway for the substrate transport across the lipid bilayer. The dimeric nucleotide binding domain (NBD) present on the cytoplasmic side couple conformational changes induced by ATP binding, hydrolysis and ADP release to the transport process (Higgins and Linton 2004). ATP binding and hydrolysis are not required for substrate transport, but confer directionality and provide the energy required to drive substrate transport against a concentration gradient.

The above mentioned basic architecture has been observed in structures determined by x-ray crystallography (Chang and Roth 2001; Locher, Lee et al. 2002) and in 2D crystals of P-glycoprotein, a multidrug scavenging pump (Rosenberg, Kamis et al. 2003). All these structures indicate the presence of an aqueous chamber at the interface of the trans-membrane domain dimer that opens to the extracellular side but is closed intracellularly. The coupling ratio of ATP hydrolysis to substrate transport appears to be 1 to 3 which is very similar to the other primary ion pumps such as the P-type ATPases (Ambudkar, Cardarelli et al. 1997). However the structures of the ABC transporters differ significantly from the other primary transporters such as the Ca-ATPase, where the α-helices are more tightly packed and the ATP binding sites are placed away from the membrane (Toyoshima, Nomura et al. 2003). The basic architecture of the ABC transporters holds true in a wide variety of protein families but two x-ray structures (BtuCD and MsbA) differ significantly. The conclusion that can be derived from these structures is that the NBD domains share a common

evolutionary origin and mechanism, but the differences arise from the TM domains, which determine the substrate specificity. A recent publication on the structure of trapped intermediate and an EPR study has shed light on the possible mechanism of substrate transport with respect to ATP hydrolysis (Dong, Yang et al. 2005; Reyes and Chang 2005)

In humans, two important proteins belong to this class. P-glycoprotein, a multidrug resistance transporter implicated in drug resistance of cancerous cells (Ambudkar, Dey et al. 1999) and the cystic fibrosis trans-membrane conductance regulator protein (CFTR) which acts as a chloride channel but has the signature motifs of the ABC transporters that are broadly known as the non-transporter ABC proteins (Gadsby and Nairn 1999). A very recent 3D map of the P-glycoprotein (Rosenberg, Callaghan et al. 2004) highlights the necessity for a high-resolution structure since it differs significantly from the prokaryotic homologues. To answer how the TM domain's handle different substrates one would need to study many different structures as implicated by the three different transporters explained above.

1.9 SECONDARY TRANSPORT

Secondary active transporters utilize the free energy stored in the electrochemical ion gradient to drive the uphill translocation of the substrates. Primary and secondary transport processes frequently interact with each other via the membrane potential. Circulation of protons, forced against a gradient through one system and flowing back downhill through another, enables energy to be transferred from redox reactions to phosphorylation reactions and vice versa, or it allows the energy from either process to be utilized for solute transport or other membrane processes such as drug extrusion or flagellar rotation.

Secondary transporters have multiple membrane-spanning □-helices. They are classified into different families based on their sequence homology and their function. From the numerous genome sequences that have been

completed, the family of the secondary transporters are one of the largest classes of membrane proteins (Paulsen, Sliwinski et al. 1998). They carry out a wide variety of functions including transport of various metabolites, maintaining ion homeostasis. Indeed they have been reported to transport every low-molecular weight compound found in nature (Sobczak and Lolkema 2005). Clustering of transporters according to the hydropathy profile analysis reports specific folds and detects distant relationships between the protein families (Lolkema and Slotboom 2003) indicating that they are likely to be evolutionarily related, and the high number of encoded protein families is likely to represent a much smaller number of structures and translocation mechanisms.

H^+ and Na^+ is the most common coupling ions used by secondary transport systems. Most cells maintain electrochemical gradients of both H^+ and Na^+ across the cytoplasmic membrane by primary or secondary ion translocation processes. In many organisms, the proton motive force generated by substrate oxidation via the respiratory chain is used to extrude Na^+ from the cell by a Na^+/H^+ antiport mechanism, thereby establishing an electrochemical Na^+ gradient across the cytoplasmic membrane called “smf” (sodium motive force). Alternatively, a variety of prokaryotic cells possess primary Na^+ pumps that can also generate smf (section 1.7.1.1).

Transport of a given substrate can be coupled to H^+ in one organism and to a Na^+ in another. There is no relation between substrate and ion specificity (Lolkema, Speelmans et al. 1994). So, H^+ and Na^+ coupled transport systems exist within one organism, and therefore overlapping substrate specificities can occur (Poolman and Konings 1993). There appear to be no major structural differences between H^+ and Na^+ dependent transporters. Furthermore, significant differences in the catalytic efficiency of ion coupled transport systems are not apparent. Therefore, the existence of H^+ and Na^+ coupled systems cannot be due to a need to optimize catalytic efficiency of secondary transporters during evolution but must be related to specific environmental conditions (Lolkema, Speelmans et al. 1994). Obvious

environmental parameters that influence the choice of the coupling ion are temperature, pH and salinity (Tolner, Poolman et al. 1997). In this context it has to be considered that high internal Na^+ concentrations are toxic and cells are required to keep the concentration of the ion at a low level (Padan, Venturi et al. 2001). Furthermore, many cellular functions require pH homeostasis and in this process Na^+/H^+ antiport plays a pivotal role. The choice of the transport system and thereby of the coupling ion for a given substrate can also be determined by metabolic requirements and the demand of the environment, e.g., upon a switch from aerobic to anaerobic growth conditions or a shift to higher salt (Bott 1997; Dimroth 1997)

The mechanism of substrate translocation by secondary transport has been explained by a “carrier model” (Figure 1.6), where the carrier alternates between two conformations, C_o and C_i in which the substrate site faces either outward or inward, respectively. This model holds good for transporters of any kind.

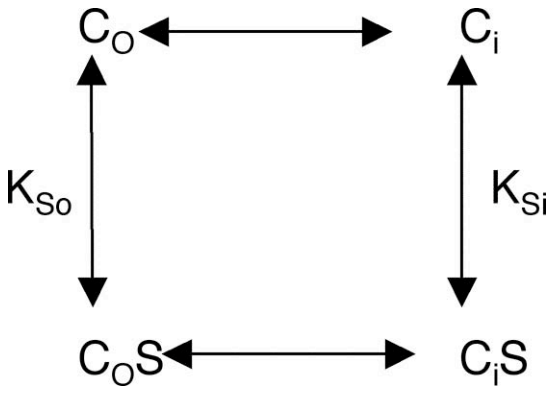

Figure 1.6: Carrier model involving a single substrate, two different conformation of the carrier either facing outward or inward allows the transport of a substrate.

The simplest mechanism is the “exchange only” transport (antiport) where a substrate molecule on one side of the membrane is exchanged for another substrate on the opposite side of the membrane. Co-transport (symport) is a more complex process, where two different substrates move together in the same direction, which makes it possible for a downhill gradient in one substrate to drive the uphill flow of the other. Much experimental evidence has indeed confirmed the carrier model in many different transporters. In most of these cases, a six-state kinetic model has been

proposed, to account for a series of conformational changes that occur by substrate binding and eventual translocation (Figure 1.7). In the case of co-transport, the six states account for empty transporter, one substrate bound and both substrates bound in outward and inward facing states respectively.

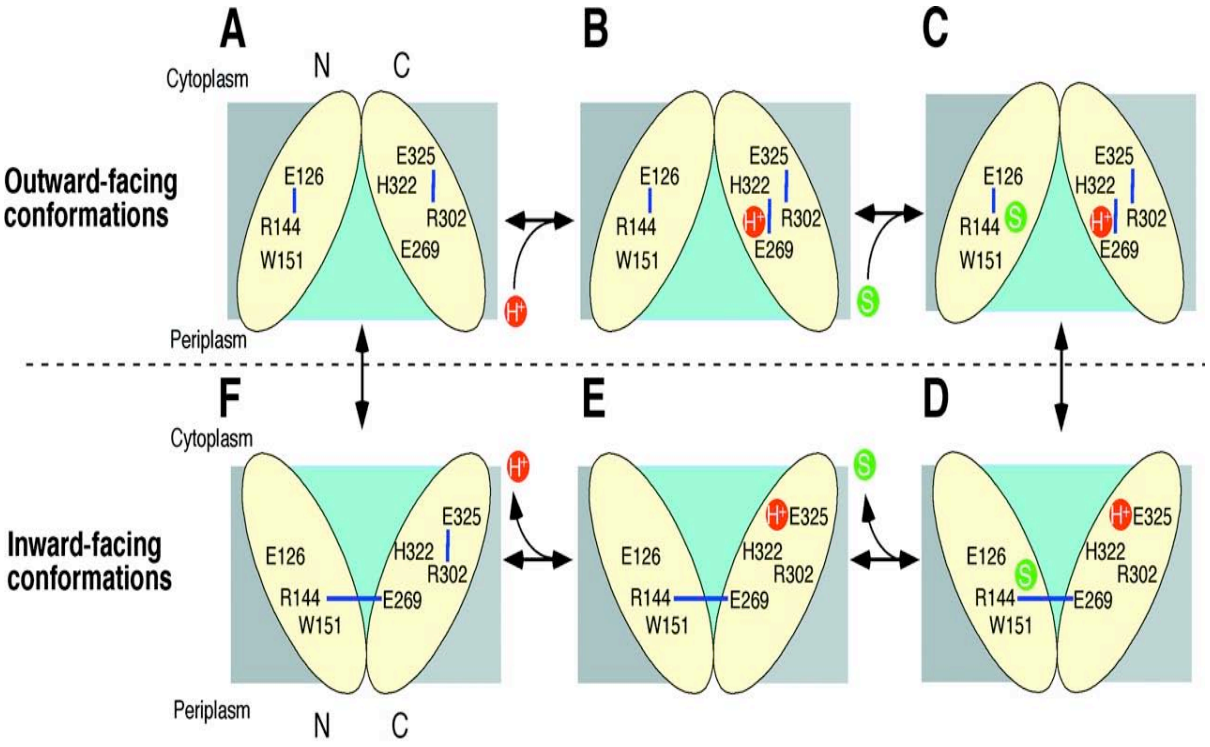

Figure 1.7: Six-state model explaining the uphill transport of □-galactoside using the downhill movement of protons with key residues that take part in transport are shown (Abramson, Smirnova et al. 2003)

Two processes will be coupled if they are combined in a single overall reaction sequence. For the coupling protein to guide the reaction along a path involving both processes, its specificity and transport properties have to be systematically altered in the course of the reaction while avoiding pathways involving one of the processes. These changes can be brought about by substrate binding energy; it can be shown that the greater the increase in the strength of substrate binding at branch points between coupled and uncoupled paths, the greater the preference for the coupled path. Hence, the ratio of coupled to uncoupled rates, which may be called the tightness of coupling, is a function of binding energy. This strong binding of the substrate

also tends to retard the dissociation of substrate in a subsequent step of the coupled reaction (Krupka 1999). Secondary active (also primary) transport systems are subjected to this limitation because the coupling mechanism necessarily involves intermediates in which the substrate is strongly bound. The uncoupled reaction is called the slippage and under natural selection coupling should have become as efficient as possible and slippage reduced to a minimum. But one does observe such slippages in many transport systems (Nelson, Sacher et al. 2002). These slippages are necessary and act as safety valves to prevent damage that can occur by building up of a gradient. They are observed most frequently in eukaryotic transporters.

1.9.1 EVOLUTION OF TRANSPORTERS

The sequence analysis and the recent structures of secondary transporters describe a possible role of gene duplication and fusion in the process of evolution. The primitive carriers possibly consisted of multimers of identical domains, presumably pairs of helices (Maloney and Wilson 1993). A remnant of this primitive carrier we possibly see today in the subunit c of the F-type ATPases. They have only a pair of trans-membrane segments connected by short intracellular loops (Figure 1.9A). This structure is replicated many times (various with species ~9-15) to form a ring resulting in a proton /sodium translocating carrier (Meier, Polzer et al. 2005). The presence of tripartite structure in mitochondrial carriers has been known for long time from the sequence (Klingenberg 1981) and the recent structures of the ATP/ADP translocase both in 2D and 3D crystals (Pebay-Peyroula, Dahout-Gonzalez et al. 2003; Kunji 2004) confirm the presence of three homologous sequence repeats of about 100 amino acids, each resulting in a six trans-membrane helical bundle (Figure 1.9B).

The small multi drug resistance family of transporters such as EmrE comprises 4 trans-membrane helices from each monomer, which associate to form a dimer resulting in a central cavity that forms the translocation pathway (Figure 1.9D). The helices in this protein are structurally related (Ubarretxena-

Belandia, Baldwin et al. 2003). The transport of metal ions such as magnesium has been predicted to bring about residues from different helices to form an oligomer, probably a tetramer (Warren, Kucharski et al. 2004). The structure of an ammonium channel has an eleven trans-membrane helical bundle with a pair of five helices related to each other (Khademi, O'Connell et al. 2004). This quasi-two fold symmetry is not evident in the sequence but notable in the structure (Figure 1.9C). The majority of the MSF protein families have 12 TM helices that can be divided into two halves, which are related to each other. The two bundles of the six helices form a central hydrophilic cavity that forms the substrate binding cleft (Figure 1.8). This particular architecture has to date been shown independently in three structures of MSF family of transporters (Hirai, Heymann et al. 2002; Abramson, Smirnova et al. 2003; Huang, Lemieux et al. 2003).

In addition, the structure of the chloride channel (Dutzler, Campbell et al. 2002) that has been recently shown to be an antiporter (Accardi and Miller 2004) spans the membrane 18 times. The helices are highly tilted and variable in length. Only from the three-dimensional structure, the relatedness between the N-terminal and C-terminal half was evident. They exist in opposite orientation (antiparallel) and create a pseudo two-fold axis within the membrane. These two subunit halves in a monomer wrap around a common centre such that the amino acids from segments of different □-helices are brought together (Figure 1.8). The presence of the pseudo two-fold symmetry or the structural relatedness in a subunit is not confined only to transporters but also found in the aquaporins (Fu, Libson et al. 2000; Murata, Mitsuoka et al. 2000) even though the membrane spanning topology is unrelated to the transporters.

It is probably logical to think that from a simpler structure of multiple subunits, evolution favored the reduction in subunits but increasing the complexity of the sequence thereby allowing for greater specificity of a given protein. Thus the secondary transporters are dynamic and diverse (Table 1.1). The structures of the seven different transporters that have been solved differ

significantly from one another. However, in a given family they tend to have the same quaternary structure and similar architecture in terms of membrane spanning domains (Hirai et al 2002; Abramson et al 2003; Huang et al 2003). Most of these proteins contain a cavity lined by trans-membrane helices to form the substrate translocation pathway. From these structures it has been possible to speculate mechanism for transport essentially based on the long-standing alternate access mechanism (Jardetzky 1966).

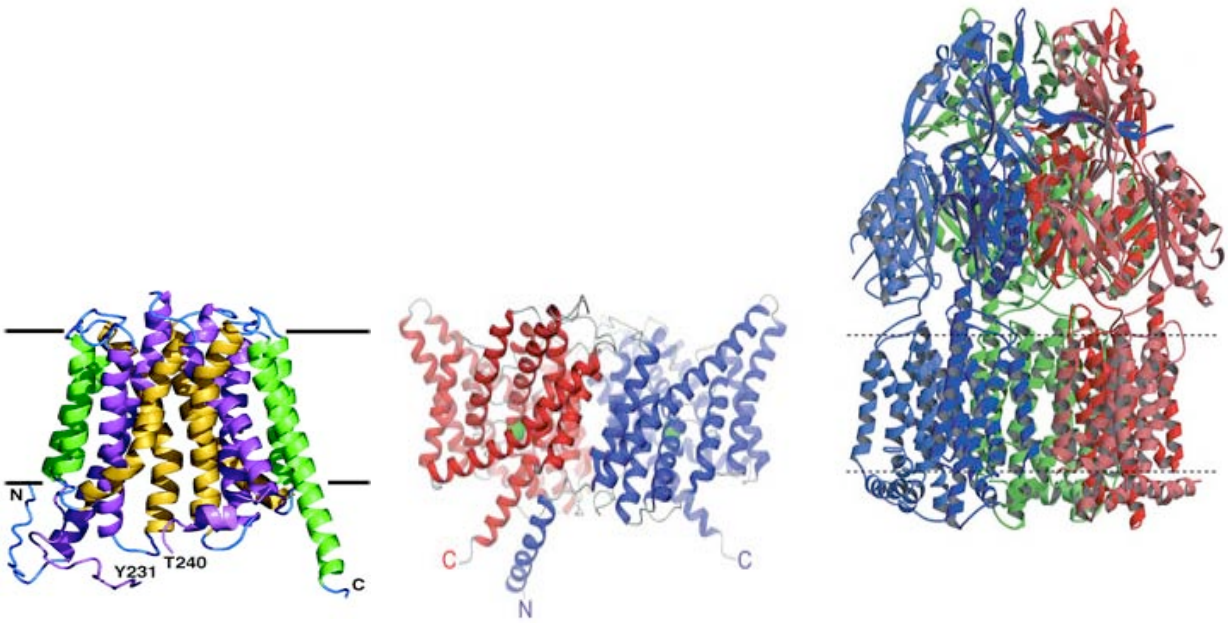

GlpT CLC AcrB

Figure 1.8: Structures of three different secondary transporters illustrating the diversity found in them. GlpT is glycerol phosphate transporter belonging to the MSF family (Huang, Lemieux et al. 2003), CLC is the chloride antiporter, belonging to the ion transporters (Dutzler, Campbell et al. 2002), AcrB is a proton/drug antiporter belonging to the RND family (Murakami, Nakashima et al. 2002).

Table 1.1: SMALL SELECTION OF SECONDARY TRANSPORTER FAMILIES

Transporter	No. of TM helices /type	Family[a]	Oligomeric state	Method	Resolution (inÅ)	Reference
LacY	12,symporter	MSF	monomer	X-ray	3.5	Abramson et al., 2003
GlpT[b]	12,antiporter	MSF	monomer	X-ray	3.3	Huang et al., 2003
OxlT	12,antiporter	MSF	monomer	Cryo-EM	6.5	Hirai et al 2002
ADP/ATP	6,antiporter	M.carrier	dimer	Cryo-EM	8.0 (P)	Kunji E., 2003
			monomer	X-ray	2.2	Pebay-Peyroula et al 2003
EriC[c]	18,antiporter	Ion transporter	dimer	X-ray	3.0	Dutzler et al., 2002
NhaA	12,antiporter	Ion transporter	dimer	Cryo-EM	4.0	Williams et al., 1999
			monomer	X-ray	3.45	Hunte et al 2005
Band 3	12,antiporter	Ion transporter	dimer	EM	20	Wang et al., 1994
EmrE	8,antiporter	SMR	dimer	Cryo-EM	7.0	Tate et al., 2001
AcrB	12,antiporter	RND	trimer	X-ray	3.4	Murakami et al., 2002
BetP[d]	12,symporter	BCCT	trimer	Cryo-EM	7.5 (P)	Ziegler et al., 2004
CaiT[e]	12,antiporter	BCCT	trimer	EM	25 (P)	This work
PutP[f]	13,symporter	SSF	trimer	EM	20 (P)	This work
GltPh[g]	8,symporter	GTF	trimer	X-ray	3.4	Yernool et al., 2004
Glt1	8,symporter	GTF	trimer	BN gel	-	Gendreau et al.,2004
TetA	12,antiporter	MSF	trimer	EM	20(P)	Yin et al 2000

[a] - MSF -Major facilitator family, M.carrier – mitochondrial carrier, SMR –Small multidrug resistance family, RND-Root nodulation division family, BCCT-Betaine,choline,carnitine family, SSF-Sodium solute symporter , GTF-Glutamate transporter family.
[b]-glycerol phosphate transporter, [c]-chloride transporter, [d]-sodium/betaine transporter, [e]-carnitine transporter, [f]-proline symporter,
[g]- glutamate transporter from *P.horikoshii*
P – Projection map

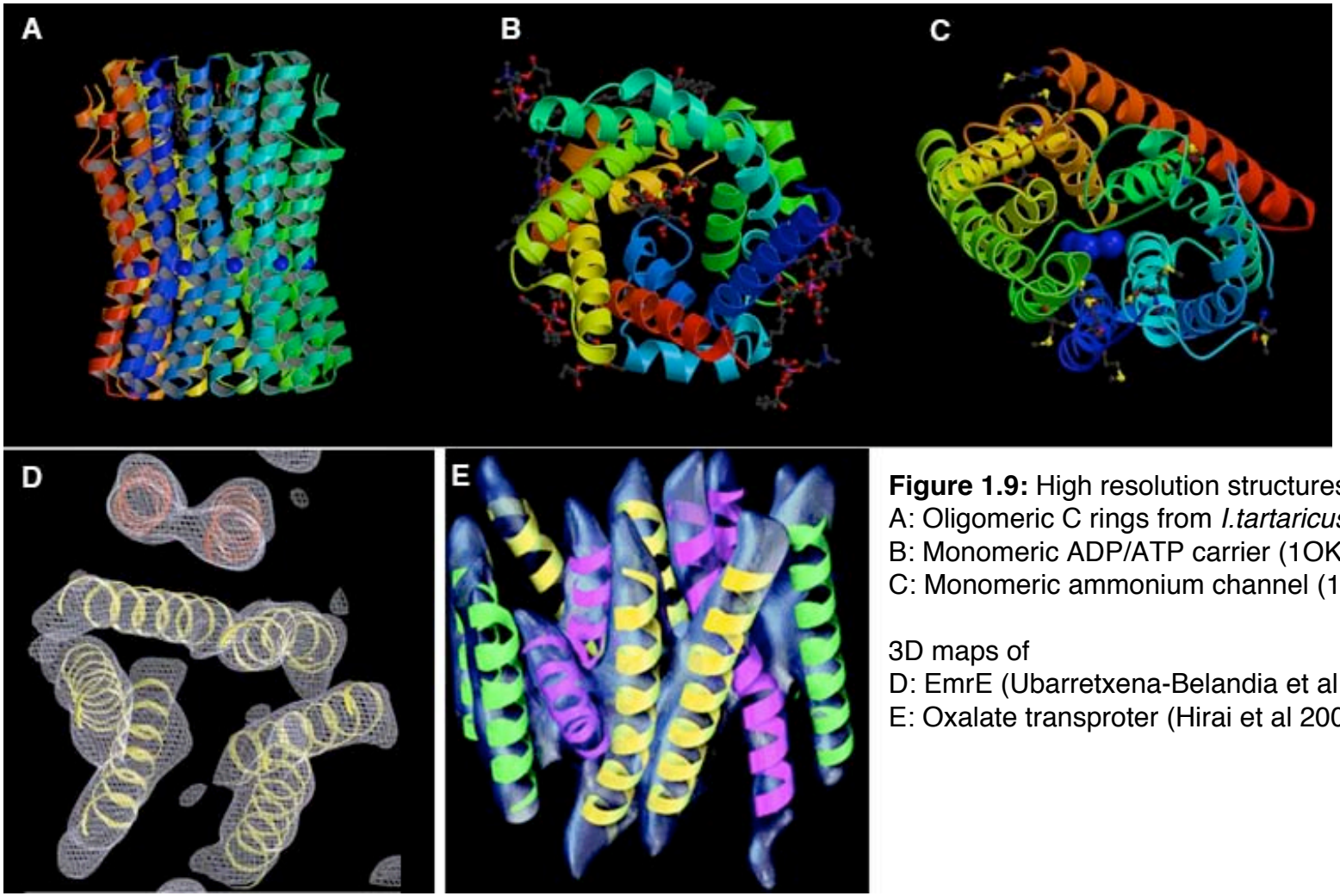

Figure 1.9: High resolution structures of
A: Oligomeric C rings from *I.tartaricus* (1YCE)
B: Monomeric ADP/ATP carrier (1OKC)
C: Monomeric ammonium channel (1U7G)

3D maps of
D: EmrE (Ubarretxena-Belandia et al 2003)
E: Oxalate transproter (Hirai et al 2002)

A small representation of structures showing the presence of internal pseudo symmetry that possibly arose by duplication best viewed in C, D and E.
The tripartite architecture of ADP/ATP carrier shown in (B). The subunit C of F_1F_0ATPase is shown here as a possible remaining ancestor (A).

1.10 APPROACHES FOR STUDYING MEMBRANE PROTEINS

In recent years an increasing number of structures of membrane proteins have been solved. This has been possible due to multiple reasons including the wealth of genome information, better understanding of proteins and crystallization and new generation synchrotron sources. X-ray crystallography, NMR and cryo-EM are the three techniques that are used to obtain structural details of membrane proteins. These techniques have been used complementarily, often giving greater understanding of a given protein.

1.10.1 3D CRYSTALLIZATION AND X-RAY CRYSTALLOGRAPHY

Two of the major hurdles that lie on the way to structure determination of protein by x-ray crystallography are

a) a sufficient amount of protein to screen for suitable crystals

b) a crystal that is sufficiently well ordered and diffracts to a limit that would make the structure determination (4Å or better) possible.

In the initial stages of the crystallization of the membrane proteins, naturally abundant proteins such as those from the respiratory chain (Abrahams, Leslie et al. 1994; Iwata, Ostermeier et al. 1995; Lancaster, Kroger et al. 1999; Kurisu, Zhang et al. 2003) or photosynthesis (Deisenhofer, Epp et al. 1984; Kühlbrandt, Wang et al. 1994; Nogi, Fathir et al. 2000; Jordan, Fromme et al. 2001), Ca ATPase (Toyoshima and Inesi 2004) and the porins (Schulz 2002) were solved. A lack of efficient expression systems for eukaryotic proteins resulted in looking for homologues of these proteins in prokaryotes, which can be expressed at high level in *Escherichia coli*. Homologous proteins from different organisms were screened and the one that gave the best crystals was used for high resolution studies (Chang, Spencer et al. 1998; Locher, Lee et al. 2002; Van den Berg, Clemons et al. 2004).

This approach has yielded high-resolution structures of several different

membrane proteins including the bacterial potassium channels (MacKinnon 2003), secondary transporters (Murakami, Nakashima et al. 2002; Abramson, Smirnova et al. 2003; Huang, Lemieux et al. 2003; Yernool, Boudker et al. 2003; Ma and Chang 2004), ABC transporters (Chang, Spencer et al. 1998; Locher, Lee et al. 2002) and the protein translocation machinery (Van den Berg, Clemons et al. 2004). The success of this approach has been nicely illustrated in the structural solution of the ABC transporter BtuCD (Locher, Lee et al. 2002). The authors screened 28 distinct ABC transporters from different biological sources and transporting diverse substrates for their expression and then crystallization. This resulted in the crystals of the BtuCD diffracting to 3.2Å whose structure was subsequently solved.

Eukaryotic proteins are phylogenetically more closely related to archaeal proteins than to those from eubacteria (Olsen and Woese 1993). The extreme environments where the archaea thrive have gained a great deal of attention and since their proteins show greater stability, structural biologists have started preferring them to mesophilic homologues. The series of potassium channel structures support this idea. The calcium activated potassium channel from *Methanobacterium thermoautotropicum* [equivalent to BK channel in eukaryotes; (Jiang, Lee et al. 2002)] and the voltage-gated channel from *Aeropyrum* [equivalent to Kv channel (Jiang, Lee et al. 2003)] are two examples. The prokaryotic channels possess many properties of the eukaryotic channels if not all but have formed the basis for understanding the functions of channels (Roux 2005). Apart from the channels, the structure of GltP from *Pyrococcus horikoshii* [equivalent to Glt1 (Yernool, Boudker et al. 2004)] is another example. Does this mean one should always look for an archaeal (thermophilic) homologue to get better crystals? A clear answer cannot be given at this stage. It is worth considering that the highest resolution achieved for a membrane protein structure to date is that of an ammonium channel at 1.35Å (Khademi, O'Connell et al. 2004) which is not of thermophilic origin.

The second hurdle in the structure determination of membrane proteins

is getting well-diffracting crystal. The presence of a flexible and dynamic detergent micelle may be a big problem as any degree of flexibility in the crystal lattice is detrimental for high-resolution x-ray crystallography. The importance of detergents and use of mixtures of detergents in crystallization has been implicated in some of the recent publications (Kuo, Bowler et al. 2003; Lemieux, Song et al. 2003). Different thoughts have been applied to overcome this specific problem of detergents in membrane protein crystallization. These include:

1) Use of antibodies or their fragments generated against an epitope (Hunte and Michel 2002), thereby improving the quality of the crystals by increasing the number of protein-protein contacts and decreasing the weaker and less stable protein-detergent/detergent-detergent contacts. To state one example, the chloride antiporter was first crystallized without antibody and the crystals diffracted to 3.0Å (Dutzler, Campbell et al. 2002), subsequently co-crystallization with Fab fragment resulted in crystals diffracting to 2.0Å (Dutzler, Campbell et al. 2003).

2) Bicontinuous cubic phase, where protein is reintroduced into membrane bilayer environment (Landau and Rosenbusch 1996) seems to have lot of potential but so far has been successful only with particularly stable, colored proteins.

3) Importance of lipids in crystallization has been emphasized in many different cases (Lemieux, Reithmeier et al. 2002; Palsdottir and Hunte 2004). The complex of cytochrome b_6f (Zhang and Cramer 2004) was stabilized by addition of lipids and the crystals obtained thus yielded the structure (Figure 1.10). Recently the crystals of Lac permease were improved to 2.7Å by the addition of negatively charged lipid, phosphatidylglycerol before crystallization (Ron Kaback, personal communication).

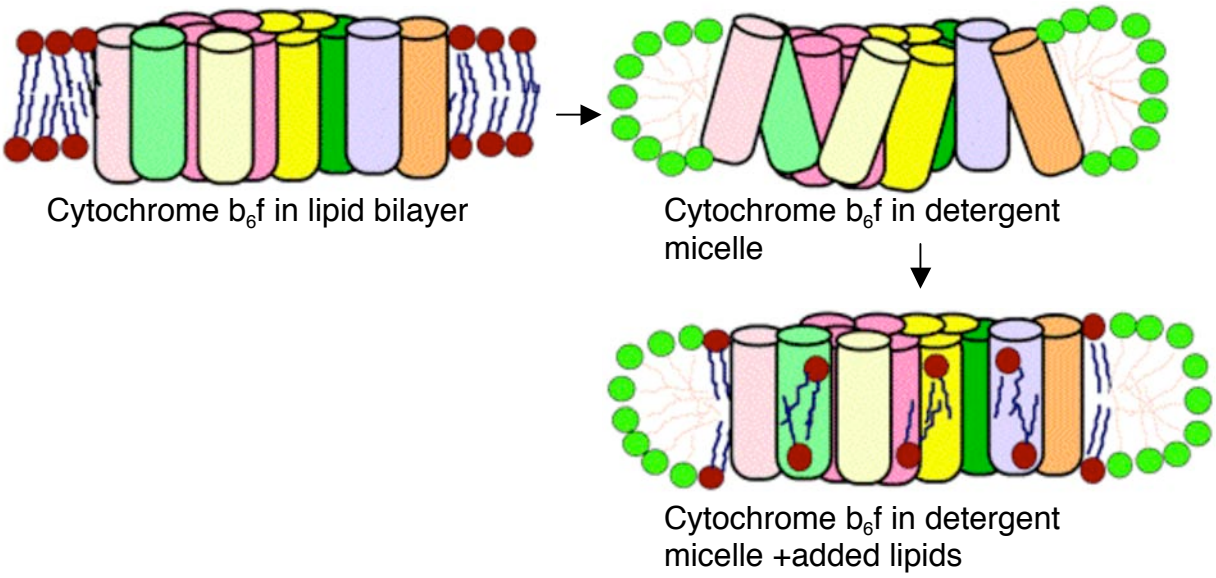

Figure 1.10: The logic behind the addition of lipids in the case of cytochrome b_6f, redrawn from Zhang and Cramer, 2003. The authors have shown that the addition of lipids to the protein-detergent micelle yields protein that is more stable against proteolysis as well as in yielding well diffracting crystals. This particular cartoon explains the flexibility of the helices in detergent micelle.

1.10.2 ELECTRON MICROSCOPY

3D crystallization and X-ray crystallography are the front-runners in structural determination of membrane proteins. However, the importance of studying proteins in a native-like lipid bilayer has been emphasized in many cases. This can be achieved either by lipid cubic phase or 2D crystallization. The lipid cubic phase approach is still generally not applicable to all proteins. On the other hand 2D crystals and electron microscopy have resulted in structural determination of different proteins, initially from the native sources (Henderson and Unwin 1975; Kühlbrandt, Wang et al. 1994; Unwin 2003). Progress has been extended to proteins that have been over expressed in homologous/heterologous systems, initially yielding a projection map and then to a 3D map (Kühlbrandt 1992; Mosser 2001). Emphasis of studying membrane proteins in detergent as well as lipid bilayers has been

strengthened in some of the recent structures. The structure of the mitochondrial ADP/ATP carrier in detergent was solved as a monomer (Pebay-Peyroula, Dahout-Gonzalez et al. 2003) but the protein crystallized as dimer in 2D crystals (Kunji and Harding 2003). The 3D map of EmrE in the lipid bilayer (Ubarretxena-Belandia, Baldwin et al. 2003) and in detergent (Ma and Chang 2004) differ significantly. The 2D crystals of SecYEG from *E.coli* shows a dimeric arrangement in the membrane (Breyton, Haase et al. 2002) but the 3D crystals of SecYE from *M.jannaschii* yielded a monomeric structure (Van den Berg, Clemons et al. 2004). These are some examples to illustrate the fact that for a given protein one may need to carry out both 2D and 3D crystallization.

2D crystallization and cryo-EM can provide a medium resolution map in relatively short period. The other advantage of cryo-EM is the ability to trap functional intermediates in the native membranes (Unwin 1996; Subramaniam and Henderson 1999). The protein-protein contact as found in cell junctions of eukaryotes can possibly be studied only in 2D crystals. In the double membrane structure of AQP0 (Aquaporin 0) the extracellular domains of the tetramer from each layer face each other mimicking an in-situ state in cell-cell association (Gonen, Sliz et al. 2004), whereas in detergent the cytoplasmic domain of one tetramer is in contact with the extracellular domain of the adjacent tetramer (Harries, Akhavan et al. 2004). When possible it is thus worth pursuing both 2D and 3D crystallization to get complementary information.

1.10.3 NUCLEAR MAGNETIC RESONANCE SPECTROSCOPY

In the case of membrane proteins the use of solution-state NMR has been hampered due to the slow molecular motion of the protein-membrane particles (detergent micelles or bilayers). The larger size of the protein-detergent micelle and reduced molecular motion may induce line broadening, which effectively limits the size-range of the NMR experiment. This leaves

NMR with three possibilities:

i) To study protein constructs with a relatively low molecular mass including the micelle

ii) Use of special NMR methods that will reduce the problem of increasing line broadening and increasing the size limit such as TROSY

iii) To use solid-state NMR, which does not rely on the molecular motion, so there is no upper limit in the size of the molecules that can be studied.

Small membrane proteins like the phage coat proteins have been studied in detergent micelle and this has been extended to smaller □-barrel outer membrane proteins such as OmpX (Fernandez, Hilty et al. 2002), OmpA (Arora, Abildgaard et al. 2001) and PagP (Hwang, Bishop et al. 2004). They were studied using transverse optimized NMR spectroscopy (TROSY), which partially alleviates the effect of line broadening with increasing molecular size and is well suited to study large proteins and those incorporated into membranes (Fernandez and Wüthrich 2003).

Solid state NMR has the potential to observe anisotropic nuclear spin interactions such as dipole-dipole coupling, chemical shielding anisotropy etc., which provide detailed information on structure and dynamics. These anisotropic interactions are orientation dependent and hence regular protein powder samples are extremely complex. To circumvent this problem, solid-state NMR of membrane proteins has been studied in two different ways magic-angle spinning (MAS) experiments, which remove the effect of anisotropic interactions through fast sample rotation, while selectively recouple the interactions needed to obtain structural information during specific periods of the experiment (Griffin 1998) and orientation of the sample in one direction simplifies the spectra and the magnitude and orientation of the chemical shift and dipolar coupling tensors provide structural information (Opella 1997).

Apart from these three techniques that can in principle provide information about the co-ordinates of all atoms in a macromolecule, all biophysical techniques have been used in the study of membrane proteins to get different information. Few techniques that have gained greater importance are:

1) FTIR - Fourier transfer infra-red spectroscopy: This technique has been used to determine the number of trans membrane helices and their relative tilt to the membrane and for probing the micro environment of a given protein (Tatulian 2003).

2) EPR - Electron paramagnetic resonance: Even when there is no paramagnetic center in the protein, EPR can be used to study the conformational changes and accessibility of residues in a membrane protein. This is achieved by the so called “Site-directed spin labeling” (SDSL) where a nitroxide side chain is introduced via cysteine substitution mutagenesis followed by modification of the unique sulfhydryl group with a specific nitroxide reagent (Hubbell, Cafiso et al. 2000). Subsequent EPR spectrum gives four different parameters:

a) Solvent accessibility of the side chain (of the spin label) that is determined from the collision frequency of the spin label with paramagnetic reagents such as O_2 and Ni EDDA (Ni (II) ethylenediamine diacetic acid)

b) Mobility of the side chain

c) Polarity index for its immediate environment

d) Distance between two paramagnetic centers in the protein

This approach has been nicely illustrated with the KcsA channel (Perozo, Cortes et al. 1998), the mechanosensitive channel (Perozo, Kloda et al. 2002) and recently KvAP (Cuello, Cortes et al. 2004). The dynamics of transporters have also been studied (Wegener, Tebbe et al. 2000; Omote and Al-Shawi 2002) and very recently a pH induced oligomerization was reported

for a sodium/proton antiporter (Hilger, Jung et al. 2005).

3) The minimal protein core required for obtaining well diffracting crystals has been elucidated with mass spectrometry. Some examples include the KcsA channel and the glycerol phosphate transporter (Doyle, Morais Cabral et al. 1998; Huang, Lemieux et al. 2003). In addition the substrate binding sites have also been explored with mass spectrometry (Weinglass, Whitelegge et al. 2003).

When starting a project it would be worth to bear in mind all the possibilities to experiment on a particular protein and the following flow diagram is one I found useful to determine the needs and time required for a project.

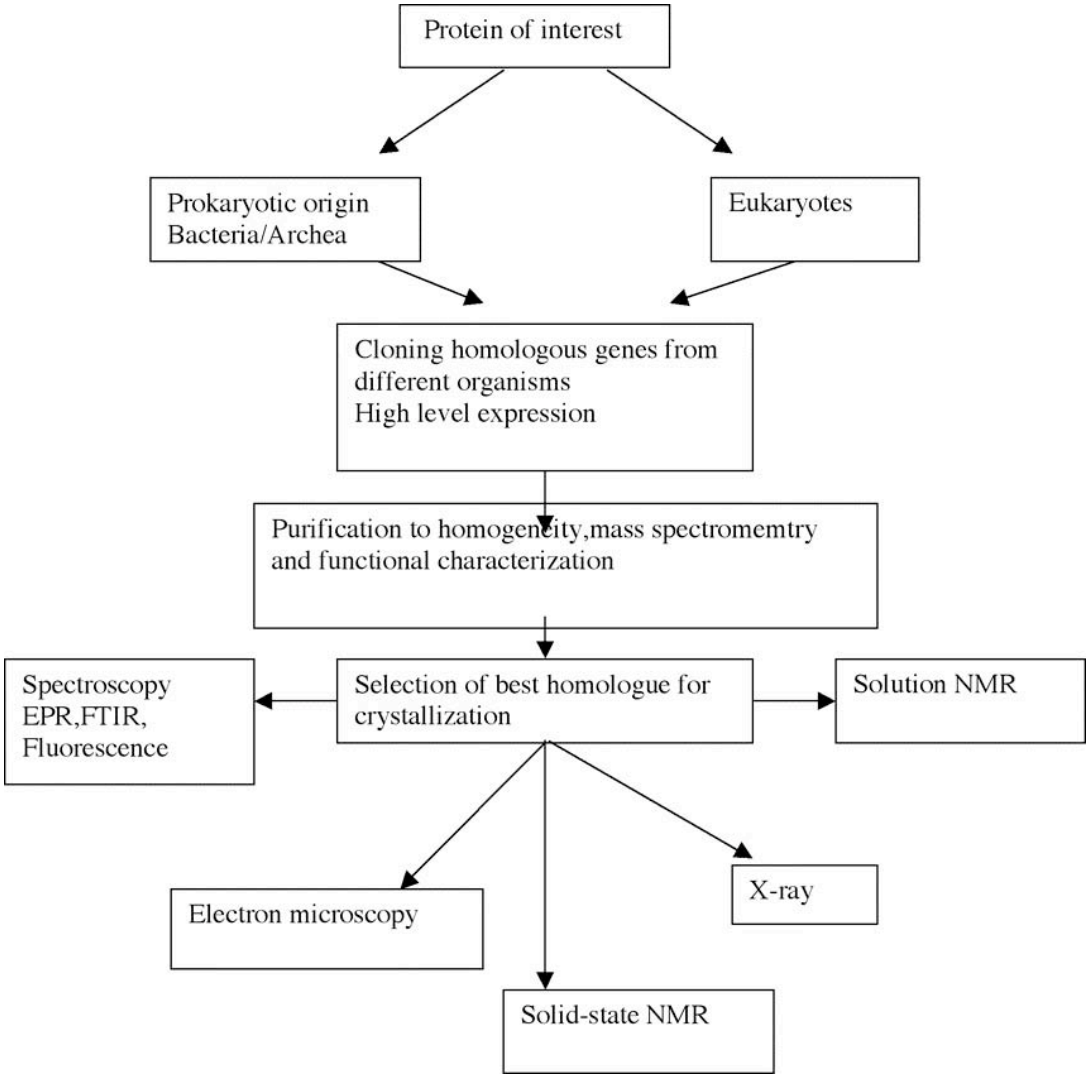

Figure 1.11: A flow diagram summarizing the different options for studying the structure and function of a membrane protein.

1.11 LEARNING ABOUT MEMBRANE PROTEINS

The topic of my doctoral work is broadly called “Structural studies of membrane transport proteins”. As mentioned earlier, prokaryotic homologues of a few families of secondary transporters constitute the main part of the work. One of the porin was also studied due to interest in MAS-NMR. Initially, 2D crystallization and electron microscopy were the main techniques used but towards the end focus also shifted towards 3D crystallization. The following pages describe in detail the information available for the proteins that I have been working on.

1.11.1 SODIUM/PROTON ANTIPORTERS

Na^+/H^+ antiporters are ubiquitous membrane proteins that counter-transport sodium ions and protons. They play a central role in pH homeostasis and in the extrusion of Na^+, which is toxic at high concentrations (Padan, Venturi et al. 2001). They are thus crucial for maintaining the electrochemical gradient across the membrane, which provides the driving force for many other transport systems that use either Na^+ or H^+ as the counter ion. In the non-epithelial cell of higher eukaryotes, Na^+/H^+ antiport is thought to be most important in the regulation of intracellular pH since it has been shown to be induced by various growth promoters and to have a central role in regulation of cell volume (Kapus, Grinstein et al. 1994). A fascinating property of these antiporters is their response to pH. Apparently, a change in pH, acting directly on a small set of amino acid residues, triggers a conformational change that results in activation or inactivation of the transporter (Padan, Tzubery et al. 2004). Biochemical studies suggest that distinct groups of residues are involved in substrate binding and pH response (Padan, Tzubery et al. 2004). These transporters have been described in many different organisms. They share a common functional feature but evidently differ in terms of regulation. These differences probably arise from the environment where the organism lives. A small representation of the Na^+/H^+ antiporters in the following table explains the profile of the protein in terms of its response to pH and the ion it

extrudes.

Table 1.2:

Organism/protein	Active in pH range	pH inactive at	Ion extruded
E.coli NhaA	7-8.5	<6.5	sodium
V.cholerae NhaA	7-8.5	<6	sodium
V.cholerae NhaD	7-8.5	<6.5 & >8.8	sodium
H.pylori NhaA	6-8.5	<6	?
M.jannaschii NhaP1	6-7	>7	protons
Human NHE1	6-7	>7	protons
P.aeruginosa NhaP	7-8	<6.5 & >8.5	protons

In my opinion, the Na^+/H^+ antiporters can transport both ions in a functional state and it is the necessity of the cell that results in extrusion or import of either ion. Based on their ability to grow at different pH, it is possible to classify the organisms into three categories acidophiles, neutrophiles and alkaliphiles (Booth 1985). Acidophiles have an internal pH of ~6-6.5, while the neutrophiles tend to have around 7.5-8, and the alkaliphiles have 8.5-9. This property of cytoplasmic pH and the primary pump possibly determine the role of Na^+/H^+ antiporters in a given cell.

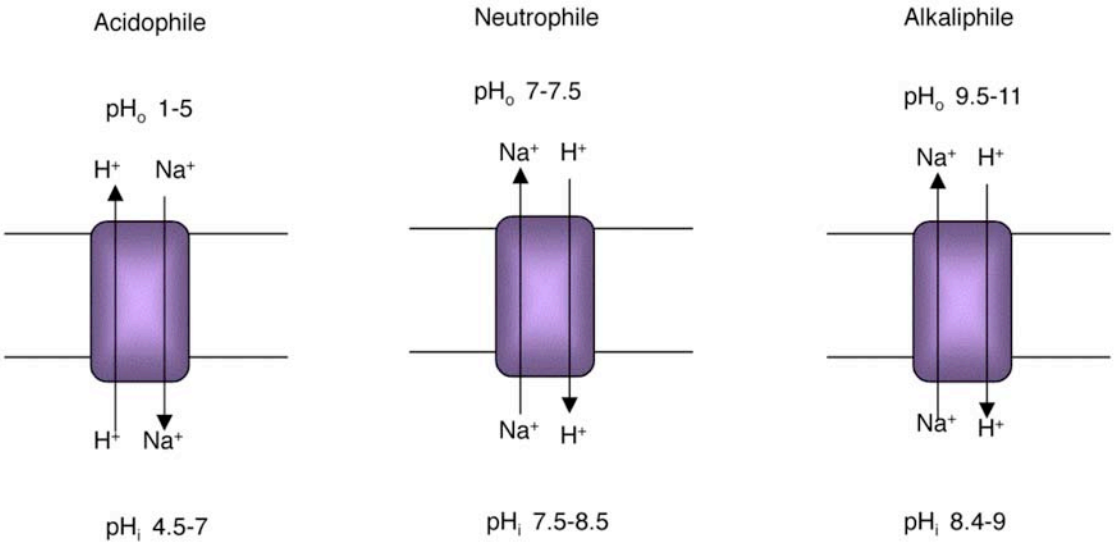

Figure 1.12: A diagram explaining the functional role of sodium/proton antiporters in organisms that grows under different external pH.

The projection structure and the 3D map of NhaA from *E.coli* was the first structural information obtained for a sodium/proton antiporter describing two bundles of 6 helices arranged asymmetrically in each monomer (Williams, Geldmacher-Kaufer et al. 1999; Williams 2000). This was the first instance where the author had clearly pointed out that the ion translocation site is not at the dimer interface but resides on each monomer. The recent x-ray structure of NhaA solved as a monomer in detergent reveals a novel fold 'short helix-extended polypeptide chain-short helix' of TM helices that are in antiparallel orientation (Hunte, Screpanti et al. 2005). Although the x-ray structure has been solved as a monomer, the domain architecture and organization of the helical bundles are essentially the same as in lipid bilayer. These two structures represent the inactive closed state of the transporter.

MjNhaP1

Three homologues of sodium/proton antiporters have been identified in the genome of *Methanococcus jannaschii*, a hyperthermophilic archaeon

growing optimally at 85°C. Two of them are closely related and possibly arose by gene duplication (MJ0057 and MJ1526) and third gene (MJ 1321) resembles the NapA family members. One of this MJ0057 has been shown to be active in *E.coli* inverted membrane vesicles at acidic pH (Hellmer, Patzold et al. 2002) and named MjNhaP1. Sequence comparison places MjNhaP1 in the NhaP family of Na^+/H^+ antiporters, which show greater homology to eukaryotic proteins such as the human sodium-proton exchanger NHE1 rather than to NhaA from *E.coli*, the best-characterized sodium/proton antiporter (Padan, Venturi et al. 2001). The activity profile and the pH response are very similar to that of NHE homologues of humans (Hayashi, Szaszi et al. 2002). Based on the sequence, the protein is predicted to span the membrane 13 times. Two aspartate residues (D132 and D161) and an arginine (R320) found in the putative trans-membrane regions have proven to be important for activity of MjNhaP1 (Hellmer, Teubner et al. 2003).

1.11.2 SODIUM/SOLUTE SYMPORTER FAMILY

This family consists of more than 40 different proteins from all the kingdoms. They use only Na^+ as the coupling ion, in other words a sodium gradient acts as a driving force. The proteins in this family include the well studied Na^+-glucose cotransporter (SGLT1), mutations of which is implicated in inherited disorder glucose-galactose malabsorption (Wright, Loo et al. 2004) and the Na^+-iodide symporter, whose understanding is critical in treatment of thyroid cancers (Dohan and Carrasco 2003). Some of the remarkable properties of the SGLT1 include its ability to act as uniporter in absence of sugar. It can act as channel for water and other hydrophilic solutes (Wright, Loo et al. 2004). The members of the SSF family are predicted to have 11-14 trans-membrane helices from their sequence and most proteins are thought to function as monomers. The stoichiometry of sodium and substrate differs but the binding of sodium to the transporter results in a conformational change that favors substrate binding. The reaction scheme is very similar to that shown in figure 1.7 for Lac permease. None of these eukaryotic proteins have been expressed to a level suitable for crystallization

so far and the attention has been on the prokaryotic homologues.

Proline Transporter

The *E.coli* proline transporter PutP catalyzes the coupled translocation of Na^+ and proline according to a symport mechanism with a Na^+ to proline stoichiometry of 1:1. Li^+ but not H^+ can substitute for Na^+. An electrochemical potential (□□) can drive proline accumulation if Na^+ ions are present. The K_m values for Na^+ and proline uptake by PutP in whole cells and right-side-out membrane vesicles were determined as 30 and 2□M, respectively. However, the apparent K_m (Na^+) of PutP reconstituted into proteoliposomes in an inside-out orientation was calculated to be 730□m. The lower affinity can be explained as a functional asymmetry of the transporter that appears to have a lower cation affinity at its cytosolic side. Binding of Na^+ to PutP causes a conformational change in the protein that results in increased affinity for proline (Jung 2001).

Reporter fusion and EPR studies of PutP suggest a 13 TM helical protein (Jung 1998; Wegener, Tebbe et al. 2000). Structure-function studies of PutP have yielded residues important for substrate binding. The ion binding site is proposed to be located in the N-terminal half, with only a single aspartate essential for activity located in TM II (Pirch, Quick et al. 2002).The hydrophilic residues in the cytoplasmic half of TM II form an aqueous cavity in the membrane that possibly allows the release of Na^+ and proline (Pirch, Landmeier et al. 2003). Purified PutP could be obtained in amounts suitable for crystallization (Jung, Tebbe et al. 1998) and would be a model system for the SSF transporter family.

1.11.3 BCCT family

The BCCT family of secondary transporters comprises a large group of membrane proteins, which share the common functional feature of transporting molecules with a quaternary ammonium group. Most members of this family utilize electrochemical ion gradients for substrate accumulation.

Sequence alignment of the proteins in the BCCT family shows atleast three conserved regions, which are possibly involved in binding of the substrate. This region includes the trans membrane helix 8 and the loop that continues this helix (Figure 1.13). Binding of the substrate causes a conformational change, which has been studied in the case of CaiT by analyzing changes in tryptophan fluorescence emission (Jung, Buchholz et al. 2002).

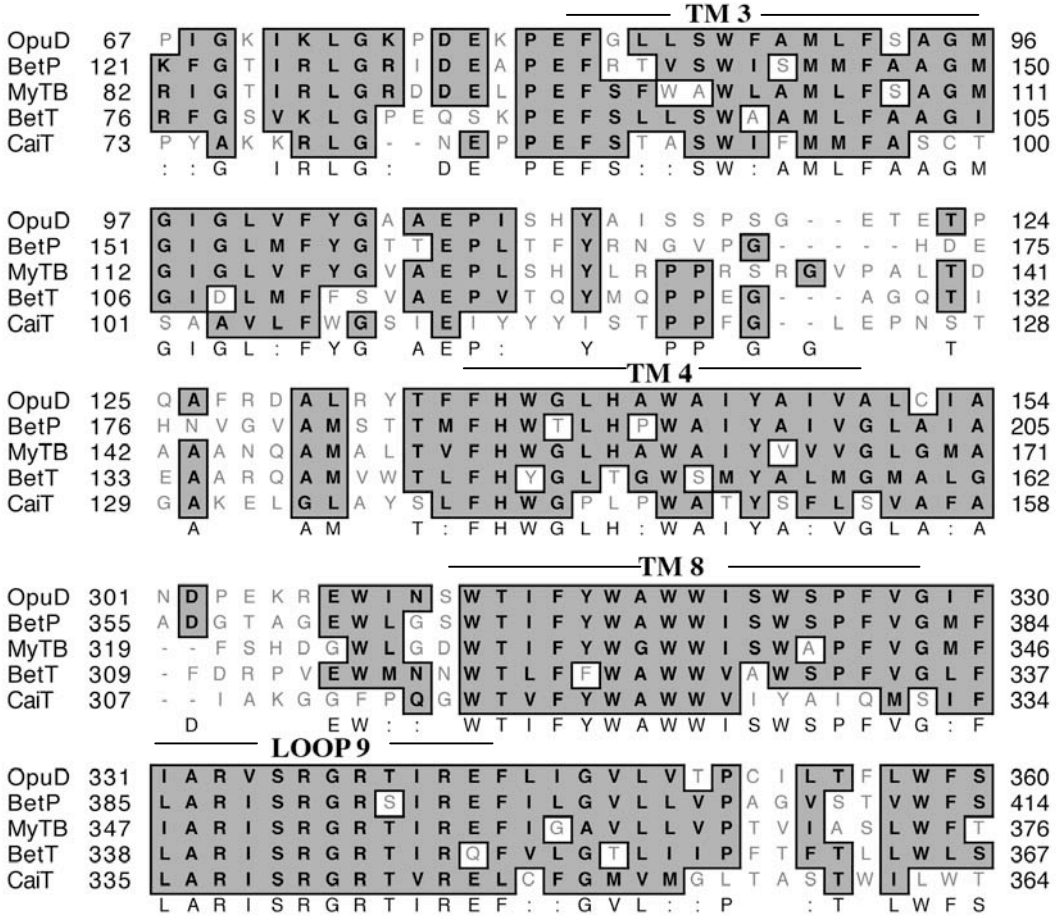

Figure 1.13: Multiple sequence alignment of transporters from the BCCT family. The conserved residues are boxed and shaded. The proteins selected for alignment are OpuD from *Bacillus subtilis* (P54417), BetP from *Corynebacterium glutamicum* (P54582), MyTB from *Mycobacterium tuberculosis* (P63695),CaiT from *Escherichia coli* (P31553) and BetT from *Escherichia coli* (P17447).

However, the proteins in the family differ among themselves in their ability to respond to osmotic stress. One of the well-studied members of this family is BetP from *Corynebacterium glutamicum* that is a symporter. It uses the sodium gradient to import betaine, in a process regulated by N and C terminal extensions of the protein (Rubenhagen, Ronsch et al. 2000; Kramer

and Morbach 2004). The projection map of BetP from *Corynebacterium glutamicum* was reported at 7.5Å (Ziegler, Morbach et al. 2004) revealing an asymmetric trimer with two pore like features suggesting putative transport pathways.

Carnitine Transporter

The *Escherichia coli* carnitine transporter is a member of the BCCT family. The protein sequence shows no N-or C-terminal extensions, unlike its homologue BetP. CaiT differs from the other members of this family with respect to its use of electrochemical gradient. It acts as L-carnitine/□-butyrobetaine exchanger and does not respond to osmotic stress (Jung et al 2002). *E.coli* dehydrates L-carnitine accumulated by CaiT and the resulting crotonobetaine is used as an electron acceptor under anaerobic conditions, which results in the end product □-butyrobetaine (Jung, Jung et al. 1990).

1.11.4 OUTER MEMBRANE PROTEINS

As many as 22 structures of □-barrel membrane proteins are known, many differing in the number of strands and function they carry out (Schulz 2002). □-barrel proteins are very stable in comparison to the □-helical proteins, mainly due to the large number of intra-strand hydrogen bonds. The H-bond energy has been calculated as roughly 0.5kcal/mol/residue and this must be one reason for their greater success in x-ray crystallography. They carry out diverse functions in different organisms. Crystals have been obtained for the outer membrane proteins that have either been expressed to the membrane or by refolding from inclusion bodies. Both approaches have yielded crystals diffracting to high resolution, with the amount of protein obtained from inclusion bodies largely greater than from that expressed in the membrane. However, yield of fully functional protein after refolding is not 100%.

The following table summarizes the various classes of β-barrel membrane proteins and the number of β-strands.

Table 1.3:

Functional category	Protein	No. of strands	Oligomeric state
Non – specific	OmpF	16	trimer
Facilitated transporter	LamB	18	trimer
Energy dependent efflux	TolC	12	trimer
Energy dependent influx	FepA	22	monomer
Protein secretion	PulD	?	?
OM-Usher pore	PapC	18-24	?
Adhesion	OmpX	8	monomer
Phospholipase	OmpLA	12	dimer
Protease	OmpT	12	dimer
Pore forming toxin	β-hemolysin	14	heptamer
Autotransporters	NalP	12	monomer

OmpG

OmpG is a protein encoded by a cryptic gene. It was discovered by mutagenesis (Misra and Benson 1989). In the absence of major maltoporins OmpG is probably expressed to import sugars. Based on the sequence it has been predicted to have a 14-stranded barrel and exists as a monomer. It forms large cation selective channels of 80pS and the pore is blocked by gadolinium chloride (Fajardo, Cheung et al. 1998; Conlan, Zhang et al. 2000). A projection structure of OmpG from 2D crystals of protein isolated from the native membrane showed a roughly circular pore with a few internal densities,

probably helices (Behlau, Mills et al. 2001). The dimension of OmpG was different from that of other known porins, probably reflecting a difference in the number of β-strands.

Why study OmpG?

There are many different structures of β-barrel membrane proteins known, so why do we need another one? The protein OmpG was chosen for the following reasons:

1) Unlike most other pore-forming outer membrane β-barrels, OmpG is a monomeric protein and its medium size (~33kDa) makes it a suitable candidate for solid-state NMR studies. MAS-NMR (Magic angle spin-NMR) is still in its initial stages of structural determination and requires ordered material rather than a powdered sample. Either a 2D or 3D crystal can fulfill this need. This additional demand means the protein of interest should be expressed in large amounts so that one can get sufficient quantities after labeling. OmpG fulfills both these needs. Moreover, the possibility of studying protein dynamics makes it a good candidate for solid-state NMR.

2) In physiological membranes, membrane bound receptors and channels perform the function of discriminating a multitude of stimuli. Using this idea from nature engineered membrane pores can be used to make rapid and sensitive biosensors that have potential applications in detection of biological warfare agents and pharmaceutical screening. Using engineered pores in stochastic sensing, a single molecule detection technology will reveal the identity and the concentration of the analyte. In the past years small ions, organic molecules, proteins and DNA have been detected (Howorka, Cheley et al. 2001).

A sensor element has two states – occupied and unoccupied, which results in different output (current). One possible application of this system is the ability to do sequencing of nucleic acids. The transit time and extent of current blockage reveal information about the length of the nucleic acid and its

base composition. This system when optimized has the potential of sequencing large genomes in shorter period.

What are the requirements for a pore to be used as a biosensor?

1) the protein of interest should be easily amenable for protein engineering

2) it should have high conductance

□-barrel proteins suit both these needs. Their advantage over the □-helical pore formers is their ability to tolerate mutations while maintaining their structure. The pore used till date in the sensing is the staphylococcus □-hemolysin, which is a heptamer of identical subunits forming a 14-stranded □-barrel. OmpG has a very large conductance; it has the advantage being a monomer and should be relatively easy for genetic manipulation

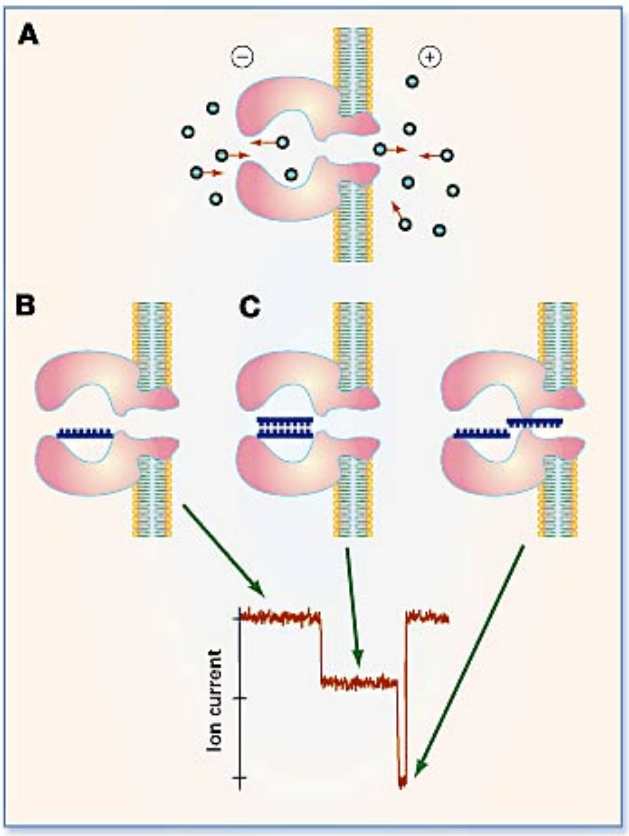

Figure 1.14: A schematic representation of nanopores, based on haemolysin to detect the mismatches in nucleic acid (Bayley and Jayasinghe 2004).

A - in a lipid bilayer the pore forms a large conducting channel that allows the passage of the ions

B – a tethered single stranded nucleic acid in the pore does not affect the conductance in the channels.

C – subsequently when another test sample is added, due to the base pairing it forms double stranded and blocks the pore resulting in change in conductance. But due to the applied current the strand is moved and resulting in differential conductance state, based on the nucleotide present. This system has been used to detect the mutations that occur frequently in the genome of HIV virus (Howorka, Cheley et al.).

2 MATERIAL AND METHODS

2.1 BASIC MOLECULAR BIOLOGICAL TECHNIQUES

Basic techniques for handling of DNA and cells were essentially followed as described in the manual "Molecular Cloning" by Sambrook and Maniatis.

2.1.1 PREPARATION OF COMPETENT CELLS

Transformation buffer (TB):

Reagents	Final concentration
$MnCl_2.4H_2O$	55mM
$CaCl_2.2H_2O$	5mM
KCl	250mM
PIPES (0.5M,pH6.7)	10mM

Divided into aliquots and stored at -20^{O}C.

An overnight culture of the desired *E.coli* strain was sub-cultured in 50 ml of Luria broth (LB) and grown at 37°C till the OD_{600} reached 0.6. The cells were immediately placed in ice and incubated for 10 minutes. Cells were harvested by centrifugation at 2500g for 10 minutes. The pellet was washed once with ice-cold transformation buffer and resuspended in 4ml of TB. 0.3ml of DMSO (dimethyl sulfoxide) was added and mixed by swirling followed by incubation in ice for 10 minutes. Cells were aliquot (50□l), flash frozen in liquid nitrogen and stored at -80°C. The competent cells thus obtained were used up to a year.

2.1.2 DNA TRANSFORMATION

Frozen competent cells were thawed in ice and the required amount of DNA (typically in ng) was mixed and incubated for 30 minutes on ice. Cells were heat shocked at 42°C for 90 seconds followed by incubation on ice for 10 minutes. 0.8ml of LB was added and incubated in a shaker for 45 minutes at 37°C to allow the expression of the transformed marker. The transformed

cells were then selected on the respective plates.

2.1.3 MAINTENANCE OF BACTERIAL STRAINS

Freshly transformed strains of bacteria were grown in 4ml of LB overnight at 37°C. Cells were diluted to a final glycerol concentration of 20% and frozen at -80°C. For a reproducible expression always the strains were streaked from the stock thus made.

2.2 CELL GROWTH

For expression of proteins, single colonies of cells harboring the respective plasmid were inoculated in 50 ml of Luria broth (Tryptone 10g, Yeast extract 5g and NaCl 10g per liter) and grown overnight at 37°C. The cells were then sub cultured in 2 liters of 2XYT media (Tryptone 20g, Yeast extract 10g and NaCl 5g) and grown at 37°C. Expression was induced when the cells reached an OD_{600} of 0.6 with 1mM IPTG (or 0.2% arabinose) and grown further for 3-4 hours.

CELL STRAINS AND CONSTRUCTS:

Protein	Vector[a]/Promoter	Strain/Phenotype	Protein yield (per liter)	Comments
OmpG	pET 26b/T7	BL21□(DE3)-C41[b]	10-15 mgs	Expressed as inclusion bodies (IB)
ProOmpG	pET 26b/T7	BL21□(DE3)-C41	-	OmpG was either in IB or found attached to membrane
PutP	pTrc99A/Tac*	WG170 (□putp,puta)	1-1.5mgs	Growth stops after induction
PutP	pBAD/Ara*	" "	"	
CaiT	pT7-UV5* pET 15b/T7	BL21□(DE3) pLysS " "	2-2.5mgs	Normal growth
MjNhaP1	pET 26b/T7	BL21□(DE3) pLysS	0.5-0.7mgs	Slow growth after induction

[a] – Sources of vector are pET series of vector from Novagen, pTrc99A from Amersham/Pharmacia, pBAD from Invitrogen. * - Clones provided by Prof.Jung

[b] – this particular strain is derivative of normal *E.coli* BL21 □(DE3) strain but has higher capability to hold expressed protein

2.3 MEMBRANE PREPARATION AND SOLUBILIZATION

Cells were harvested and broken with a cell disrupter (Constant Systems) or a microfluidiser. Unbroken cells were removed by low speed centrifugation. The membrane fraction was collected by centrifugation at 100,000g at 4°C for 1 hour, resuspended in 25mM Tris pH8 and stored at a final protein concentration of 25 mg/ml at -80°C. Membranes were solubilized in 1.5 % □-D-dodecyl maltoside (DDM, Glycon) for 45 minutes at room temperature or 4°C. The unsoluble fraction was removed by ultracentrifugation at 100,000g for 20 minutes at 4°C. Prior to the affinity column, 0.3M NaCl and 10mM imidazole were added to the soluble fraction.

2.4 ESTIMATION OF TOTAL PROTEIN IN MEMBRANES

A modified Lowry method was used to estimate the total protein in the membrane (Peterson 1977). Membranes were diluted in water to a final volume of 500□l. 50□l of 0.15% of deoxycholate was added, vortexed and incubated for 10 minutes. Subsequently 50□l of 90%TCA (tri chloroacetic acid) was added and centrifuged for 10 minutes at 13,000 RPM. The pellet was dried and resuspended in 500□l of water and 500□l, of Reagent A was added, and the sample was incubated for 10 minutes. 250□l of Folin's reagent was added and incubated for 30 minutes and absorbance was measured at 750 nm. BSA (Bovine Serum Albumin) at a concentration range of 10-80□g was used as a standard.

2.5 PROTEIN PURIFICATION

2.5.1 AFFINTIY PURIFICATION WITH HIS TAG

Chelating sepharose from Amersham was washed free of ethanol with water. 50mM $NiCl_2$, equivalent to the bed volume was used to activate the column, followed by washing off the unbound nickel. The column was then equilibrated with buffer A (25mM Tris pH8, 10% glycerol, 2mM □-ME, 0.3M NaCl, 0.05% DDM) with 10mM imidazole. The soluble fraction was allowed to

bind to the nickel column in batch for one hour. Column material was packed and the flow through was collected to check the efficiency of binding. This step was followed by two washes in buffer A with 10mM and 30mM imidazole (20 column volumes each) to remove non-specifically bound proteins. Protein was eluted either directly with 0.2M imidazole in buffer A or by an imidazole gradient (10-250mM).

2.5.2 GEL FILTRATION

Gel filtration in buffer A was carried out either with a Superdex 200 (16/60) or a Superose 6 column (Amesham/Pharmacia). When required the pH of the buffer or the detergent was changed.

2.6 PROTEIN ESTIMATION

Protein estimation was done by Coomassie dye binding method (Bradford 1976). Alternatively, the absorbance of protein denatured in 6M guanidium hydrochloride at 280 nm was used with the extinction coefficient calculated from the amino acid sequence (CaiT – 154510 and OmpG - 85060).

2.7 POLYACRYLAMIDE GEL ELECTROPHORESIS

2.7.1 SDS GEL ELECTROPHORESIS

Stock solutions:

A) Acrylamide/bis (30%T, 2.67%C) – prepared by mixing of 29.2 g acrylamide and 0.8g N'-N'bis-methylene-acrylamide, filtered and stored at 4°C in the dark.

B) 1.5M Tris pH8.8

C) 0.5M Tris pH6.8

D) 10% SDS

E) 10% ammonium persulfate (prepared fresh)

F) Sample buffer

0.5M Tris pH6.8	1ml
Glycerol	0.8ml
10% SDS	1.6ml
2-mercaptoethanol	0.4ml
0.05% (w/v) BP blue	0.4ml
water to	8ml

G) 5X Electrode buffer (for a liter)

Tris	15g
Glycine	72g
SDS	5g

Components	Separating gel	Stacking gel
Acrylamide (30%)	15ml	3ml
1.5M Tris pH8.8	15ml	-
0.5M Tris pH6.8	-	7.5ml
10% SDS	0.6ml	0.3ml
10% APS	0.3ml	0.15ml
TEMED	30□l	75□l
Water to final volume	60ml	30ml

12% gels were cast with a multiple casting unit from Biorad. After polymerization, gels were stored at 4°C and used up to a month. For sample preparation, the protein sample at desired concentration was mixed with sample buffer (to a final of 1X). Samples were not boiled unless otherwise indicated.

2.7.2 BLUE NATIVE GEL ELECTROPHORESIS

3X gel buffer: 1.5M aminocaproic acid and 150mM bis-tris buffered to pH7

Cathode buffer: 50mM Tricine and 15mM bis-tris pH7 with or without 0.02% Servablue G

Anode buffer: 50mM bis-tris pH7

Gel loading dye: 5% CBB, 500mM 6-amino-n-caproic acid in 100mM bis-tris buffer pH7

For a 12x15cm gel the following composition was used.

COMPONENTS	GRADIENT-SEPERATING GEL 6%	16%	STACKING GEL 4%
3X Gelbuffer	3ml	3ml	1.33ml
30% Acrylamide	1.8ml	4.8ml	0.53ml
87% Glycerol	-	1ml	-
10% APS	38µl	30µl	30µl
TEMED	3.8µl	3µl	3µl
Water to final	9ml	9ml	4ml

A gradient (6-16%) of separating gel was made using a Hoefer gradient maker, followed by overlaying a 4% stacking gel. The gel run was carried out at 125V for 12-14 hours and then increased to 300V for 1-2 hours till the dye reached the bottom of the gel. The run was carried out at 4°C. The cathode buffer could be changed to a Commassie free buffer without having any effect on the migration of the bands. The buffer exchange was carried out after an hour of gel run. This exchange yielded gels with better background.

2.8 VISUALIZING PROTEIN AFTER ELECTROPHORESIS

2.8.1 COOMASSIE STAINING

Coomassie brilliant blue R250/G250 was dissolved in 45.5% of methanol and 7% acetic acid and filtered before use. Gels were stained for 20 minutes and destained with 5% methanol and 7% acetic acid.

2.8.2 SILVER STAINING

A – Fixing solution contains 40% of methanol and 35% of formalin

B – 0.2% stock solution of sodium thiosulfate (STS)

C – 0.1% of silver nitrate solution (prepared fresh)

D – Developing solution made of 0.3% sodium carbonate, 0.02% sodium

thiosulfate and 0.05% formalin

E – Stopping solution was 5% acetic acid

The procedure for silver staining was as follows:

1) The gel was fixed for ten minutes and washed in water two times for 5 minutes.

2) Subsequently, the gel was treated with 300ml of 0.02% STS for a minute and washed with water for a minute.

3) The gel incubated with 300ml of 0.1% silver nitrate solution for 10 minutes and rinsed with water.

4) The gel was developed with 300ml of the developer until the bands started appearing.

5) The reaction was stopped with 5% acetic acid.

2.8.3 WESTERN BLOTTING

BUFFERS AND REAGENTS:

A – Transfer buffer
25 mM Tris
192 mM glycine
20% methanol (added just before the transfer)

B- TBS (for washing)
10 mM Tris pH7.5
150 mM NaCl

C – TBS –Tween buffer (TBS +0.05% Tween 20)

D – Blocking buffer was made of 5% milk powder or 3% BSA in TBS

E – Antibody stock solution (11000) was made in blocking buffer

Transfer of the protein from the gel to PVDF membrane was carried out with a semi dry blotting system from BIORAD for 30 minutes at 15V. The membrane was subsequently treated with blocking buffer for an hour and

washed 2 times each with TBS-Tween buffer and TBS buffer for 10 minutes. The membrane was allowed to bind primary antibody (anti-his) for an hour and washed as in the previous step. Subsequently the secondary antibody, a conjugate of alkaline phosphatase was allowed to bind to the membrane for an hour and washed as before. The membrane was developed with BCIP tablets (sigma).

2.9 CD SPECTROSCOPY

The CD spectrum was measured using a JASCO spectrometer with a 1mm cuvette. The wavelength range of 300-190 nm was used for measurement at 24°C unless otherwise stated. Typically 0.05-0.1mg/ml of protein in the respective detergent was used for spectrum measurement. The spectra were analyzed by CDNN, a neural network program.

2.10 FLUORESCENCE SPECTROSCOPY

2.10.1 Tryptophan fluorescence

Fluorescence measurements were made with a Hitachi fluorimeter. For tryptophan fluorescence an excitation wavelength of 285nm was used with a slit width of 5nm. Spectra were measured with a 10x10-mm cuvette. Emission spectra were recorded in the region of 300-400nm with a slit width of 5nm.

2.10.2 Determination of CMC

For determining the CMC of detergents the increase in ANS fluorescence upon micelle formation was used. The excitation and emission wavelength used were 410nm and 450nm respectively with a fixed slit width of 5nm.

2.10.3 Activity measurements of MjNhaP1

For activity measurements, 4 μl of proteoliposomes (section 2.16.1) or control liposomes not containing the transporter were diluted in 1 ml MTCB

without sodium at pH 6 or 7.5 with 1μM of the fluorescence dye 9-amino-6-chloro-2-methoxyacridine (ACMA). The excitation wavelength was 409 nm and the emission wavelength 474 nm, with a slit width of 5 nm. Finally, the pH gradient was dissipated with 25mM NH_4Cl. All measurements were done at 23°C.

2.11 ESTIMATION OF TOTAL DETERGENT

The amount of detergents with a carbohydrate head group was measured by the phenol-sulfuric acid method (Rao and Pattabiraman 1989). A known concentration of protein was diluted in water to 1ml. 50μl of water-saturated 95% phenol was added, thoroughly mixed until the solution was clear. 2.5ml of conc. sulfuric acid was added and allowed to cool at RT for 30 minutes. The absorbance at OD_{490} was measured using a Perkin Elmer spectrometer with an appropriate blank. The detergent β-D-dodecyl maltoside (DDM) was used as a standard.

2.12 MALDI MASS SPECTROMETRY

A robust technique to analyze membrane proteins in detergent was followed as described previously (Cadene and Chait 2000). The matrix α-cyano-4-hydroxy-cinnamic acid (BRUKER) was prepared as saturated solution in acetonitrile/water mixture (3:1). A thin layer was made on the target plate and allowed to dry. Sample proteins at a concentration of 5-8mg/ml were diluted 20 fold in saturated matrix solution (low protein concentration resulted in high background). 1μl of sample was laid on the thin layer of matrix and allowed to air dry. As the crystal of the matrix formed the sample was washed with 4μl of 0.1% TFA twice and allowed to dry.

Spectra were acquired using a MALDI time-of-flight mass spectrometer from Bruker, operating in linear delayed extraction mode. Spectra from 120 individual shots were averaged with software provided by the manufacturer. The spectra were smoothed and analyzed using the program M-over-Z (From

the prowl website of Rockefeller University).

2.13 THIN LAYER CHROMATAGRAPHY

Two different solvent systems were used to separate the lipids. Acidic and basic solvent was used in the first and second dimension respectively.

COMPONENTS	SOLVENT (in ml) ACIDIC	BASIC
CH_3OH	10	25
$CHCl_3$	30	65
CH_3COOH	10	-
$(CH3)_2CO$	40	-
H_2O	5	-
NH_3	-	5

Lipids from the protein sample (~200-500μg) was extracted with chloroform/methanol (3:1) and dried in nitrogen. The dried sample was redissolved in 10-20μl of chloroform. 1-2μl of sample and standard were spotted on silica gel coated plates and air-dried thoroughly. The run was carried out until the solvent front was 1cm from the edge in both dimensions. Chromatogram was developed with iodine vapor for non-specific staining. Molybdenum blue staining was used to identify phospholipids.

2.14 PREPARATION OF LIPID STOCKS

Lipids were obtained from Avanti Lipids as stocks in chloroform. Lipid was dried under argon and traces of chloroform were further removed in vacuum for 2 hours. Lipid was resuspended in 1% of detergent solution to a final concentration of 4-5mg/ml, sonicated till a clear solution was obtained. This stock of solubilized lipid was aliquot and stored at –20°C.

2.15 DETERMINATION OF ONSET/TOTAL SOLUBILIZATION OF LIPIDS

E.coli polar lipids were dried under argon and rehydrated with aqueous

buffer to a final concentration of 1mg/ml. Turbidity measurements were performed with a Perkin Elmer spectrophotometer at 500nm. The change in turbidity upon the addition of detergent was allowed to reach a steady state before further addition of detergent.

2.16 RECONSTITUTION OF PROTEINS

2.16.1 RECONSTITUTION FOR FUNCTIONAL STUDIES

The following procedure was carried out to reconstitute MjNhaP1 into lipids for functional studies. *E.coli* polar lipids were dried and resuspended in MTCB (10mM Mes-Tris, 140mM Cholinechloride pH8) buffer with 0.3M NaCl. MjNhaP1 was added at a lipid-to-protein ratio of 50:1 (weight by weight) and incubated for 10 minutes at room temperature. Detergent was removed by overnight incubation with biobeads at 4°C. Proteoliposomes were collected by centrifugation (100,000g for 20 minutes) and resuspended in 100μl of MTCB+0.3M NaCl.

2.16.2 2D CRYSTALLIZATION

Protein typically at 1mg/ml final concentration was mixed at the desired LPR (lipid to protein ratio) with lipid, incubated in ice for 1hour before being transferred to dialysis bags for crystallization. The temperature and time period for dialysis depended on the protein, lipids and detergents.

2.17 ELECTRON MICROSCOPY

2.17.1 NEGATIVE STAINING AND SCREENING

4μl of the dialyzed sample was placed on a carbon coated copper grid (400 mesh size). The sample was allowed to adsorb for a minute. The grid was stained by floatation on drops of 1.5% uranyl acetate placed on parafilm. The grid was subsequently transferred to fresh drops. This ensured that any ingredients (phosphate, glycerol) in the sample buffer were removed in the first drops, resulting in better staining. The grids were screened in a Philips

CM12 or CM120 microscope equipped with a LaB6 filament and operating at 120KV. Images were recorded in low dose mode typically at a magnification of 35,000 with an exposure resulting in 20 electrons per $Å^2$.

2.17.2 PREPARING SPECIMEN FOR CRYO ELECTRON MICROSCOPY

Specimens for cryoEM were prepared by back injection method (Kühlbrandt and Wang 1991). A fresh piece of carbon floated on embedding medium of choice (typically 4% glucose or 4% trehalose) and the grid was coated with carbon from one side. The sample was applied to the side of the grid that carried the embedding medium and was mixed several times to ensure the adherence of the membranes onto the carbon. The grid was blotted on a filter paper for 10 seconds and air dried for 5 seconds before plunging into liquid nitrogen.

2.17.3 IMAGE COLLECTION

Images were recorded using a JEOL 3000 SFF electron microscope equipped with a field emission gun and liquid helium cooled top entry stage, with an accelerating voltage of 300 kV at a specimen temperature of 4K and a magnification of 53000x, using a spot scan procedure with an exposure time of 35 ms per spot. Images recorded on Kodak SO-163 electron emulsion film were developed for 12 min in full strength Kodak D19 developer. The quality of negatives was evaluated by optical diffraction and those exhibiting strong reflections to 10 Å were selected for further processing.

2.17.4 IMAGE PROCESSING

Selected image areas of 4000x4000 pixels were digitized with a pixel size of 7 □m on a Zeiss SCAI scanner. Images were processed using the MRC image processing programs to correct lattice distortions and contrast transfer function (Crowther, Henderson et al. 1996).Typically 3-4 cycles of unbending were carried out for each lattice. The program ALLSPACE was used to determine the phase residuals (Valpuesta, Carrascosa et al. 1994).

The best lattices were used for merging different data sets from which projection maps were calculated.

2.18 GENERATION OF PROJECTION MAP FROM PDB COORDINATES

The orientation of the model of the protein of interest was adjusted manually using the program O. Structure factors were then calculated from the pdb file to the desired resolution. A projection map was then calculated by using various programs of the CCP4 package. These include SFALL (for structure factor calculation), FFT (for calculating a map), MAPMASK (for extending the map) and NPO (for plotting).

2.19 CALCULATION OF MjNhaP1 DIFFERENCE MAP

Difference maps were calculated using phases and scaled amplitudes of structure factors obtained of the structure to be compared. Alternatively, a dimer from the pH4 projection map was masked out and placed into the pH8 unit cell by molecular replacement, using the program MOLREP (Vagin and Teplyakov 2000). Projection amplitudes and phases were calculated, scaled and subtracted from the pH8 data as above. In addition the dimer from each pH was cut out and subtracted in real space using the program SPIDER (Frank, Radermacher et al. 1996) or with the program OVERLAPMAP in the CCP4 package.

2.20 3D CRYSTALLIZATION

Protein at a concentration of 10-15 mg/ml was mixed with 1□l of reservoir solution and allowed for equilibration either by hanging drop or sitting drops method, incubated at 18°C. Crystals were harvested and frozen in liquid nitrogen with appropriate cryo protectant. Frozen crystals were checked for their ability to diffract x-rays at a synchrotron source. The information of the unit cell parameters was obtained with either DENZO or MOSFLM.

3 MjNhaP1

3.1 RESULTS

3.1.1 CLONING OF MJ0057 FROM GENOMIC DNA

The gene encoding the antiporter was amplified from the genomic DNA of *Methanococcus jannaschii* in two steps. In the first step the flanking primers on either side of the gene were used to get a PCR product (5' ata aaa tat tta tat gat ttt tag 3' and 5' caa gct tcg aaa cta ctt ctc cc 3'). The purified PCR product was used to amplify the gene encoding for MJ0057 using second set of primers (5' tta ttg tga tca tat gga act tat g 3' and 5' ata att tta ctc gag gga gga ttc ttc 3'). These primers had the restriction site for cloning into an expression vector (NdeI and XhoI). The sequence was verified and found to match with the published sequence in genbank. The clone MJ0057 hereafter is called MjNhaP1 as per the nomenclature introduced by Hellmer et al 2002. The cloning in the pET vector 26b (Novagen) resulted in protein with a His_6-tag at the c-terminus for purification.

3.1.2 EXPRESSION AND PURIFICATION

Expression of MjNhaP1 in *E.coli* strain BL21 pLysS yielded typically 0.5 – 0.7mg of pure protein per liter of culture. Of several detergents tried, DDM solubilized the protein most efficiently. MjNhaP1 was >85% pure after Nickel affinity chromatography, as judged by SDS gel electrophoresis and Coomassie staining (Figure 3.1A), which indicated a single band at ~36kDa. The predicted molecular weight from the amino acid sequence is 46789 daltons and this apparent difference in mobility in SDS gel is a common feature observed with membrane proteins. Immediately after the elution from the nickel column, the protein was dialyzed to pH4 buffer containing 0.05% DDM. It was observed that the protein was more stable in acidic pH and this dialysis step also ensured the removal of imidazole. Among the detergents checked for protein stability, maltosides were the best.

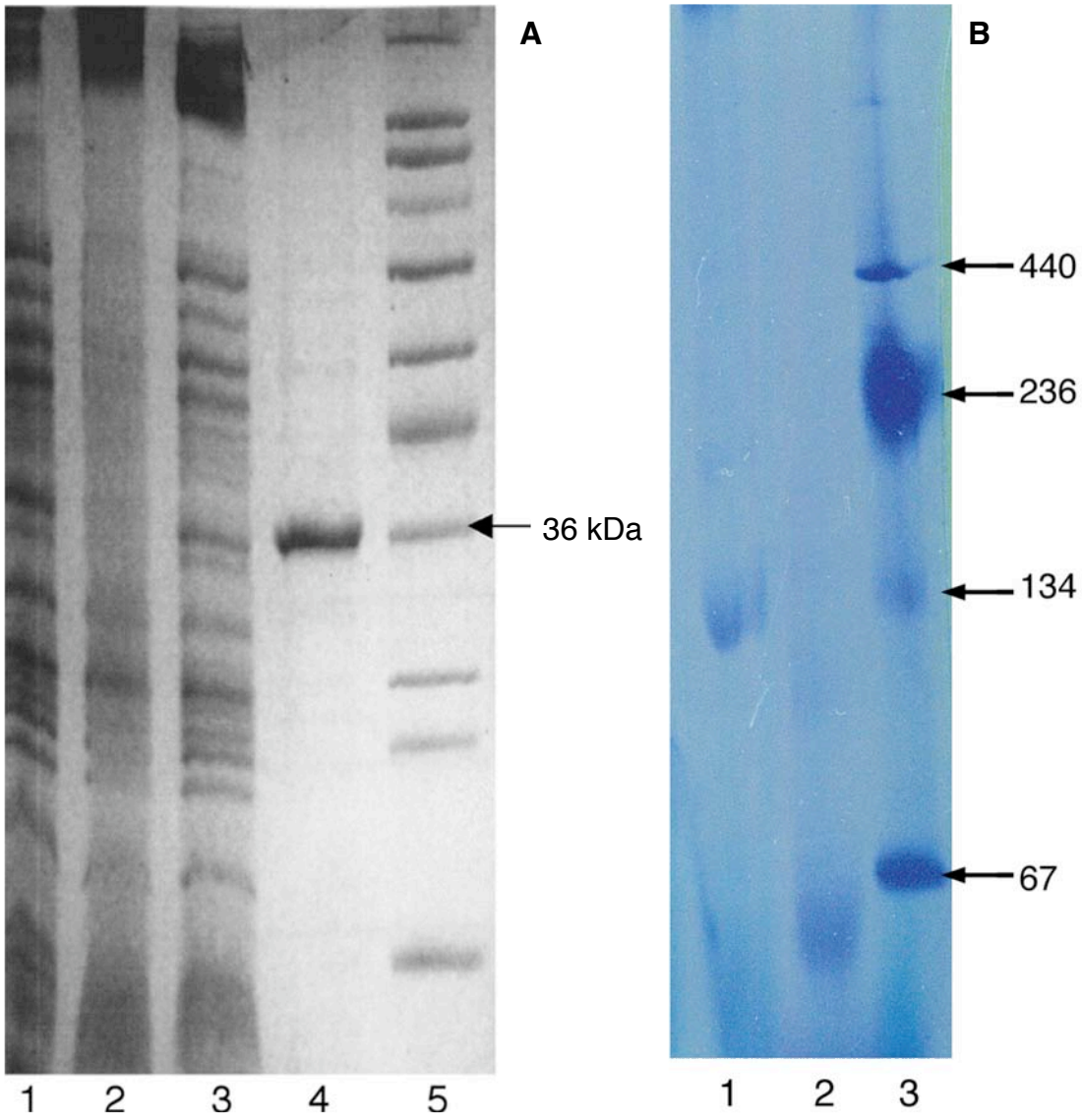

Figure 3.1 A: 12 % SDS-PAGE gel stained with Coomassie brilliant blue.
Lane 1, membrane fraction (15□g); Lane 2, insoluble fraction after detergent extraction (15□g); Lane 3, soluble fraction after detergent extraction (15□g); Lane 4, protein after affinity purification on nickel column (3□g); Lane 5, Sigma wide range marker

B: Blue native gel (6-20%) showing the protein is a dimer in detergent solution. Lane 1, purified protein (6□g); Lane 2, purified protein + 2% SDS added before loading (6□g); Lane 3, markers in kDa (from top to bottom: ferritin, catalase, BSA dimer and monomer)

The oligomeric state of the purified protein was examined by blue native gel electrophoresis. MjNhaP1 migrated as a dimer. No higher aggregates were observed at the concentrations used for crystallization. Increasing detergent concentration had no effect on the dimeric nature of the protein. SDS dissociated the dimer into monomers (Figure 3.1B). This property was used as a control to determine the oligomeric state in blue native gel. The momomeric band of MjNhaP1 migrates a little lower than 67kDa and the dimeric band migrates at twice the mass.

3.1.3 GEL FILTRATION OF MjNhaP1

The oligomeric nature of MjNhaP1 was further analyzed by gel filtration on a calibrated Superose 6 column. The retention volume of the protein-detergent micelle was approximately 1.62 ml corresponding to a Stoke's radius of 46Å (aldolase, 157kDa). Since dodecylmatloside was used in the buffer, the size of the detergent plays a role and hence this information could not be used for an exact determination of the oligomeric state of the protein.

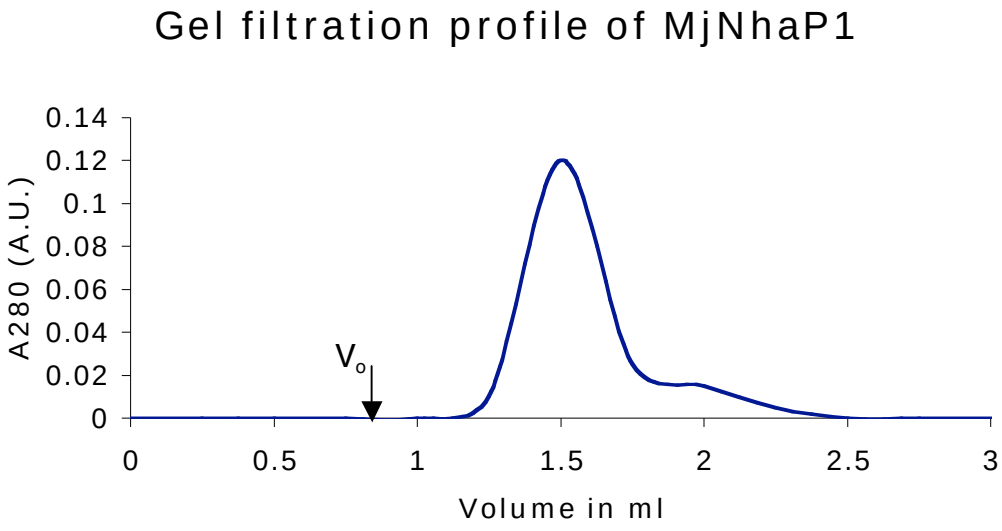

Figure 3.2: Gel filtration profile of MjNhaP1 applied on a calibrated Superose6 column eluted in pH4 buffer. Total volume of the column is 3ml and the void volume is 0.8ml.

The stability of the protein in different buffers was analyzed. When both protein and the elution buffer were at pH8, the eluted peak was very broad. In contrast when protein in either pH8 or pH4 eluted with pH4 buffer a sharp peak with a retention volume of 1.62 ml was obtained. The following table summarizes the elution profile of the protein under different conditions.

Table 3.1:

Protein in pH	Elution in	R_{tv} in ml	Comments
In pH4/DDM	pH4 in DDM	1.62	sharp peak with a small shoulder
In pH8/DDM	pH4 in DDM	1.61	broader peak
In pH8/DDM	pH8 in DDM	1.32	broad peak with no clear bands visible in BN gel
In pH4/DDM	pH8 in DDM	1.62	similar to pH4 peak

3.1.4 ACTIVITY ASSAY

The purified protein was active when reconstituted into liposomes as judged by the generation of Δ pH in response to a Na^+ gradient (Figure 3.3). Proton transport caused a fluorescence recovery of the ΔpH sensing dye 9-amino-6-chloro-2-methoxyacridine. This activity was dependent on the external pH. MjNhaPI was active in H^+ transport at pH 6-7, but inactive at pH above 7. Control experiments with the same Na^+ concentration on both sides of the membrane indicated that the Na^+ gradient was necessary to bring about the pH-induced fluorescence change. Liposomes without the transporter did not show fluorescence recovery, indicating that the liposomes were not leaky.

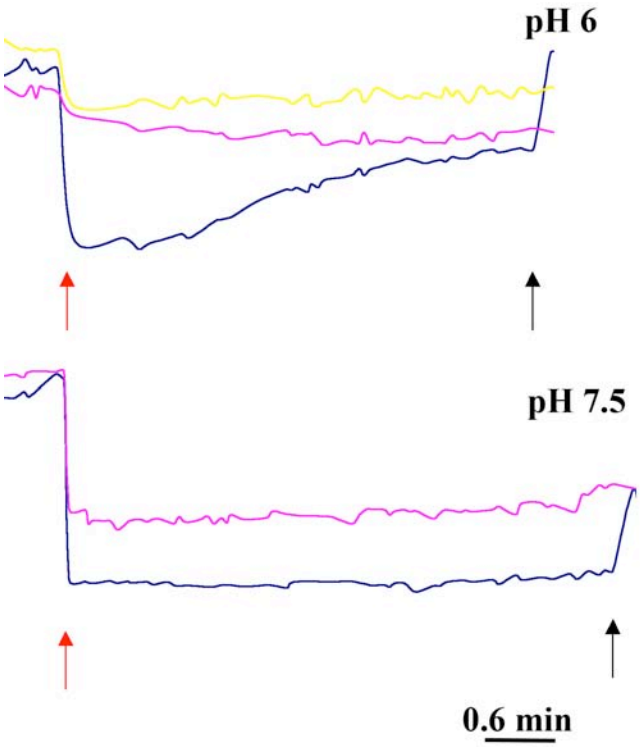

Figure 3.3: Activity of purified MjNhaP1 as measured by ΔpH induced ACMA fluorescence (arbitrary units) at pH6 and pH7.5. The blue line refers to proteoliposomes containing MjNhaP1, the pink line to control liposomes without protein and the yellow line to proteoliposomes diluted with MTCM buffer containing 0.3M NaCl (no sodium gradient). The red arrow indicates the addition of liposomes and the black arrow the addition of NH_4Cl to dissipate the pH gradient.

3.1.5 2D CRYSTALLIZATION

MjNhaP1 reconstituted in to lipid bilayers formed 2D crystals readily at ~pH 4-5. Tubular crystals measuring 0.3-0.6 μm in width and 0.5-1 μm or more in length were obtained at a lipid-to-protein ratio (LPR) of 0.4-0.55 (w/w). Crystalline membranes were observed at pH ranging from 4 to 7 but the best lattices were obtained at pH4.

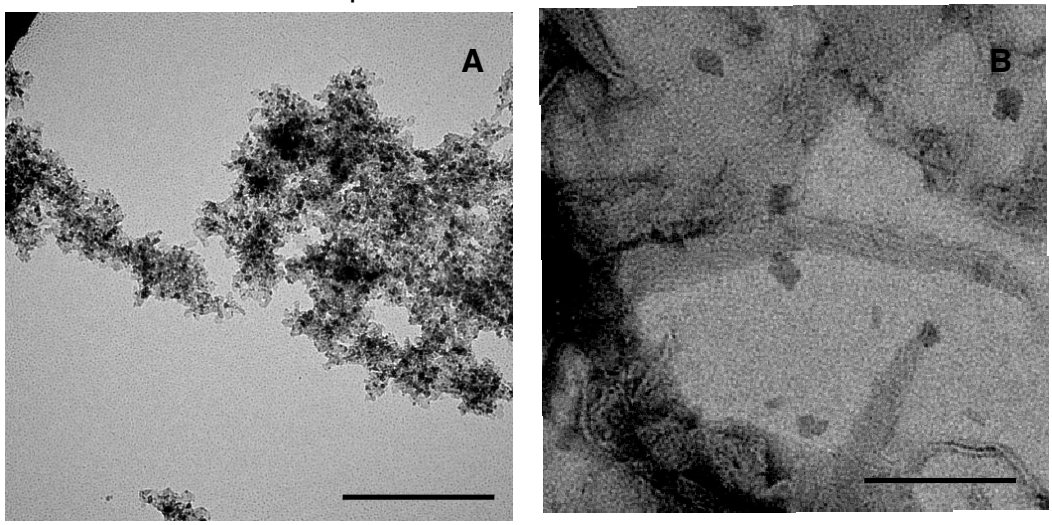

Figure 3.4: A- morphology of the membranes obtained at low LPR and B- at higher magnification shows the multiple layers of membrane as well the ordered arrays of protein (scale bar – 1 μm and 100 nm in A and B respectively).

At very low LPR below 0.35, ordered membranes were found but instead of having a defined structure they were clumped together (Figure 3.4). At increasing LPR, round crystalline vesicles were observed, but only the tubular crystals contained well-ordered lattices (Figure 3.5). The optimal conditions for crystallization was 0.2M NaCl, 5% each of glycerol and methyl pentane-diol (MPD) buffered with acetate to pH4, dialyzed at 37°C for six days. The presence of MPD was crucial for the formation of crystals.

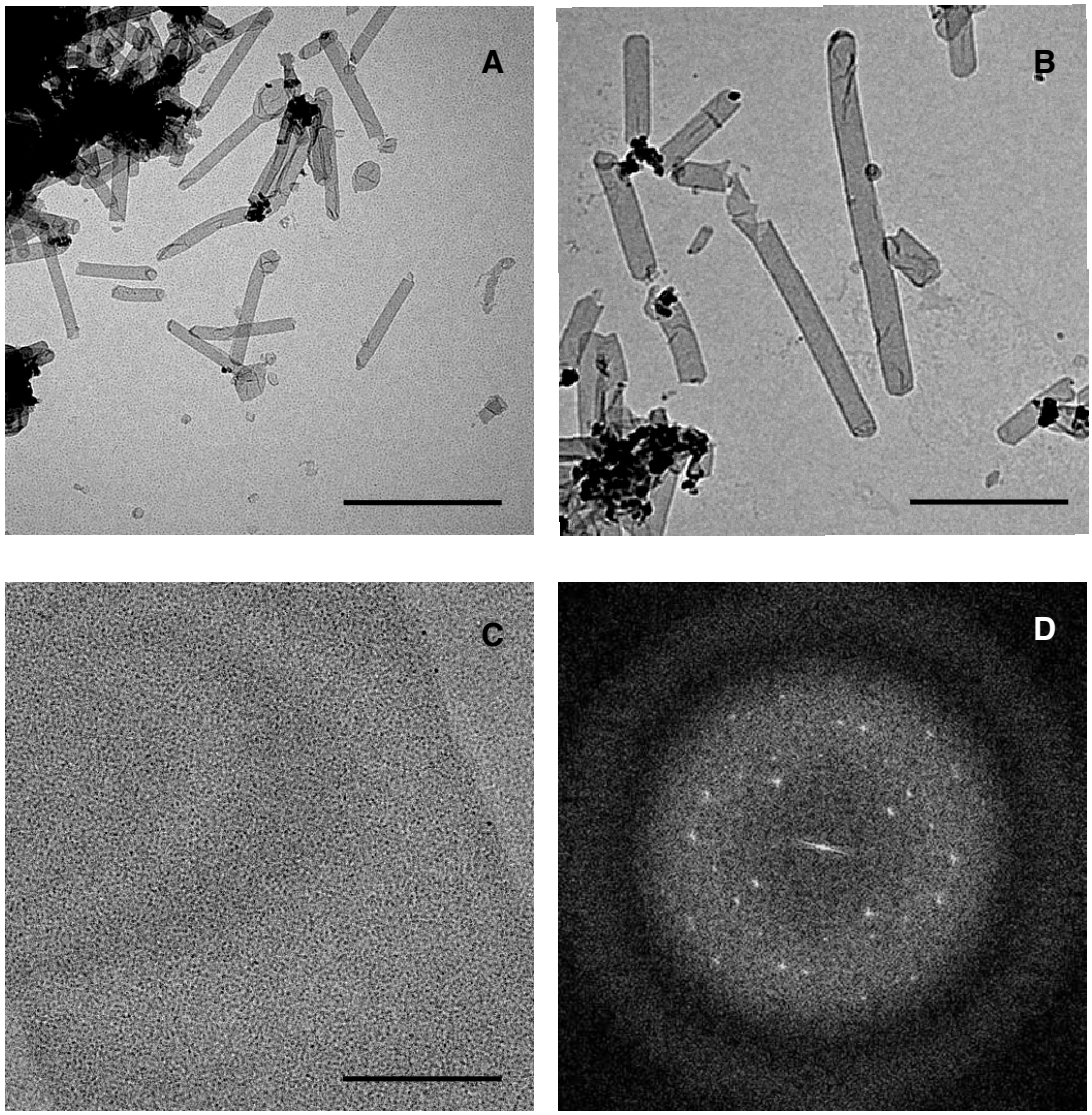

Figure 3.5: A and B – Tubular crystals obtained at pH4 growing from aggregates and isolated (scale bar – 1 □m). C- Crystal lattice as observed at higher magnification (scale bar –100 nm) D- a power spectrum of the tubular crystal

The amount of glycerol used in the crystallization buffer had a clear effect, with increasing glycerol concentration resulting in vesicles with no order. Crystals were also obtained in the presence of trivalent cations such as gadolinium but under these conditions the tubular crystals had a greater tendency to clump together. Similar results were obtained with divalent cations such as magnesium.

3.1.6 DIFFERENTIAL SCREEN OF LIPIDS

Generally, *E.coli* polar lipids were used for 2D crystallization. The reasoning was that the protein expressed well in *E.coli* cells and therefore lipid from this source was used for crystallization. As shown in the pictures above, well-ordered crystals formed with this lipid (Figure 3.5). When negatively charged lipid such as cardiolipin was used for reconstitution, no crystals were observed. Use of neutral and synthetic lipids like POPC yielded similar tubular crystals.

However, *Methancoccus* is a thermophilic archeaon, which has ether and cyclic lipids instead of conventional ester and linear lipids. Experiments were carried out to reconstitute the protein into pure ether lipids such as diphytanyl lipids with either phosphatidylethanolamine or phosphatidylcholine head group. With phosphatidylcholine, big vesicles with no crystallinity were observed. In contrast, diphytanyl phosphatidylethanolamine gave tubular crystals (Figure 3.6B). Tubes were ~0.2-0.3 □m wider and predominantly arising from aggregates. These tubes showed weak, fuzzy spots and were poorly ordered. The diphytanyl PE lipids also showed some irregularly shaped membranous structures. These membranes were also ordered, possibly twisted ribbons (Figure 3.6A).

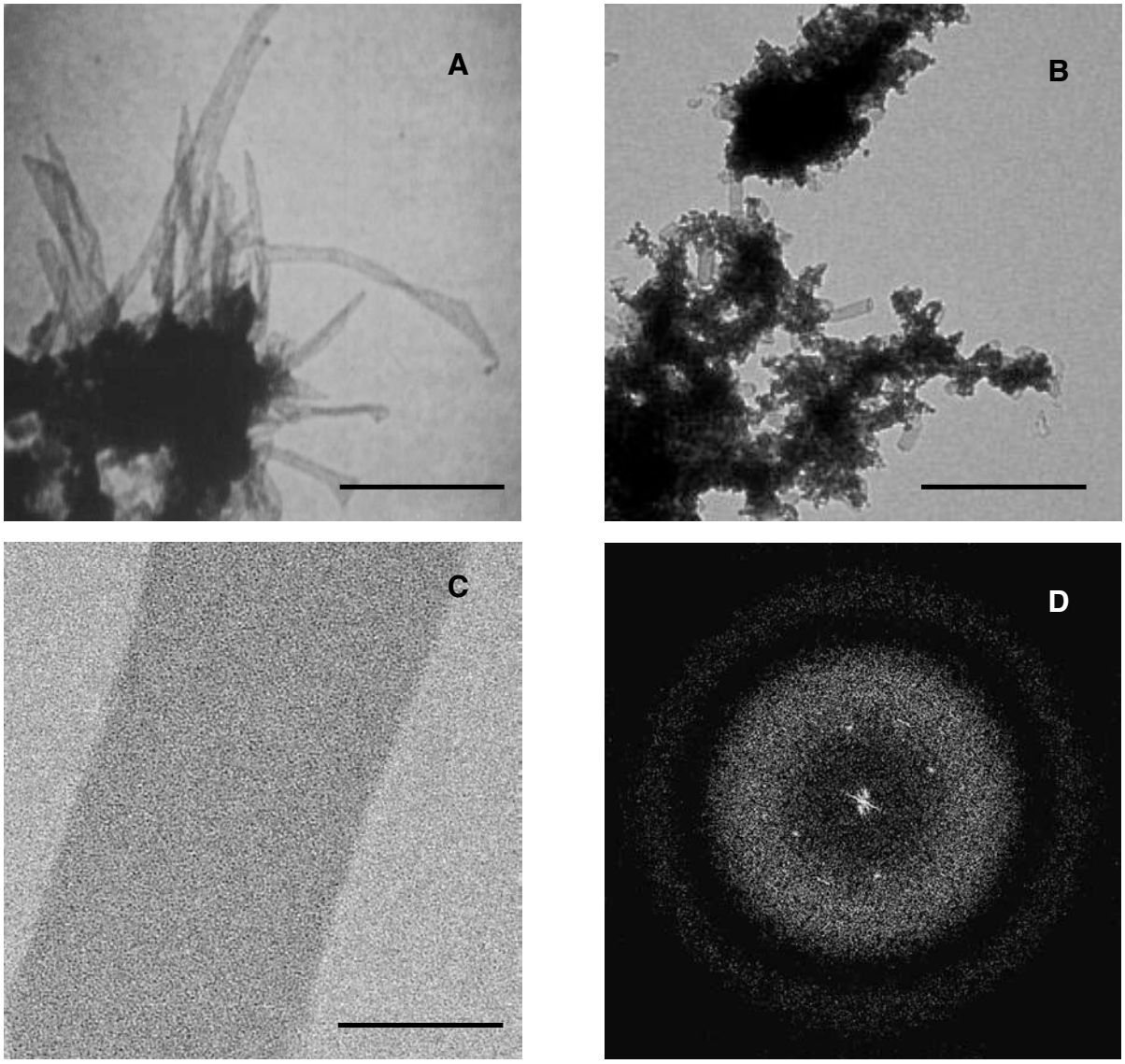

Figure 3.6: A and B The morphology of crystals from diphytanyl PE (scale bar –1 □m)

C and D: Higher magnification of one such tube showing the crystal lattice (scale bar –100 nm) and its power spectrum

3.1.7 CRYO-EM AND CALCULATION OF PROJECTION MAP

The tubular crystals grown at pH4 were used to collect images by electron cryo-microscopy using 4% trehalose or 4% glucose (measured pH~4.9). The quality of the images was assessed by optical diffraction. Images that showed spots to 10Å in all directions were chosen for scanning and subsequent processing. Images of crystals in glucose or trehalose were indistinguishable, as were the two planar lattices that formed as the tubular crystals flattened on the carbon film, which were processed separately. After three to four rounds of unbending these crystals showed spots to 6Å (Figure 3.7, 3.8), above background. The crystals had $P22_12_1$ symmetry as indicated by phase comparison of symmetry related reflections (Valpuesta et al 1994) with a unit cell of a=80Å and b=108Å.

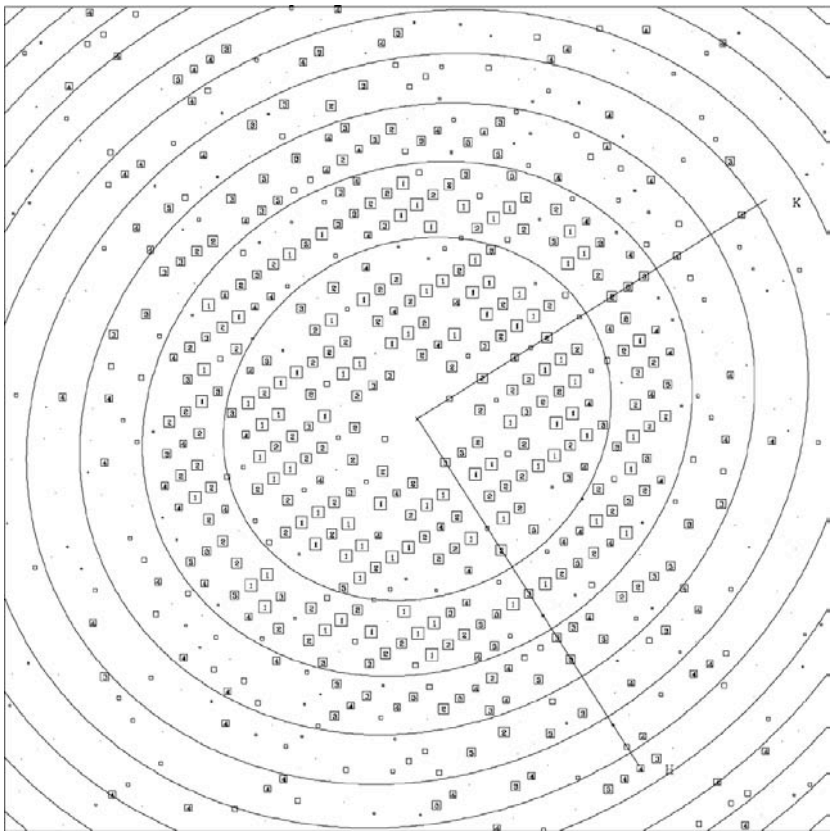

Figure 3.7: Calculated Fourier transform of a single image of MjNhaP1 at pH4. Each square on the reciprocal lattice describes a Fourier component with the size of the square and number reflecting its signal to noise ratio. The largest boxes and the smallest numbers describe the most significant reflections. Concentric rings indicate the zero crossings of the contrast transfer function. The resolution at the edge is 5 Å.

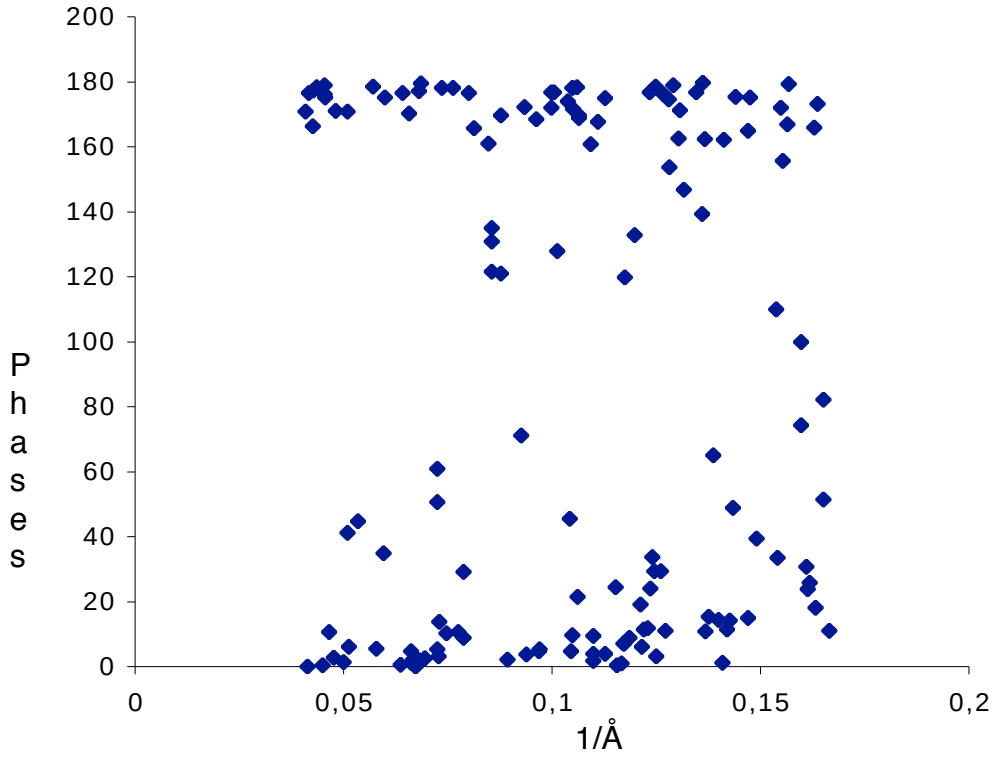

Figure 3.8: An assessment of the quality of the experimental phases from the merged dataset at pH4. The space group $P22_12_1$ requires the phases to be either 0 or 180. The quality of the phases was thus used to determine the optimal resolution for the data set at higher resolution (<6 Å) the phases tend to become random.

A projection map of MjNhaP1at pH 4 was calculated with data truncated to 8Å resolution (Figure 3.9). The unit cell contains four molecules of MjNhaP1 arranged in two dimers with a 2-fold axis perpendicular to the membrane. The 2-fold screw axes perpendicular along *a* and *b* give rise to the alternating up and down orientation of adjacent dimers.

The dimer of MjNhaP1 has overall dimensions of ~51Å x 84Å. Within the projected density of the protein, two regions can be distinguished. The central region, which consists predominantly of elongated peaks, forms the dimer interface. The shape of the density peaks suggests that this region represents a number of highly tilted membrane-spanning helices. On either side of this central core lies a cluster of 4 to 6 strong density peaks, characteristic of a bundle of helices oriented roughly perpendicular to the membrane.

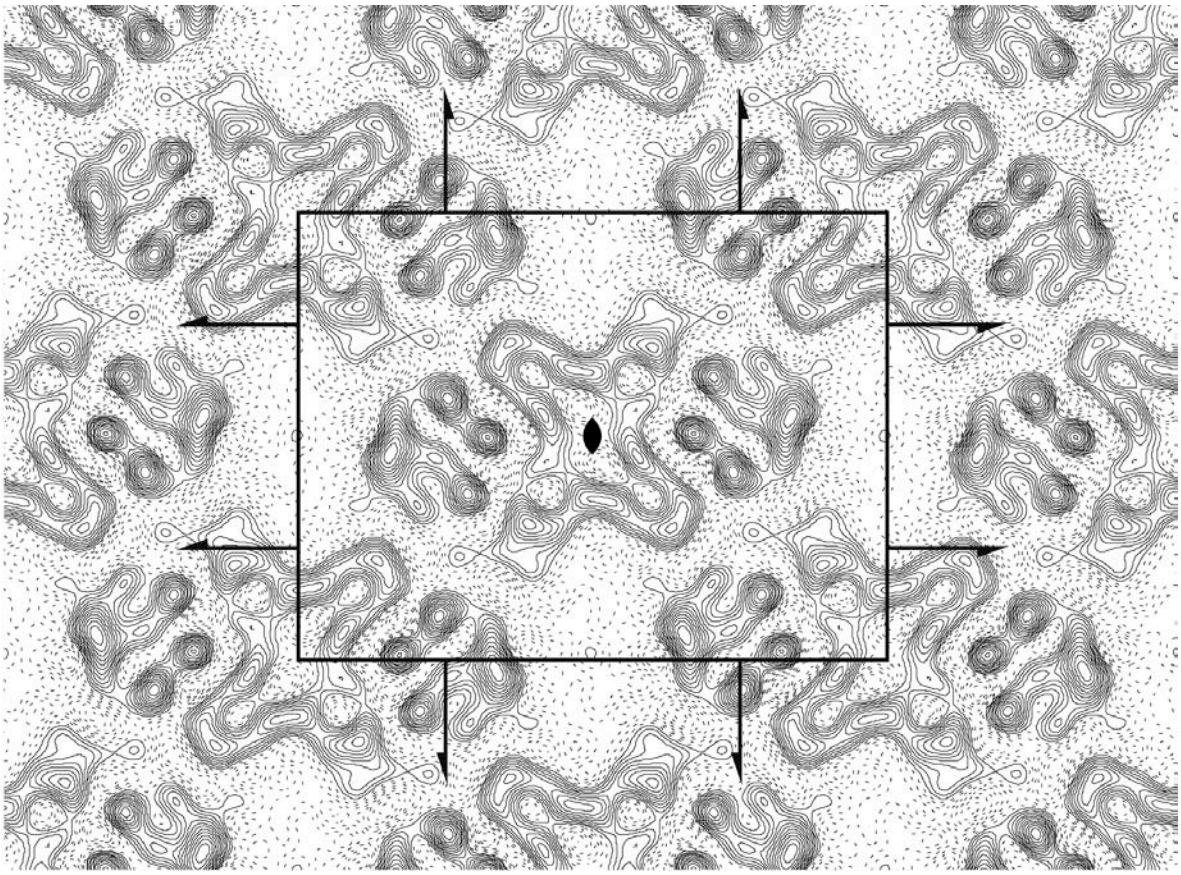

Figure 3.9: Projection density map of MjNhaP1 at 8Å resolution at pH 4 calculated from merged amplitudes and phases of five independent lattices with $P22_12_1$ symmetry applied. The 2-fold axes perpendicular to the membrane plane and the screw axes parallel to a and b are indicated. A unit cell is displayed with the a axis vertical and the b-axis horizontal. One unit cell contains 4 molecules of MjNhaP1. Solid lines indicate density above the mean while negative contours are shown as dotted lines. An isotropic temperature factor (B = -200) was applied to compensate for the resolution-dependent degradation of image amplitudes. The map was scaled to a maximum peak density of 250 and contoured in steps of 21.

3.1.8 CRYSTALLIZATION AT HIGHER pH

An important functional aspect of the MjNhaP1 is its ability to respond to pH. Attempts to grow crystals at higher pH resulted in vesicular membranes that had no significant ordering. It was possible to obtain tubular crystals at pH7 measuring 0.2-0.25 □m in width and variable in length. These crystals were rare and difficult to reproduce.

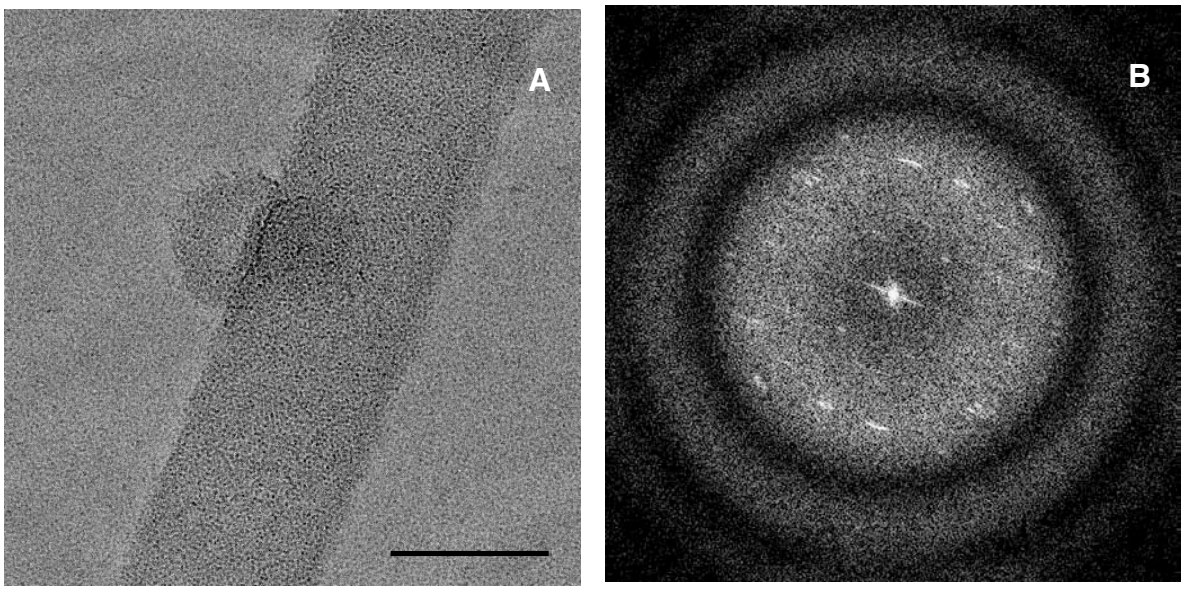

Figure 3.10: A- high magnification image of tubular crystal from pH7 (scale bar –100 nm) and the power spectrum shown in B

These crystals showed fuzzy spots and were poorly ordered. Hence they were not suitable for image processing. However, an important potential of cryo-EM is to study the effect of pH in situ on 2D crystals. Prior to this experiment, it was important to know the effect of pH on the crystals. The tubular crystals in pH4 buffer were therefore dialyzed to the crystallization buffer at pH8, at room temperature. Samples were taken at various time points and checked by negative stain EM with respect to the crystal morphology and crystal quality.

For a time period of up to 10 minutes after incubation, no difference was observed both in terms of morphology and quality of crystals as judged from the power spectrum of the crystal. However after 30 minutes of incubation, the

tubular crystals tended to clump together and showed only weak spots. Samples after an hour or more showed no tubular crystals but positively stained membranes only.

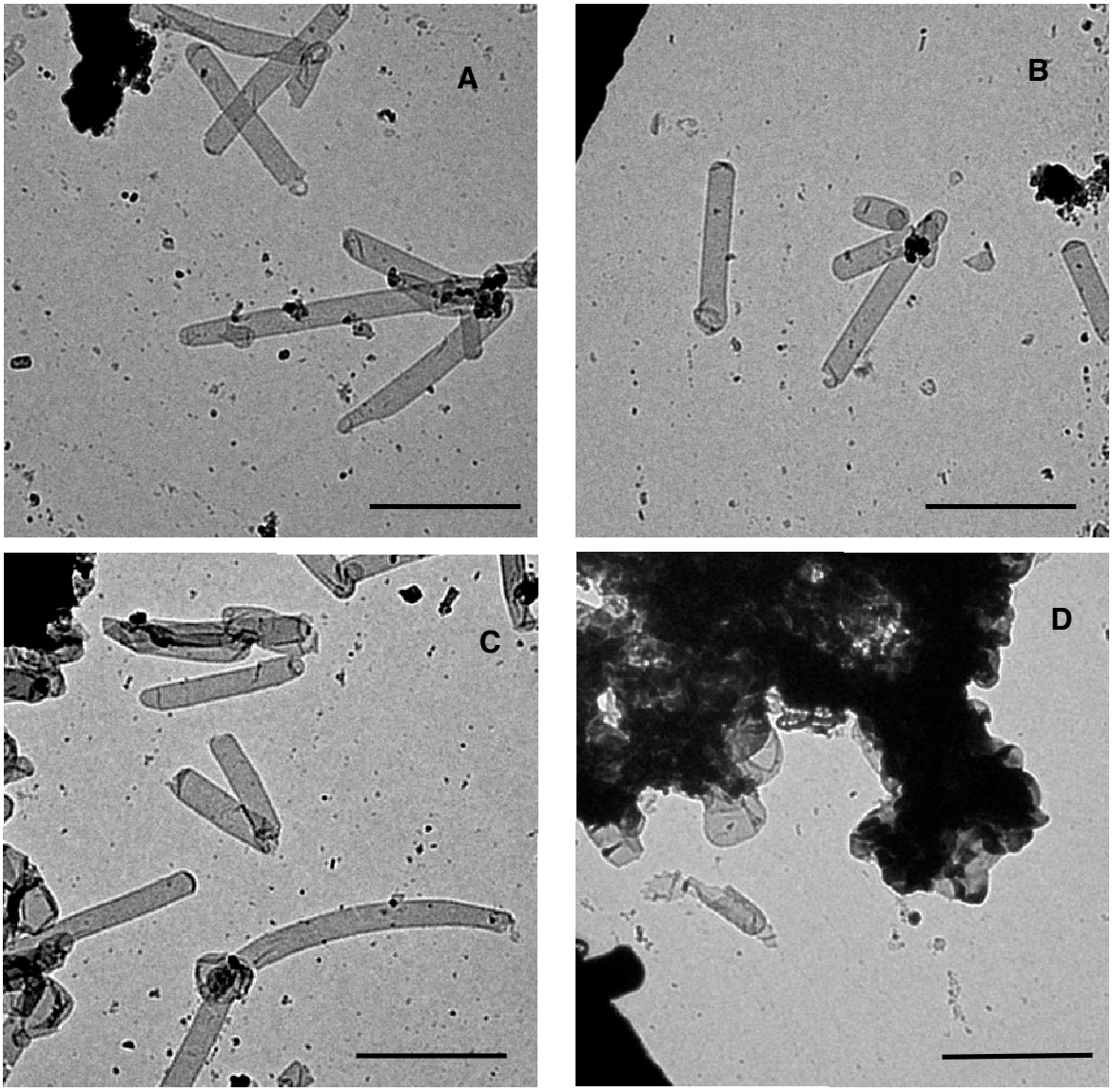

Figure 3.11: Time course of the effect of pH on the crystals A- crystals at pH4, B- after 5 minutes incubation at pH8, C- after 10 minutes incubation and D- after 30 minutes (scale bar 1 □m).

It was clear from the above observation (Figure 3.11) that the crystals were stable up to 10 minutes at higher pH. Therefore, the effect of pH on the crystals was examined in situ on the grid by incubating the crystals at higher

pH for a minute. Images were then collected as before. The calculated projection map from the crystals treated in this way showed a difference in the unit cell (a=82.1Å b=103.6Å) but had the same space group as the crystals at pH4.

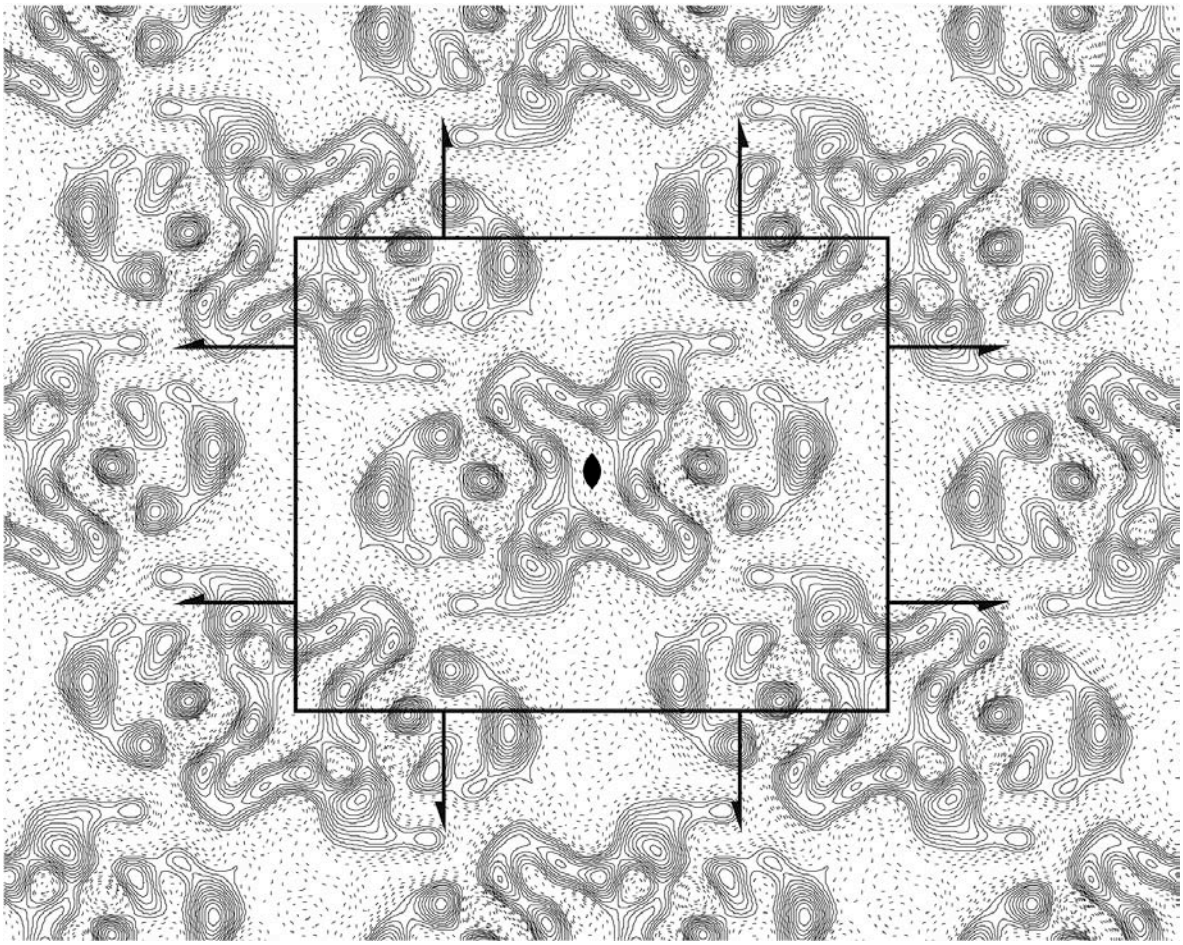

Figure 3.12: Projection density map of MjNhaP1 at 8Å resolution at pH 8 calculated from merged amplitudes and phases of five independent lattices with $P22_12_1$ symmetry applied. Map was contoured similar to that of pH4 in figure 3.9.

Significant differences in the projection structures at pH4 and pH8 were evident by visual comparison (Figure 3. 9 and 3.12). The IQ plot of the data sets from both pHs shows that exposure to pH8 results in a slight loss of

resolution (Figure 3.13). Therefore both projection maps were calculated at 8Å where both data sets are comparable (Table 3.2). The projection map at pH8 obtained in this way indicated a ~2Å displacement of the helix bundle relative to the central dimer core, and a significant rearrangement of densities in the helix bundle (Figure 3.23 A and B).

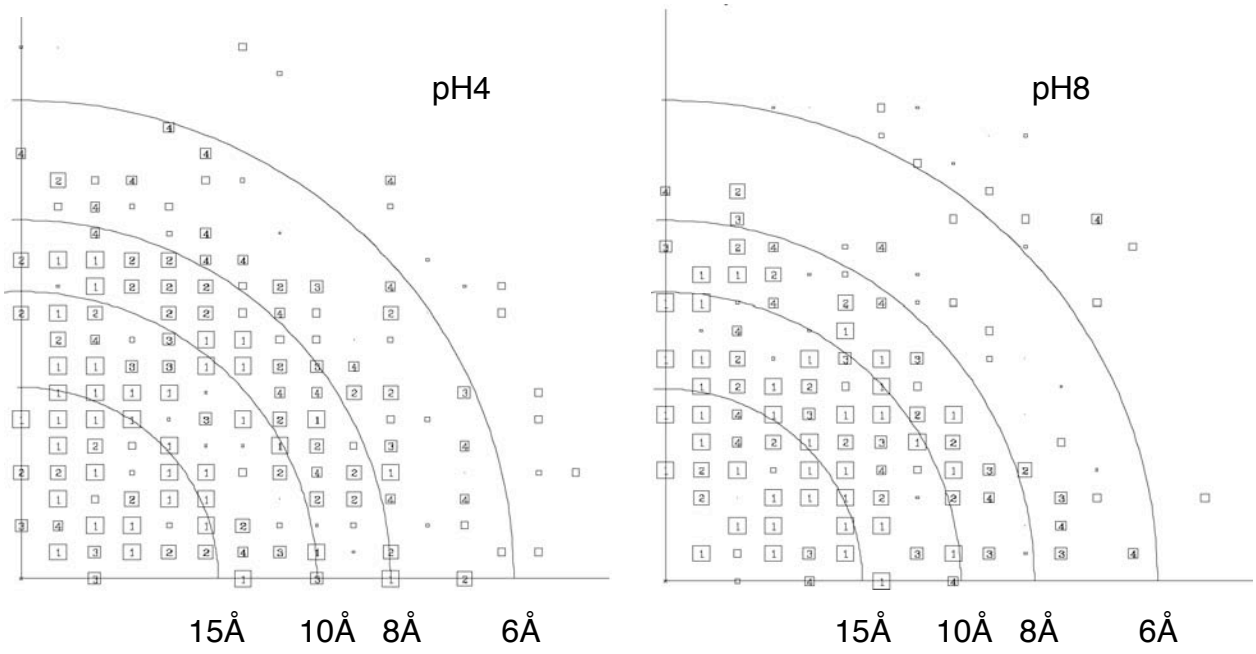

Figure 3.13: Combined phase error to 5Å after merging of five lattices from separate images at pH 4 and 8 respectively. The size of the boxes corresponds to the phase error after averaging and rounding to 0° or 180° associated for each measurement (1, <8°: 2, <14°; 3, <20°; 4, <30°; 5, <40°; 6<50°; 7, <70°; 8, <90°, where 90° is random). Values from 1-4 are shown as numbers inside boxes, whereas those from 5-8 are indicated with decreasing box size.

Table 3.2: Electron crystallographic data

	pH4.0		pH8.0	
Plane group symmetry	$P22_12_1$		$P22_12_1$	
Unit cell dimensions	A= 80±0.5Å B=108±1Å □=90°		A=82±1Å B=103.6±1Å □=90°	
No. of images	5		5	
Range of defocus	3000-7000		2500-8500	
No.of unique reflections[a]	125(7Å)		103(7Å)	
Overall phase residual[b] (random = 45°)	14.6		15.0	
Resolution range (Å)	No.of unique reflections	Phase residual (random =45°)	No.of unique reflections	Phase residual (random =45°)
-16.0	26	10	24	12.6
15.9-11.3	25	14.6	23	8.1
11.2-9.2	24	17.9	25	12.3
9.1-8.0	24	13.4	15	22.3
7.9-7.1	23	16.7	15	25.8
7.0-6.5	13	26.5		
6.4-6.0	10	28.8		

[a] - Reflections included to IQ□ 4 to 7Å

[b] - Amplitude weighted, vectorially averaged phase residual which shows the phase deviation from theoretical 0°/180° (45° is random).

3.1.9 DIFFERENCE MAP

To demonstrate that the observed differences are genuine, a difference map was calculated. The amplitudes from different data sets were scaled and a vector difference map was generated. The difference observed was localized on either side of the dimer core. The structure of the central core at

the dimer interface did not change visibly in response to pH. As a control a difference map was calculated from two data sets collected at the same pH. This map showed no major difference and indicated that the background noise level was two contours.

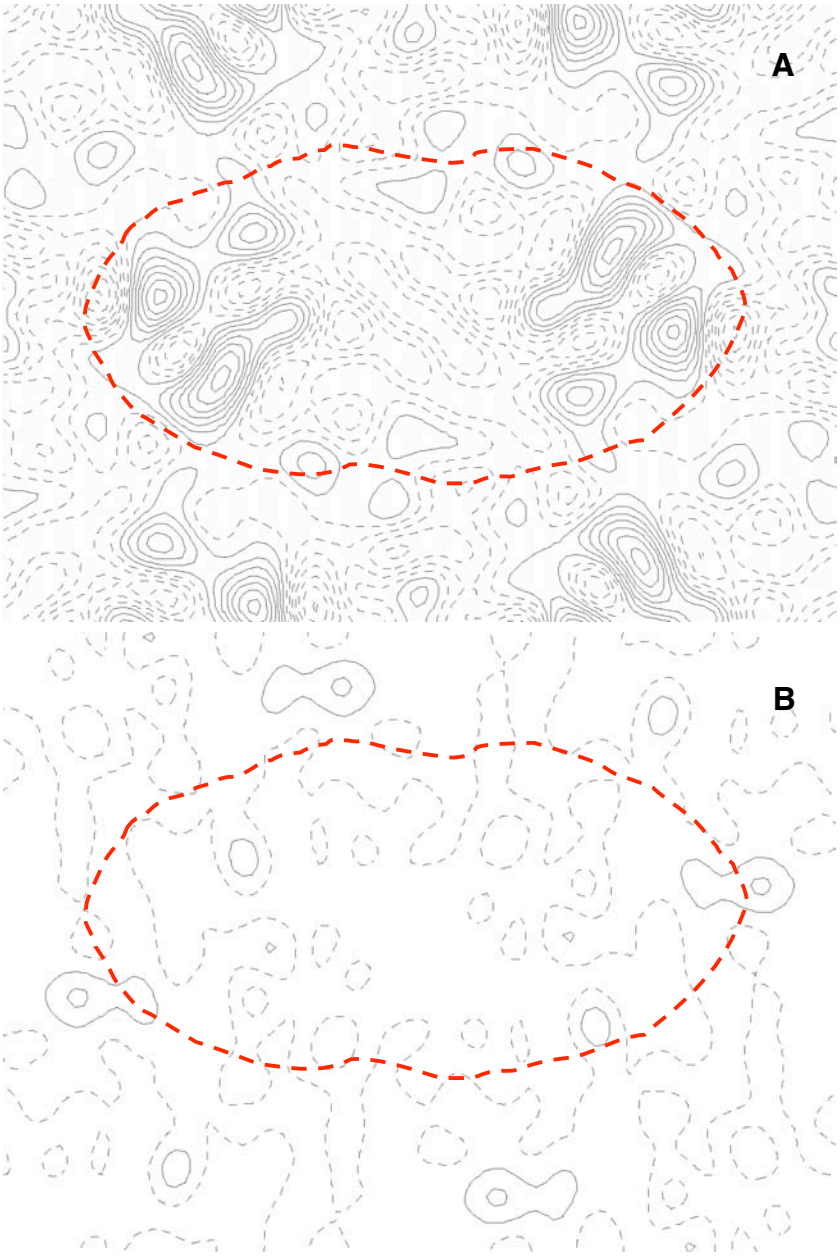

Figure 3.14: Difference map of MjNhaP1 projections at pH4 and pH8 (A) Difference map generated from pH4 data divided randomly into two halves (B). Both maps were contoured to a maximum of 2 in steps of 0.05. The dashed red line indicates the dimer boundary.

3.1.10 RESAMPLING OF DATA

The calculation of a difference map strictly requires isomorphic crystals. The unit cell of pH4 and pH8 differed by roughly 4% in one axis and hence it was necessary to rule out the possibility that the differences arise from the lack of isomorphism on differential packing of the protein on the crystal lattice. A pH8 data set was used as reference against a masked pH4 dimer to calculate structure factors by molecular replacement, which results in a map of the pH4 structure in the pH8 unit cell (Figure 3.15). Since the success of the molecular replacement depends on the quality of the experimental data, the resolution limit was set to 8 Å where the quality of the both data sets was comparable.

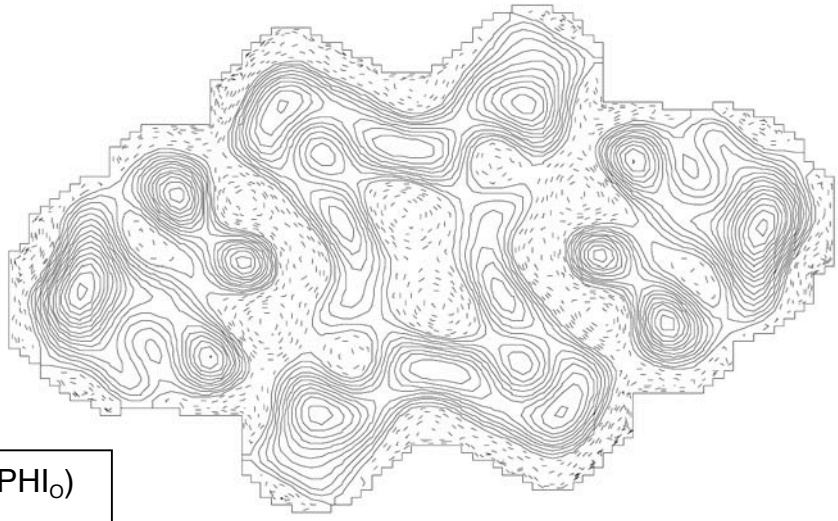

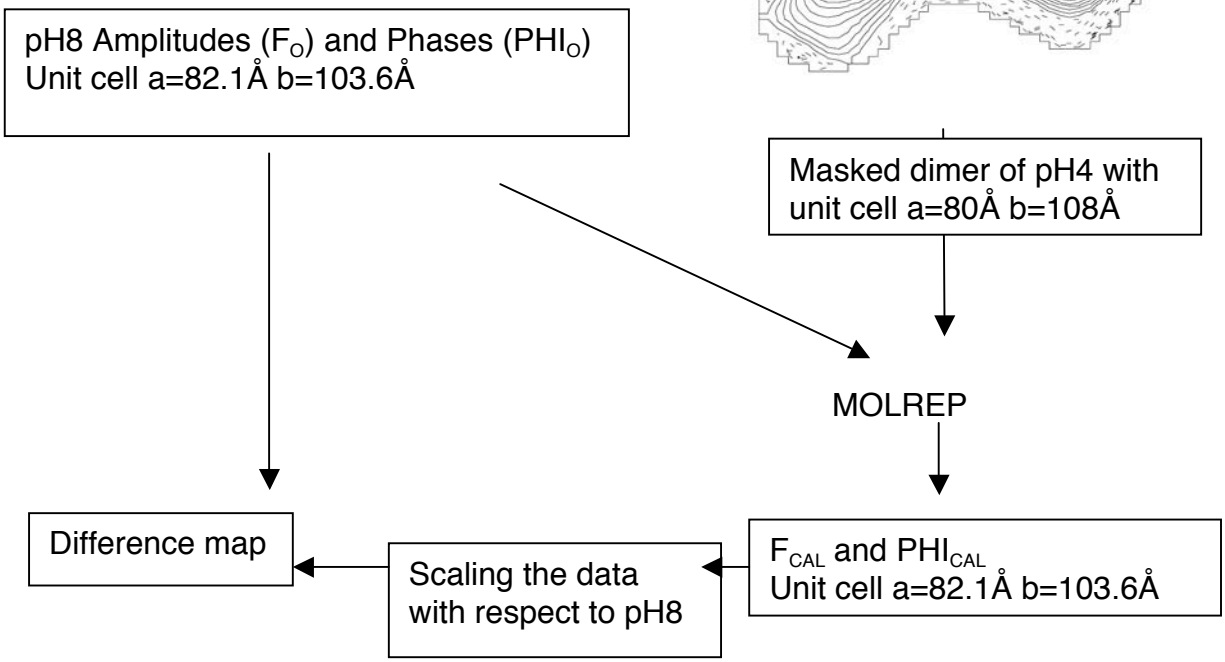

Figure 3.15: Steps involved in calculating the difference map by molecular replacement.

The program performs molecular replacement first with a rotation function to orient the model and then using the translation function to search for the position of the orient the model. A correlation coefficient gives the measure of how well a given data set agrees with the model (if, as in this case, both amplitudes and phases are used).

The following table shows the correlation coefficient of different data sets using a dimer from a pH4 data set.

Table 3.3:

Data set	Correlation coefficient
pH8 data 1	0.852
pH8 data 2	0.786
pH4 data 1	0.897
pH4 data 2	0.924 (self corr.)
pH4 data 3	0.904
NhaA at pH4	0.367

In theory a self-correlation should give a value of 1 but what I observed was 0.924. It was clear from the high correlation coefficient of different data sets from pH4 and 8 that the pH induced change occurring was not drastic and the two structures were quite similar. For a comparison, when a data set of *E.coli* NhaA crystallized at pH4 with a unit cell of a=77Å, b=122Å in the same space group gave a very low correlation coefficient suggesting that these two sodium/proton antiporters differ significantly.

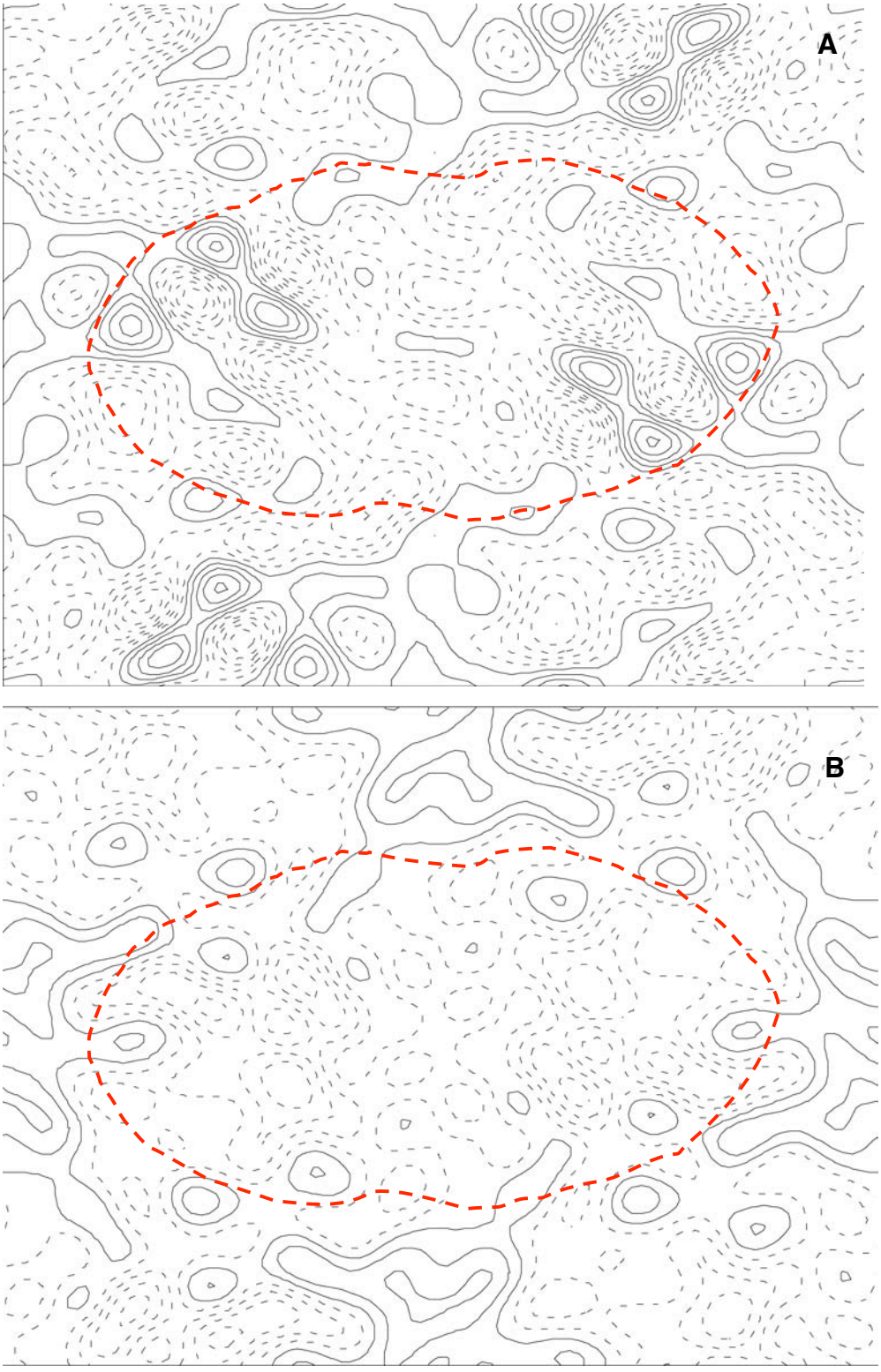

Figure 3.16: Difference map calculated after molecular replacement A- pH4-pH8 and B pH4-pH4, contoured to a maximum of 1 in steps of 0.02.

3.1.11 CALCULATION OF DIFFERENCE MAP IN REAL SPACE

In another approach the masked dimers from both pH were subtracted in real space. This was carried out either with SPIDER or programs in the CCP4 package. Both approaches yielded essentially the same result.

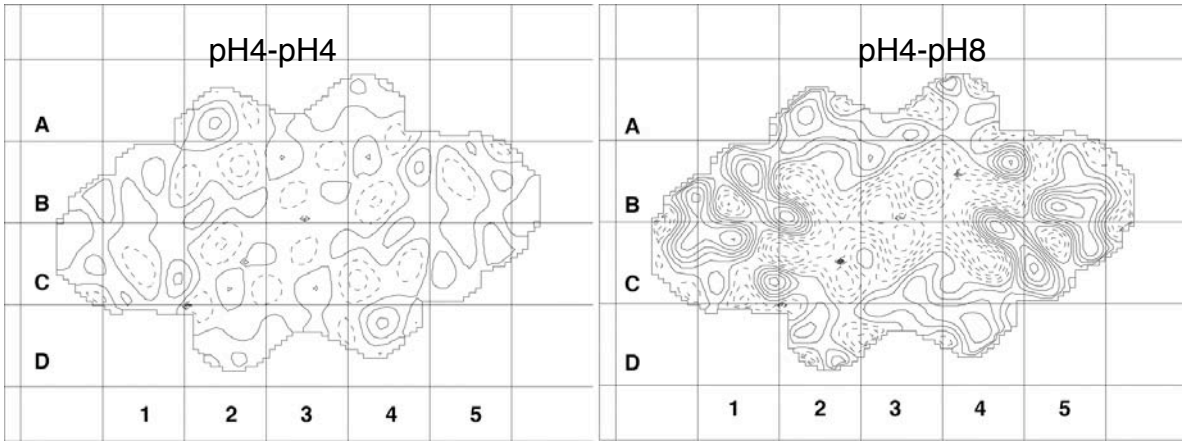

Figure 3.17: A real space difference map calculated with the use of programs from CCP4 package. The maps are contoured to a final of 10 in steps of 1.

The background noise as observed in the control pH4-pH4 difference map was three contour levels. The pH4-pH8 difference map was largely similar to those calculated in Fourier space or after molecular replacement (Figure 3.14 and 3.16).

3.1.12 OBSERVATION AT INTERMEDIATE pH

Since two different structures were obtained at pH extremes, it was of great interest to perform similar experiment at an intermediate pH around 6. When the tubular crystals were incubated at pH6.2, it yielded a very interesting observation. Tubular crystals flatten to form two layers on the carbon grid and at pH6.2 occasionally both conformations of pH4 and pH8 could be observed in single tube. One of the layers had the pH4 conformation while the other had the pH8 conformation. This particular observation told that the change occurring as a result of pH was not a gradual process. At this pH

the lattices with pH4 conformation had an unit cell very similar to that of pH4, however lattices with pH8 conformation showed a slightly different unit cell a=81.5Å, b=104.5Å.

3.1.13 PRELIMINARY 3D CRYSTALLIZATION

The stability of MjNhaP1 at acidic pH prompted me to screen for 3D crystals at acidic pH. Protein at a final concentration of 4mg/ml was used in a hanging drop with either PEG 400 or 350 as precipitant, buffered at pH4. Small crystals were obtained after a week at 20°C, measuring ~20 μm in width. These crystals grew from a spherulite and were clumped together. Apart from the rod like crystal some small tetragonal crystals were also obtained. They did diffract but the resolution was limited to 15Å. This trial of 3D crystallization was just to see if the conditions from 2D could be used as a starting point for screening in detergent solution. The validity and the reproducibility of crystals need to be verified.

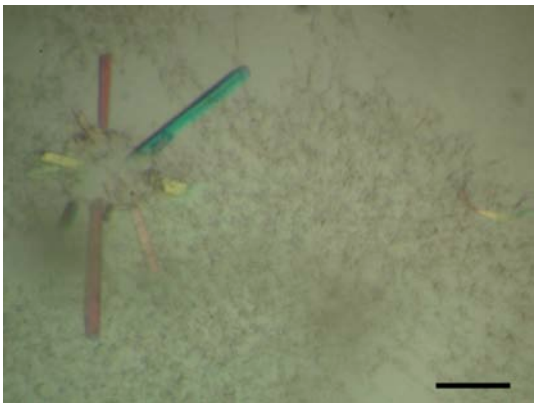

Figure 3.18: Preliminary rod shaped crystals of MjNhaP1. Scale bar - 100μm.

3.2 DISCUSSION

3.2.1 CLONING AND COMPARISON OF SODIUM/PROTON ANTIPORTER FROM *Methanococcus jannaschii*

Sodium/proton antiporters have been classified into different families based on their sequences. These include the Nha A, B C and D, NapA and the NhaP family. The affinity to sodium or lithium and the pH profile in relation to activity differs for each subfamily and allows a given organism to make use of different subfamilies for maintaining pH and intracellular sodium levels. For example, the genome of *E.coli* encodes three different genes, nhaA, nhaB and chaA. NhaA is required for adaptation to high salinity and growth at alkaline pH in presence of Na^+, while NhaB confers a limited tolerance to sodium but becomes essential when NhaA is deleted (Herz, Vimont et al. 2003). The relative activities of NhaB and NhaP from *Pseudomonas aeruginosa* showed that NhaP had higher affinity for sodium and NhaB for lithium. The activity of NhaP showed a sharp pH profile with maximum activity at 7.5 while NhaB had a broader pH range (Kuroda, Fujita et al. 2004). In most of the sequenced genomes thus one finds more than one homologue of sodium/proton antiporters.

From the genome of *M.jannaschii* three ORF's for sodium/proton antiporters have been identified. Two of them, MJ0057 and MJ1521, are 48% identical to one another and possibly arose by gene duplication (APPENDIX) while the third ORF encodes a gene that shows greater homology to the NapA family of Na^+/H^+ antiporters. All the three genes have been cloned and only one of them (MJ0057) has been shown to be active in membrane vesicles of *E.coli* (Hellmer et al 2002). The function of the other gene products is not clear. It is likely that *M.jannaschii* uses the three homologues in different situations and regulates their expression at the level of genes.

A multiple sequence alignment of the NhaP subfamily of sodium/proton antiporters show three conserved regions that can be implicated for ion transport (Figure 3.19). These include:

a) TDP motif – conserved in many of the sodium/proton antiporters (APPENDIX). The presence of a hydroxyl group along with an acidic side chain is also conserved in the sodium dependent ATPases (Kaim, Wehrle et al. 1997). In two structures of sodium ATPases, these residues (acidic and hydroxyl) have been shown to take part in sodium binding (Murata, Yamato et al. 2005).

b) FNDP motif – conserved in the NhaP family. In the NhaA subfamily, an equivalent motif with two aspartates is found. The aspartates are essential for the activity in both families of transporters.

c) RPL- a positive charge that is present in the middle of a predicted trans-membrane helix grasps immediate interest. Indeed this residue is essential for activity and an equivalent lysine is found in most members of the NhaA subfamily. Interestingly, a proline residue is present next to this positive residue in both NhaA and NhaP subfamilies presumably to allow flexibility during transport.

d) GPRG motif – conserved only in the NhaP family. The exact role of this motif is not clear. When the arginine was mutated in MjNhaP1 the protein retained low activity at pH6 (Hellmer et al 2003).

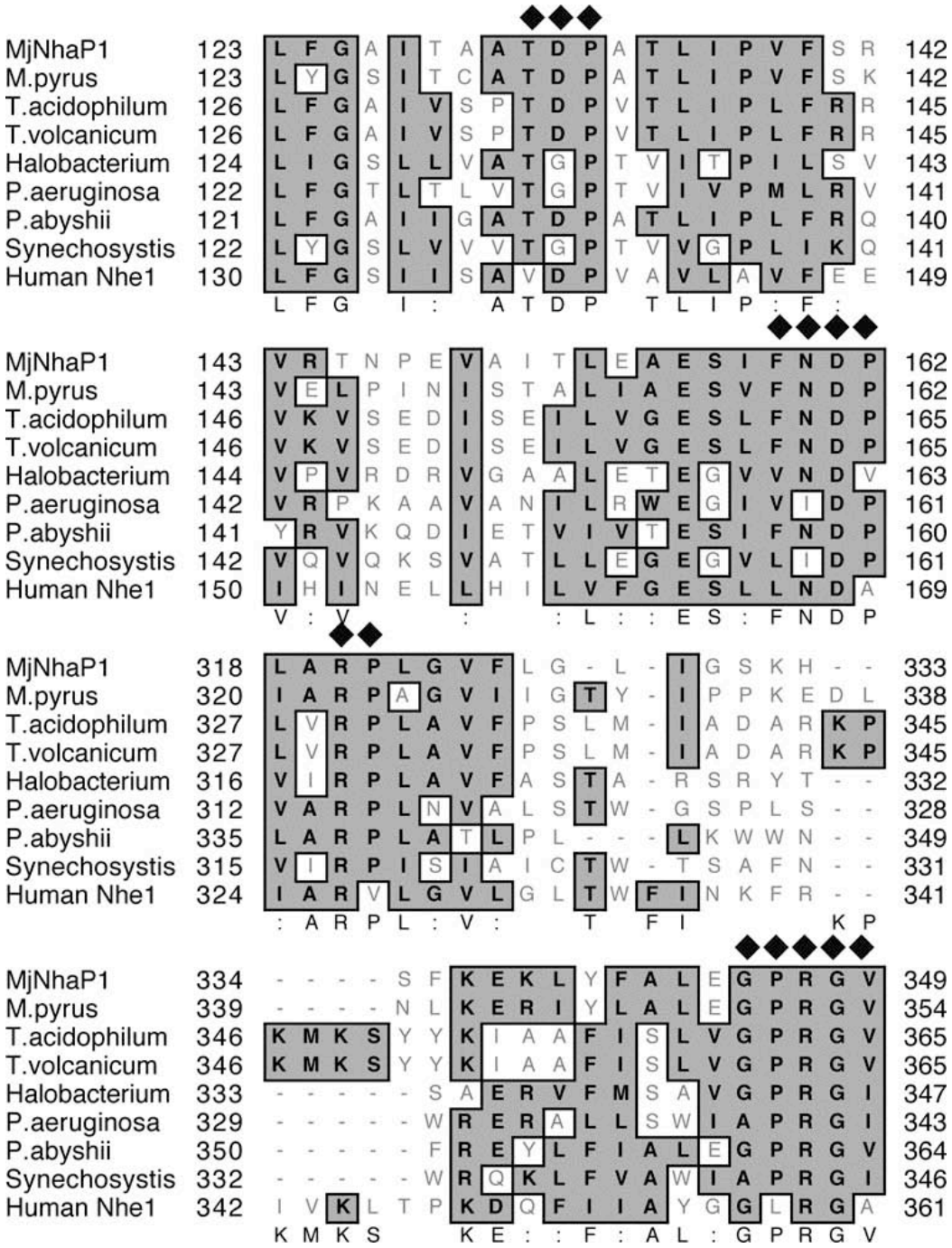

Figure 3.19: A multiple sequence alignment of sodium/proton antiporters from the NhaP subfamily. The conserved motifs are highlighted with black diamonds. The accession numbers are *Methanococcus jannaschii* NhaP1 (Q60362), *Methanopyrus kandleri* (NP_613837), *Thermoplasma acidophilum* (NP_394359), *Thermoplasma volcanicum* (NP_111535), *Halobacterium sp.* (NP_280739), *Pseudomonas aeruginosa* (NP_252428), *Pyrococus abyshii* (NP_126974), *Synechocystis sp.* (BAA10477) and Human NHE1 (P19634).

3.2.2 SECONDARY STRUCTURE OF MjNhaP1

The secondary structure prediction of MjNhaP1 suggests 13 membrane-spanning helices. There is no experimental evidence to support this. A previously published article (Hellmer et al 2003) claims that the C-terminus is on the periplasmic side but following the positive inside rule (von Heijne 1998), it would be more like likely that the N-terminus is on the outside and the C-terminus on the cytoplasmic side. It is interesting to note that most membrane proteins with odd numbers of TM domains have their N-terminal end on the extracellular side (Jung et al 1998; Khademi et al 2004).

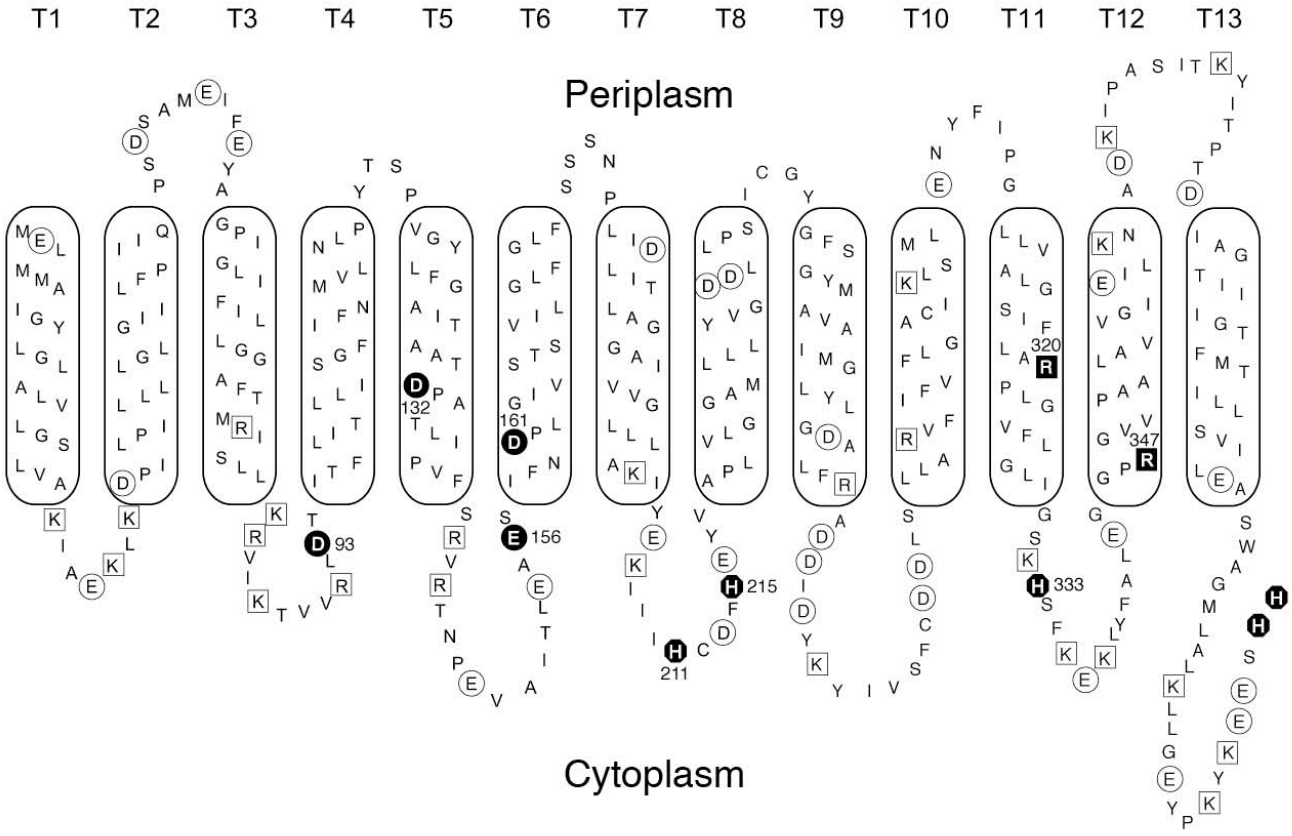

Figure 3.20: A putative secondary structure of MjNhaP1 showing a 13 trans-membrane helical protein. The orientation of the protein in the membrane was inverted from Hellmer et al 2003.

3.2.3 OLIGOMERIC STRUCTURE OF PROTEIN

The oligomeric structure of MjNhaP1 was analyzed by gel filtration and blue native gel electrophoresis. The calculated mass of the protein from the amino acid sequence is ~47 kDa and a dimer would correspond to 94kDa. When MjNhaP1 is dissociated with SDS, a single band migrating at less than 65 kDa was observed in the blue native gel. This would correspond to a monomeric protein and the corresponding dimer would be ~130kDa. I observed that the undissociated protein migrates at ~134kDa confirming it as dimer (Figure 3.1B). This ratio corresponds to 1.4 that is slightly different from the reported ratio of 1.8 (Heuberger et al 2002). These results correlate with the observed migration behavior of other membrane proteins of the same class (transporters) or a porin (chapters 4,5 & 6). Due to the presence of detergents the determination of the oligomeric state of the protein is difficult. When sufficient controls are used, the blue native gel system can be used with some confidence as has been shown with different proteins here.

The gel filtration profile of MjNhaP1 suggested that the protein was unstable or aggregates at higher pH. However, when the protein was applied to the column at pH8 and eluted with pH4 buffer, a peak very similar to that observed to that of pH4. Hence, the instability at pH8 is reversible (Table 3.1).

3.2.4 2D CRYSTALLIZATION

Due to the greater stability of the protein at acidic pH compared to pH8 it is not surprising that MjNhaP1 crystallizes readily at pH4. The optimal conditions for 2D lattice formation obtained are similar to those published for *E.coli* NhaA (Williams et al 1999). The possible reason could be the protonation of the acidic residues that are essential for transport and presumably make the protein more rigid. The involvement of surface charges in crystal formation on the protein is also likely to play a role.

E.coli polar lipid was used regularly to obtain 2D crystals. Other lipid like POPC yielded crystals that were of similar quality. However, negatively

charged lipid cardiolipin did not yield crystals. *Methanococcus*, being a hyperthermophile, grows at an optimum temperature of 85°C. Membranes of the thermophiles contain lipids with a distinct chemical structure that confers a higher stability to the cytoplasmic membrane. The amount of saturation increases with increasing temperature and in archaeabacteria the degree of cyclization of the biphytanyl chains increases with increasing growth temperature. Such changes in the fatty acid composition are supposed to maintain the membrane fluidity at a constant level over the growth temperature range. Since, MjNhaP1 was of thermophilic origin, my interest was to check the formation of crystals in ether lipids. Other examples where 2D crystals have been obtained in archael lipids are from the family of rhodopsins (Henderson and Unwin 1975; Kunji, Spudich et al. 2001). In fact, the sensory rhodopsin from *Natronobacterium* was crystallized with lipids obtained from *Halobacterium*.

Synthetic ether lipids with either ethanolamine or choline as head group were used for screening. Both lipids had a fatty acid chain length of 16. Narrow crystalline tubes were obtained with phytanyl-PE while the phytanyl-PC yielded large vesicles with no order. The tubular crystals from the phytanyl-PE had a rectangular lattice but the spots were fuzzy (Figure 3.6). This lipid also yielded structures that were irregular. The present crystals in *E.coli* polar lipids yield only a resolution of 6.5 Å. The use of native lipids from *M.jannaschii* would be worth a try for improving the quality of crystals to obtain higher resolution.

3.2.5 COMPARISON OF MjNhaP1 and NhaA

MjNhaP1 has been identified as a Na^+/H^+ antiporter by sequence comparison, but it is clear from the projection maps (Figure 3.22) that its structure differs considerably from that of its *E.coli* homologue, NhaA (Williams et al, 1999). The overall dimensions of the dimer of *E.coli* NhaA and MjNhaP1 are 38x96Å and 51x84Å respectively, suggesting major differences in helix packing. Another 2D crystal form of *E.coli* NhaA with a similar unit cell

to that of MjNhaP1 shows an unchanged projection structure of the NhaA dimer (Figure 3.21), suggesting that the crystal packing does not affect the monomer interactions or the arrangement of helices in the Na^+/H^+ antiporters.

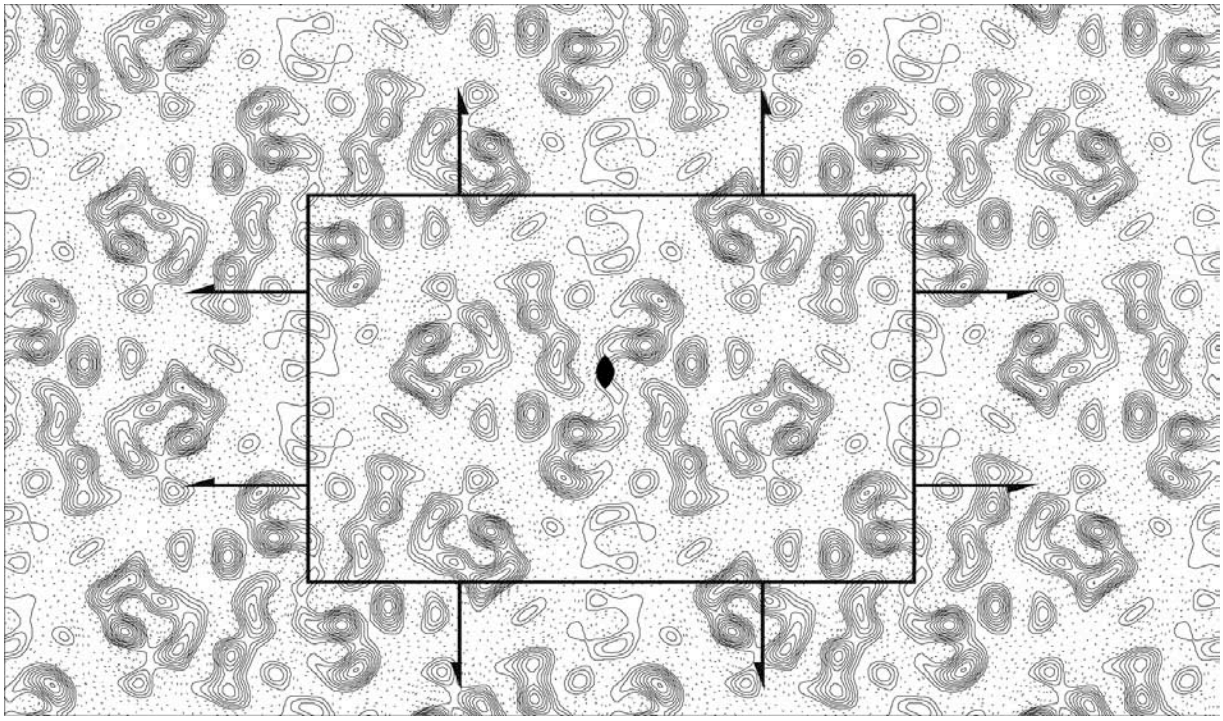

Figure 3.21: Projection density map of new crystal form of NhaA at 8Å resolution. Crystals were obtained in the same way as described by Williams et al 1999. However, the unit cell of the crystal is a=77.3 Å, b=122.2 Å belonging to $P22_12_1$ space group. The structure of the NhaA is unchanged, when compared to published maps (Williams et al 1999; 2000 and Figure 3.22A).
When the structure factors from this data was used with MOLREP against a pH4 dimer of MjNhaP1, a correlation coefficient of 0.367 was obtained indicating that two homologues differ significantly (Table 3.3).

Like *E.coli* NhaA, the MjNhaP1 dimer can be divided into two distinct regions with a central core and a helix bundle at either side. The structure of the dimer core looks quite different in the two proteins, reflecting different interactions of membrane-spanning helices across the dimer interface. The helix bundles on either side of this core show some similarity but in the case of MjNhaP1 they suggest a more or less perpendicular orientation of the membrane-spanning helices whereas the helices in *E.coli* NhaA are known to

be predominantly tilted (Williams KA, 2000). The different activity profiles of the two antiporters are likely to be related to these structural differences.

The projection map of both these transporters show two less dense regions that could be the possible ion translocating pathway. It has been known from the studies of the human sodium/proton exchanger (NHE) that protons compete for sodium both at the external and internal site (Aronson 1985). This suggests that both ions take the same pathway and the direction is determined by the gradient. The x-ray structure of NhaA (Hunte et al 2005) confirms this observation.

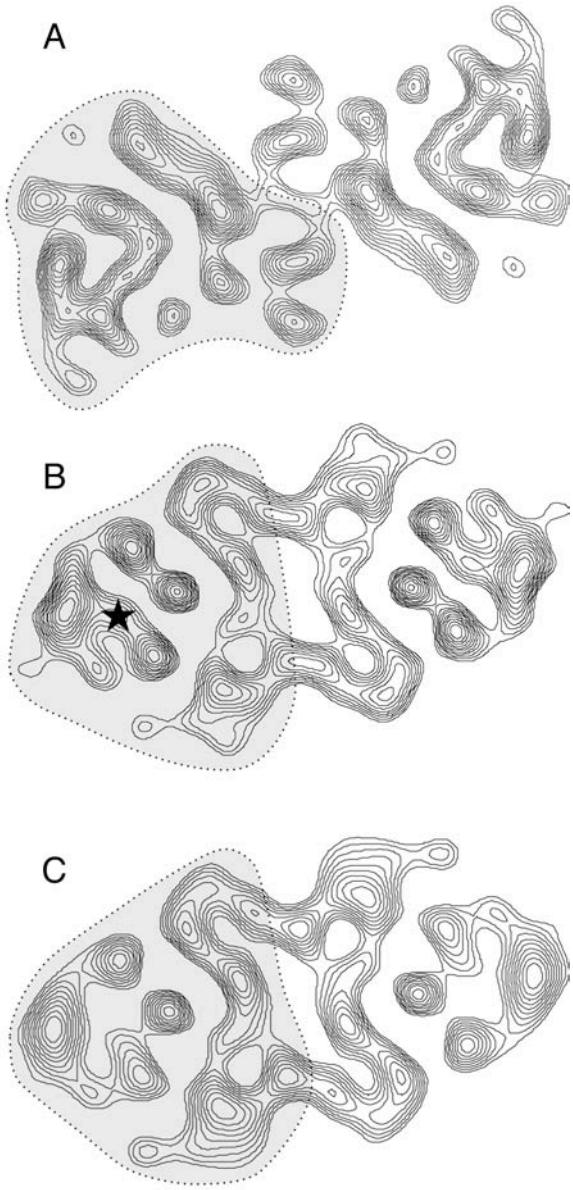

Figure 3.22: Comparison of sodium/proton antiporters

A: Dimer of NhaA from *E.coli* at pH4

B: Dimer of MjNhaP1 at pH4

C: Dimer of MjNhaP1 at pH8

The map resolution is 8Å with only positive contours shown. The putative monomer is labeled with dotted lines. The projection map of NhaA was calculated from the data in Williams et al., 1999.

The asterisk marks a density in pH4 (B) that is not present in pH8 (C).

3.2.6 pH-INDUCED CONFORMATIONAL CHANGE

MjNhap1 is active in the pH range from 6 to 7 (Hellmer et al 2002) and inactive at alkaline pH (Figure 3.3). NhaA on the other hand is active at pH7 and above but inactive at acidic pH. The 3D map of NhaA has been reconstructed from crystals grown at pH4 (Williams 2000), hence in addition to the projection map of MjNhaP1 at low pH it was of great interest to obtain crystals at higher pH. Attempts to crystallize MjNhaP1 at higher pH resulted in poorly ordered tubes or small crystalline patches, which were difficult to reproduce and which I was not able to improve (Figure 3.10). The quality of the crystals obtained by detergent dialysis deteriorated with increasing pH. When preformed 2D crystals of MjNhaP1 were dialyzed against a pH8 buffer and monitored at various time points, it was clear that the crystals were stable up to 10 minutes. With time they tended to clump and eventually lost their crystallinity (Figure 3.11).

Hence an insitu approach was carried out, exposing the crystals to higher pH on the grid, a method inspired from the success of bacteriorhodopsin (Subramaniam, Gerstein et al. 1993) and acetylcholine receptor (Unwin, Toyoshima et al. 1988). This approach yielded a projection map at pH8 (Figure 3.12) that showed visual differences from that of pH4 (Figure 3.9). The validity of the observed differences was carried out by three different approaches that yielded similar results (Figure 3.14, 3.16 & 3.17). The position of the difference peaks as shown in figure 3.23B indicates clearly that the ion translocation pathway is located within the monomer and not at the dimer interface, either within the helix bundle or at the bundle-core interface. The two monomers in the dimer appeared to be active independently of one another, as both undergo the same pH induced conformational change in the 2D crystals. The limited extent of this change is consistent with one translocation pathway per monomer.

When a pH of 6.2 was used instead of pH8 one could observe both conformation in a single tubular crystal, implying that the observed change is not gradual but a change that is occurring around this pH. The observation of

both conformations is possibly a result of time required to induce such change on a carbon grid.

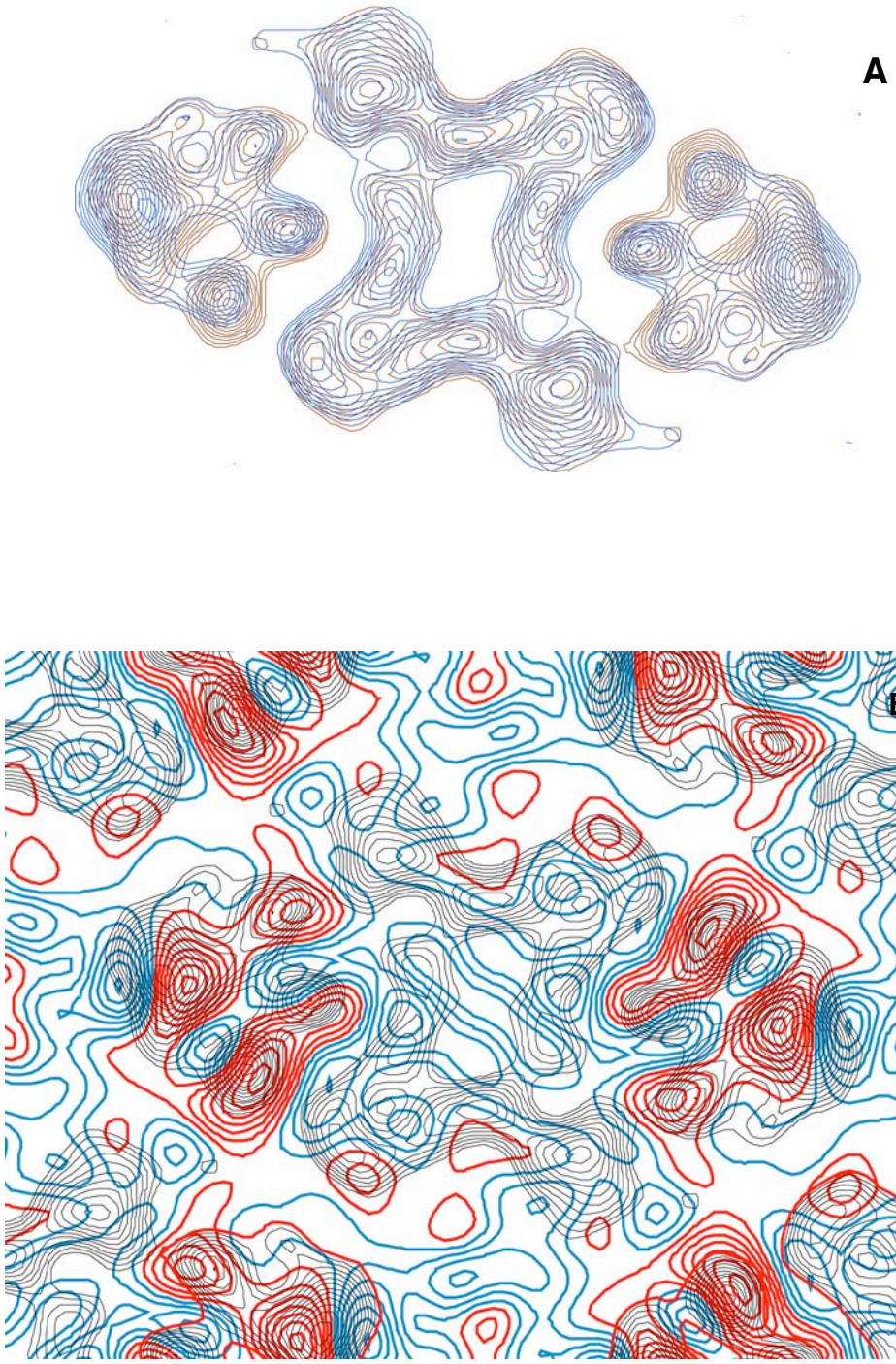

Figure 3.23: A – an overlay of pH4 dimer (red) and pH8 dimer (blue) with only positive contours, map contoured as in figure 3.12.
B- Overlay of projection map of pH4 (black) and the difference map. The positive contours of difference map in red and negative contours in blue. Maps were contoured as in figure 3.14.

3.2.7 OPEN AND CLOSED STATE

In NhaA, the protonation of particular residues apparently blocks ion translocation. Our results indicate that this process is associated with a conformational change in the homologous archaeal antiporter, and I therefore believe that the low pH conformation shown in figure 3.9 represents the inactive, closed conformation of MjNhaP1. The simultaneous occurrence of both conformations at pH 6.2 indicates a conformational switch around this pH rather than a gradual change with increasing pH. Presumably, a similar switch occurs in NhaA at a pH above 7. Interestingly, the 8Å projection map of MjNhaP1 does not show a further change at increasing pH, although the protein becomes inactive at pH greater than 7 (Hellmer et al 2002). This inactivation is therefore possibly associated with a minor change that would not be visible at 8Å resolution, such as the deprotonation of a residue or set of residues (see below). Because the 8Å projection maps of MjNhaP1 look the same at pH6.2 (where the protein is active) and pH8 (where it is inactive), I conclude that figure 3.12 shows the open state of the transporter.

3.2.8 IMPLICATIONS FOR THE REGULATORY MECHANISM

Having said that it is the ion gradient that determines the direction of translocation of sodium ions or protons, an important property of these transporters is the allosteric regulation of proton concentration in the cell that determines the functional state of the protein. For the Na^+/H^+ antiporters, conformational changes in response to pH are thought to activate or inactivate the protein. Such changes have been postulated for *E.coli* NhaA (Padan et al, 2004) and human NHE3 (Hayashi et al, 2002). The change we observe with MjNhaP1 is therefore likely to be related to the pH-mediated regulation of transport activity. Ion transporters have a very much higher transport rate in the order of 10^5 translocation events per second (Taglicht, Padan et al. 1993; Accardi and Miller 2004), requiring dynamics on the timescale of a few microseconds. Rather than rigid-body movements of whole domains, such

rapid dynamics are likely to involve the rearrangement of individual helices or sets of residues, consistent with the scale of the confined conformational changes I observe.

In contrast to ion channels, transporters need two gates for regulating the translocation of substrates. In the Na^+/H^+ antiporters, these two gates are likely to be two distinct sets of residues that are protonated or deprotonated in response to pH, thereby closing or opening the ion translocation pathway. The conformational change closing the translocation path at low pH may be brought about by the protonation of acidic side chains, a number of which have been shown to be functionally important in Na^+/H^+ antiporters. In MjNhaP1, Asp 132 and 161 are essential for transport (Hellmer *et al*, 2003). Asp132 is a key residue in the TDP sequence motif that is characteristic of Na^+/H^+ antiporters and conserved in bacteria, archaea and mammals. Conversely, the deprotonation of these residues at ~pH6 and above may activate ion translocation.

At a pH above 7 MjNhaP1 again becomes inactive. This step might involve the deprotonation of Arg320, the equivalent of Lys300 in NhaA, which are both directly involved in ion translocation (Hellmer *et al*, 2003; Padan *et al* 2004). The observation that Arg320 can be replaced by a histidine without affecting activity or pH response (Hellmer *et al*, 2003) suggests that a positive charge is required in this position, perhaps because it forms an ion pair with one of the negatively charged side chains in the active conformation. The drawing in figure 3.24 summarizes a simplified mechanism of ion translocation in MjNhaP1. However, it is likely that the process of ion translocation and regulation in MjNhaP1 is much more complex, involving many different residues and water molecules.

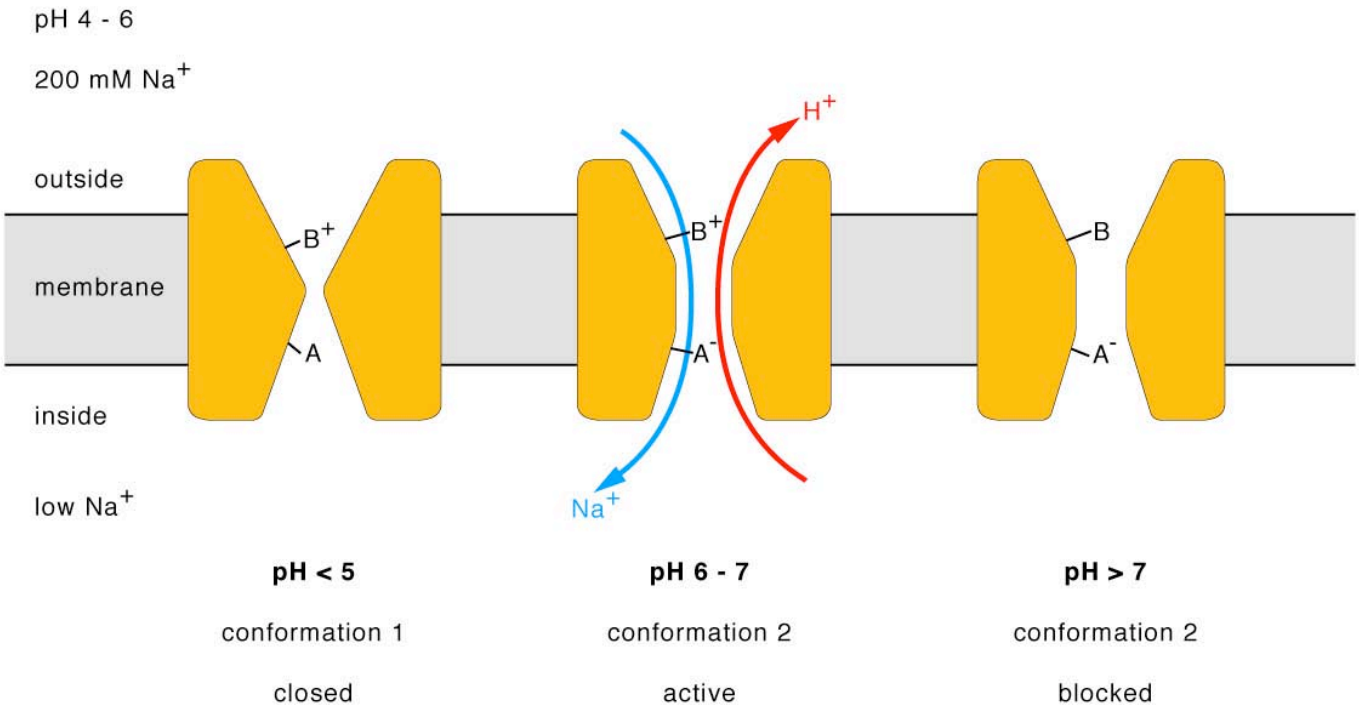

Figure 3.24: Schematic diagram of the *Methanococcus* Na^+/ H^+ antiporter (MjNhaP1) monomer, showing the proposed response to cytoplasmic pH. At normal internal pH (centre) the antiporter is open and active, balancing the Na^+ and pH gradients to maintain the intracellular pH at an optimal level. Closure at low pH (left) is associated with a conformational change that may be caused by the protonation of acidic side chains **A** and is visible in the projection maps of figure 3.12. At pH7 and above (right), the channel is blocked, presumably due to the deprotonation of basic residues **B** in the translocation pathway. This change is not visible in the 8Å projection map.

3.2.9 PHYSIOLOGICAL ROLE OF MjNhaP1

Methanogens are uniform group of strictly anaerobic archaea. The genome of *Methanococcus jannaschii* was the first archaeal genome to be sequenced (Bult, White et al. 1996). Methanogens grow by converting a small number of compounds to methane that is used to generate ion gradients rather than substrate-level phosphorylation (Schäfer, Engelhard et al. 1999). This pathway of methane generation is simultaneously coupled to generation of both proton and sodium gradients. The interrelationship between Na^+ and H^+ cycles is well documented in many organisms (Skulachev VP 1991). In methanogens and *Methanococcus*, the components of the electron transport

chain involve some unique enzymes, which includes the heterodisulfide reductase and hydrogenases that pump protons. In addition, the production of methane from formaldehyde and hydrogen is catalyzed by methyl transferase, a primary sodium pump that extrudes Na^+ from the cytoplasm during methanogenesis (Gottschalk and Thauer 2001). The proton gradient generated thus is used to generate ATP by the ATP synthases (A_0A_1).

From the genome it is evident that *M.jannaschii* encodes for more ABC transporters (23) than secondary transporters (13). Among the secondary transporters for which substrates are known most are sodium coupled. These include 3 sodium/proton antiporters and a chloride/proton antiporter. It is known that many thermophilies tend to use sodium rather than protons for transport. It was reasoned that at high temperatures, the membranes are more permeable to protons than to sodium and presumably to circumvent this leakage, sodium as coupling ion is preferred over protons.

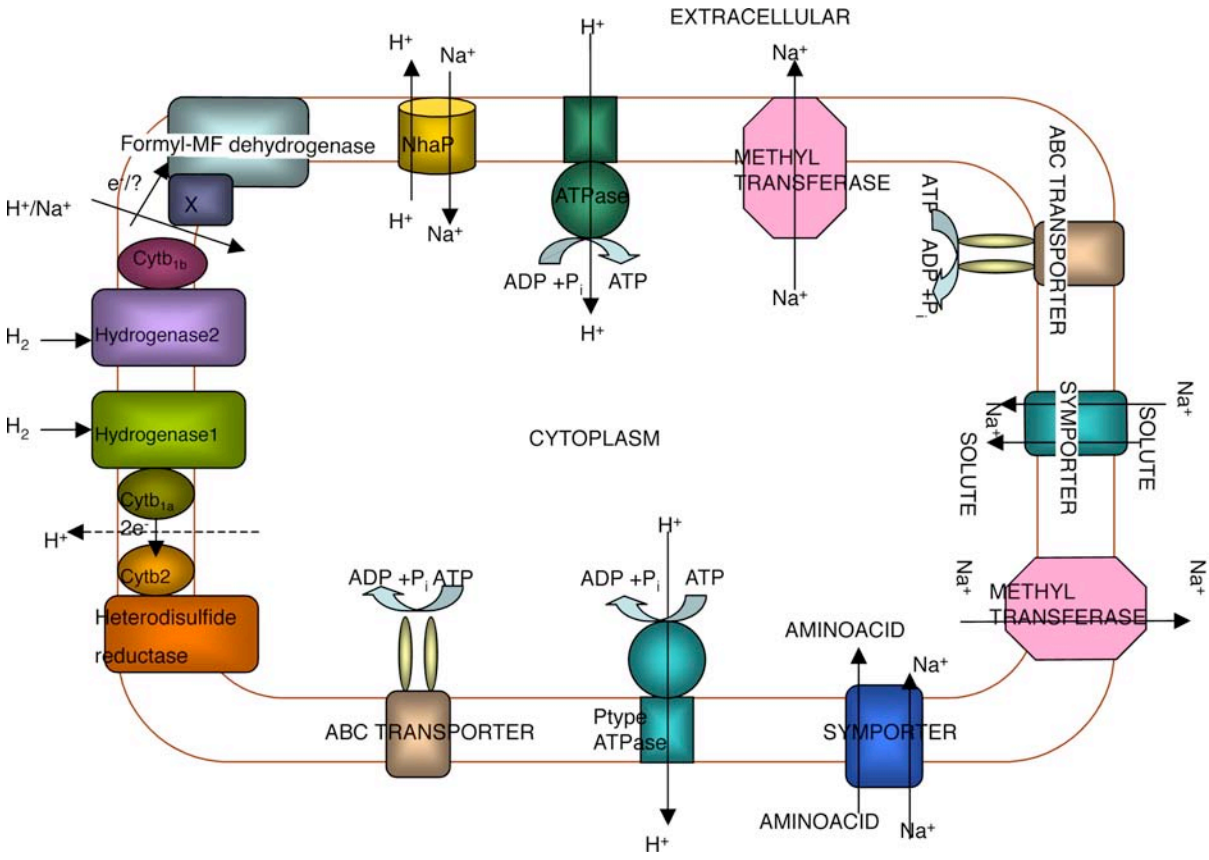

Figure 3.25: Schematic representation of membrane of *Methanococcus* with different membrane protein involved in generation of gradients, energy and transporters are shown.

The natural marine habitat of *M. jannaschii* has a salinity of ~10-15mg/l and a pH of 4-6 (K.O. Stetter, personal communication). Around this external pH *M.jannaschii* would like to keep its cytoplasmic pH close to neutral and would require proton-pumping machineries to achieve this. A detailed appraisal of the exact physiological role of the MjNhaP1 would require additional information on the internal pH and Na^+ concentration, and in particular the transport stoichiometry, whether it is electrogenic (like NhaA) or electroneutral (like NHE1). Without this information, I can only speculate on the role of MjNhaP1 in pH regulation *in vivo*.

Assuming that the activity profiles of the Na^+/H^+ antiporters are adapted to their particular environment and tuned to ensure pH homeostasis in the cell (as is the case for NhaA and *E. coli*), the internal pH of *M. jannaschii* is likely to be around 6.5. MjNhaP1 is evidently designed to correct minor changes of the intracellular pH that arise due to metabolic activity. If the internal pH drops slightly, protons are pumped out by using the Na^+ gradient. If the internal pH rises by a small amount, the antiporter responds by letting protons in, using the increasing pH gradient to extrude Na^+. However, in the event of more extreme pH differences, the antiporter must be switched off to prevent an uncontrolled influx of Na^+ that would result from a large outward proton gradient, either at high external or low intracellular pH.

Conversely, a large inward proton gradient, associated with either a high internal or a low external pH, might cause an almost complete loss of Na^+ from the cell, which may be undesirable as several of the unique enzymes of *M. jannaschii* are Na^+-dependent, amongst them the *M. jannaschii* methyl transferase, a primary Na^+ pump.

The Na^+ gradient thus formed is used by MjNhaP1 to extrude protons. Correspondingly, in human cells the Na^+ gradient formed by the Na^+/K^+ ATPase is used by NHE1 and its isoforms to extrude protons and maintain the intracellular pH. A 3D map by cryo-EM and further a high-resolution x-ray structure will be essential to understand the effect of pH on the protein and mechanism of transport.

4 PutP

4.1 RESULTS

4.1.1 EXPRESSION AND PURIFICATION

Wild type PutP with a flag epitope and a histidine tag at the C-terminus was used to large extent in this study, while a mutant D187C that is functionally inactive was also studied at a later stage of the project. Expression of PutP from a strong promoter such as the 'tac" yielded 1-1.5 milligrams from a liter of shaker flask culture. Solubilization of protein from membranes was achieved with either decyl or dodecyl maltoside as detergent. A single step of metal affinity purification yielded protein that was > 90% pure as judged from Coomassie stained SDS gel.

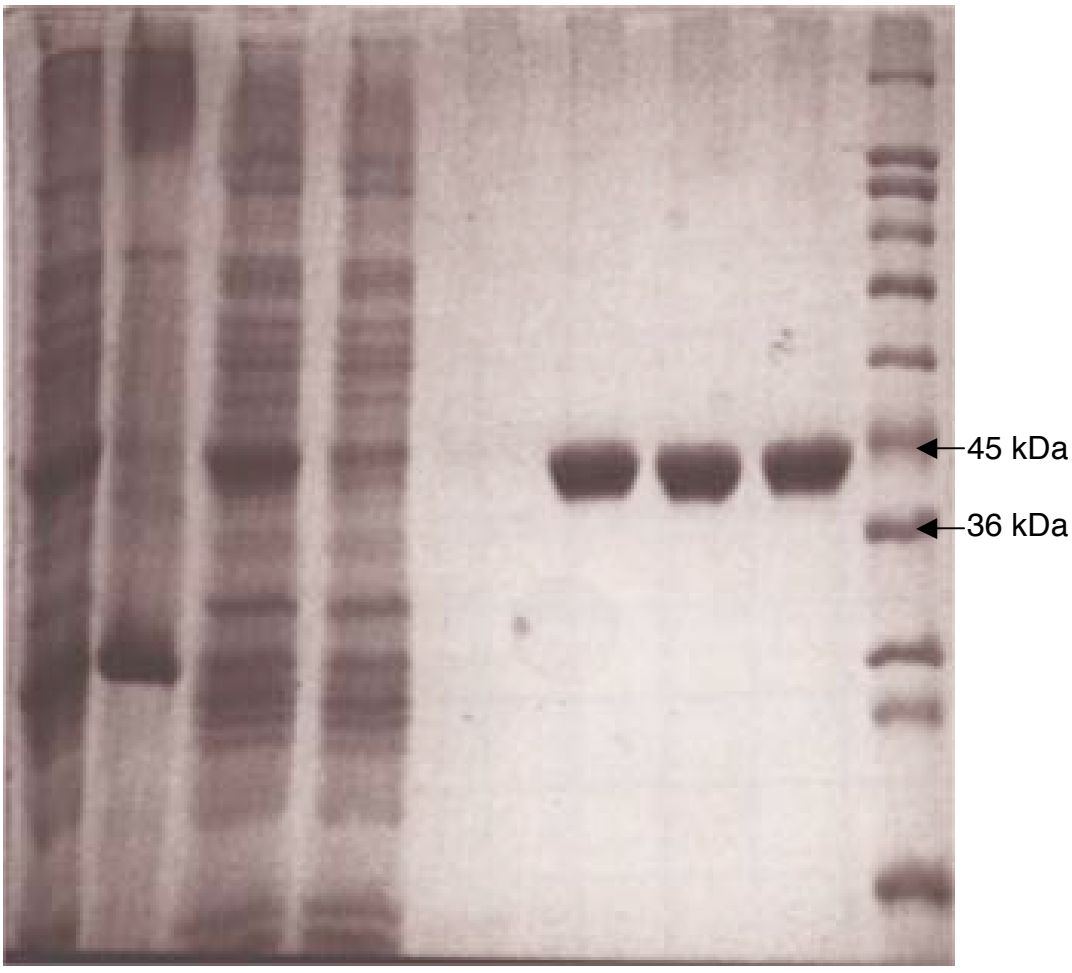

Figure 4.1: Coomassie stained SDS gel of PutP after affinity column Lanes 1,2,3 are membranes, unsoluble and soluble fractions respectively (20□g each). Lanes 4,5 flowthrough and washing with 15mM imidazole, Lanes 6,7,8 are purified fractions of PutP (~3□g) and Lane 9 is Sigma wide range marker.

On a SDS gel PutP migrates a little less than 45kDa (Figure 4.1). PutP in imidazole-containing buffer when incubated overnight at 4°C showed a tendency to form aggregates (Figure 4.2). Hence it was essential to remove imidazole immediately after affinity purification. The aggregates of PutP move at approximately twice the mass of the monomer and could be visualized in the SDS gel when stained with Coomassie. A transport deficient mutant D187C showed similar behavior. Parameters such as final concentration of detergent or glycerol or the addition of lipid had no effect in preventing the formation of the aggregates. These aggregates could be removed by centrifugation at 100,000g for 20 minutes prior to crystallization. The protein was most stable in DDM but could also be purified with DM or $C_{12}E_8$. But most of the work described here was carried out using DDM.

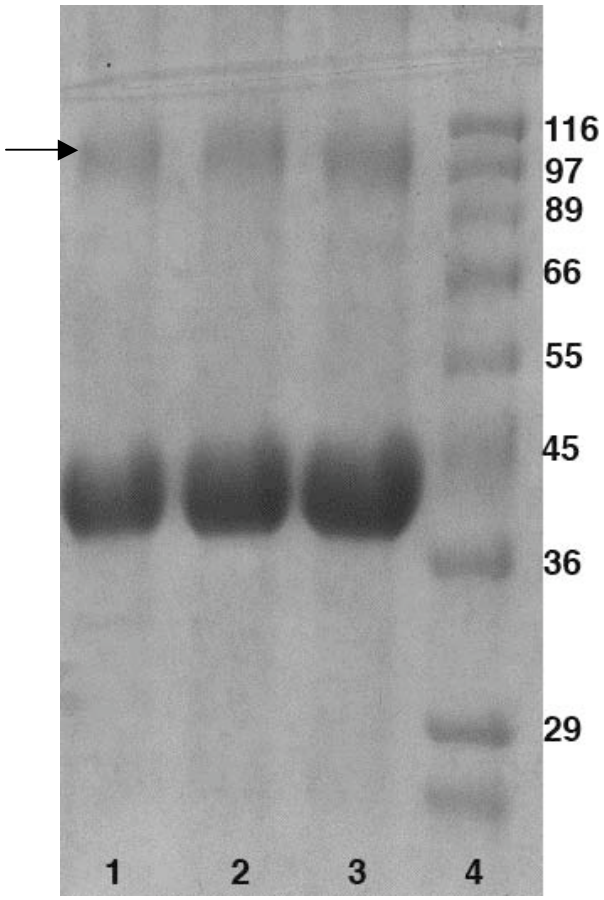

Figure 4.2: SDS gel of PutP after a day of incubation at 4°C.

Lane 1,2,3 – different samples of PutP in DDM showing the formation of higher aggregate shown with black arrow

Lane 4- marker

4.1.2 BLUE NATIVE GEL ELECTROPHORESIS OF PutP

Analysis of PutP by blue native gel yielded complex results. No single band was observed. Instead a distinct band migrating at ~75kDa and streaky higher molecular weight bands were observed. Upon dissociation with 2% SDS a single band migrating at ~70kDa was observed that probably corresponds to a monomer. To verify if the final DDM concentration had any effect on the oligomeric state, PutP was incubated with different DDM concentrations (0.2 to 1.5%) for 1 hour before loading in the gel. No difference was observed with any concentration of DDM. The protein band was visualized better with silver staining (Figure 4.3). Unlike other proteins analyzed in my work (chapters 3,5 and 6) an excess of protein was required to visualize the bands clearly. It was not clear why higher molecular bands would be streaky.

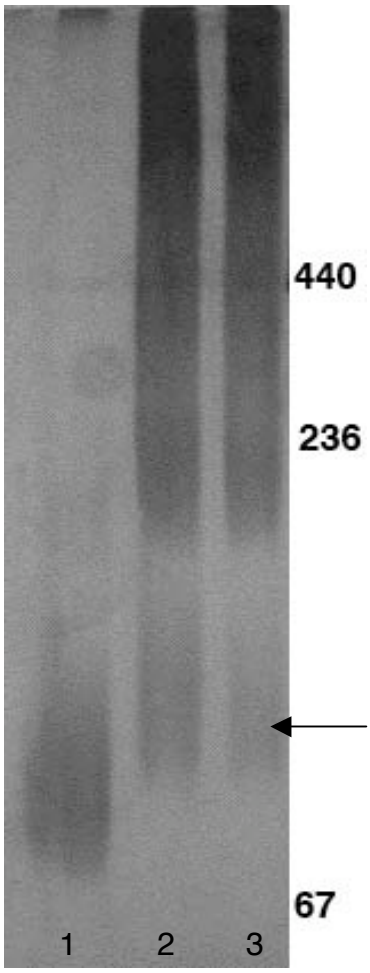

Figure 4.3: Silver stained blue native gel.

Lane 1: PutP in DDM +2% SDS (8□g)

Lane 2,3: PutP in DDM (8 and 15 □g)

The arrow indicates the monomeric band

4.1.3 GEL FILTRATION

An additional chromatographic step was carried out on a Superose 6 gel filtration column. Protein in DDM (0.1%) eluted with a retention volume of 13.94 ml (Figure 4.4). However, the peak obtained was very broad indicating multiple states of protein in detergent solution, consistent with the observed bands in the blue native gel (Figure 4.3). The stability of the protein in DDM was greater than in DM.

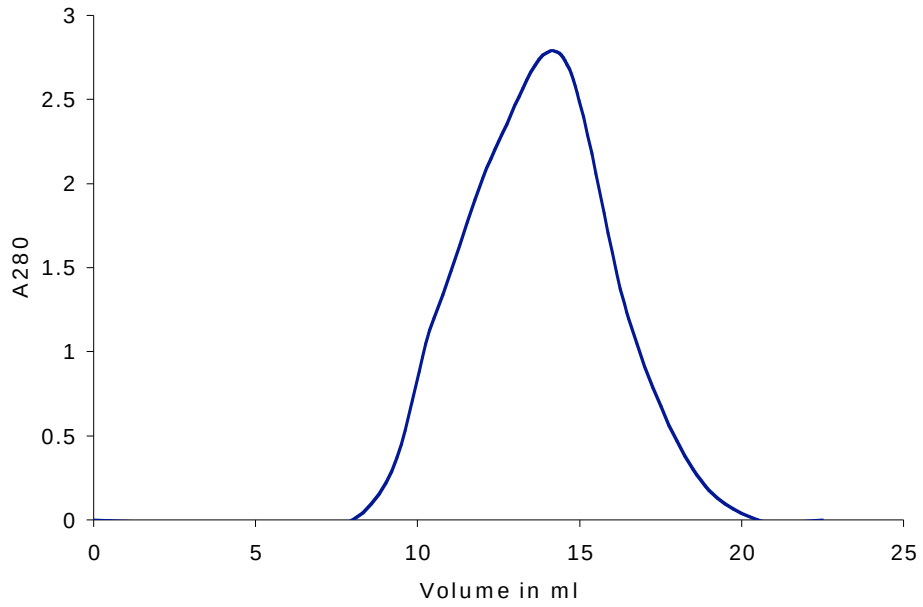

Figure 4.4: Gel filtration of PutP on a Superose 6 column (24ml). The void volume of the column is 8ml.

4.1.4 2D CRYSTALLIZATION

Initial reconstitution experiments were carried out in a dialysis bags (Spectrum) with many parameters varied such as the LPR, pH and ionic strength, lipid and temperature. Most of the conditions yielded membrane vesicles that were clumped together with very little protein incorporated in them. When observed in EM these membranes stained positively. When magnesium was included in the crystallization buffer (pH7), membranes with

small patches of ordered protein were observed (Figure 4.5). These crystalline patches were very small and showed a hexagonal diffraction pattern. On a positive note this indicated that PutP liked to form ordered aggregates.

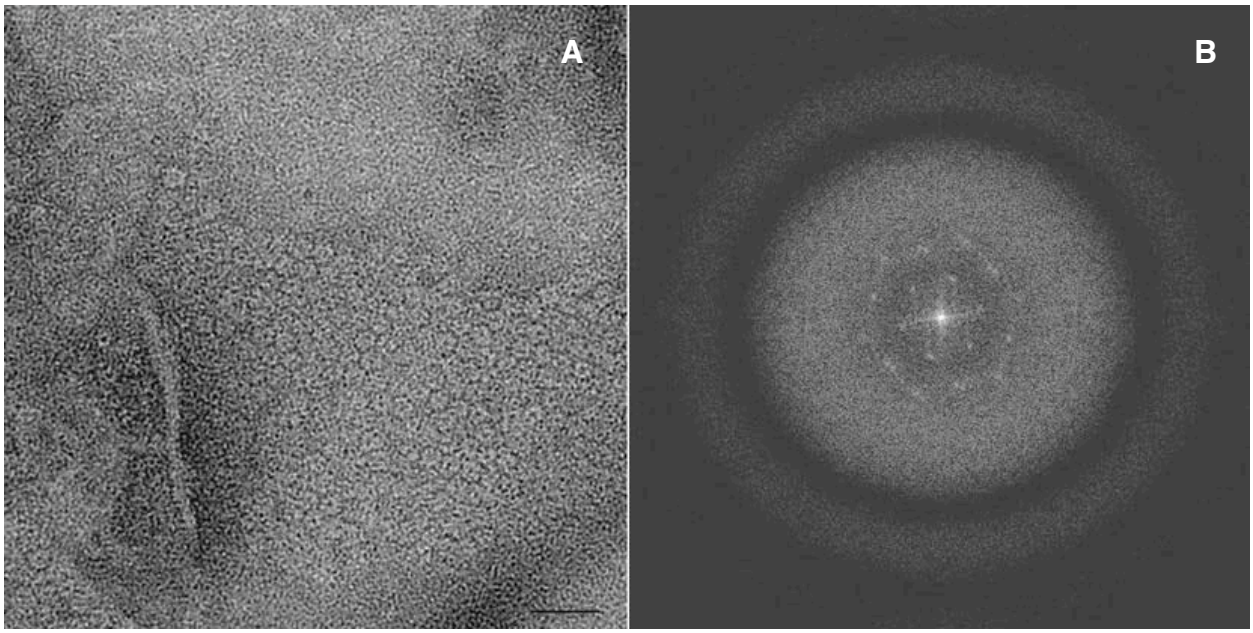

Figure 4.5: A – Crystalline patches of PutP observed by negative staining at pH7 (scale bar –100 nm) and the power spectrum showing a hexagonal lattice (B).

These patches obtained at alkaline pH were difficult to reproduce. Hence, a pH screen was carried out. This yielded 2D crystals of PutP at pH5 that were vesicular in nature. It was also possible to get small patches of crystalline membranes at intermediate pH such as 5.6 or 6 and occasionally narrow tubular crystals. Most of these crystals invariably had a hexagonal lattice. The formation of crystals required the presence of methyl-pentane-diol. When only glycerol was used in the buffer the resulting membranes were not ordered.

The following parameters were important for obtaining well-ordered 2D crystals of PutP:

a) It was essential to pre-incubate the protein with lipid on ice or at room temperature prior to dialysis.

b) Crystals were obtained most reproducibly when the final detergent concentration was raised to 0.1%, five times higher than the CMC of DDM. Irrespective of DDM concentration (0.05% or 0.1%) the gel filtration profile was essentially the same. Hence, it is unlikely that more detergent was necessary to keep the protein stable.

c) Initially, detergent removal was carried out in dialysis tubing (molecular weight cutoff of 12-14kDa) that yielded crystalline membranes with low yield. Incubation at different temperatures was attempted to get better crystals. But when the dialysis was carried out at lower temperature, no distinct membrane structures were observed indicating that the rate of dialysis was important. Based on this observation, different methods were used to remove detergent, which differ in the rate of detergent removal.

When biobeads were used to remove the detergent, this yielded small vesicles with little incorporation of protein and lot of protein aggregates (Figure 4.6B). The best crystals were obtained with Slide-A-Lyzer mini dialysis units (PIERCE) with a molecular weight cut off of 10kDa. Since this device had only a single outlet for detergent removal, presumably a slow rate of detergent removal accompanied by incorporation of protein into lipid bilayer was the success behind the mini dialysis units.

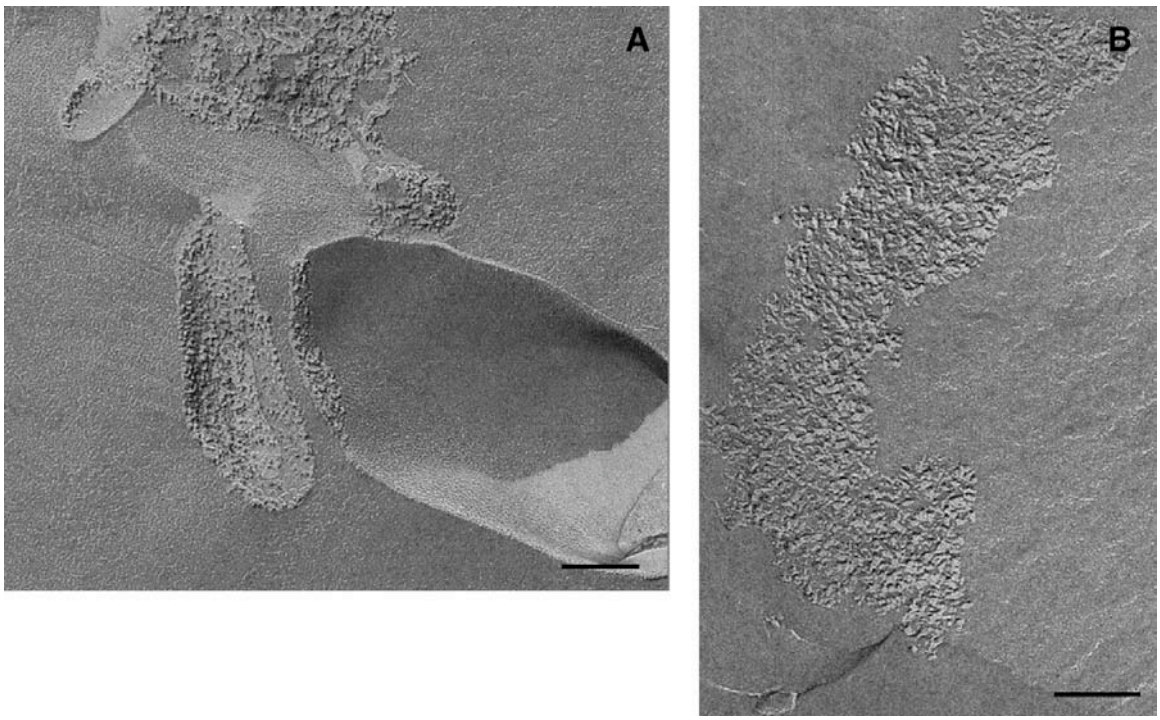

Figure 4.6: Freeze fracture electron micrographs of PutP membranes. A – Membranes obtained by dialysis at pH5.
B – PutP reconstituted by biobeads.
Scale bar-100 nm.

In a given grid or grid square, the number of crystalline vesicles were random. Sometimes one could observe a lot of crystalline vesicles in a single grid square but many a times no crystal was observed on the whole grid. This observation and the freeze fracture analysis of the membranes clarified that the efficiency of reconstitution was very low (Figure 4.6A). Subsequent efforts were attempted to increase the amount of protein incorporated and the yield of single or double-layered crystal. D187C, a transport deficient mutant that I thought might be less flexible yielded similar results. An optimal condition was reached based on the various factors discussed above. Protein in 0.1% DDM at an LPR of 0.25-0.4 was dialyzed in a slide-A-lyzer mini dialysis units at 37°C against 25mM acetate buffer pH5, 0.25M NaCl, 5% each of MPD and glycerol for 7 days.

The 2D crystals obtained were vesicular in nature. Most of these crystals were multiple layers with only two orders visible in the power spectrum (Figure 4.7B), but some of these crystals were better ordered and spots up to the fifth order in the power spectrum of CCD could be seen (Figure 4.7D).

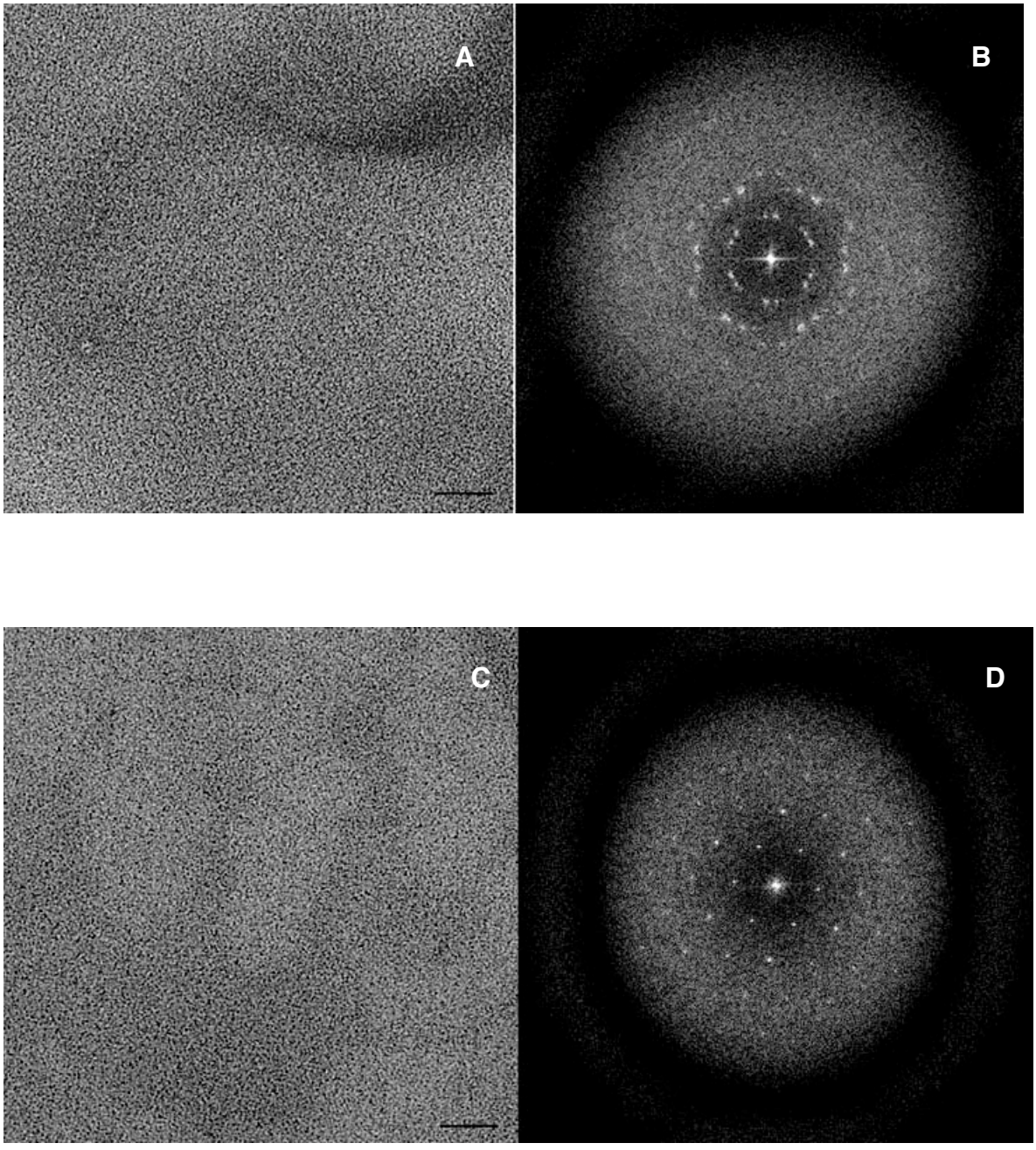

Figure 4.7: A and C: High magnification images of multiple layered and isolated crystal of PutP (scale bar- 100 nm) and their respective power spectrums in B and D.

The isolated membranes measured 0.5-0.7 □m in width and were uniformly crystalline. The amount of salt present in the crystallization buffer was directly proportional to the formation of stacked membranes. When no salt was used during reconstitution very small vesicles without any order were obtained. An optimal concentration of 250 mM was used to balance the equilibrium between the stacked membranes and the non-crystalline vesicles.

To improve the efficiency of reconstitution a screen for detergents was carried out. The stability of PutP was best in DDM and hence this screen could be done only with solubilization of lipid with different detergents. The efficiency of the reconstitution of a given protein depends on the choice of the detergent and its concentration. The solubilization of lipids by detergent involves two distinct points called the “onset and complete” solubilization based on the change in the turbidity (Figure 4.8). Since I was using *E.coli* polar lipids it was essential to determine the break points of this lipid for different detergents.

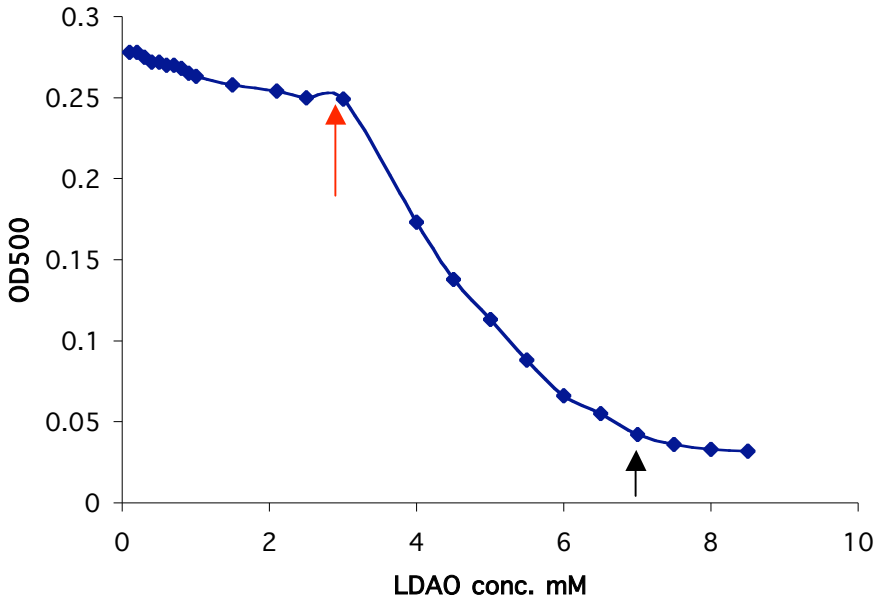

Figure 4.8: Plot showing the breakpoints (onset and total solubilization) of *E.coli* polar lipids (1mg/ml) at 25°C for LDAO. The red arrow indicates the onset of solubilization and the black arrow indicates the total solubilization. Onset is defined as the point when the turbidity of the lipid suspension starts decreasing and the total solubilization is the point where no change is observed with further increase in the concentration of detergent.

The onset and total solubilzation of *E.coli* polar lipids for different detergents was determined and tabulated below.

Table 4.1:

Detergent	Onset (mM)	Total (mM)
LDAO	3	7.5
$C_{12}E_8$	0.7	2.5
DM	1	3
OG	17	23
MEGA-9	19	25
DDM[a]	-	-
TX100[b]	1	3

a – clear break point was not observed
b – Jung et al 1998

The onset of solubilization for maltosides were not clearly defined in particular for DDM where both onset and total solubilization were indistinguishable and the turbidity kept decreasing gradually.

The following approach was then used for reconstitution. Lipids were dried under inert atmosphere and rehydrated with aqueous buffer. The steps involved were:

a) The required amount of liposomes based on the LPR was taken, typically 0.4-0.5 (w/w).

b) The detergent of choice was added at the concentration required for the onset of solubilization of *E.coli* polar lipids as determined from the turbidity measurements (Table 4.1) and incubated for 10 minutes at RT.

c) Protein eluted in 0.1% DDM was mixed with destabilized liposomes and incubated on ice for 1 hour.

d) The solution was transferred to mini dialyzers for detergent removal and

incubated at 37°C for 5-7 days.

As controls, completely solubilized lipids or rehydrated liposomes with no additional detergent were used. The rationale for using liposomes with no detergent was due to fact that the protein after purification would have enough free detergent (in this case DDM) to destabilize the lipids and promote the incorporation of the protein. All these trials with different detergent yielded 2D crystals of PutP.

Most conditions yielded stacked crystals but the frequency of crystalline membranes was greater, reflecting a better efficiency of incorporation when compared to the completely solubilized lipids. The membranes obtained just with liposomes were equally good indicating that the amount of free detergent after purification was sufficient for getting 2D crystals. In fact, these yielded better results with respect to stacking. Detergents such as CHAPS or $C_{12}E_8$ yielded only stacked membranes and the spots obtained with TX100 were blurred (Figure 4.9). Hence liposomes without any detergent were directly used for further reconstitution. Crystals were obtained reproducibly and one could distinguish between stacked and isolated vesicles in negative stain easily. Several attempts to get good images by cryo-EM were not successful.

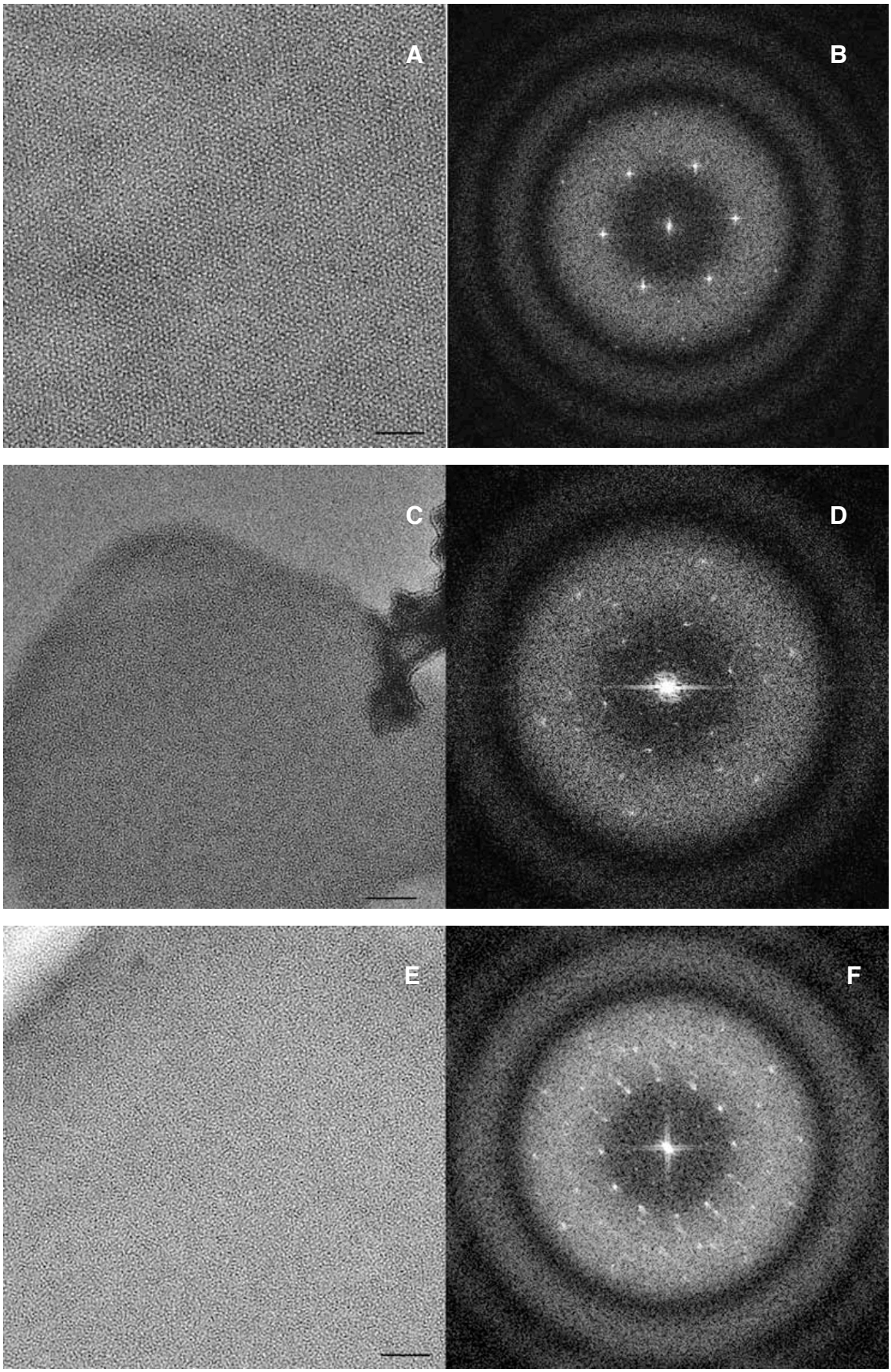

Figure 4.9: Crystalline membrane observed with different detergents. High magnification images of membranes with no detergent added (A), TX100 (C) and CHAPS (E) (scale bar is 100 nm). B, D and F show the respective power spectrum.

Along with these vesicular crystals, occasionally I also observed some thin 3D crystals that stained positively. Some of these were hexagonal in shape and could be observed in a pH range 4-6. Most of these were clumped and found on the edge of the grid square. In a grid square they were few in number. These membranes indicated that PutP has a tendency to form 3D crystals.

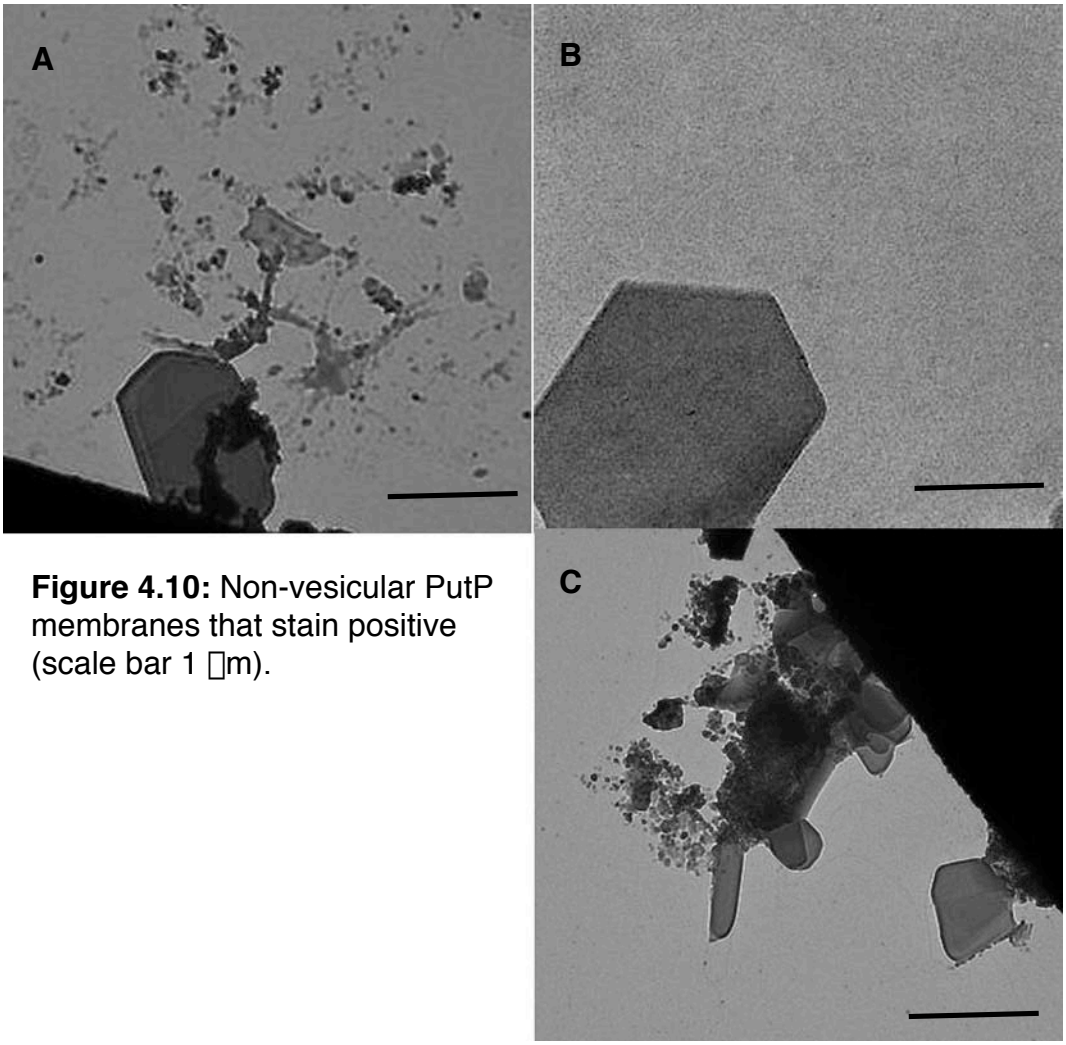

Figure 4.10: Non-vesicular PutP membranes that stain positive (scale bar 1 □m).

4.1.5 IMAGE PROCESSING

Negatively stained images were used for image processing that yielded two different classes. One set of images after three to four rounds of unbending showed spots to 20Å and unit cell was a=b=108Å. The program ALLSPACE indicated the presence of three-fold symmetry. A projection map was calculated from averaged images to 20Å with symmetry applied (Figure 4.11). The approximate dimension of trimer was 100Å.

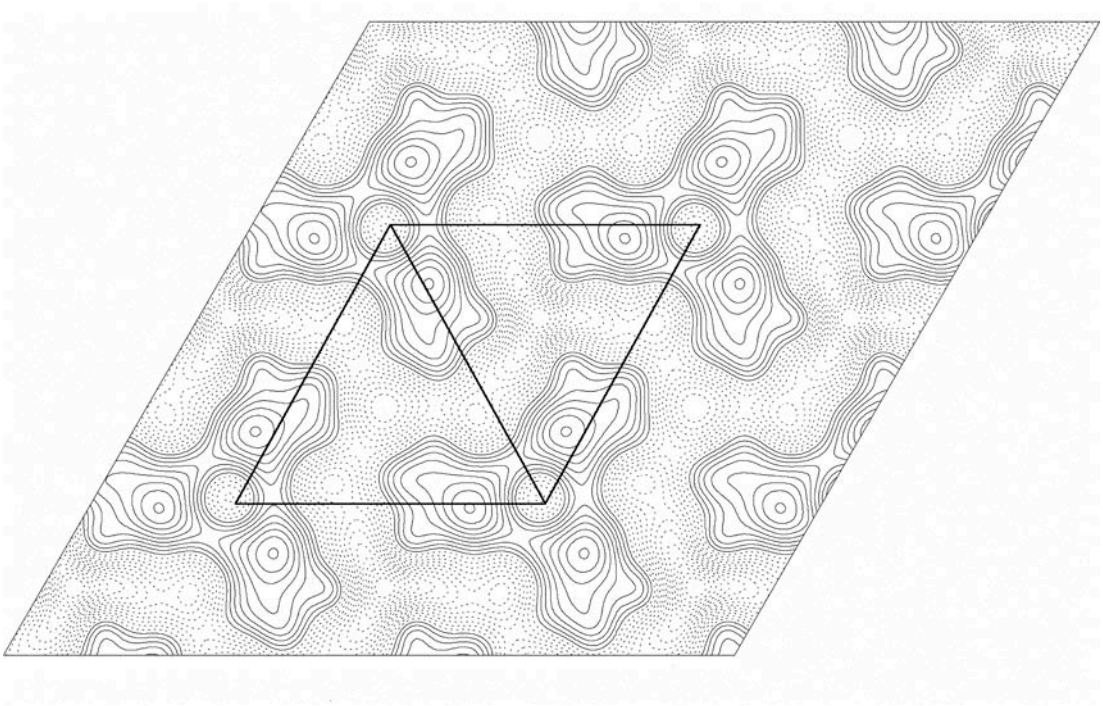

Figure 4.11: Projection map of PutP membranes at 20Å with P3 symmetry applied.

The second set of images showed spots after unbending of lattice to 15Å (Figure 4.12B) and no symmetry was detected by ALLSPACE at 15Å. However when only low-resolution spots were included for determining the

space group the presence of P3 or P321 was evident. These images had very similar unit cell (a=b=108Å) but with greater variability. Projection map calculated from a single image was very similar to that of isolated vesicles.

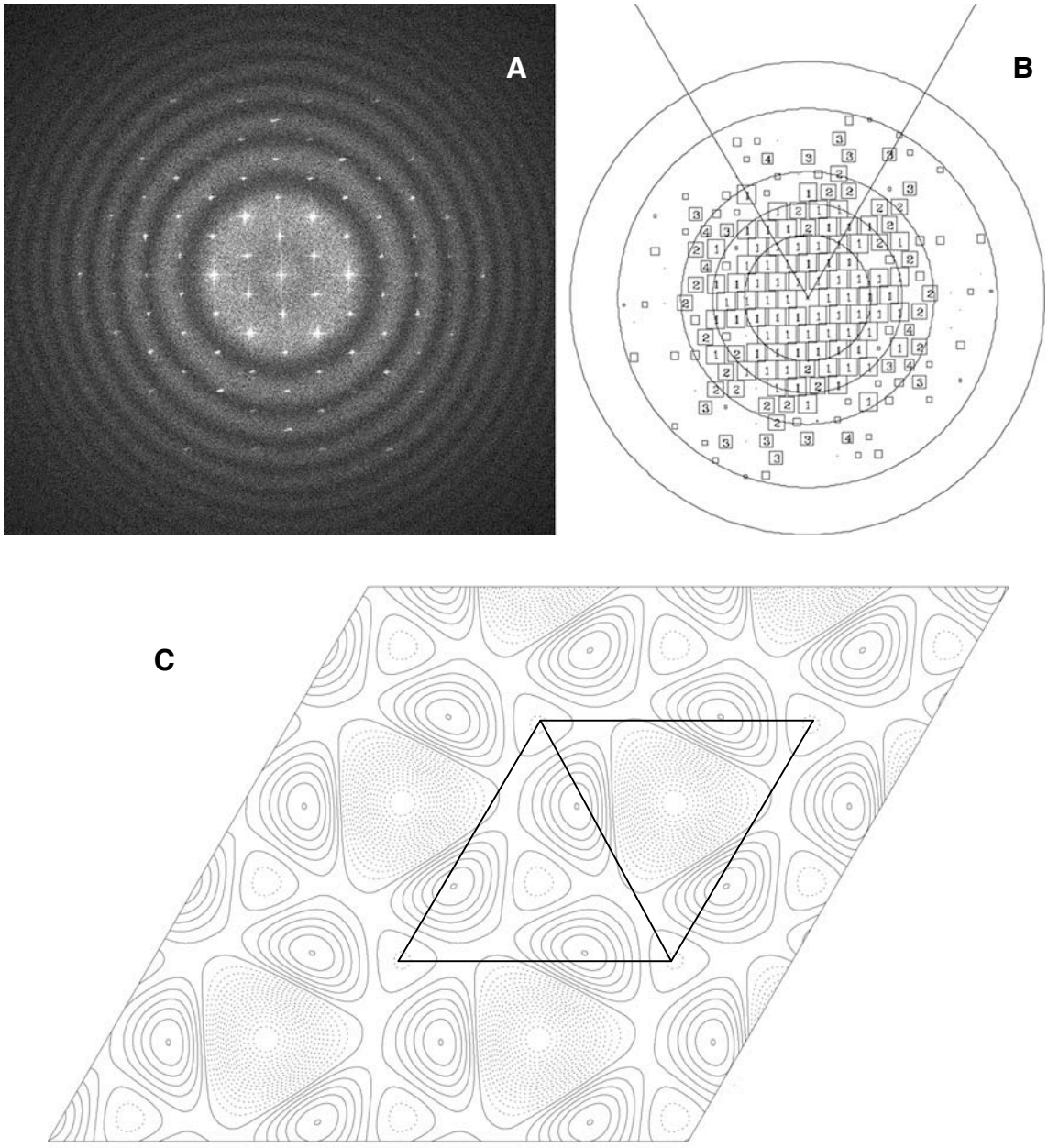

Figure 4.12: Fourier transform of one single PutP image of multiply stacked membrane (A) and the IQ plot (B) after three rounds unbending of lattice (circles denote 30,20,15,10 and 8Å from the center). C - projection map with P3 symmetry applied.

4.2 DISCUSSION

4.2.1 PURIFICATION OF PutP

Wild type PutP yielded more protein than the transport deficient mutant. After a single affinity chromatography step both protein showed greater than 90% purity. Both the wild type and the mutant protein showed similar behavior in detergent solution and had a tendency to aggregate (Figure 4.2). Many different parameters tried to prevent the aggregation were not successful. The best way to tackle this problem was to work fast and reconstitute the protein into lipid bilayers, the native environment of the protein before it had time to aggregate.

4.2.2 OLIGOMERIC STATE OF PutP

The oligomeric state of PutP has not been reported before. Two different members of the SSF (sodium solute symporter family) have been reported as monomers (Eskandari, Wright et al. 1998; Turk, Kim et al. 2000).These studies are based on freeze fracture electron microscopy of particles in proteoliposomes or on oocyte membranes. The dimensions of known proteins (such as aquaporin and connexin) were used as a reference to determine the possible oligomeric state for both SGLT from rabbit or *V.parahaemolyticus*. However, the thickness of the metal film is very critical and this can make all difference between the diameter of a monomer or dimer, hence I would like to be very cautious on conclusions drawn from these freeze fracture studies.

The gel filtration profile of PutP showed a broad peak with a retention volume of ~14ml (Figure 4.4). No conclusion could be drawn from this because of the presence of larger detergent micelles. Blue native gel analysis of PutP showed a strong band at ~75kDa and higher molecular bands that were not clearly resolved (Figure 4.3). Upon addition of SDS, PutP showed a single band with an apparent mass of ~70kDa, indicative of a monomer (Figure 4.3). The calculated mass of PutP from the amino acid sequence is ~56.5kDa. The observed mass on blue native gel would correspond to a ratio

of ~1.4 as calculated for other membrane proteins in this study.

It is tempting to conclude that the very broad band observed at ~230kDa is an oligomeric form of PutP (Figure 4.3). This band would correspond to a trimer. Whether this oligomerization is a property of PutP or due to aggregation needs to be verified. Many different membrane proteins have been observed in equilibrium between oligomeric states. This includes the secondary transporter LacS from *Streptococcus lactis* that has been shown to be in equilibrium between a monomer and dimer (Heuberger et al 2002). Depending on the detergent concentration, the equilibrium of this transporter shifted to either a monomer or dimer. However, different concentrations of final DDM had no effect on the bands of PutP observed by blue native gel.

4.2.3 2D CRYSTALLIZATION

2D crystals of PutP were not obtained readily. It took nearly a year for me to understand the requirement of the protein for forming ordered arrays. Initial screens for PutP 2D crystals in dialysis tubes invariably resulted in protein aggregates most of which stained positively with uranyl acetate. The first hint for the formation of crystals was found with a buffer at pH7 with magnesium. These membranes had small crystalline patches that showed a hexagonal lattice (Figure 4.5). However efforts to improve the size or the number of these patches were not successful.

The large number of lipid-protein aggregates indicated that the rate of dialysis was probably fast. Incubation at different temperatures to control the rate of dialysis or the use of bio beads that remove the detergent rapidly yielded similar results (Figure 4.6B). Following this indication, dialysis was carried out either in hockey sticks (Kühlbrandt 1992) or mini dialyzer. The latter was chosen for easy handling. 2D crystals could be immediately obtained at pH5. Most of these crystals were stacked and poorly ordered (Figure 4.7A).

The amount of final detergent present in the purified protein has been

shown to play a major role in obtaining bigger and well-ordered crystals (Schmidt-Krey, Lundqvist et al. 1998). When the protein was eluted with 0.1% DDM and subsequently used for crystallization, more reproducible and larger crystals were obtained. Some of these were isolated vesicles and had only two layers. These isolated vesicles were better ordered (Figure 4.7C) but their frequency on a given grid was low indicating less efficient reconstitution.

Different approaches for reconstitution of membrane proteins have yielded proteoliposomes of different sizes and compositions, largely depending on the nature of the detergent, the choice of the method of removing detergent, and naturally the protein and lipid composition. In 2D crystallization, it is possible to use two different detergents, one to solubilize the protein and the other for the lipid. The efficiency of reconstitution of a given protein tends to depend on many different factors. One among them is the choice of the detergent and its concentration. The choice of detergent has shown to have great impact on reconstitution of membrane proteins when used for functional studies (Paternostre, Roux et al. 1988; Rigaud, Pitard et al. 1995). When a detergent is added to a lipid suspension, two different break points are obtained, at onset and total solubilization. A wealth of information has been published for lipids such as eggPC (Levy, Bluzat et al. 1990). Most of these data is based on the reconstitution of primary pumps that showed a marked behavior on the type and amount of detergent indicating preferences for efficient reconstitution (Rigaud et al 1995).

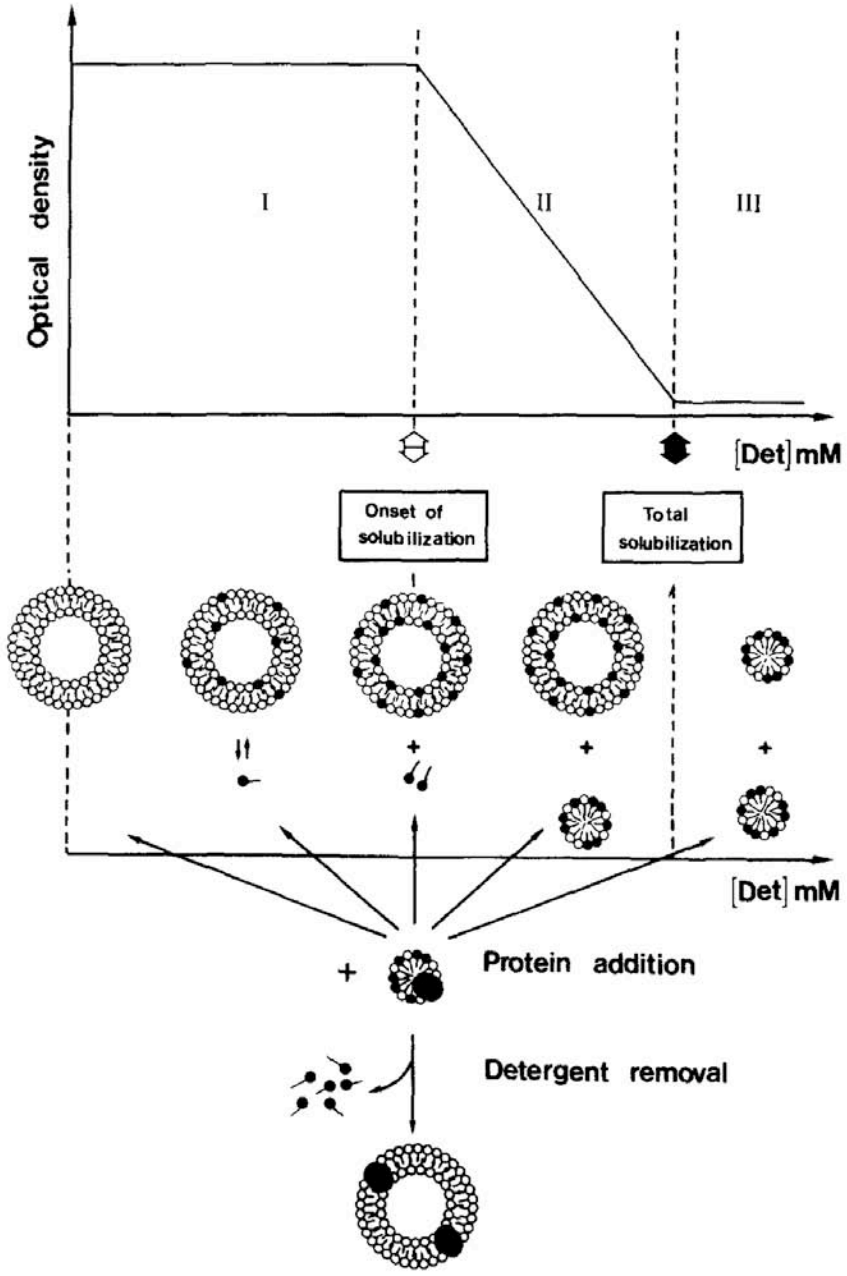

Figure 4.13: Schematic diagram explaining the different steps in lipid solubilization and stages where protein can be added (from Rigaud et al 1995).

Protein for reconstitution can be added at many different points. Based on the detergent and the nature of the protein one could get efficient reconstitution at any of these points (Figure 4.13). The effect of different detergents used for 2D crystallization is not well documented. But some of the

recent studies on the eukaryotic proteins has shown that apart from finding the right detergent to keep the protein stable it is also essential to use a second detergent to obtain good 2D crystals (Parcej and Eckhardt-Strelau 2003; Schmidt-Krey, Kanaoka et al. 2004). In these cases the best 2D crystals were obtained when the protein was purified with a detergent that has a low CMC (such as DDM or TX100) in combination with lipid solubilized in a detergent that has a higher CMC (cholate or CHAPSO) yielded better crystals. One explanation is the formation of mixed micelles that could remove the detergents faster, but it is likely to involve a more complex process.

When PutP was reconstituted into liposomes for functional assays, it was observed that detergent concentration at the onset of solubilization showed greater activity than the fully solubilized liposomes. The profile was also dependent on detergent used (Jung et al 1998). I wanted to test the possibilities from the above discussion in crystallizing PutP. Since I was using *E.coli* polar lipids dominantly, it was essential to determine the amount required for the onset and complete solubilization of *E.coli* polar lipids by different detergents (Figure 4.8 and Table 4.1).

PutP reconstitution was carried on with liposomes destabilized with detergents at a concentration corresponding to onset of solubilization. Many of these trials invariably yielded crystals. The best condition was obtained with just free detergent present with the protein after purification. The yield and frequency of crystalline membrane in a given grid was higher. Some of these membranes showed sharp spots and could correspond to two layers of membranes exactly in register (Figure 4.9B). Even though the efficiency of reconstitution was increased, lot of stacked membranes was found all over the grid. Reconstitution with other detergents yield predominantly stacked membranes (Figure 4.9 E and F). It was possible to distinguish them by visualizing in low magnification.

4.2.4 IMAGE PROCESSING

Image processing of crystals in negative stain was divided into two different categories. One set of images from isolated vesicles presumably made of two layers of membranes, showed the presence of three-fold symmetry with spots good only till 20Å. The other set of images showed very good spots till 15Å. It is likely that these images are made of multiple layers of membranes stacked upon one another presumably all in register as seen from the strong diffraction spots (Figure 4.12A). The phases of the spots at the higher resolution in these stacked crystals showed a lot of deviation and only at low resolution of 35-40Å the phase residuals for the image were within the error (< 45°) for P3 symmetry. The space group P321 was a possibility in both isolated vesicles as well as stacked crystals. However, I thought it was just safer to impose three-fold symmetry at this stage of negatively stained crystals.

PutP in detergent solution exists predominantly as a monomer (Figure 4.3) but in lipid bilayer a trimeric architecture (Figure 4.14) is observed, which is interesting. This could be due to ordered aggregation of protein at high concentration in the lipid bilayer. The dimension of the trimer calculated from the projection map (Figure 4.11) is comparable to the dimensions of CaiT or BetP both trimeric protein, made of multiple spanning TM helices.

Such differences in oligomeric state of membrane proteins in lipid bilayer and detergent solution are not uncommon. Some examples include the ADP/ATP carrier and the lac permease (Kunji et al. 2003; Pebay-Peyroula et al. 2003; Zhuang et al. 1999; Abramson et al. 2003). Mitochondrial ADP/ATP carrier for long time was thought to be a dimer (Klingenberg 1981) and it came as a surprise when the x-ray structure was solved as a monomer (Pebay-Peyroula et al. 2003). But the structures in detergent and lipid bilayer are very similar indicating that protein is in its native state in detergent solution (Kunji 2004).

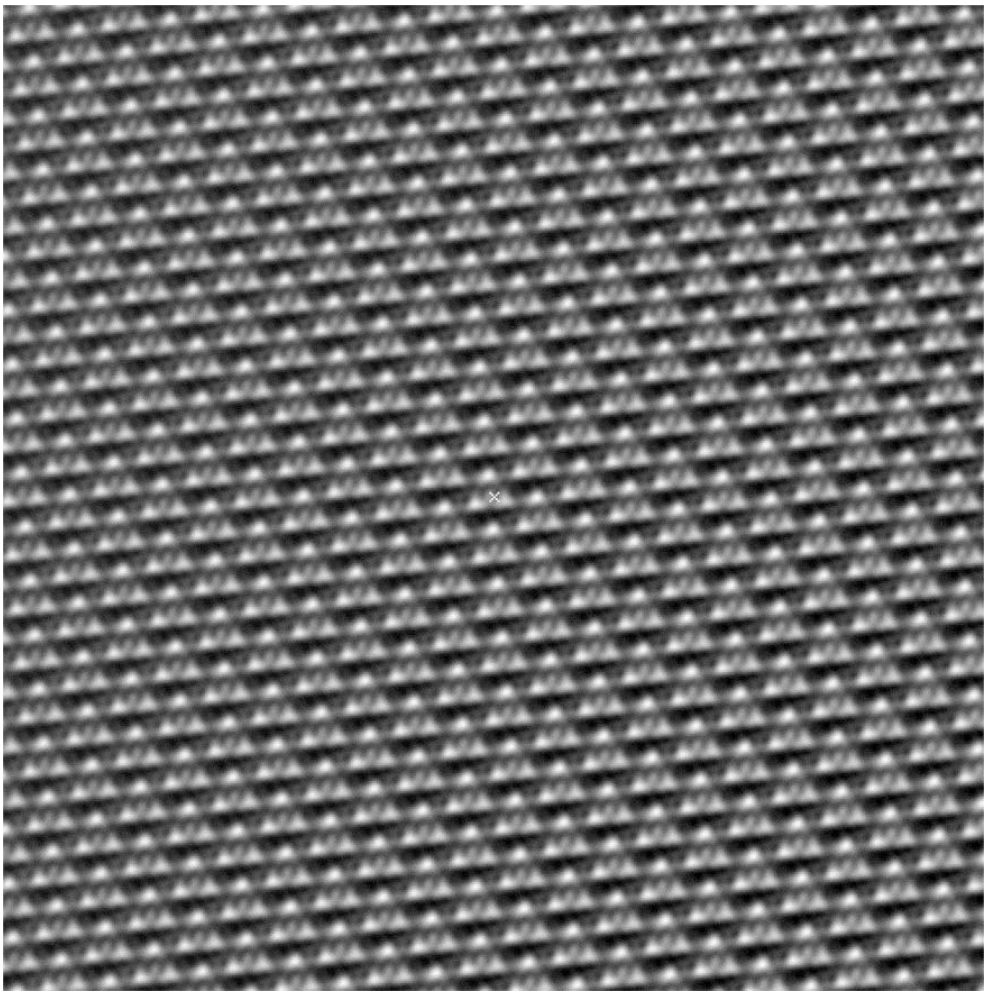

Figure 4.14: A filtered image of negatively stained PutP showing the trimeric assembly of the protein in lipid bilayer.

Lac permease, a monomeric sugar transporter (Abramson et al 2003), when expressed as a red permease (fusion of cytochrome b_{562}) and crystallized in lipid bilayer yielded a trigonal or rectangular crystal form (Zhuang, Prive et al. 1999). In both crystal forms trimers of red permease were observed. It is known from different experimental approaches that Lac permease is a functional monomer (Kaback, Sahin-Toth et al. 2001). The high protein concentration in 2D crystallization might result in packing of protein to form trimer and might be influenced by the crystallization conditions. In analogy to Lac permease it is likely that PutP can function as a monomer and crystallizes in the lipid bilayer as a trimer. Whether the trimer of PutP could be

observed *in vivo* membranes and if so what is the functional importance of this trimeric arrangement needs to be studied.

The tendency to form stacks (Figure 4.7) and the formation of thin 3D crystals (Figure 4.10) indicates the willingness of PutP to form 3D crystals. One could ask if these stacks and thin 3D crystals could be analyzed by electron microscopy. Different groups have devoted a lot of effort to tackle this particular problem but there has been no clear solution till date. So, 3D crystallization with multiple approaches such as the use of antibodies to stabilize the protein or a mutant that locks the protein in one conformation and addition of lipids would be things to try.

5 CaiT

5.1 RESULTS

5.1.1 EXPRESSION AND PURIFICATION

Different constructs of carnitine transporter were expressed and purified essentially as described previously (Jung et al 2002). The protein had either a N-terminal cleavable or a C-terminal histidine tag. All the clones from the shaker flask culture yielded about 2-2.5 milligrams per liter of culture. Solubilization of the protein was achieved by dodecyl maltoside. A gradient of imidazole was used for purification and CaiT eluted at ~150mM. Greater than 90% purity was obtained with a single affinity chromatography step as judged from Coomassie stained gel.

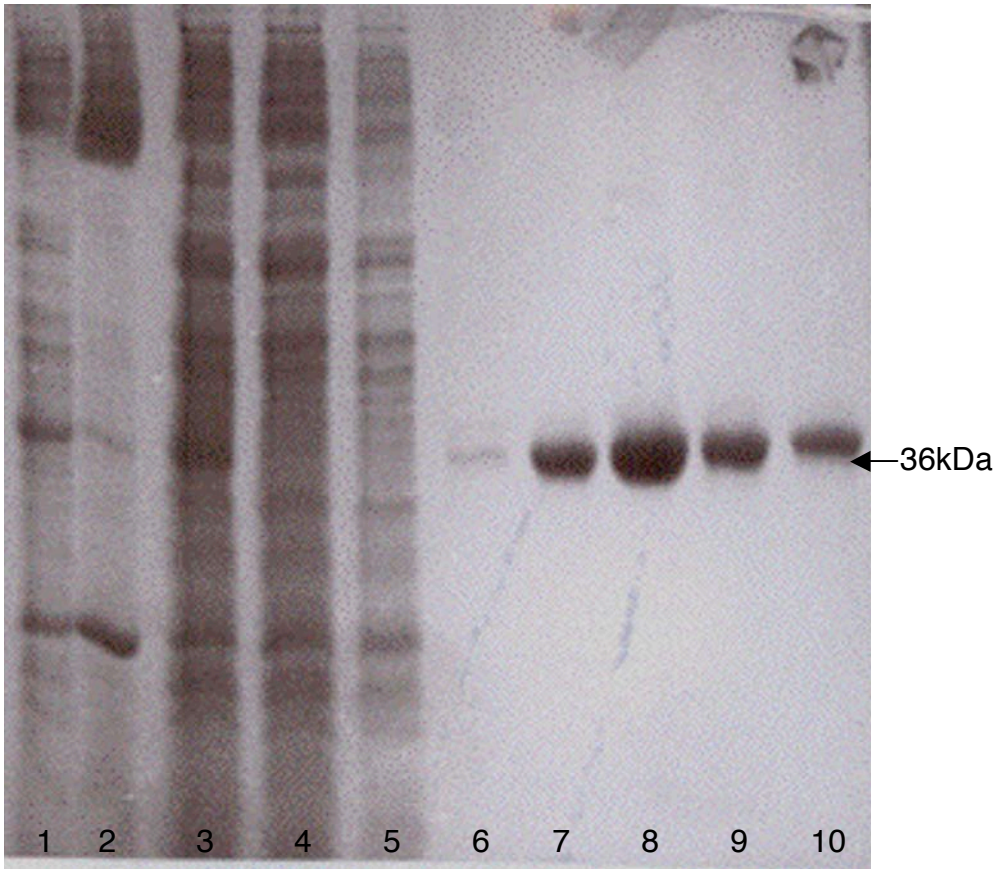

Figure 5.1: Coomassie stained SDS gel after affinity purification
Lane 1 Membranes, Lane 2 unsoluble fraction, Lane 3 soluble fraction, Lane 4 flow through, Lane 5 column wash with 10mM imidazole (all 20□gs), Lanes 6-10 different fractions of purified protein.
The arrow indicates the migration of 36kDa marker.

The cleavage of the histidine tag was achieved by digestion with thrombin. Different concentrations of thrombin were used for a protein concentration of 1mg/ml and incubated overnight, at room temperature. Cleavage of the histidine tag was confirmed by Western blot using anti-his antibody and the size difference was also observed on SDS gel (Figure 5.2A)

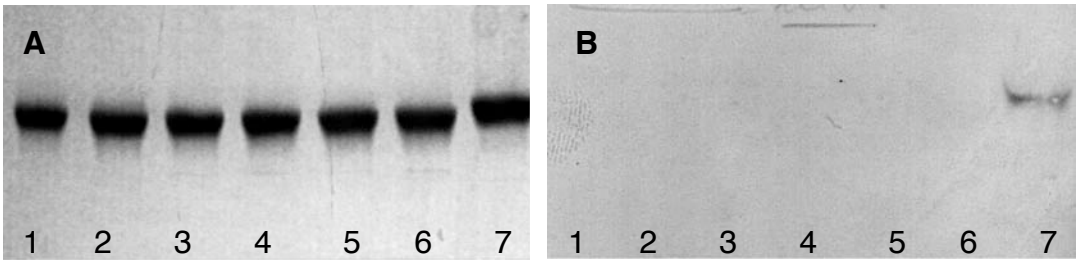

Figure 5.2: Cleavage of histidine tag by thrombin
A – Coomassie stained SDS gel, B - Western blot with anti-his antibody. Lanes 1 to 6 – increasing concentration of thrombin 0.5,1,2,3,4 & 5 units respectively. Lane 7 – undigested protein

5.1.2 GEL FILTRATION OF CaiT

For analytical gel filtration a calibrated Superose 6 column was used in combination with the SMART system. 50□g of protein was loaded for analysis.

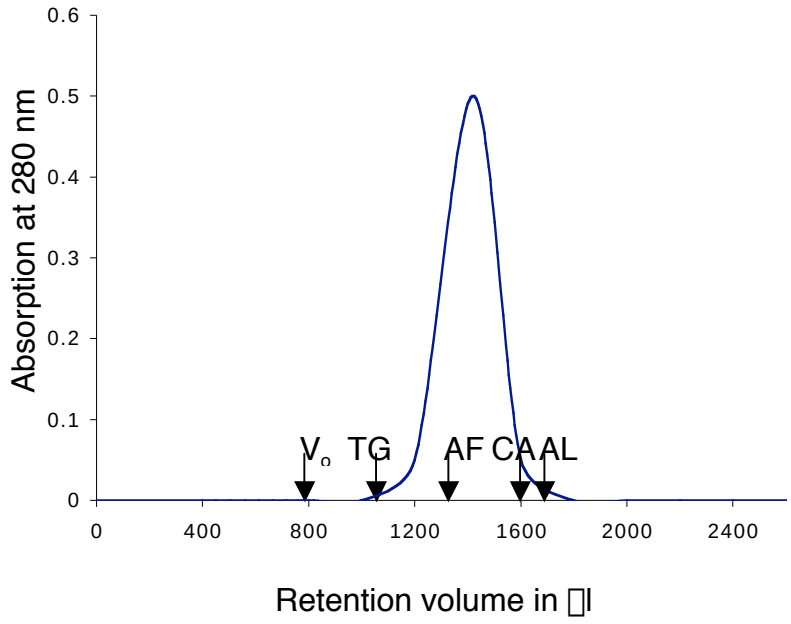

Figure 5.3: Gel filtration profile of CaiT on a Superose6 column. Elution volume of standard proteins of known Stokes radius are indicated: TG, thyroglobulin (86Å); AF, apoferritin (63Å); CA, catalase (52Å); AL, aldolase (46Å).

The retention volume in the analytical gel filtration indicated a possible oligomeric state of the protein, with CaiT eluting at ~1.42ml corresponding to a Stoke's radius of ~63Å (apoferritin). No aggregate peak was observed under normal conditions, however when buffer without reducing agent was used, a peak close to the void volume was observed. For large-scale purification a Superdex 200 column (16/20) was used prior to crystallization.

5.1.3 BLUE NATIVE GEL ELECTROPHORESIS

The oligomeric state of CaiT was further analyzed by blue native gel electrophoresis. The protein migrates a little higher than catalase (236kDa) that was used as marker. Addition of SDS prior to loading in the gel resulted in a single band migrating at ~75kDa. No change in oligomeric state was observed with the addition of substrate.

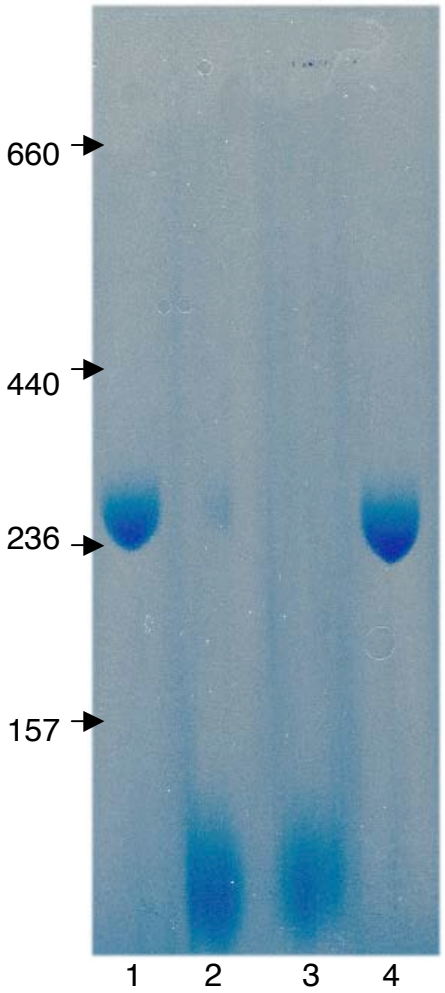

Figure 5.4: Blue native gel electrophoresis of CaiT

Lane 1- Protein in DDM

Lane 2,3 – 1% and 2% SDS added before loading in the gel

Lane 4- Protein with 25mM carnitine

5.1.4 STABILITY OF PROTEIN IN DIFFERENT DETERGENTS

After solubilizing the membranes with DDM, the protein was exchanged to the desired detergent at 2 to 3 times the CMC on the affinity column. The protein purified in different detergents was then analyzed by various methods, to assess its secondary and tertiary structure.

5.1.4.1 CD SPECTROSCOPY

CaiT in different detergents was analyzed at pH8. CaiT in DDM was used as the positive control while protein in guanidium chloride was used as a negative control. In presence of detergents such as LDAO or zwittergent 3-12, CaiT was unstable. A loss of helical content accompanied by an increase in random coil was observed (Figure 5.5, Table 5.1).

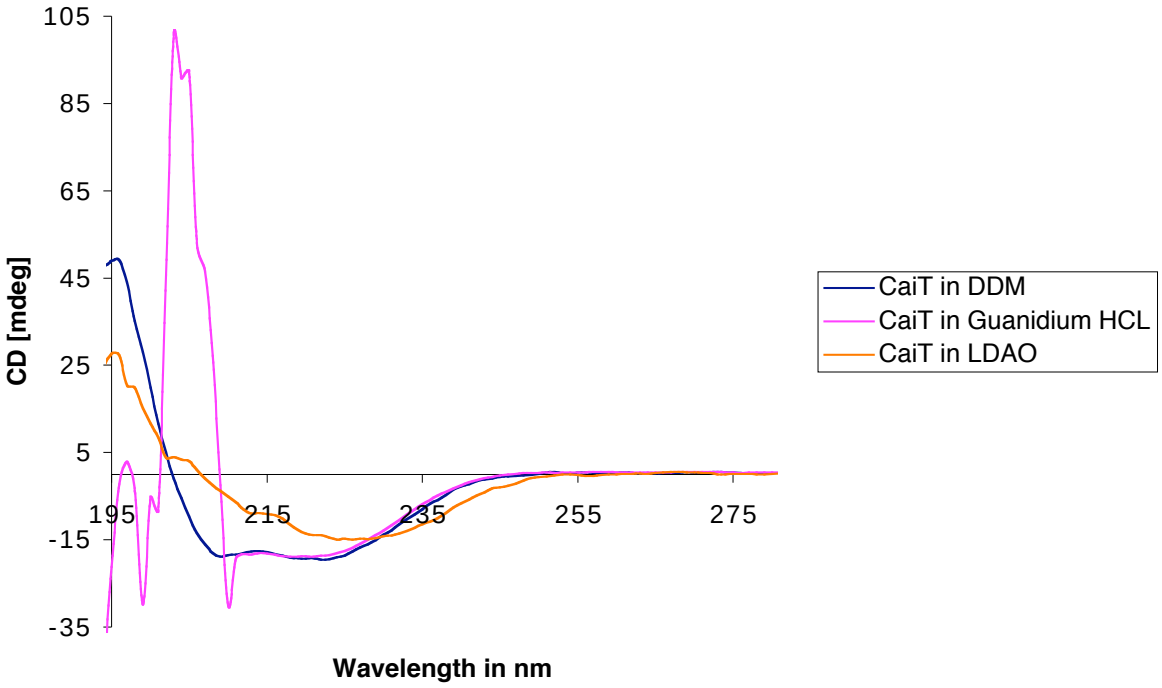

Figure 5.5: CD spectrum of three different samples of CaiT in nonionic detergent, denaturant and zwitterionic detergent.

The following table shows the estimated amount of secondary structure present in different detergents.

TABLE 5.1:

	% secondary structure in different environment			
	DDM	LDAO	GuHCl	ZW 3-12
□-helix	98.1	60.8	47.1	28.9
□-sheet	0.6	7.5	10.9	19.2
turn	5.4	12.1	12.4	16.9
random coil	1.8	19.7	31.1	38

5.1.4.2 FLUORESCENCE SPECTROSCOPY

The substrate-binding site of CaiT has numerous tryptophans (TM 8, Figure 1.11). Upon addition of substrate a conformational change occurs that can be followed by fluorescence spectroscopy (Jung et al 2002). The emission maximum of protein in DDM was 330 nm. Addition of substrate resulted in red shift by 4nm accompanied by increase in fluorescence. In contrast a similar compound such as choline produced a small increase in fluorescence, with no change in the emission maximum.

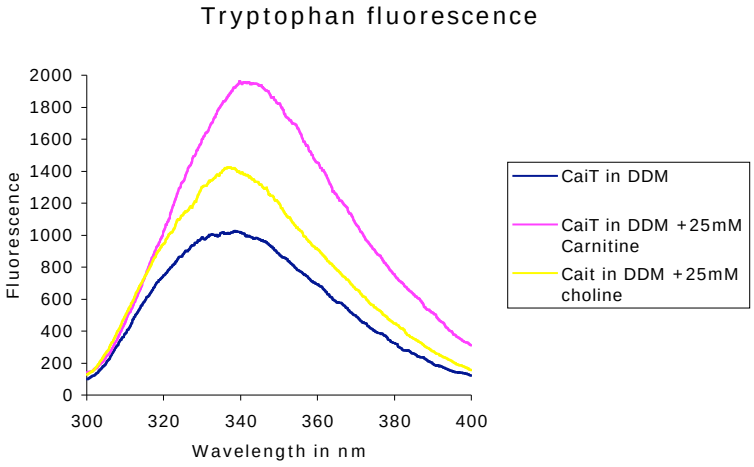

Figure 5.6: Substrate induced internal tryptophan fluorescence change in CaiT.

The emission maximum of tryptophan fluorescence changes, depending on the environment. This was used to analyze the stability of CaiT in different detergents. Completely denatured protein such as in guanidium showed a maximum fluorescence at 350 nm, similar to tryptophan measured in aqueous solution. Detergents like LDAO, OG and zwittergent 3-12 yielded similar spectra to guanidium. Detergent with maltoside as head group with carbon chain length of 10 or more showed a spectrum with a maximum at 330 nm and a red shift was observed upon substrate addition. In contrast, addition of substrate to protein in LDAO or guanidium showed no shift in the emission maximum.

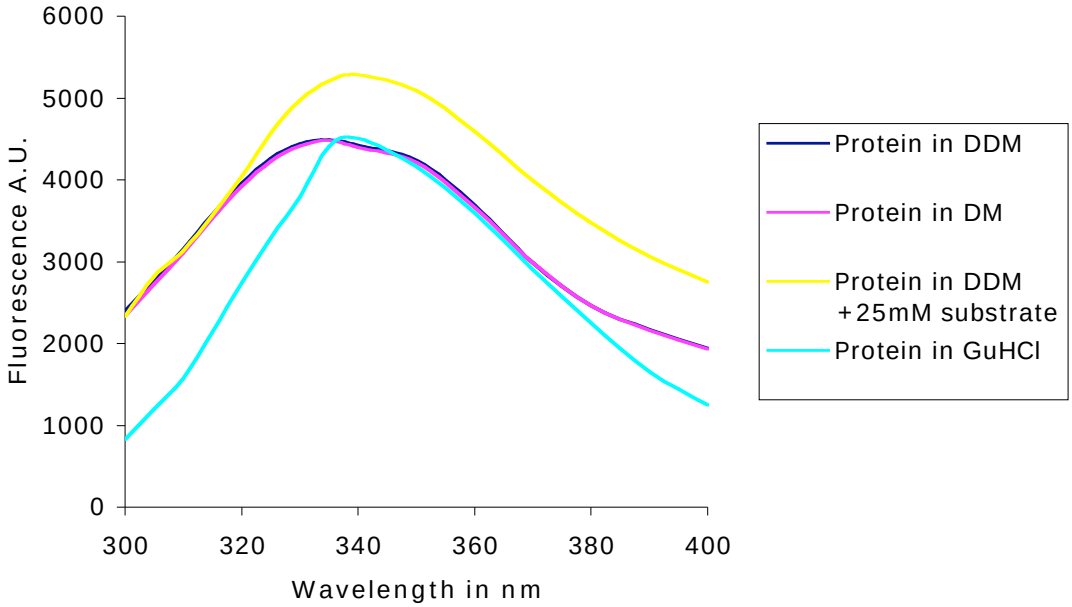

Figure 5.7: Fluorescence spectra of CaiT in different detergents

5.1.4.3 OLIGOMERIC STATE OF CaiT IN DIFFERENT DETERGENTS

To verify if CaiT forms higher aggregates in a particular detergent blue native gel electrophoresis was carried out.

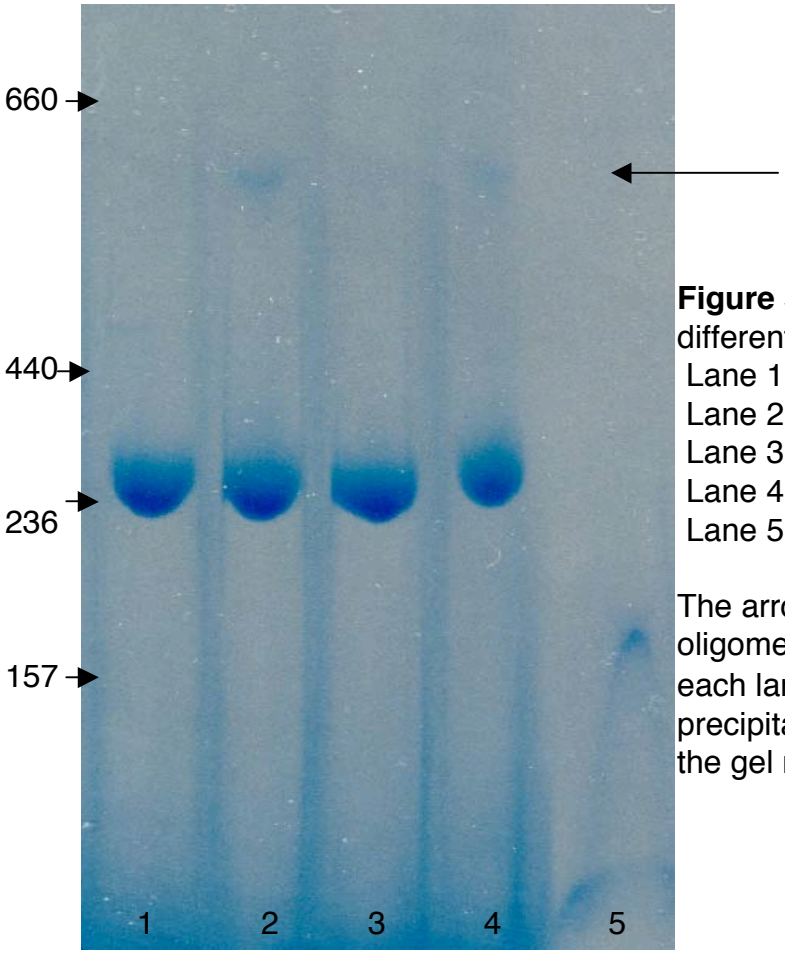

Figure 5.8: The stability of CaiT in different detergents.
Lane 1-Protein in DDM
Lane 2-Protein in DM
Lane 3-Protein in cymal6
Lane 4-Protein in nonyl glucoside
Lane 5-Protein in zwittergent 3-12

The arrow indicates the formation of higher oligomer. 5□g of protein was loaded in each lane. Protein in zwittergent 3-12 precipitates immediately, when loaded in the gel no band is observed.

As shown in figure 5.4, CaiT migrates as a single band on blue native gels. Detergents that do not keep the protein stable such as zwittergent 3-12 showed no visible band (Figure 5.8, Lane 5). Detergents with a carbon chain length >10 showed a single band migrating a little above catalase. Detergents with a carbon chain length of 9-10 showed an additional band, possibly a higher oligomer (Figure 5.8, Lane 2,4). CaiT preferred detergent with maltoside as a head group.

In the blue native gel, CaiT in polyoxyethylene detergents moved a little higher than with other detergents like maltosides or glucosides. This could be due to the bound detergent that had not been displaced by Coomassie (Figure 5.9).

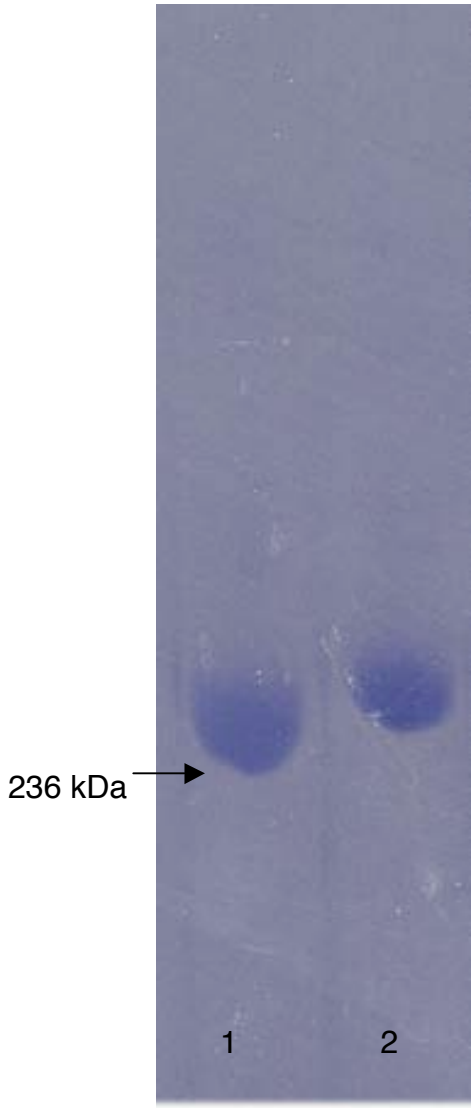

Figure 5.9: Blue native gel of CaiT in DDM (Lane 1) and in $C_{12}E_8$ (Lane 2). Equal amount of protein was loaded. The band corresponding in lane 2 is slightly shifted.
A similar shift was also observed with TX100 as detergent.

5.1.5 DISSOCIATION AND REASSOCIATION OF CaiT WITH SDS

The addition of SDS prior to loading onto the blue native gel resulted in the dissociation of the trimer into monomers (Figure 5.4). The question that occurred upon this observation was " is it possible to reassociate the monomers of CaiT into trimers by removing SDS? ". CD spectroscopy of CaiT in SDS-DDM mixed micelles showed no significant difference, indicating that

the secondary structure was largely preserved.

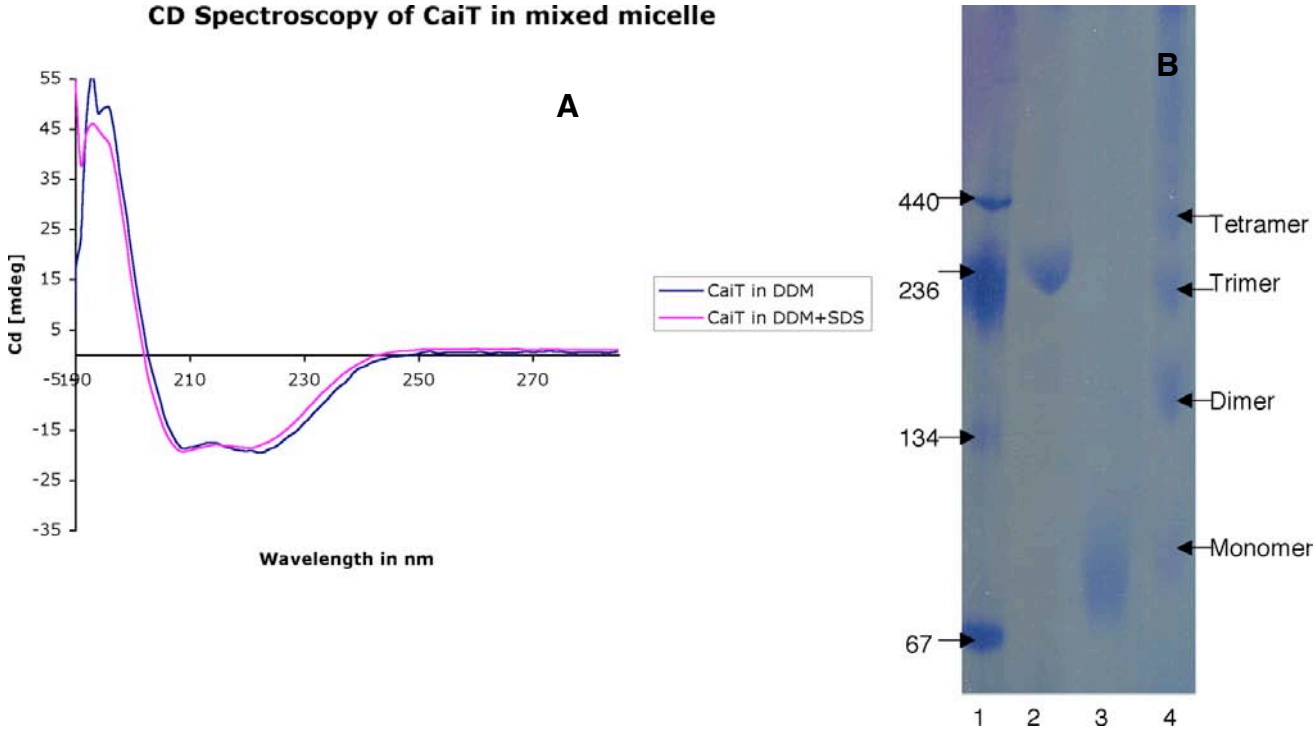

Figure 5.10 A: CD spectra of CaiT in DDM and in a mixed micelle of DDM +SDS

B: Blue native gel of CaiT in SDS-DDM mixed micelles.
Lane 1 – Marker, Lane 2 – CaiT in DDM, Lane 3 – CaiT in DDM +0.75% SDS incubated for five minutes before loading, Lane 4 – Oligomeric ladder of CaiT formed after dissociation with SDS followed by dialysis.
5□g of protein was loaded in lanes 2,3 and 4.

Dissociated trimers were dialyzed against a buffer containing only DDM to remove SDS and analyzed on a blue native gel. Interestingly, this sample formed a ladder of bands. Bands for monomers, dimers, trimers and tetramers were clearly distinguished. The band corresponding to the trimer in this ladder moved a little lower than the trimer of the native protein (Figure 5.10B, Lanes 2 and 4). No difference in the mobility of the monomeric band was observed. This indicated that SDS was not completely removed by dialysis but bound to the protein even after displacement by Coomassie stain, resulting in a slightly shifted band. However, this difference was not drastic and hence this ladder was used as calibration of the blue native gel.

5.1.6 LIPID ANALYSIS BY THIN LAYER CHROMATOGRAPHY

Lipid extracted from purified CaiT was analyzed by thin layer chromatography. One-dimensional separation showed two different peaks staining with both iodine and molybdenum blue. Based on the standards used these peaks were determined as phosphatidylethanolamine (PE) and phosphatidylglycerol (PG). Detergent was also present after extraction and stained only with iodine (Figure 5.11A, Lane 7). The peak corresponding to PE showed high variability even among standards (Figure 5.11A Lane 3 and 6). No peak corresponding to cardiolipin was found with the protein. The peaks of PE and PG were resolved more clearly on a 2D chromatogram.

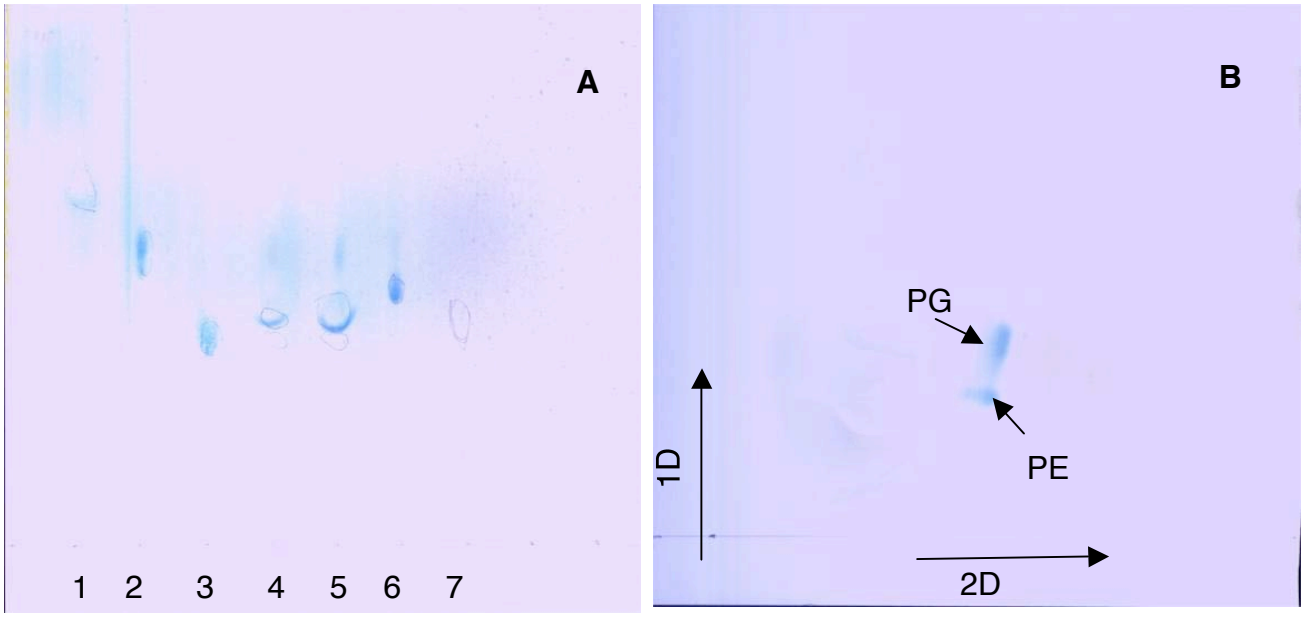

Figure 5.11: Thin layer chromatography of lipids associated with CaiT. A – 1D chromatogram developed with iodine vapor first and subsequently with molybdenum blue.
Lane 1 - cardiolipin, Lane 2 - PG, Lane 3 – PE (10 □g of each was loaded)
Lane 4, 5 - Lipid extract from CaiT (2 and 4□l)
Lane 6 – Extract of *E.coli* polar lipids (10□g),
Lane 7 - 2□l of 10% dodecyl maltoside

B – 2D chromatogram stained with molybdenum blue only

5.1.7 THERMAL STABILITY OF CaiT

The stability of CaiT with respect to increasing temperature was followed by CD spectroscopy. Three different protein samples were used. Protein that was completely denatured in guanidium HCl showed no significant change in the spectra with increasing temperature. Protein in DDM showed a sharp transition at around 70°C, above which rapid loss of helical content was observed. In contrast, protein in a mixed micelle of DDM and SDS where the protein exists as a monomer, showed a gradual loss in helical content.

The sharp transition of CaiT denaturation observed in CD spectra prompted me to analyze the effect of temperature on the oligomeric state of protein. No change in the oligomeric structure was observed when protein was heated at 55°C but at 75°C a slightly shifted diffuse band was visible. This was interpreted as a denaturation and aggregation of protein. This could possibly occur due to disruption of detergent micelles at higher temperature and/or a possible loss of interaction between the monomers in the trimer.

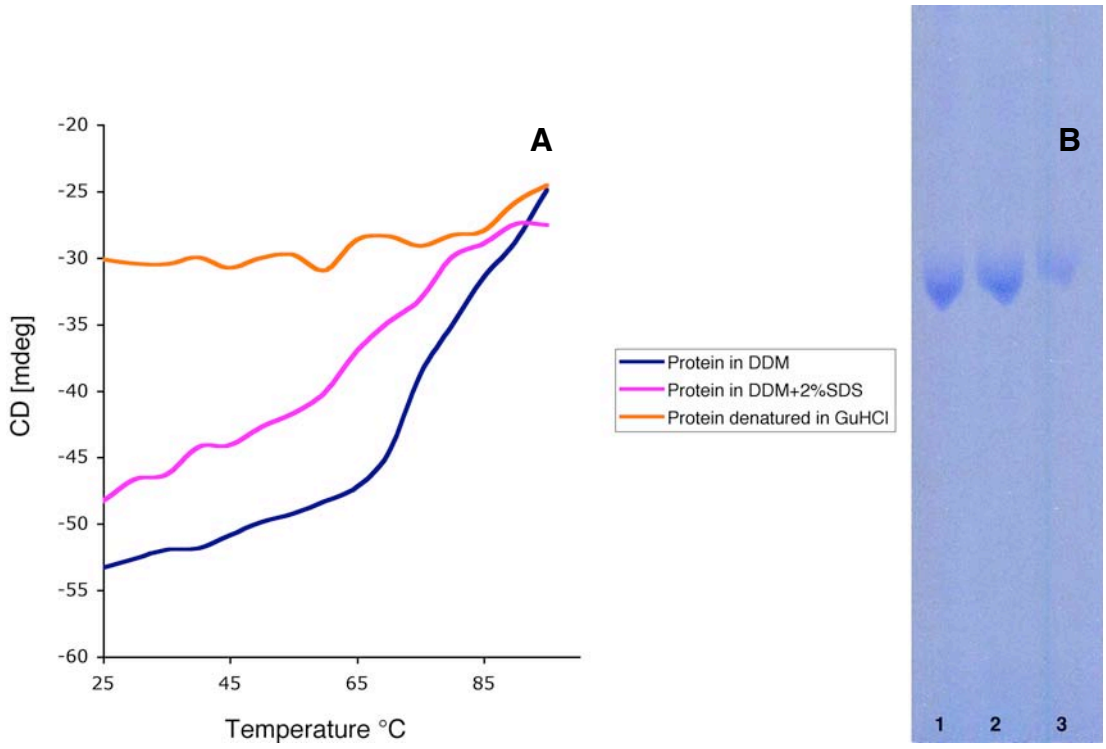

Figure 5.12: Thermal stability of CaiT
A - CD spectra of CaiT at 220 nm as a function of temperature in three different solutions. B - BN gel electrophoresis. Lane 1: Protein in DDM, Lane 2: Protein in DDM, heated at 55°C for 5 minutes, Lane 3: Protein in DDM, heated at 75°C for 5 minutes (equal amounts of protein was loaded).

5.1.8 2D CRYSTALLIZATION

The crystal screen and conditions described here were performed largely with C-terminal his tagged CaiT. The first strategy attempted for obtaining the 2D crystals was to determine the pH where the protein would tend to form an aggregate resulting in a 2D crystal. Purified CaiT was reconstituted into lipid bilayers made from *E.coli* polar lipids at different pH, but with a fixed LPR and ionic conditions. Vesicles were observed in wide pH range. Ordered arrays of protein were found only at pH above 7.5. At acidic pH, membrane structures resembling tubes and sheets were observed. However, these membranes were not ordered and in fact contained no protein when analyzed by the freeze fracture electron microscopy (Figure 5.13C). The small vesicles at this pH had protein incorporated and densely packed.

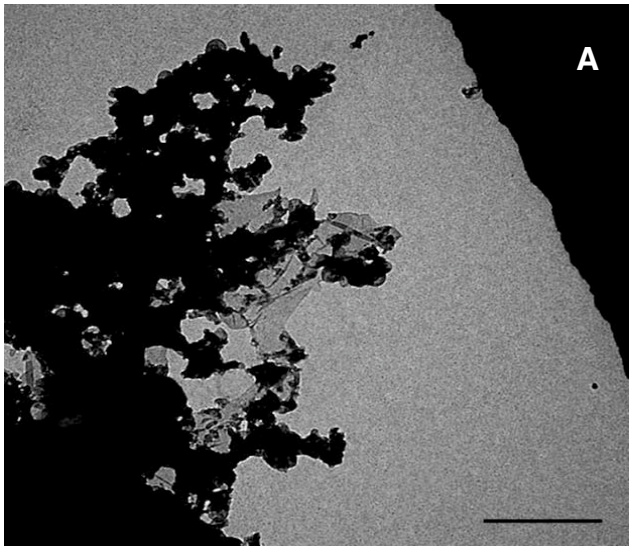

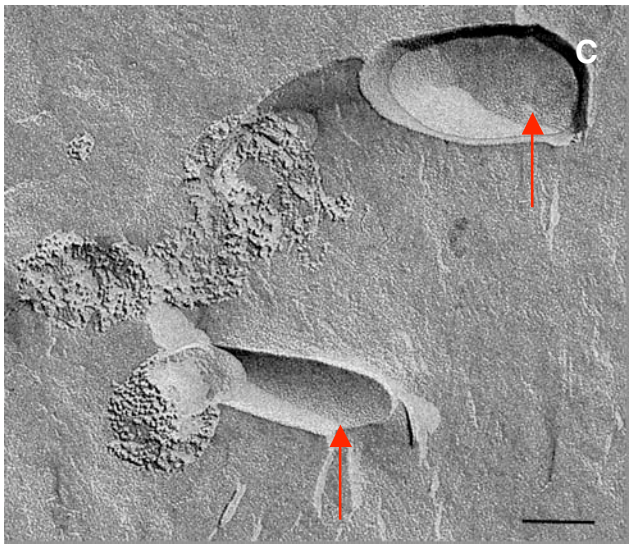

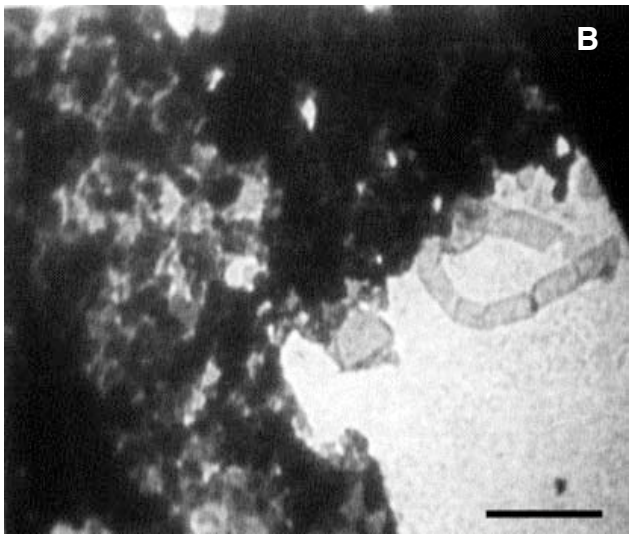

Figure 5.13: A and B – Membranes with sheet and tube like morphology observed at pH5.6 (scale bar -1□m).

C – Freeze fracture of the membranes showing protein incorporated in small vesicles but larger membranes with no protein (marked with red arrows). Scale bar is 100 nm.

The membranes at alkaline pH appeared in different morphologies with vesicles dominating. They measured up to a micron in diameter. They preferred to stack upon each other and one could observe as many as six different layers of ordered arrays.

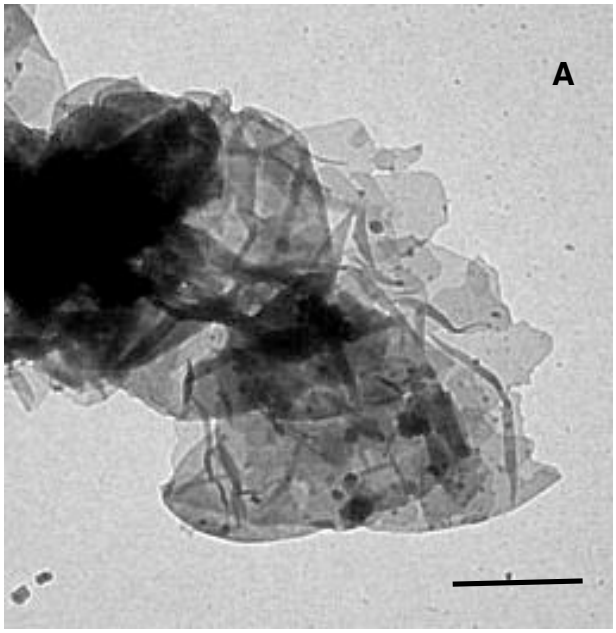

Figure 5.14: A - Negatively stained specimen showing the crystal morphology at pH9 (scale bar –1 □m).
B and C – Higher magnification of stacked crystals showing many different layers of membranes and the power spectrum (scale bar –100 nm).

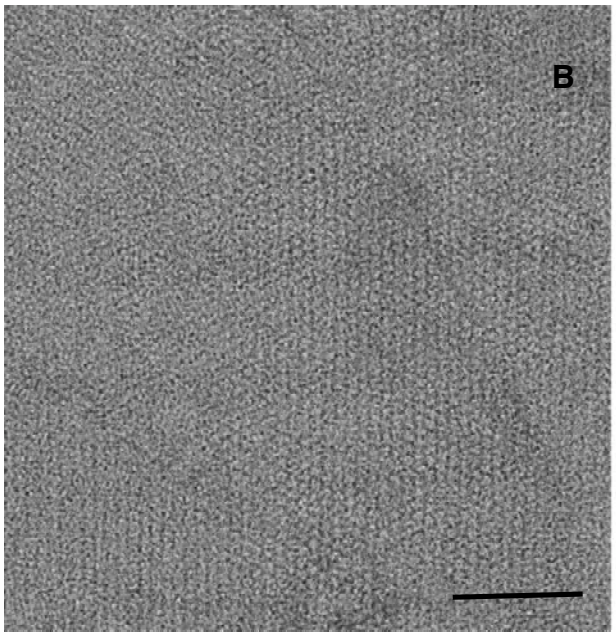

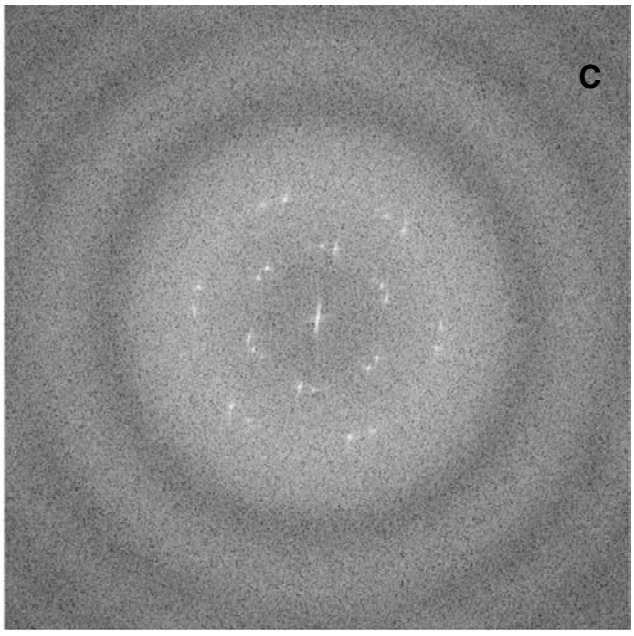

Occasionally tubular crystals were also observed. They were ~0.3-0.5 μm wide and up to an μm in length. As opposed to the hexagonal lattice obtained generally, these crystals had a rectangular lattice. However, they were difficult to reproduce and rarely found on a grid. These tubular crystals formed only with a particular detergent batch but the exact reason remained unclear.

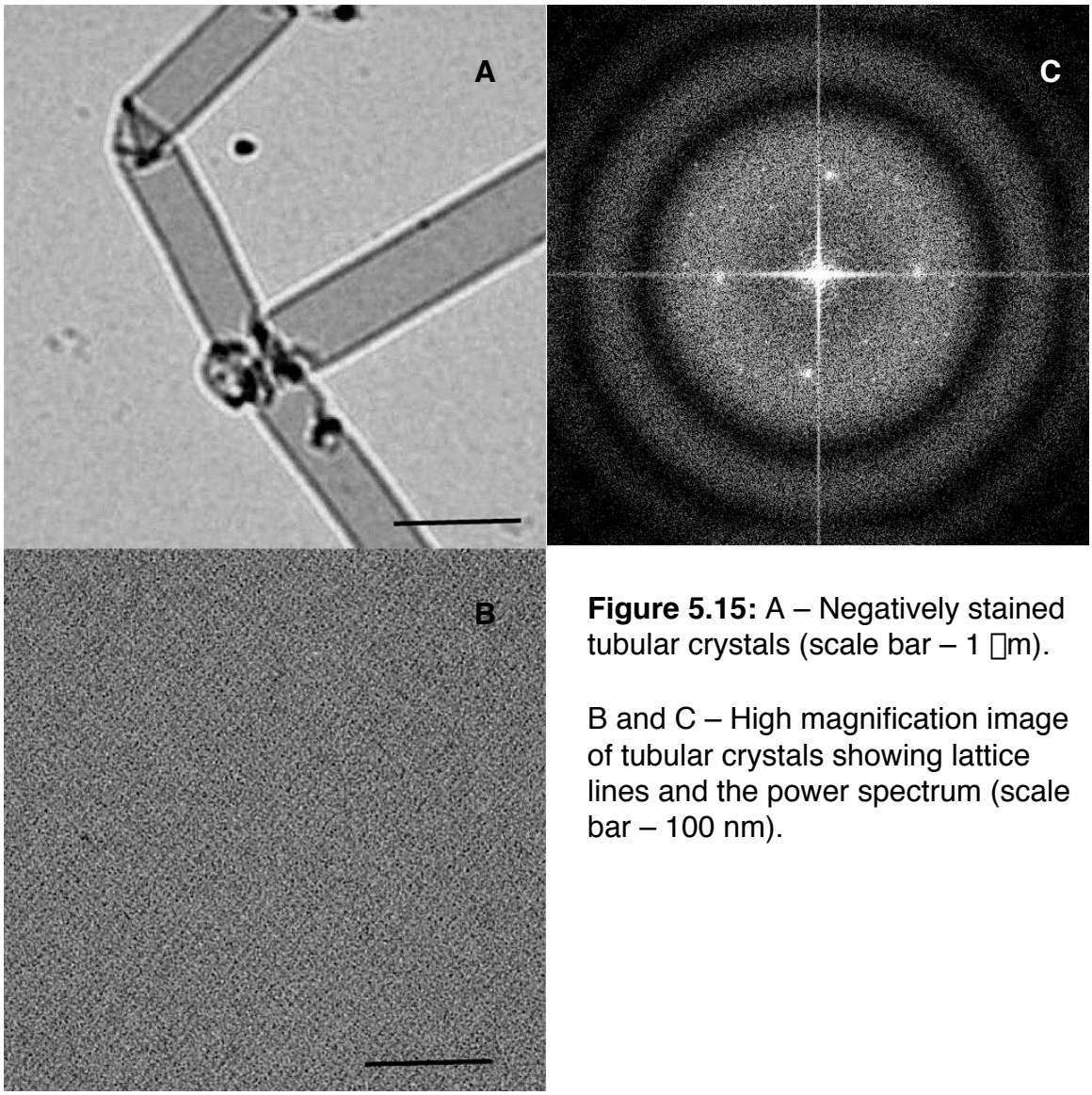

Figure 5.15: A – Negatively stained tubular crystals (scale bar – 1 μm).

B and C – High magnification image of tubular crystals showing lattice lines and the power spectrum (scale bar – 100 nm).

At low LPR around 0.2 (w/w) the membranes were small and poorly ordered. An optimal LPR was found between 0.4 - 0.5, while at higher LPR large empty vesicles formed. Since the crystals obtained had a tendency to

stack (Figure 5.14), a screen for lipids with different head groups and chain length was carried out. The screen indicated that negatively charged lipids such as PG or cardiolipin promoted the tendency to form stacks. When PE was used as the sole lipid apart from the stacked membranes, tube-like structures were also observed but they were poorly ordered.

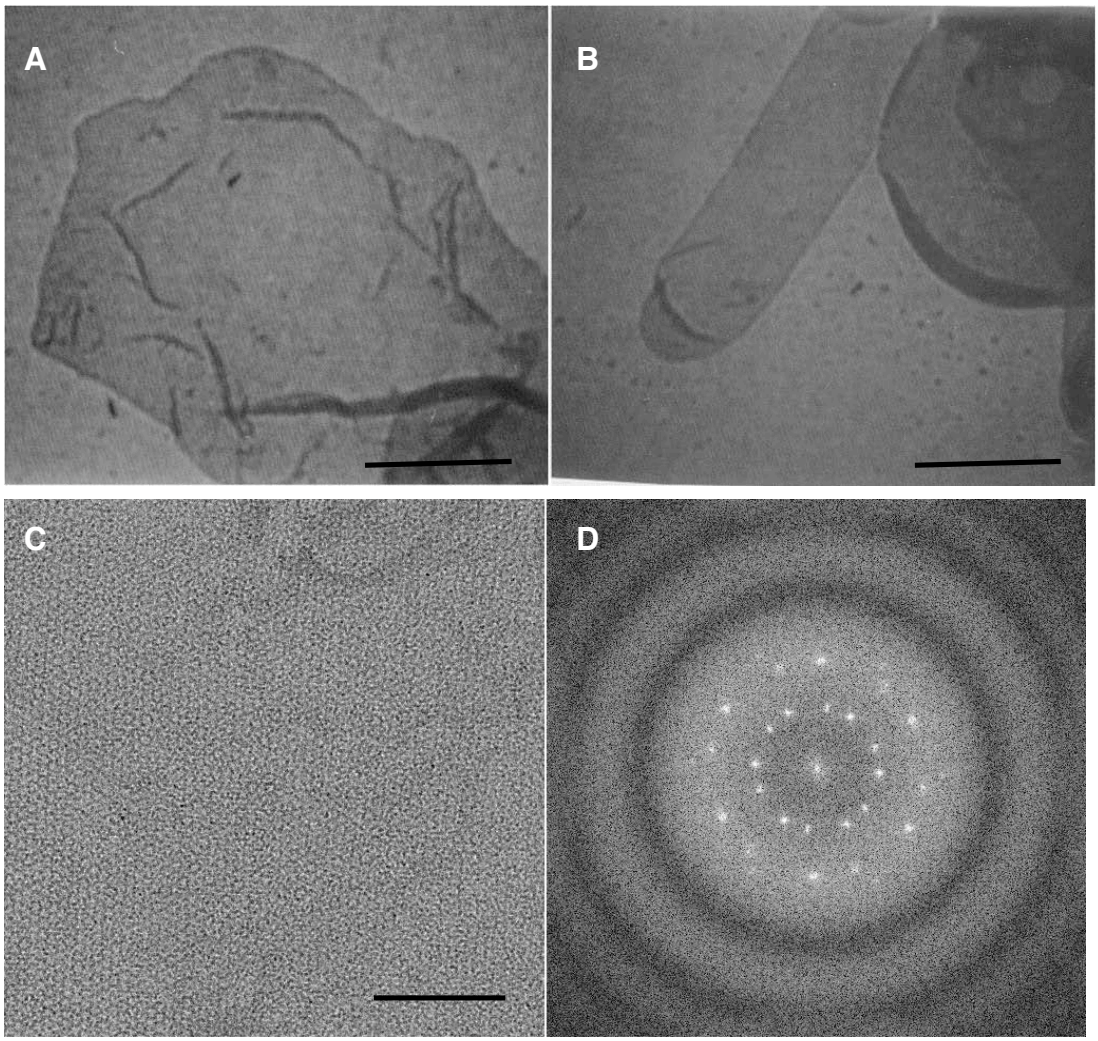

Figure 5.16: Different morphologies of crystals obtained during the screen of lipids.
A and B, multiple layered and tubular membranes observed with PE (scale bar - 1 □m).
C and D, Higher magnification image showing the numerous layers and the power spectrum (scale bar-100 nm).

Therefore neutral lipids were screened intensively. The best lattices were obtained with DPPC and POPC under similar conditions. These membranes were still vesicular in nature and measured on average 0.5-1 □m. Crystals obtained in this way were better ordered. Many of these membranes had only two layers but some stacks were also found (Figure 5.17A and B). The resolution was however limited to 20-22Å.

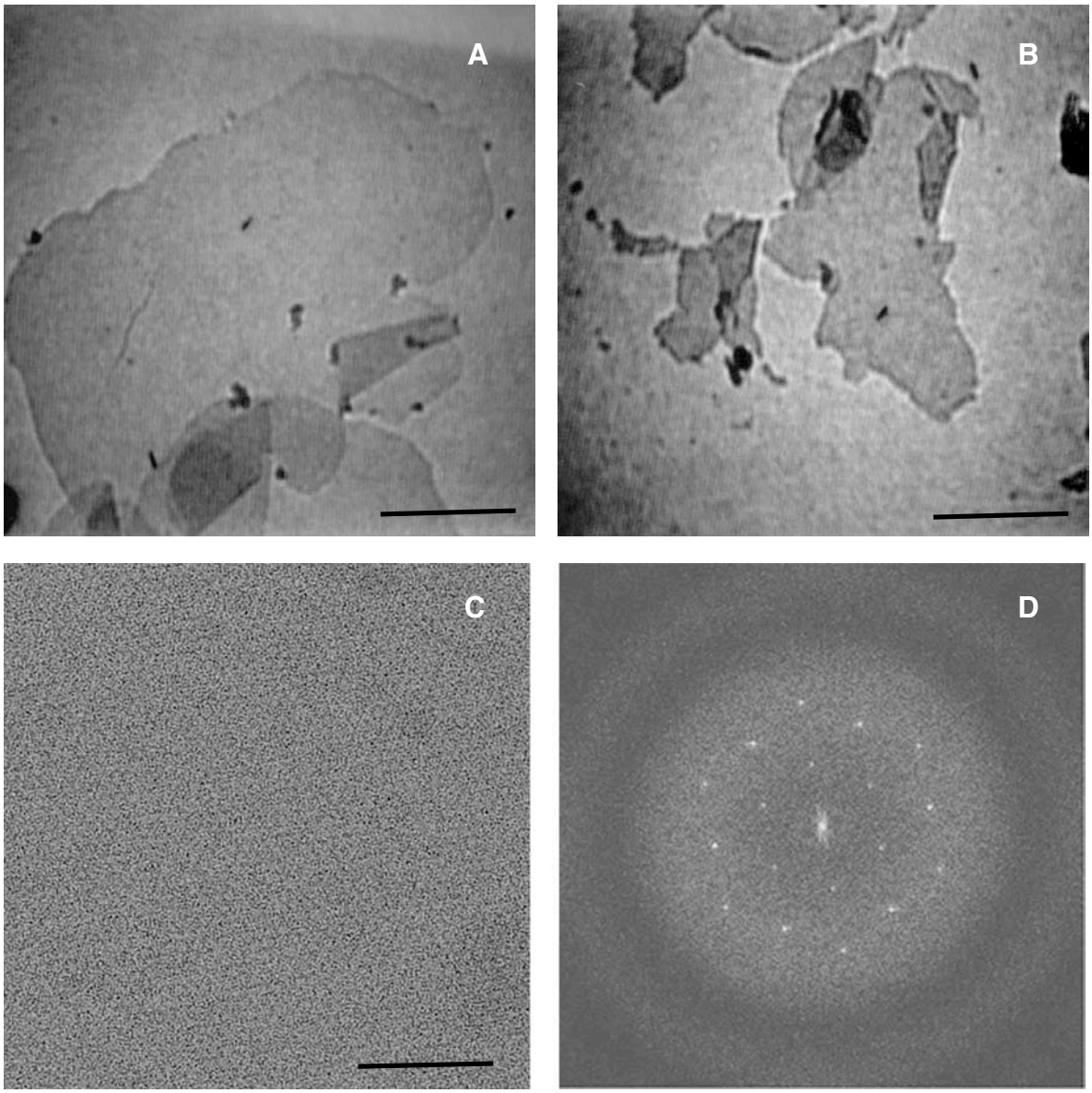

Figure 5.17: A and B – negatively stained membranes from POPC lipids showing large isolated as well as clumped membranes (scale bar – 1 □m) C – Higher magnification image of vesicles with only a single lattice evident (scale bar 100 nm). D - Power spectrum of the same membrane showing the hexagonal lattice.

The unit cell of the crystals from the stacked membranes was a=b=96Å □=120°, while that of isolated vesicles had a slightly smaller unit cell with a=b=93Å. The crystals from different lipids all had similar unit cells. The program ALLSAPCE indicated that both stacked membranes and isolated vesicles had three-fold symmetry while the stacked membranes exhibited higher symmetries such as P6 and P622. Images from the isolated vesicles were merged and a projection map at 25Å was calculated with symmetry applied (Figure 5.18). The approximate dimension of the trimer calculated from the projection map was ~90Å and the diameter of a monomer density was ~38Å.

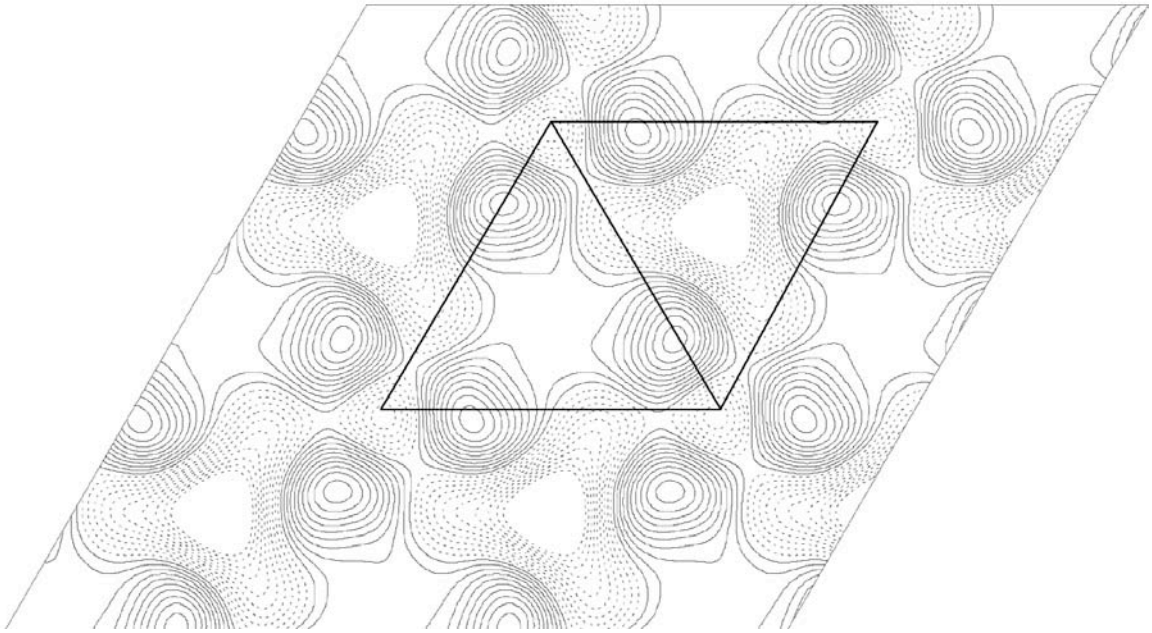

Figure 5.18: A projection map of negatively stained 2D crystal of CaiT at 25Å with P3 symmetry applied.

5.1.9 3D CRYSTALLIZATION

CaiT in DDM, either affinity purification or gel filtration yielded 3D crystals. The final concentration of DDM was critical for obtaining crystals reproducibly. When protein was concentrated to 10mg/ml using a 100kDa cut off, the final DDM concentration was measured as ~0.5% (by phenol-sulfuric acid method). It was necessary to dialyze the protein against a glycerol and salt free buffer to obtain bigger crystals. CaiT formed 3D crystals readily under different conditions. Many different polyethylene glycols gave crystals in a pH range 5.6-7. Crystals appeared with different morphologies in three to four days and measured on an average 0.25x0.3 mm. The size and the identity of the protein in the crystals were verified by SDS gel (Figure 5.19).

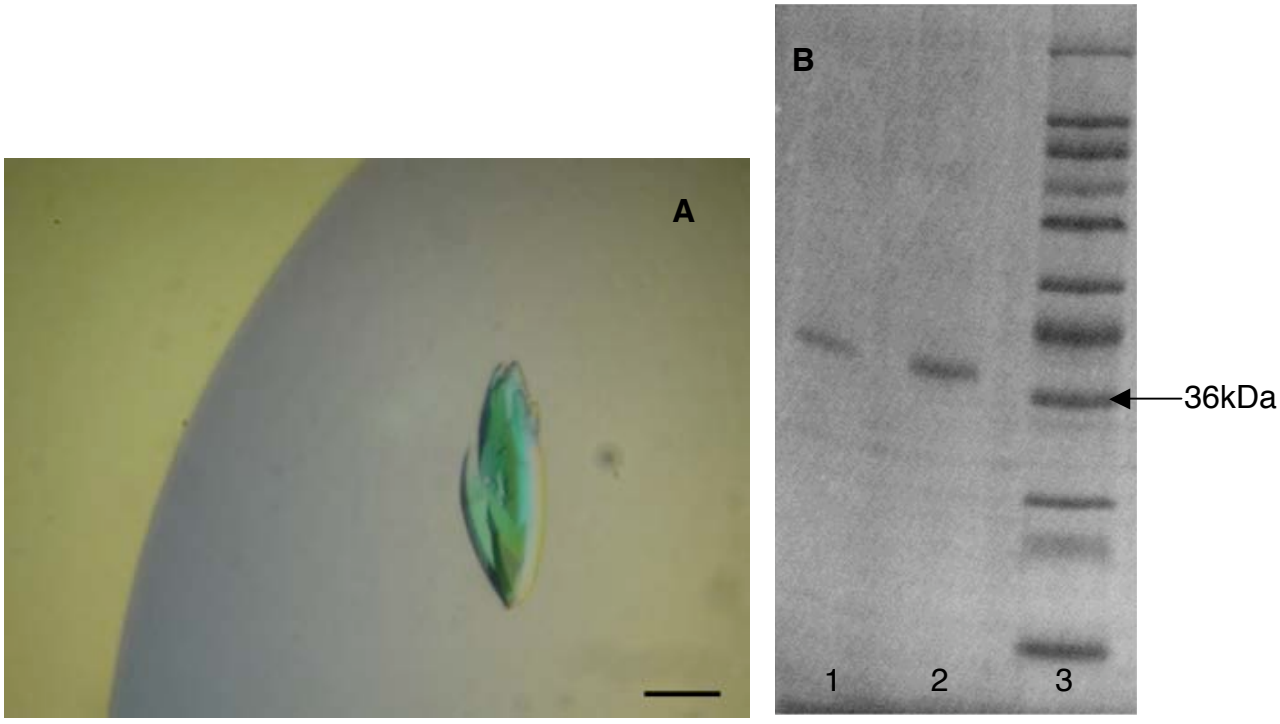

Figure 5.19: A – Picture of a multiple crystal (scale bar – 100 □m)

B – SDS gel showing that the crystal consists of CaiT. Lane 1,2 – two different crystals. Lane 3 is Sigma wide range marker.

Initial crystals obtained were multiple in nature (Figure 5.19A). Optimization of the final protein and detergent concentration yielded single crystals (Figure 5.20). Some of these crystals when checked by blue native gel electrophoresis showed the presence of the trimeric band. Many of these crystals diffracted to 7Å generally, with weak spots visible further to 6Å (Figure 5.21).

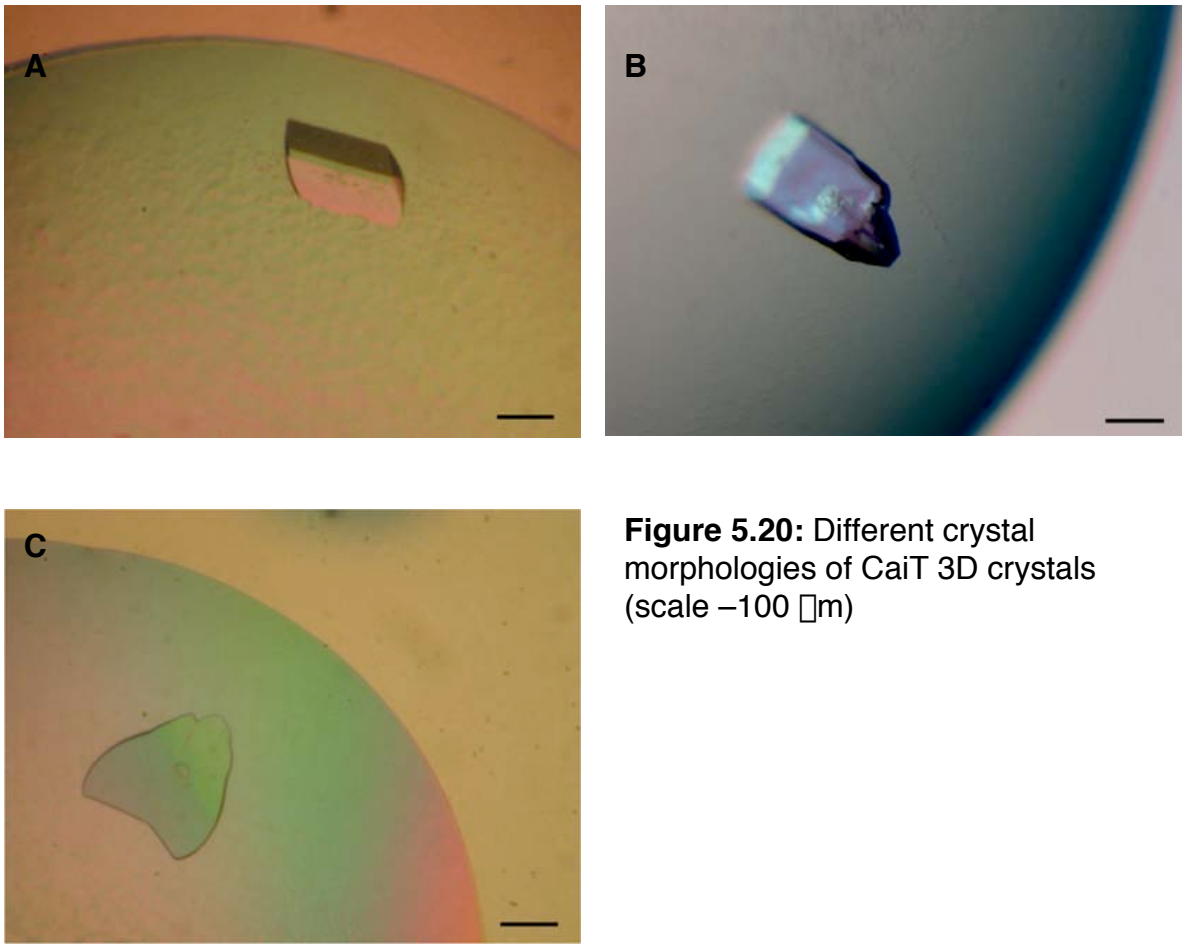

Figure 5.20: Different crystal morphologies of CaiT 3D crystals (scale –100 □m)

The diffraction pattern from some of the better crystals could be indexed. Initial analysis shows that they belong to the primitive monoclinic crystal class. The unit cell was a=123.94 b=136.60 c= 243.19, □ =107.69 with a distortion index of 0.28% as determined by DENZO.

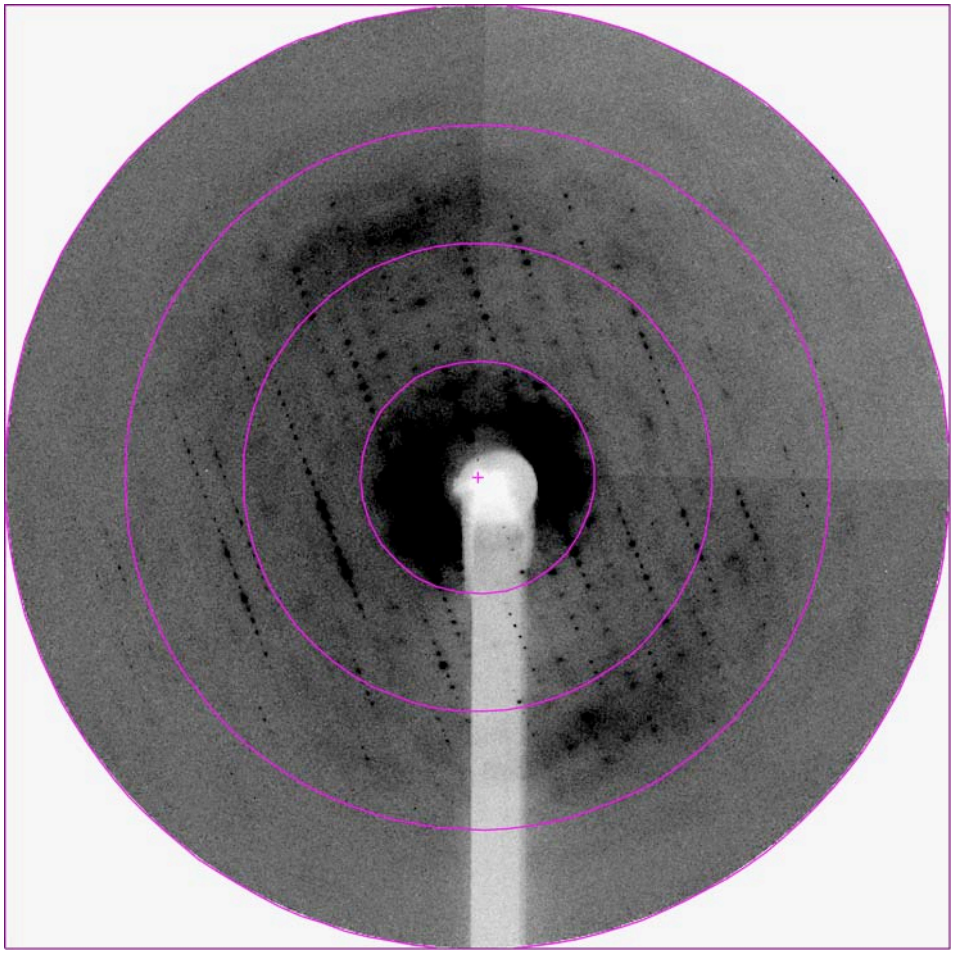

Figure 5.21: Diffraction pattern of one of the better crystals of CaiT. The circles correspond to a resolution of 22.8, 11.4, 7.6 and 5.7Å from the center.

Further screening with many different conditions including different PEGs, salts or additives that change the property of detergent micelle did not improve the order of the crystals. Use of mixed micelle was the next approach tried to improve the crystal. Prior to crystallization a fixed amount of second detergent of same class or different was mixed with the protein solution. The rationale behind this approach was that a mixture of detergent might promote better crystal contacts by reducing the size of the bulky micelle such as DDM. Screening a combination of detergents could be laborious and would require an enormous amount of protein and time. To reduce the number of detergents for this approach, the stability of the protein in a mixed micelle of DDM with different detergents was analyzed by blue native gel electrophoresis. The concentration of the second detergent was chosen to match its CMC and mixed with protein solution, incubated at room temperature for 20 minutes before loading on the gel.

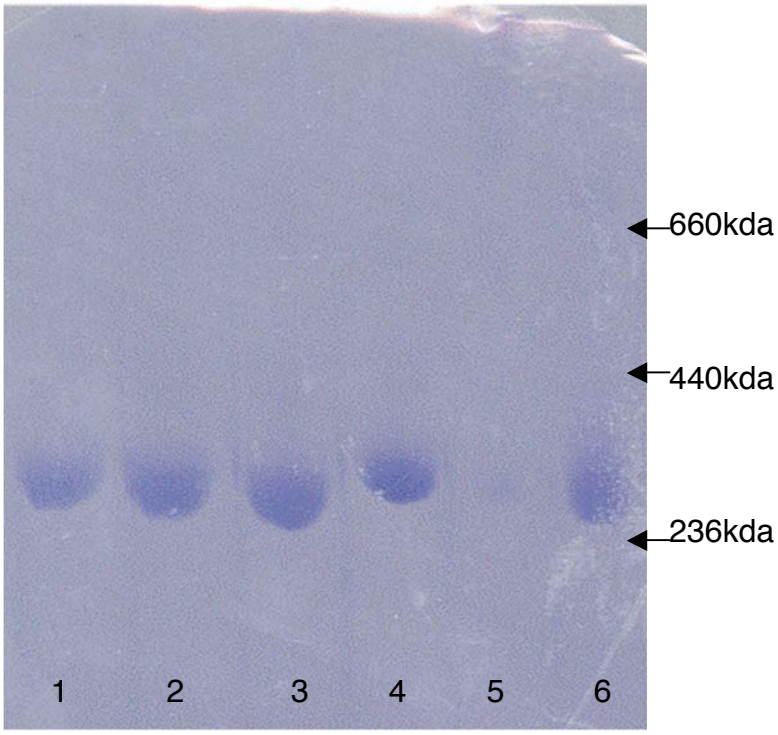

Figure 5.22: Blue native gel Electrophoresis of CaiT in Mixed Micelles
Lane 1 - Protein in DDM, Lane 2 - Protein in DDM+DM, Lane3 - Protein in DDM+Cymal5, Lane 4 - Protein in DDM+$C_{12}E_9$, Lane 5 - Protein in DDM+CHAPS, Lane 6 - Protein in DDM+OG

CaiT was stable in mixture of detergents with similar head groups or chain length (Lane 1 to 4) while chemically different detergents such as CHAPS resulted in aggregation. This trend was also observed in the crystallization behavior. The following table summarizes the effect of a second detergent on the stability and crystallization.

Table 5.2:

Detergents	Stability of protein	Crystals
DM	++	++
$C_{12}E_8$	++	++
CHAPS	-	-
Cymal 5 or 6	++	++
OG	+	-
LDAO	-	-
MEGA 9	+/-	-

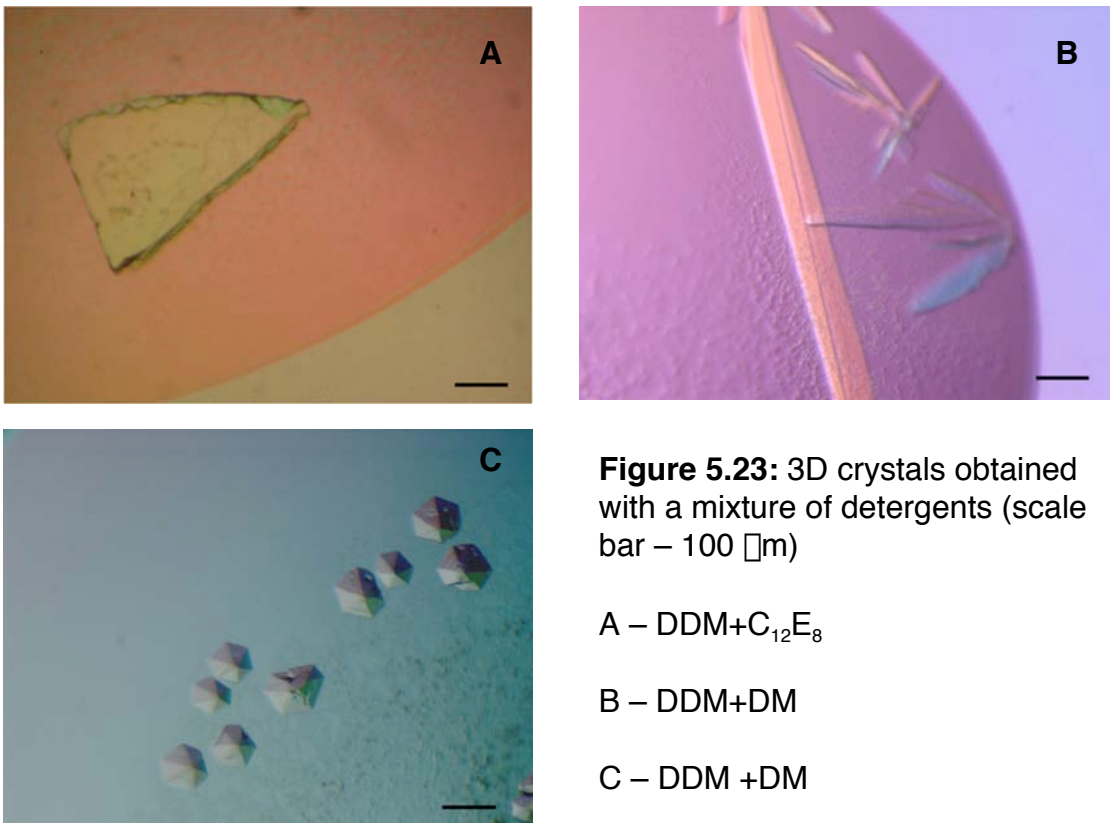

Figure 5.23: 3D crystals obtained with a mixture of detergents (scale bar – 100 □m)

A – DDM+$C_{12}E_8$

B – DDM+DM

C – DDM +DM

5.2 DISCUSSION

5.2.1 EXPRESSION AND PURIFICATION OF CaiT

CaiT expressed with either an N or C terminal histidine tag yielded comparable amounts of protein under standard growth conditions. The use of an imidazole gradient increased the purity of the protein. CaiT was stable in DDM micelle for 4-5 days at 4°C as judged from the ability to form aggregates and proteolysis by SDS gel. A minimal amount (0.5-1 unit) of thrombin was sufficient to cleave the tag from N-terminus without proteolysis of CaiT (Figure 5.2). A further step of purification in a gel filtration column yielded a single homogenous peak. Prior to crystallization, internal tryptophan fluorescence was used to check to stability of the protein (Figure 5.6).

5.2.2 OLIGOMERIC STATE OF CaiT

The retention time of CaiT on a calibrated gel filtration column was 1.42ml, close to apoferritin (440kDa) with a Stoke's radius of ~63Å. When compared with other membrane proteins with known oligomeric structure (dimeric MjNhaP1 [Chapter 3] and monomeric OmpG [Chapter 6]) the gel filtration profile of CaiT suggested a possible oligomeric state. The molecular weight of CaiT calculated from the amino acid sequence corresponds to 57.4kDa, and a CaiT trimer would have a molecular weight of 174kDa. For secondary transporters with multiple membrane spanning helices, the amount of detergent (DDM) bound is in the range of 150-180 per monomer, (Heuberger, Veenhoff et al. 2002) corresponding to ~70-90 kDa. The amount of bound detergent is thus critical to interpret the gel filtration profile. If one assumes an average of 160 molecules of DDM bound per monomer of CaiT, then the observed elution time would correspond to a trimer (~420 kDa) (Figure 5.3) rather than a dimer or tetramer (~277 or 554 kDa respectively).

In the blue native gel electrophoresis, CaiT migrates slightly above 236 kDa. The amount of CBB that displaces the detergent has been calculated to be ~1.8 for membrane proteins with 12 TM helices (Heuberger et al. 2002).

The observed mass of CaiT would correspond to a ratio of ~1.4 if it were a trimer. I did not measure the amount of Commassie stain that displaces the detergent. Hence it was essential for me to explain the observed masses in the blue native gel in an alternative way. Addition of substrate had no effect but the observed band of CaiT in DDM could be dissociated with anionic detergent SDS to an approximate mass of 74kDa (Figure 5.4).

5.2.3 DISSOCIATION AND REASSOCIATION OF CaiT

The main goal of this particular experiment was to verify if the dissociated protein monomers could reassociate spontaneously into a defined oligomer upon removal of SDS. Addition of SDS to the protein in DDM results in a mixed micelle. The carbon chain length of both these detergents are same and they have been shown to form mixed micelle although the head groups are different. It is well known that membrane proteins do not completely denature in SDS and tend to maintain the secondary structure to a large extent (Otzen 2002). A similar observation was made with CaiT in a mixed micelle of SDS and DDM (Figure 5.10A). The dissociation is presumably due to the disruption of the ionic interaction between protein monomers or lipid molecules. After dissociation and removal of SDS by dialysis, the protein was rebound to a nickel column and washed with buffer with or without lipids. Unfortunately, binding of SDS was so strong with the protein that only a fraction of protein bound to the nickel column.

After dialyzing to remove SDS when the protein was analyzed by blue native gel electrophoresis, a ladder starting with a monomer was observed. I took advantage of this to calibrate the mass observed in the blue native gel (Figure 5.10B). In this ladder the band corresponding to a trimer migrated a little lower than the native protein. This may be due to bound SDS that has not been displaced by Coomassie. But this difference was very small and therefore the ladder could be used for determining the oligomeric state of not only CaiT but also for other membrane proteins.

5.2.4 STABILITY OF CaiT IN DIFFERENT DETERGENTS

Choice of the right detergent is one of the most critical parameter for successful crystallization of membrane proteins. Stability of CaiT in different detergents was analyzed by multiple approaches. CD and internal tryptophan fluorescence yielded information on the secondary structure. The CD spectrum of protein in DDM shows ~95% helical content while detergents like LDAO show a loss in helical content and an apparent instability in this and other zwitterionic detergents (Figure 5.5 and Table 5.1). In both these experiments completely denatured protein in guanidium HCl was used as a negative control. A similar result was obtained with fluorescence spectra (Figure 5.6 and 5.7).

The formation of higher aggregates was analyzed by blue native gel electrophoresis. Detergent with shorter chain lengths or smaller micelles tends to form higher aggregates. CaiT in zwittergent showed no distinct band indicating complete denaturation. In summary CaiT prefers detergents with maltoside as head group with a carbon chain length of 10 or more. Polyoxy ethylene detergents were equally good in preserving the protein in solution. In blue native gel CaiT in $C_{12}E_8$ moved a little higher than the protein in DDM (Figure 5.9) that might be due to undissociated detergent molecules.

5.2.5 TRIMER IS THE STABLE FORM OF CaiT

For other transporters such as LacS (Heuberger et al 2002), an equilibrium between monomer and dimer has been observed whereas a detergent mediated change in the oligomeric state was found for SecYEG from *E.coli* (Bessonneau, Besson et al. 2002).The trimer of CaiT is very stable and dissociates only upon addition of SDS. The high stability may be due to the ionic interaction between the protein monomers or to lipid-protein interactions. In fact, negatively charged lipids have been shown to be important in the stability of oligomers such as KcsA (Valiyaveetil, Zhou et al. 2002) and LHCII (Standfuss and Kühlbrandt 2004). The structures of the AcrB

and GltPh suggest that the central region between trimers may be filled with lipids (Murakami et al 2002, Yernool et al 2004). When purified CaiT is subjected to lipid analysis, both PE and PG co-purifying with the protein is observed (Figure 5.11). The stability of the CaiT trimer could therefore be due to lipid-protein interactions.

5.2.6 THERMAL STABILITY OF CaiT

Oligomeric membrane proteins of mesophilic origin such as those of *E.coli* have been shown to be stable at high temperature around 70°C. Well-known examples are the trimeric outer membrane proteins of *E.coli,* which need to be boiled at 95°C for their dissociation into monomers (Rosenbusch 1974), and the prokaryotic potassium channel KcsA migrates as a tetramer in a denaturing gel, resisting the action of SDS. The stability of the tetramer in DDM with respect to temperature was analyzed by SDS gel (Perozo, Cortes et al. 1998). The mid point transition of KcsA dissociation into monomers was 73.2°C (protein in DDM).

The secondary structure of CaiT when followed at different temperatures showed a sharp transition at ~75°C when the protein was in DDM. While control protein sample in guanidium HCl showed no change and in a SDS-DDM mixed micelle showed a gradual loss in helical content (Figure 5.12A). CaiT does not migrate as a stable trimer on SDS gels but it could be observed by blue native gel that at 75°C the trimeric band tends to disappear, indication of denaturation (Figure 5.12B). Multiple explanations could be given for this observed transition in CD as well as in blue native gel that includes the disruption of the detergent micelle and or disruption of the interaction between the monomers or with lipids. It is interesting to note that both CaiT and KcsA co- purify with PG as lipid and behave similar with respect to stability with increase in temperature even though both proteins are structurally distinct.

5.2.7 2D CRYSTALLIZATION

The initial thought based on previous 2D crystallization conditions was to try and find the right condition on the opposite extreme of the theoretical isoelectric point (Chapter 7). The theoretical pI of CaiT is 8.5 and I initially expected the 2D crystals to form at acidic pH. Hence, the membranes and tubular structures observed at pH 5.6 deceived me for a while. Subsequent freeze fracture revealed that the larger membranes in this condition were empty and the small vesicles had little protein incorporated in them (Figure 5.13). As the pH increased vesicular membranes were observed in all conditions. However, the ordering of the protein into 2D lattices was observed only at a pH above 7.5 (Figure 5.14). CaiT yielded 2D crystals irrespective of N or C terminal his tag.

The membranes obtained with *E.coli* polar lipids were predominantly multiple layers and poorly ordered (Figure 5.14). Most of these membranes showed hexagonal lattice. Occasionally tubular crystals with a rectangular lattice were observed but these crystals were irreproducible (Figure 5.15). The exact reason how and why these tubular crystals formed remains unclear. I thought it was due to the detergent batch used for purification and the possible presence of the □- isomer of DDM. But when the alpha isomer was used alone, it did not solubilize the protein as efficiently as the □-isomer from the membranes and protein tended to aggregate in a short time scale. Thus formation of the tubular crystals might be due to a particular detergent batch and hence may not be reproducible.

The main problem with the CaiT crystals obtained with *E.coli* polar lipid was stacking. To overcome this a screen for different lipids was carried out based on head group and charge, the fatty acid chain length and saturation. It was clear that negatively charged lipids promoted the formation of stacked membranes and so did ethanolamine (Figure 5.16). The best conditions were obtained with choline as the head group. It is interesting to note that the head group of phosphatidylcholine lipids has a quaternary amine that might resemble a non-transportable substrate due to the presence of longer carbon

chain. Previous studies (Jung et al 2002) and my own fluorescence assay suggest that choline does not cause any change in the protein (Figure 5.6) indicating that better crystals obtained with PC lipids is not because of inhibition. The best 2D crystals obtained with DPPC and POPC were vesicular in nature (Figure 5.17). Subsequent electron microscopy and image processing of crystals from PC lipids gave information about the structure and the oligomeric state of the CaiT.

As assessed by the program ALLSPACE both the stacked and the isolated membranes showed three-fold symmetry while the stacked membranes showed additional symmetry. The dimensions of the trimer calculated from the projection map (Figure 5.18) are very similar to that of the single particles (Figure 5.24), indicating a near-native structure in the detergent micelle (Raunser S, unpublished observation), as well confirming the observed oligomeric state in the blue native gel.

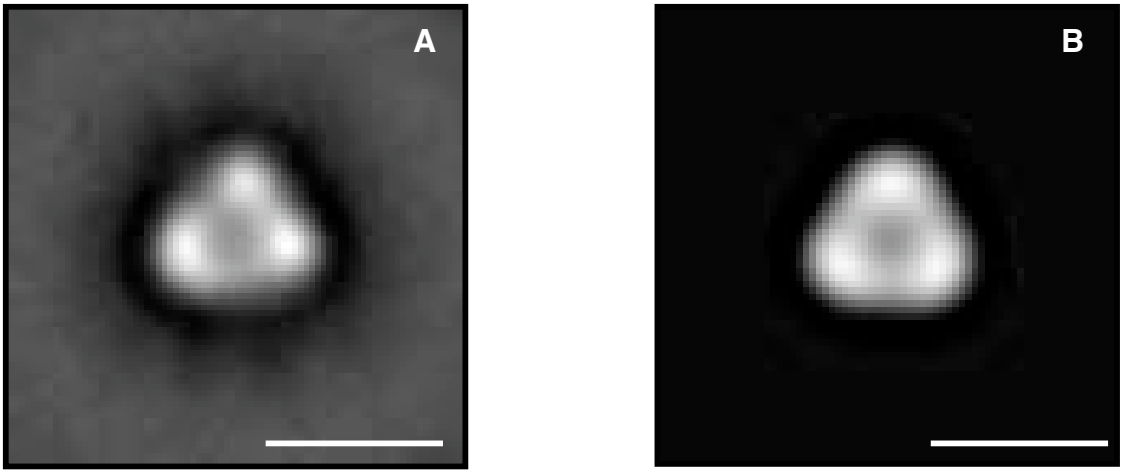

Figure 5.24: 2D averages of single particles of CaiT in DDM showing a trimeric structure. A – with no symmetry applied or B with three fold symmetry applied (scale bar –10nm). The edge to edge length of triangular mass is 85Å and each monomeric density is ~38Å.

Although the membranes obtained by reconstituting CaiT in POPC lipids yielded isolated and two layered crystalline membranes, efforts to get images from cryo-EM were unsuccessful. Among several images only one

image showed a sufficient number of spots that was useful for processing. The resolution of this particular membrane was limited to 18Å, indicating that the crystalline membrane were not well ordered to yield good images by cryo-EM. The freeze fracture analysis of the protein reconstituted into POPC lipid bilayer showed that the density and packing of the protein was not uniform all over the sample, with some vesicles showing very little protein (Figure 5.25). Some of the membranes showed good incorporation but they were hard to distinguish in cryo-EM.

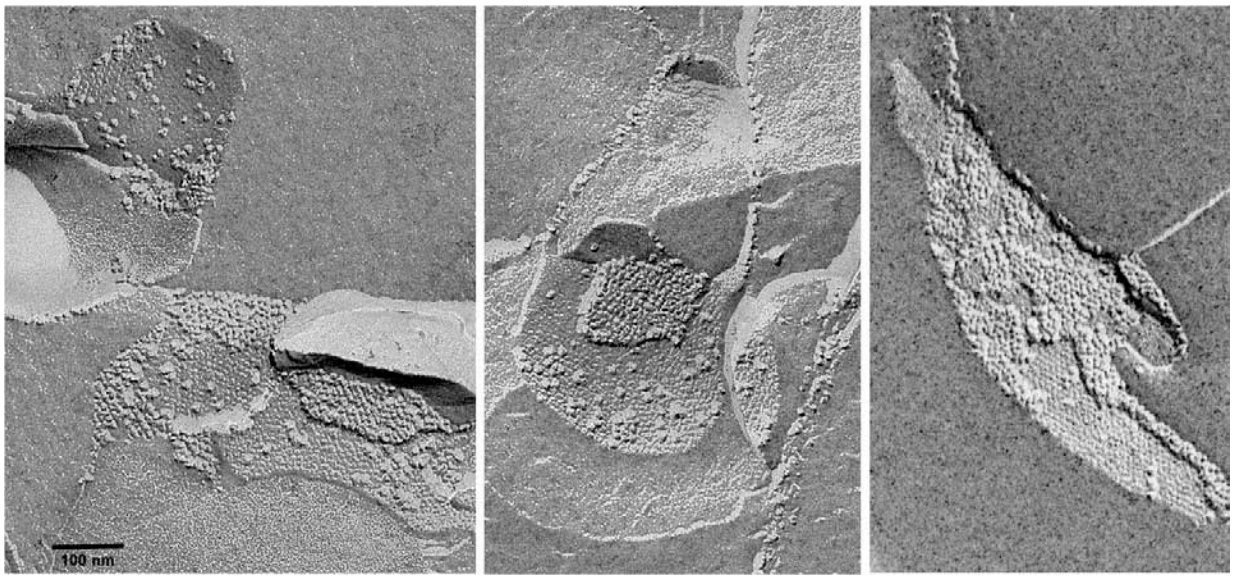

Figure 5.25: Freeze fracture images of POPC membrane of CaiT showing vesicles with less dense protein and membranes with patches of ordered aggregates.

The preliminary projection map obtained in cryo-EM was very similar to that obtained from negative stain. The oligomeric state of CaiT is in agreement to its homologue BetP that is also a member of the BCCT family (Ziegler et al 2004) confirming that in a given family of transporter the oligomeric state of the protein is conserved.

5.2.8 3D CRYSTALLIZATION

3D crystals of CaiT were obtained readily in a wide range of conditions. One important concern was the oligomeric state of the protein in the crystal.

Recent examples of membrane protein structures in detergent and in the membrane have yielded contrasting results (Kunji et al 2003;Pebay-Peyroula 2003). Analyzing the CaiT 3D crystals by blue-native gel showed a trimeric band confirming that crystallization conditions did not alter the oligomeric state. Most of these crystals diffracted to 7-8Å with some of them showing spots to 6Å (Figure 5.21). Screening for better conditions through the use of additives or incubation at different temperatures did not improve the order of the crystals.

Since the detergent DDM forms a large micelle, many of the recent structures where this detergent has been used included an additional second detergent that improved the diffraction quality significantly (Huang et al 2003;Abramson et al 2003;Kuo et al 2003). In fact the quality of the glycerol phosphate transporter crystals improved dramatically by use of mixture of detergents (Lemeuix et al 2003). However, there is no rationale to use a particular detergent for improving the quality of the crystals. Different mixtures were used to collect data sets for native and derivative sets of KirBac channel (Kuo, Gulbis et al. 2003).

Hence, instead of trying a large number of detergents for crystallization, the stability of the protein in a mixture of detergents along with DDM was checked by blue native gel electrophoresis. This experiment reduced the number of detergents to screen (Table 5.2 and Figure 5.22). For example, in a mixture of DDM and CHAPS the protein was unstable and no visible band was observed on blue native gel. Consistently no crystal was obtained with a mixture of DDM and CHAPS. But chemically similar detergents such as any of the maltoside or $C_{12}E_8$ yielded crystals. These crystals showed different morphologies ranging from very small hexagonal shapes to long, thin scale-like structures (Figure 5.23). The crystals obtained in this way were highly reproducible but their diffraction quality did not improve. Many of these crystals were thin in the third dimension, possibly forming as layers that can occasionally be observed during freezing when they crack.

Some of the recent articles describe that the addition of lipids prior to crystallization resulted in better crystals (Zhang et al 2003; Kaback R, personal communication). The addition of lipid possibly reduces the flexibility of the protein-detergent micelle. Since PG co purifies with CaiT, this was included in the crystallization mixture. Crystals were obtained under similar conditions but they were not reproducible.

Initial 3D crystallization trails of CaiT were promising. I would like to emphasize that the range of crystallization conditions explored is still quite small and more conditions need to be exploited. Thrombin could be used to cleave the 'his' tag (Figure 5.2) and subsequent crystallization screen might indicate the effect of tag on the quality of CaiT crystals. Other approaches such as finding the minimal core of the protein to get better crystals or using antibodies would be on my list to try. I feel that CaiT will yield well-ordered 3D crystals in the near future with the experience gained from the past.

6 OmpG

6.1 RESULTS

6.1.1 EXPRESSION AND PURIFICATION OF OmpG FROM INCLUSION BODIES

OmpG without its leader peptide was expressed in *E.coli* strain BL21 (DE3) C41. The protein from inclusion bodies was solubilized in 25mM Tris pH8 and 8M urea (buffer A) and purified by DEAE ion exchange chromatography. After binding the protein to the column, up to 165mM NaCl was used in steps to remove the impurities. The protein was eluted with 250mM NaCl. This procedure yielded up to 10 milligrams of pure protein per liter of culture. OmpG migrates at around 33kDa, as expected from the amino acid sequence (Figure 6.1).

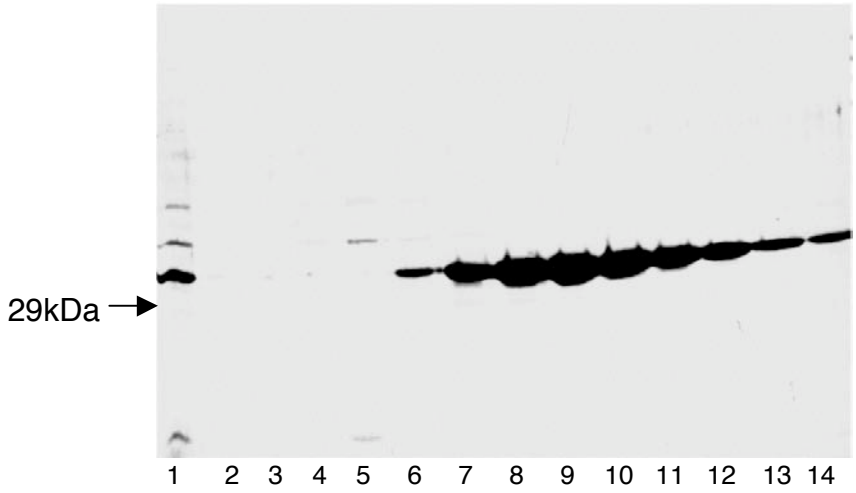

Figure 6.1: Coomassie stained SDS gel of OmpG purification from inclusion bodies
Lane 1: Inclusion bodies in buffer A
Lane 2: Flow through
Lane 3,4: Wash fractions with buffer A and with 50mMNaCl respectively
Lane 5: Wash fractions with 0.165mM NaCl
Lane 6-14: OmpG fractions eluted from the column
The arrow indicates the migration of 29kDa marker.

6.1.2 REFOLDING OF OMPG

OmpG was refolded by diluting in the presence of detergent micelles. A screen of detergents with different chemical properties was used. The efficiency of refolding was monitored by the differential migration of folded and

unfolded protein in the SDS gel. The completely denatured protein in urea migrates at around 33kDa. Refolding results in a shift of the band to ~28kDa. All these gels were run at 4° C for four to five hours with a low current to prevent heat denaturation during the gel run. Typically protein at a concentration of 0.4mg/ml in buffer A was diluted such that the final urea concentration was around 3M. Initially detergents belonging to the polyoxyethylene class were used because of their lower cost. Genepol X-80 and TritonX100 were used in varying concentrations, incubating at 20°C for 8 hours.

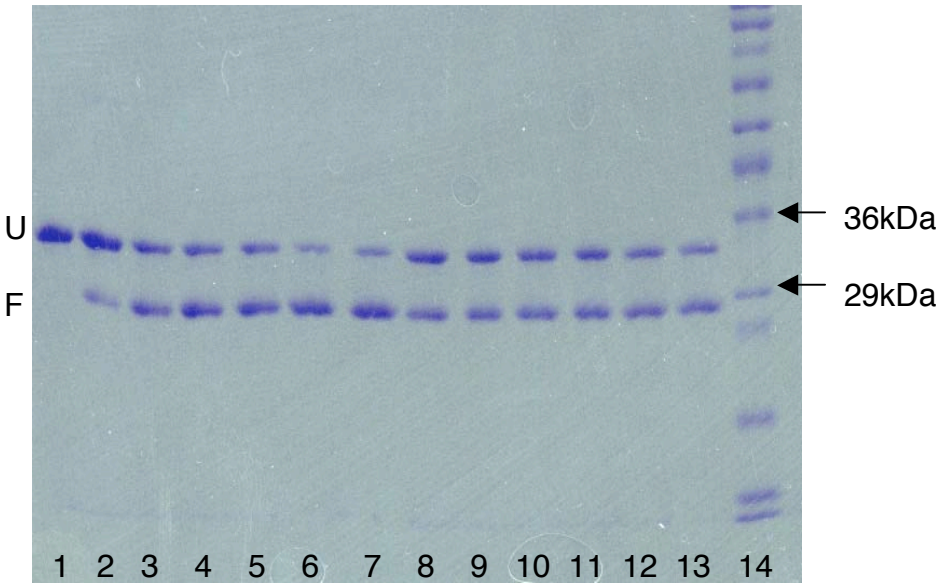

Figure 6.2: Refolding of OmpG with polyoxyethylene detergents

Lane 1: Protein in urea
Lane 2: Genepol 0.1%
Lane 3: Genepol 0,2%
Lane 4: Genepol 0.4%
Lane 5: Genepol 0.8%
Lane 6: Genepol 1%
Lane 7: Genepol 2%
Lane 8: TX100 0.1%
Lane 9: TX100 0.2%
Lane10: TX100 0.4%
Lane11: TX100 0.8%
Lane12: TX100 1%
Lane13: TX100 2%
Lane14: Marker
U and F are unfolded and folded forms.

The yield of refolded protein with these detergents was in the range of 50-60%. To improve the refolding efficiency of the protein various parameters were varied including:

1) the final concentration of urea

2) pH and ionic strength during refolding

3) temperature

4) detergents and their concentration

6.1.3 EFFECT OF UREA ON REFOLDING

Urea keeps the protein in an unfolded state and a reduction in urea concentration results in the refolding of the protein. However during this process numerous pathways are available for the protein to refold that include path to aggregation and one might need a certain amount of denaturant to prevent such a process. Refolding of protein was followed at different final concentrations of urea at constant protein and detergent concentrations. Refolding of protein was only observed when the urea concentration was less than 5M and below this value, refolding was independent of the urea concentration.

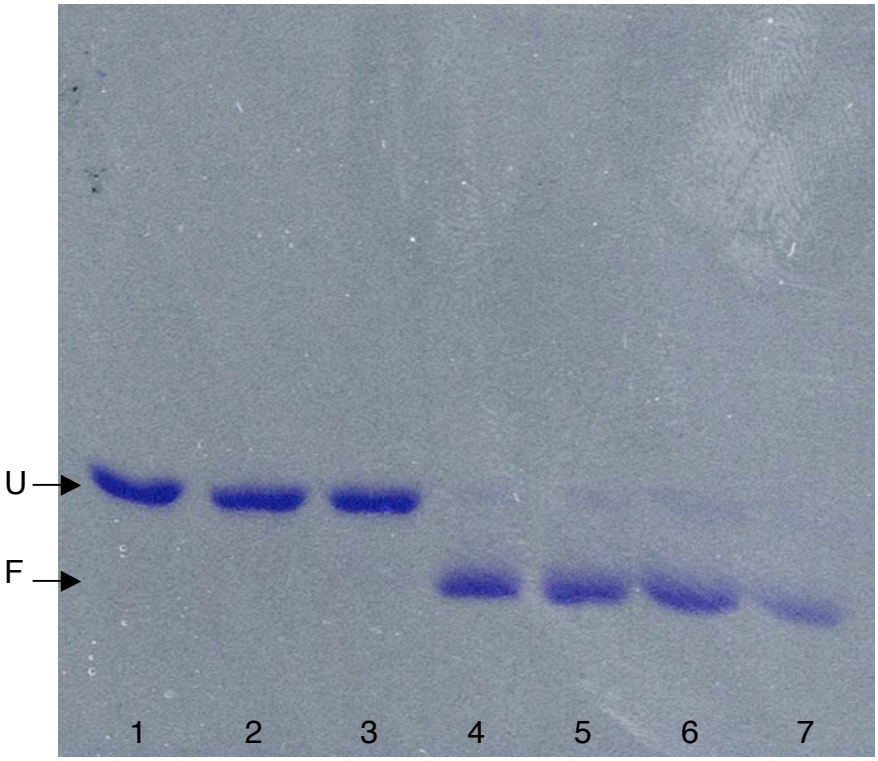

Figure 6.3: Effect of final urea concentration on refolding
Lane 1-8M, Lane 2-6M, Lane 3-5M, Lane 4-4M, Lane 5-3MLane 6-2M and Lane 7-1M.
Equal amounts of protein were loaded in lanes 1-6, in lane 7 the sample is very dilute, hence intensity of the band is low.
(U- Unfolded, F-folded)

6.1.4 EFFECT OF UREA ON CMC OF DIFFERENT DETERGENTS

Why is refolding observed only when the urea concentration is less than 5M? I reasoned it as the effect of urea on the CMC of the detergent. To verify this effect of urea, the increase in ANS fluorescence upon the formation of detergent micelles was investigated. The CMC of different detergents was determined from the break point (see figure legend 6.4) in three different solutions (water, 3.2M urea and 8M urea).

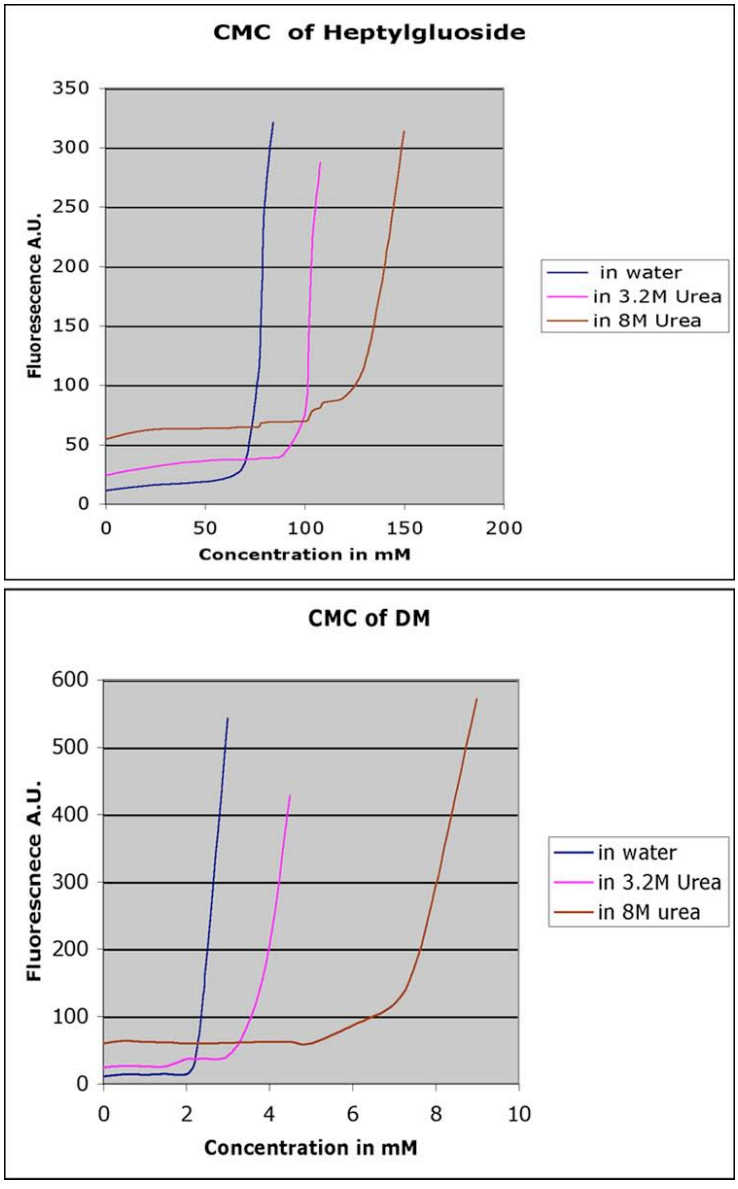

Figure 6.4: Representative graphs of two different detergents (heptyl glucoside and decyl maltoside) in different concentrations of urea. The break point is defined as the concentration when the fluorescence increases, indicating the formation of the micelles.

Table 6.1: CMC of detergents determined by increase in ANS fluorescence

Detergent	CMC in mM[a]	CMC Measured (in mM)		
		in water	in 3.2M Urea	in 8M urea
Glucosides				
Hexyl glucoside	250	250	300	400
Heptyl glucoside	79	78	102	110
Octyl glucoside	25	25	35	42.5
Nonyl glucoside	6.2	7.2	10	14
Maltosides				
Decyl maltoside	2.2	2.4	4	7
Undecyl maltoside	0.56	0.45	0.75	1
Dodecyl maltoside	0.17	0.16	0.23	0.5
Cymal 6	0.57	0.57	1.2	2.5
Cymal 7	0.19	0.19	0.45	0.8
Glucamides				
Mega 8	78	60	70	85
Mega 9	25	25	30	40
Hega 8	109	90	120	140
Hega 9	39	37	65	80
[a] – from Anatrace catalogue				

It was evident from the determination of the CMC that at higher urea concentration (8M) the CMC of the detergent was approximately 1.5 to 4 times higher than in water. This would explain the observed behavior of

refolding in different concentration of urea in figure 3.3 where CMC of OG in water was taken for calculation.

6.1.5 EFFECT OF DETERGENTS ON REFOLDING

Detergents of different classes were chosen with variable chain length, and some that are sparingly soluble such as dodecyl glucoside were not used. In all cases the protein concentration was kept constant while the final concentration of urea was 3.2M after dilution (based on figure 6.3). The refolding efficiency was assessed visually by comparing the relative amount of unfolded and folded forms present. A general trend was observed among the series of the detergents with refolding observed at the concentration that corresponds to the CMC of respective detergent in 3.2M urea (Table 6.1). Detergents with glucoside or glucamide as head group and shorter chain length were most efficient in refolding OmpG.

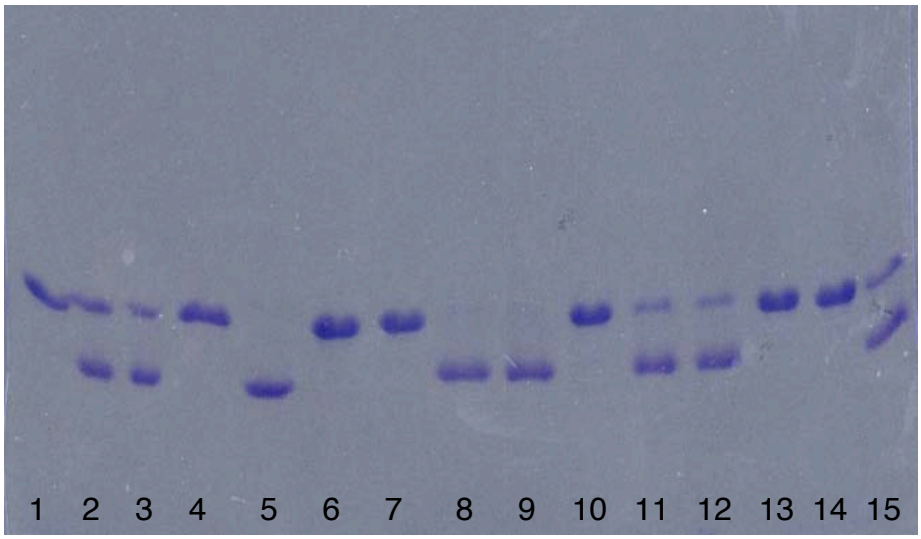

Figure 6.5: Refolding of OmpG with different chain length of glucosides

Lane 1: Hexyl glucoside 1x
Lane 2: Hexyl glucoside 2x
Lane 3: Hexyl glucoside 3x
Lane 4: Heptyl glucoside 1x
Lane 5: Heptyl glucoside 2x
Lane 6: Protein in Urea
Lane 7: Octyl glucoside 1x
Lane 8: Octyl glucoside 2x
Lane 9: Octyl glucoside 3x
Lane 10: Nonyl glucoside 1x
Lane 11: Nonyl glucoside 2x
Lane 12: Nonyl glucoside 3x
Lane 13: Decyl glucoside 1x
Lane 14: Decyl glucoside 2x
Lane 15: Decyl glucoside 3x

Equal amounts of protein were loaded in all lanes. x- denotes the CMC of detergent in water; 1x means equivalent to CMC, 2x means two times the CMC and so on.

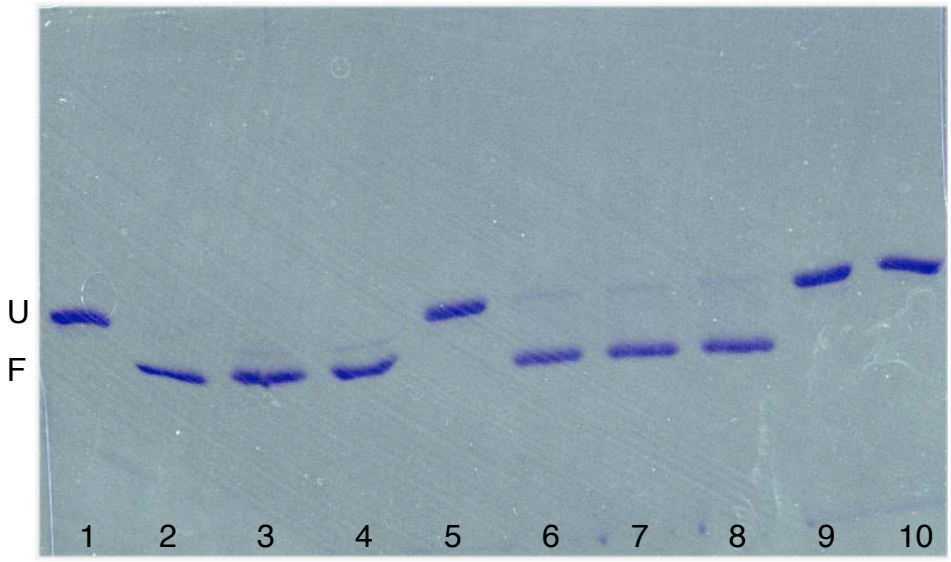

Figure 6.6: Refolding of OmpG with three glucamides

Lane 1: Mega 8 1x
Lane 2: Mega 8 2x
Lane 3: Mega 8 3x
Lane 4: Mega 8 4x
Lane 5: Mega 9 1x
Lane 6: Mega 9 2x
Lane 7: Mega 9 3x
Lane 8: Mega 9 4x
Lane 9: Mega 10 1x
Lane 10: Mega 10 2x

~90-95% of refolding was observed with glucosides with a chain length of 7 or 8. Mega 8 or 9 were equally good. However, as the chain length increased to 9 or 10 the efficiency of refolding decreased (Figure 6.5). A similar trend was observed with linear carbon chain or cyclic maltosides.

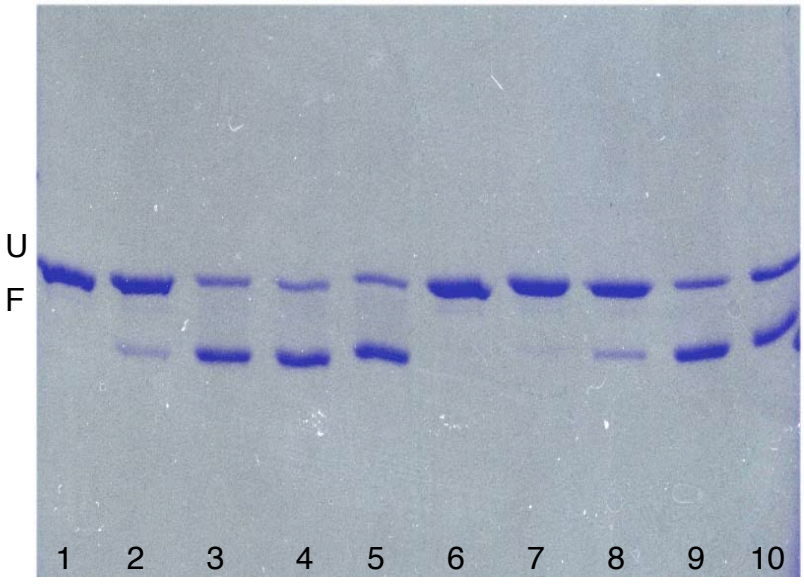

Figure 6.7: Efficiency of refolding in Cyclic maltosides

Lane 1: Cymal 6 1x
Lane 2: Cymal 6 2x
Lane 3: Cymal 6 3x
Lane 4: Cymal 6 4x
Lane 5: Cymal 6 5x
Lane 6: Cymal 7 1x
Lane 7: Cymal 7 2x
Lane 8: Cymal 7 3x
Lane 9: Cymal 7 4x
Lane 10: Cymal 7 5x

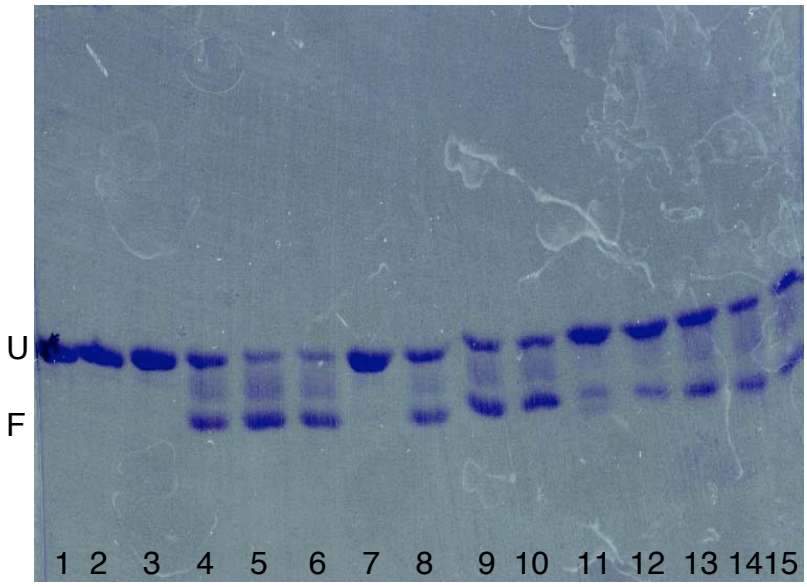

Figure 6.8: Different maltosides showing varied efficiency of refolding

Lane 1: Nonyl Maltoside 1x	Lane 9: Undecyl Maltoside 3x
Lane 2: Nonyl Maltoside 2x	Lane 10: Undecyl Maltoside 4x
Lane 3: Decyl Maltoside 1x	Lane 11: Dodecyl Maltoside 1x
Lane 4: Decyl Maltoside 2x	Lane 12: Dodecyl Maltoside 2x
Lane 5: Decyl Maltoside 3x	Lane 13: Dodecyl Maltoside 3x
Lane 6: Decyl Maltoside 4x	Lane 14: Dodecyl Maltoside 4x
Lane 7: Undecyl Maltoside 1x	Lane 15: Dodecyl Maltoside 5x
Lane 8: Undecyl Maltoside 2x	

Other detergents such as the series of polyoxyethylene and zwitterionic detergents like LDAO were able to refold OmpG only to 50% (Table 6.2). Refolding in some detergents such as Mega 8 showed a band at around 30 kDa that appeared to be an intermediate state in the refolding process (Figure 6.6). Refolding by dialysis was also possible but dilution was preferred due to the cost efficiency when refolding was scaled up. Refolding of protein on an ion-exchange column was also possible but the yield was low. Most of the protein tended to aggregate on the column, possibly due to sudden removal of denaturant. OmpG was not able to refold in lipids without detergents. However a mixture of detergent along with lipids did promote refolding but the efficiency was not greater in the presence of lipids when compared to detergent alone. Washing of OmpG bound to the column with lipid solubilized in detergent did not improve the folding efficiency. The following table summarizes the refolding efficiency of detergents and the optimal conditions achieved.

Table 6.2:

Detergents	CMC (in mM)	Optimal CMC required for refolding	Refolding efficiency
Glucosides			
Hexyl	250	2x	>85%
Heptyl	79	2x	>90%
Octyl	20-25	2-3x	>90%
Nonyl	6.5	2-3x	>75%
Decyl	2.2	2x	~60%
Glucamides			
Mega 8	108	2x	>90%
Mega 9	25	2x	>90%
Mega 10[a]	6	-	0
Maltosides			
Nonyl[b]	6	-	0
Decyl	2.2	3-4x	>75%
Undecyl	0.59	3-4x	>75%
Dodecyl	0.15	upto 5x	~50%
Cymal 6	0.56	3-4x	>75%
Cymal 7	0.19	4-5x	~50%
Polyoxyehtylene			
C_8E_5	7.1	4-5x	~50%
$C_{10}E_6$	0.9	-	0
TX100	0.23	8x	~50%
Genepol X-80	??	8x	~50%
Zwitterionic[c]			
LDAO	2	4-5x	<50%
Anergent 3-10	39	2-3x	<50%
Anergent 3-12	2.8	4-6x	<50%

[a]- The solubility of Mega-10 was very low and that may be a reason for its inability to refold

[b]- Nonylmatloside was checked repeatedly but for unknown reasons no folding was observed

[c]- with all the zwitterionic agents the efficiency of refolding was low and the protein tended to form higher aggregates.

6.1.6 EFFECT OF TEMPERATURE, pH and SALT

The efficiency of refolding was increased at higher temperature. The time required for refolding was directly proportional to increasing temperature. An optimal temperature of 20°C with overnight incubation was used in all the experiments. Little effect on refolding was observed when pH of the buffer was varied. On normal dilution conditions the end concentration of NaCl was 0.1M. No difference was observed with increasing concentration of NaCl but at very high concentration such as 1M a higher molecular weight band, possibly an aggregate of OmpG was observed.

6.1.7 OPTIMAL CONDITION FOR REFOLDING OF OmpG

Based on the various parameters screened an optimal condition was reached, where protein at a concentration of 0.4mg/ml was diluted in a buffer containing 75mM of octyl glucoside that resulted in a final concentration of 3M urea and 0.1M NaCl. Refolding was carried out at 20°C for ~8-10 hours and subsequently analyzed by SDS gel electrophoresis to check the efficiency.

6.1.8 CD SPECTROSCOPY OF OmpG

The secondary structure of the unfolded protein in urea and the refolded protein was analyzed by CD spectroscopy. The protein in detergent showed a curve expected of a □-sheet protein with a mean residue ellipiticity at 216nm was 10954.2 deg cm^2, when compared to OmpG in urea was 50-60% greater. The CD spectrum confirms the formation of correct secondary structure in correlation with the observed migration in the SDS gel, since the refolded OmpG resists the SDS denaturation and migrates faster than the completely unfolded product (Figure 6.2).

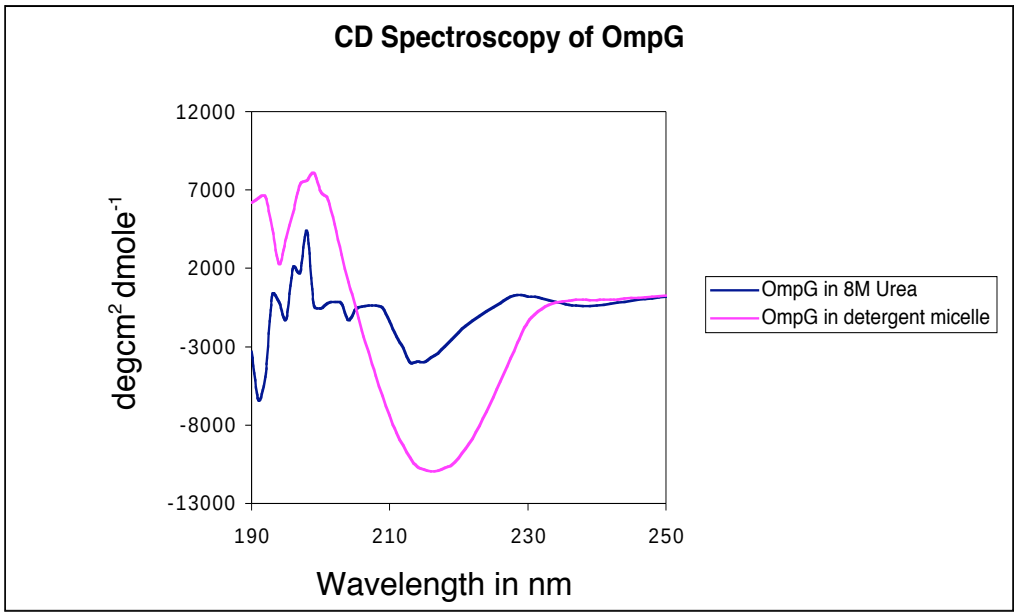

Figure 6.9: The secondary structure of OmpG is regained upon dilution in detergent micelles. The control spectrum in urea shows a random structure.

6.1.9 MASS SPECTROGRAM OF OmpG

OmpG in all these detergents showed a single homogenous peak in the mass spectrum (Figure 6.10). The mass of OmpG was determined with an apparent error of ±40 daltons, ensuring that no proteolytic digestion or modification had occurred during the long process of purification and refolding.

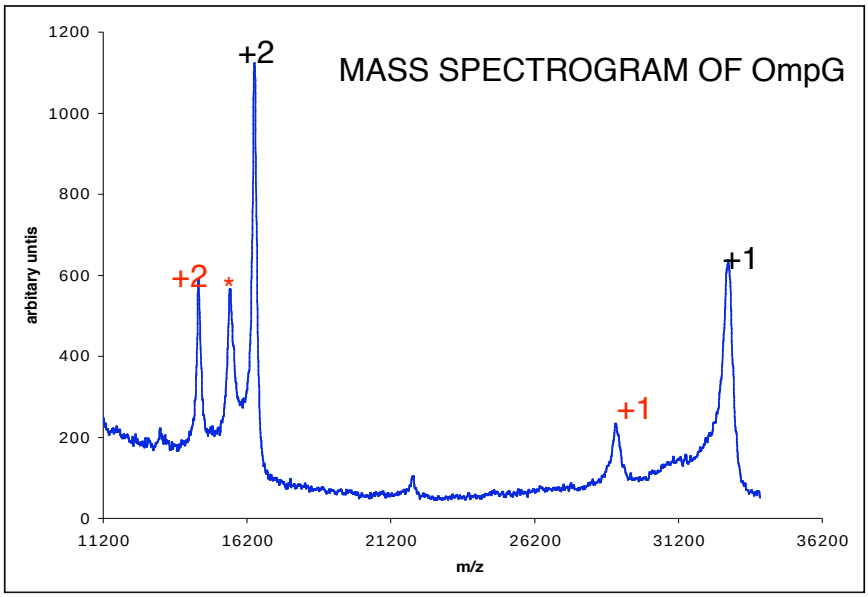

Figure 6.10: Averaged spectra of OmpG in DDM and carbonic anhydrase used as internal calibrant. The black labels indicate the peaks of OmpG 32922 and 16455 daltons (±40 Da) with one and two charges. The red labels indicate the carbonic anhydrase 29301.593 and 14516.7 daltons, while the peak marked by red asterisk arises from carbonic anhydrase.

6.1.10 GEL FILTRATION AND BLUE NATIVE GEL ELECTROPHORESIS

The refolded protein was analyzed for the formation of aggregates by gel filtration and blue native gel electrophoresis. Gel filtration on a calibrated Superose 6 column yielded a single peak with a retention volume of 1.64ml, with no aggregate peak observed. This result was consistent with the observed size on a blue native gel. The protein migrates at ~60kDa, which was expected for the monomeric protein. Unlike in SDS gels only a single protein band was observed irrespective of folded and unfolded forms, strongly supporting the idea of displacement of detergents by the Coomassie stain (Heuberger et al 2002). OmpG when incubated with SDS prior to loading in the gel migrated a little lower than the band when loaded with DDM alone (Figure 6.11B, lane2).

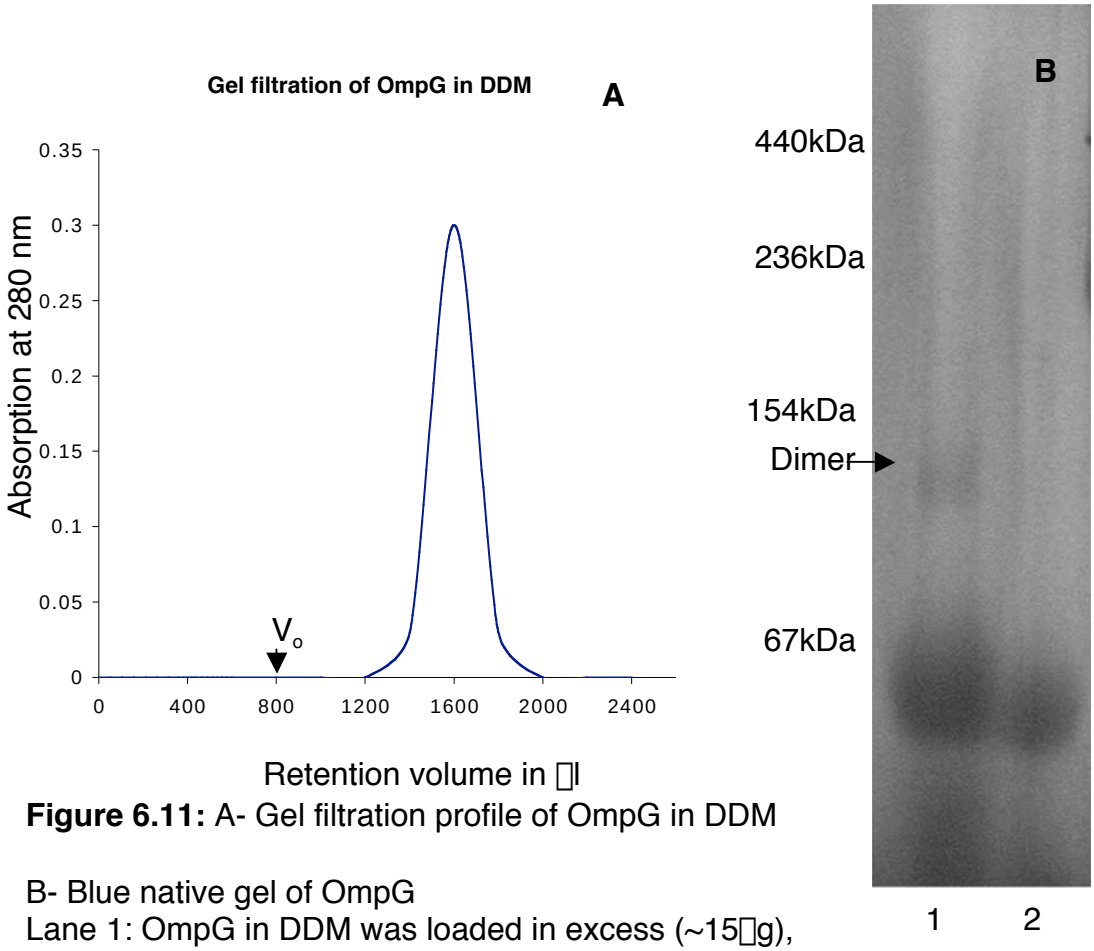

Figure 6.11: A- Gel filtration profile of OmpG in DDM

B- Blue native gel of OmpG
Lane 1: OmpG in DDM was loaded in excess (~15□g), shows a dimeric band, possibly an aggregate
Lane 2: OmpG with 2%SDS added before loading

6.1.11 ENRICHMENT OF REFOLDED OmpG

To achieve >95% of refolded protein it was necessary to optimize another step to enrich the refolded product. Several methods were tried to separate folded and unfolded protein, including sucrose density gradient centrifugation, addition of lipids, ion exchange and gel filtration chromatography. The gel filtration peak contained both forms, reflecting an intermediate form bound to the detergent micelle and denatured during the SDS PAGE. Hence it was not surprising that the two forms could not be separated by size. During a trial to refold OmpG on an ion-exchange column, it was observed that the unfolded and folded protein tends to elute at slightly different salt concentrations. This accidental observation was then used to enrich the folded product of OmpG. Prior to this step it was essential to remove the urea either by dialysis or by washing thoroughly after binding the protein on to the column. When protein was concentrated in the presence of urea (i.e., after dilution) this also resulted in an increase of urea concentration, which tended to unfold OmpG. A Mono-Q column was used for the second step of purification. Elution was carried out with a linear gradient of 0-500 mM NaCl. Three distinct peaks were observed. Peak A eluting at around 300mM NaCl was a minor fraction which had predominantly unfolded protein. The major peak designated B had >95% refolded protein. The peak C that eluted at higher salt concentration had predominantly unfolded product and was possibly a result of aggregation.

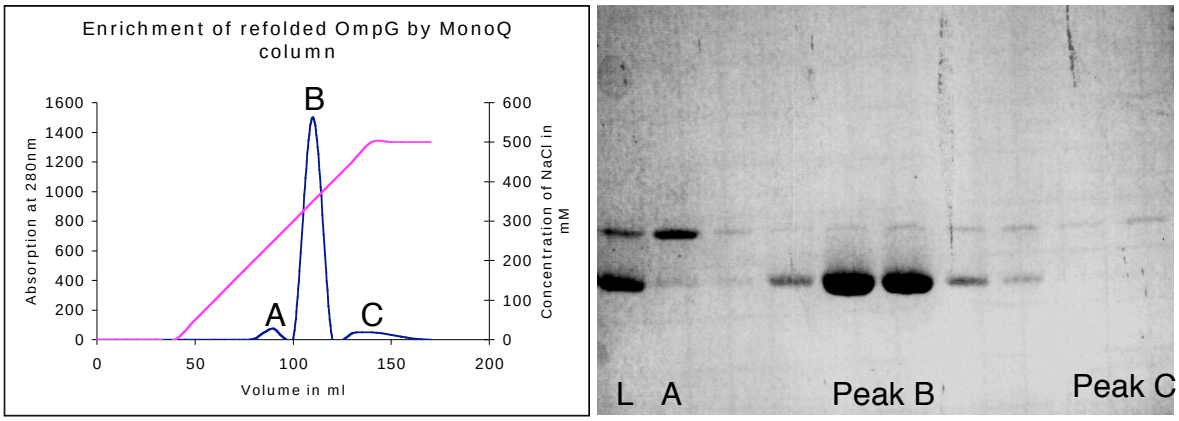

Figure 6.12: The Chromatogram from the ion exchange showing the elution profile of OmpG and the gel showing the various fractions. The lane labeled L was the protein loaded in the column.

The detergent exchange for crystallization was carried out during this step of ion exchange. Various detergents such as DDM, LDAO, C_8E_4 and OG were used to screen for both 2D and 3D crystallization. In summary starting from a liter of culture expressing OmpG in cytoplasm, refolding and further purification yielded ~5-6 milligrams of >95% refolded protein. Heating of folded protein before loading in the SDS gel resulted in a single band migrating at the same position as the unfolded protein (Figure 6.13, Lane 4).

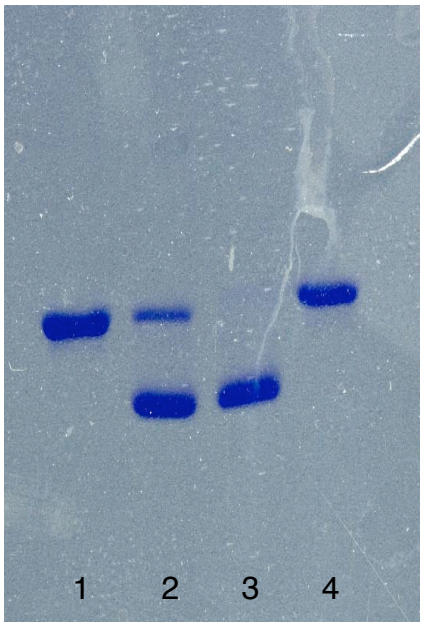

Figure 6.13:
Lane 1- Protein in 8M urea
Lane 2- Protein after refolding in OG by dilution
Lane 3- Pooled fractions of main peak from ion exchange with >95% folded protein
Lane 4- same as in lane 3 but heated at 95°C for 5 minutes before loading.

(Equal amounts of protein were loaded)

6.1.12 2D CRYSTALLIZATION

Refolded OmpG was reconstituted in to lipid bilayers of *E.coli* polar lipids for 2D crystal formation. The initial crystallization conditions were similar to those published for native OmpG (Behlau et al 2001). Protein at 1mg/ml was mixed with lipids and dialyzed to remove the detergents in a buffer containing 150mM NaCl and 25mM $MgCl_2$, pH7 at 20°C. This yielded tubular 2D crystals in 5-6 days. Tubes were 130-180nm wide and up to 1□m in length. Some of these tubes originated from vesicles. Visualization of negatively stained crystals showed the crystalline lattice (Figure 6.14).

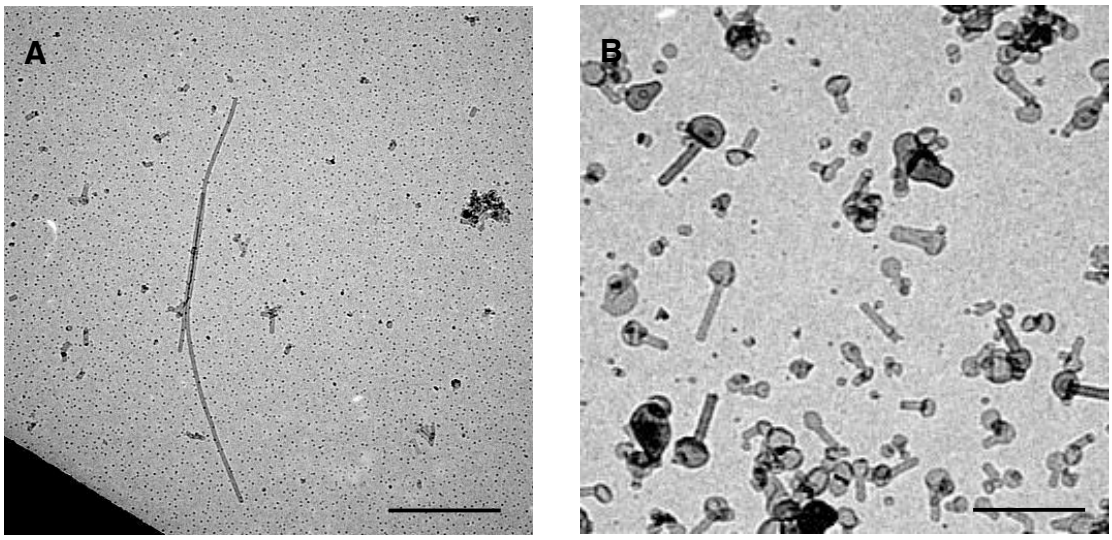

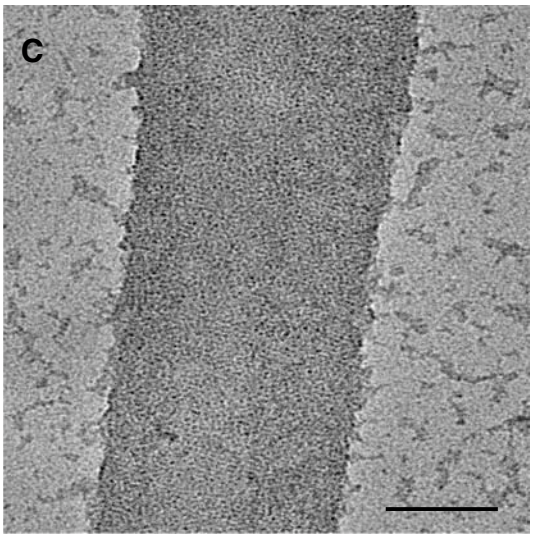

Figure 6.14:
A and B- Long narrow tubular crystals and those arising from vesicles stained negatively with uranyl acetate (Scale bar – 2 □m)

C- tubular crystal at higher magnification (Scale bar – 100 nm)

Very large numbers of tubular crystals were observed in a single grid square but their small size made it difficult to collect good images by cryo-EM and they diffracted poorly. Effort was then spent in improving the order of these crystals.

Different parameters were checked, that included the following:

a) detergents with different micelle size for fast or slow removal by dialysis

b) concentration of monovalent and divalent cations

c) temperature during dialysis

d) lipid to protein ratio

e) different types of lipids

Except for temperature all the other factors either had no significant effect or they were drastic. Formation of crystals required the presence of both monovalent and divalent cations with sodium and magnesium preferred. The concentration of the ions, sodium (0.1 –0.6M) and magnesium (10-40mM) had no influence on the size or the order of the crystals. Higher LPR resulted in some big vesicles with no particular arrangement of protein in them, tubes formed at LPR as low as 0.1. Lipids with different head groups were screened to improve the packing but had no effect. Detergent such as octyl glucoside with a small micelle or dodecyl maltoside that forms larger micelle invariably resulted in the formation of similar narrow tubes.

But when the temperature for dialysis was increased to 37°C, wider tubes and some large membrane sheets formed. The width of tubes ranged from 200-300nm while larger membranes measured a few microns. Some of the larger membranous sheets had a tendency to stack. Among these structures, narrow tubular crystals were also observed. The narrow tubes were distributed all over the grid and observed in clumps. All these crystals were of a single type made of rectangular lattices. The time for dialysis was prolonged for 6-8 weeks. This long dialysis period was not intended for complete detergent removal but to promote the formation of larger and better ordered crystals.

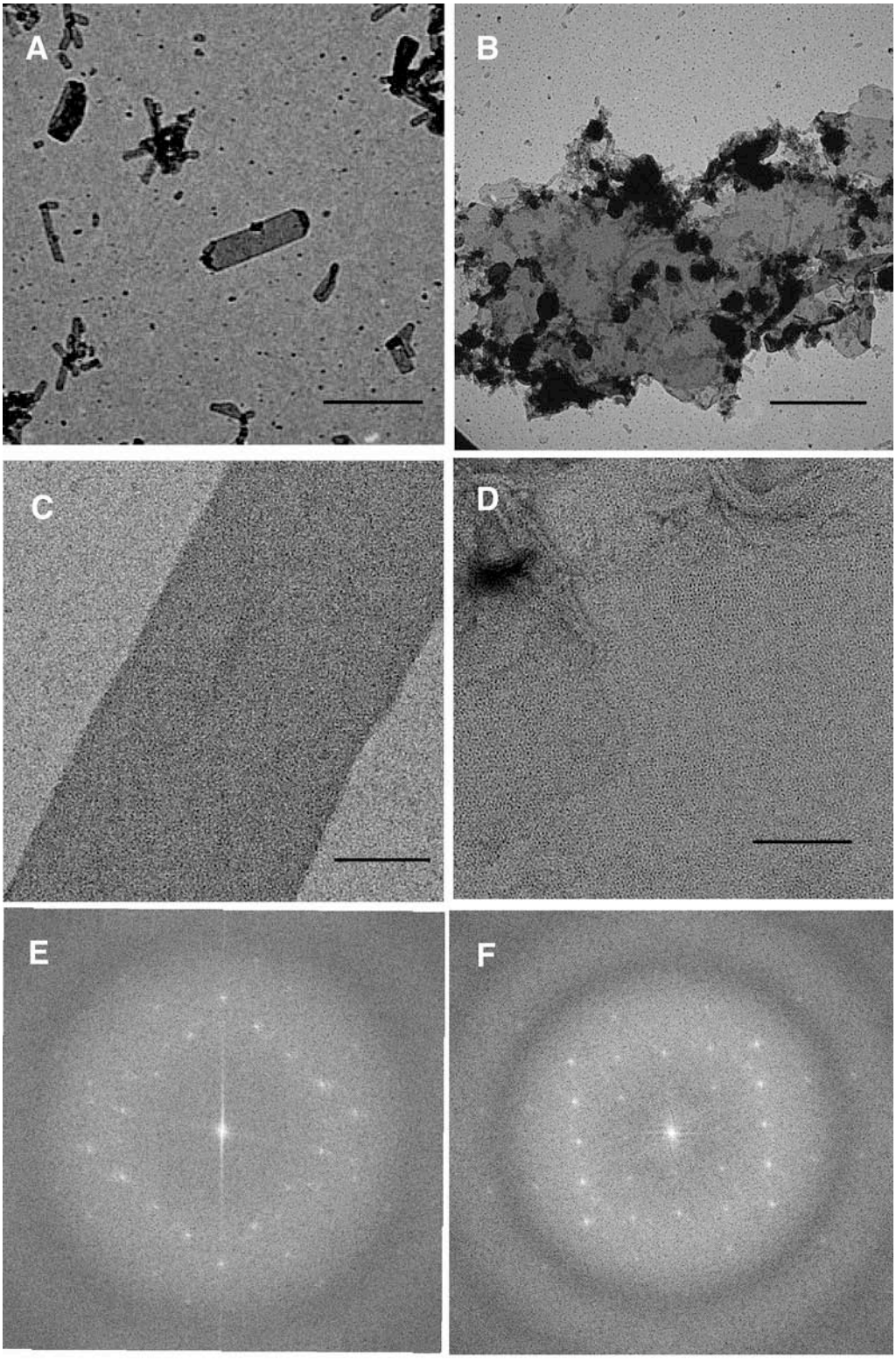

Figure 6.15: A and B – Morphology of crystals at low magnification showing wider tubes and stacked sheets respectively (Scale bar – 1 □m)
C and D – Crystals at higher magnification showing the lattice (Scale bar – 100 nm)
E and F – Power spectrum of the crystals in C and D

6.1.13 PROJECTION MAP

Images of 2D crystals with different morphologies were collected and processed. They revealed crystals with two different unit cells. The narrow tubular crystal form was poorly ordered and had a longer axis in one direction (described as OmpG_form1). The wider tubes and the larger membranes were better ordered (described as OmpG_form2).

Table 6.3: Electron Crystallographic Data

	OmpG_form1		OmpG_form2	
Plane group symmetry	$P22_12_1$		$P22_12_1$	
Unit cell dimensions	A = 72.5±1Å B = 87.2±1Å □= 90°		A = 71.5±0.5Å B = 81.6±1Å □= 90°	
No. of images	4		5	
Range of defocus	3000-7000		3500-9500	
No. of unique reflections[a]	52 (8Å)		63 (8Å)	
Overall Phase residuals[b]	19.4		13.0	
Resolution range (Å)	No. of unique Reflections	Phase residual (random=45°)	No. of unique Reflections	Phase residual (random=45°)
180-16	15	15.8	17	6.9
15.9-11.3	15	13.2	17	9.8
11.2-9.2	13	23.3	14	18.4
9.1-8.0	9	30.3	15	18.6
7.9-7.1			13	18.5
7.0-6.5			11	14.2
6.4-6.0			7	37.6

[a]- reflections included to IQ≤ 4to 8Å
[b]-Amplitude averaged, vectorially averaged phase residual which shows the phase deviation from theoretical 0°/180° (45° is random).

The shorter b axis crystals showed spots to 6Å. However the narrow tubes were good only to 10Å. Both the crystal forms had the same space group $P22_12_1$. The phase statistics of both these data sets were comparable and the eventual projection map calculated to 10Å showed no significant difference in the protein between the two crystals, but the packing was tighter in crystal form2.

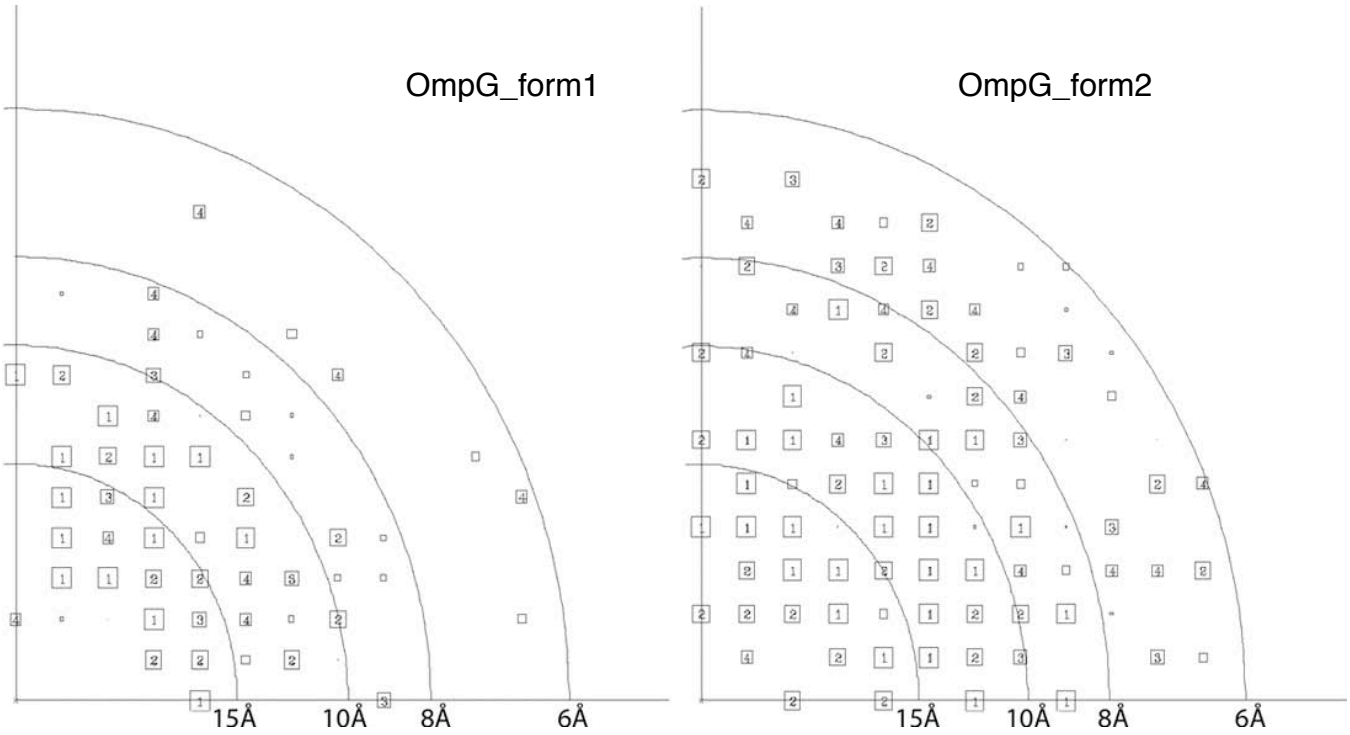

Figure 6.16: Combined phase error to 5Å after merging of lattices from separate images of crystals with differing unit cell. The size of the boxes corresponds to the phase error after averaging and rounding to 0° or 180° associated for each measurement (1, <8°: 2, <14°; 3, <20°; 4, <30°; 5, <40°; 6<50°; 7, <70°; 8, <90°, where 90° is random). Values from 1-4 are shown as numbers inside boxes, whereas those from 5-8 are indicated with decreasing box size.

Both projection maps (Figure 6.17) show almost circular molecules indicative of a ß-barrel with an approximate diameter of 25Åx27Å. In the better-ordered crystals a central strong density can be seen at this resolution, possibly reflecting the presence of internal loops.

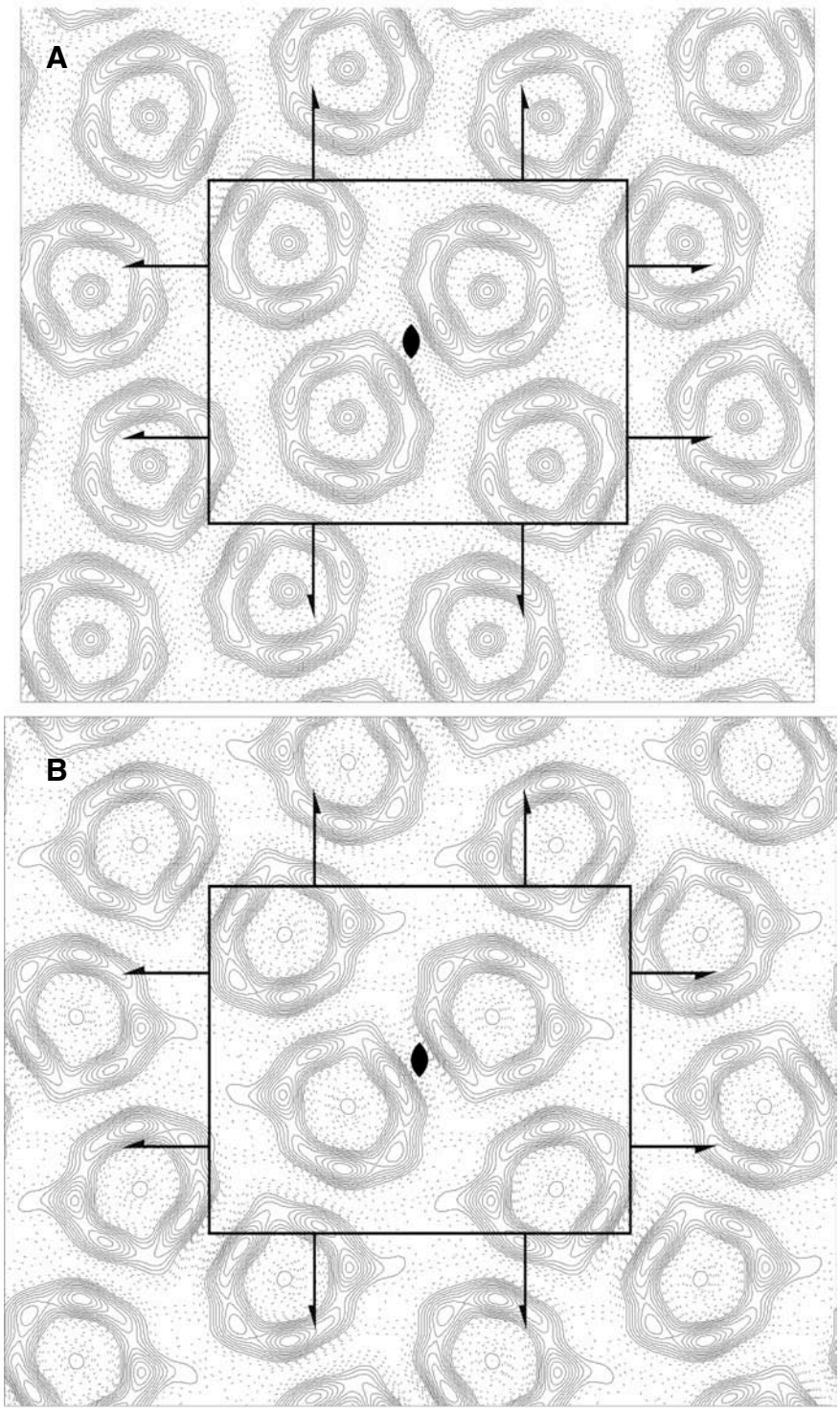

Figure 6.17A&B: Projection density map of OmpG_form2 and OmpG_form1 respectively at 10Å resolution from two different unit cells, calculated from merged amplitudes and phases of independent lattices with $P22_12_1$ symmetry applied. The 2-fold axes perpendicular to the membrane plane and the screw axes parallel to a and b are indicated. A unit cell is displayed with the a axis vertical and the b-axis horizontal. Solid lines indicate density above the mean while negative contours are shown as dotted lines. An isotropic temperature factor (B = -300) was applied to compensate for the resolution-dependent degradation of image amplitudes. The map was scaled to a maximum of 250 and contoured in steps of 25.

6.1.14 3D CRYSTALIZATION

3D crystallization conditions for OmpG were screened in LDAO as a detergent at a protein concentration of 10mg/ml. Initial screens yielded crystals in many different conditions including a wide range of pH and precipitants. These results were used for optimizing the crystals. The crystals were observed in many different forms, ranging from 0.4mm X 0.3mm growing up to 0.6mm X 0.5mm. One concern was the presence of unfolded protein in the preparation that was used for crystallization. Crystals from different batches and drops were analyzed by SDS gel electrophoresis. Most crystals showed a single band at the expected size of refolded OmpG. A higher aggregate was observed in some of the crystals but never the unfolded protein.

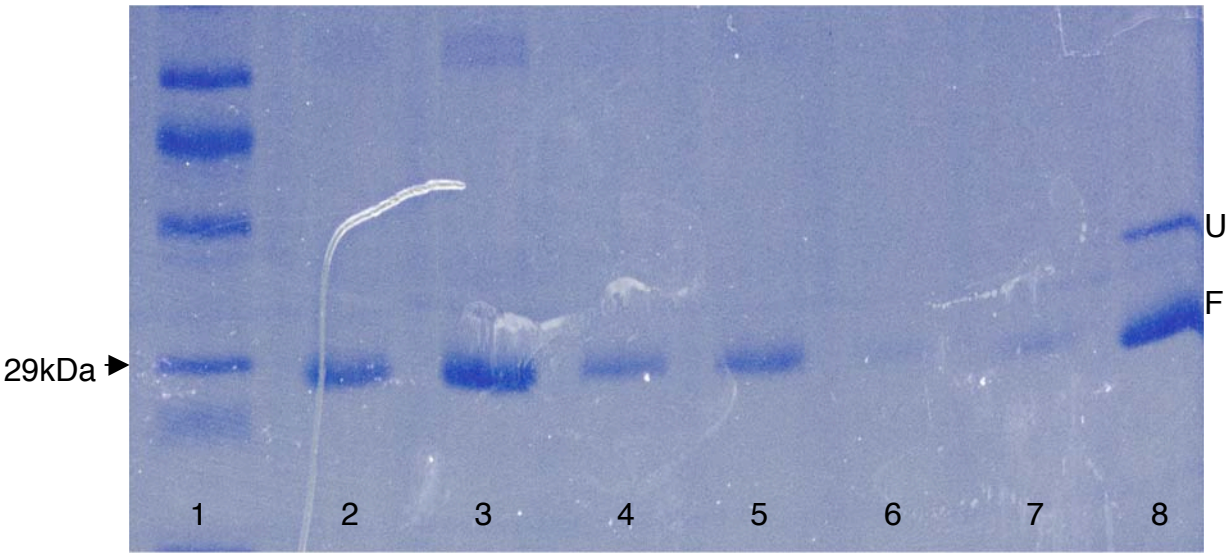

Figure 6.18: SDS gel showing the identity of the 3D crystals of OmpG
Lane 1: Marker
Lane 2-7: Different crystals
Lane 8: OmpG partially folded by detergent dilution

The absence of unfolded OmpG in the crystals was a good sign that encouraged further screens. OmpG crystals formed in a pH range of 4.5

–7.5. Polyethylene glycols 400 to 6000 or monomethyl ethers as precipitants yielded crystals invariably. Crystal formation required the presence of divalent cations such as magnesium or calcium. The crystals were very sensitive and had a tendency to crack immediately when the drop was opened for harvesting.

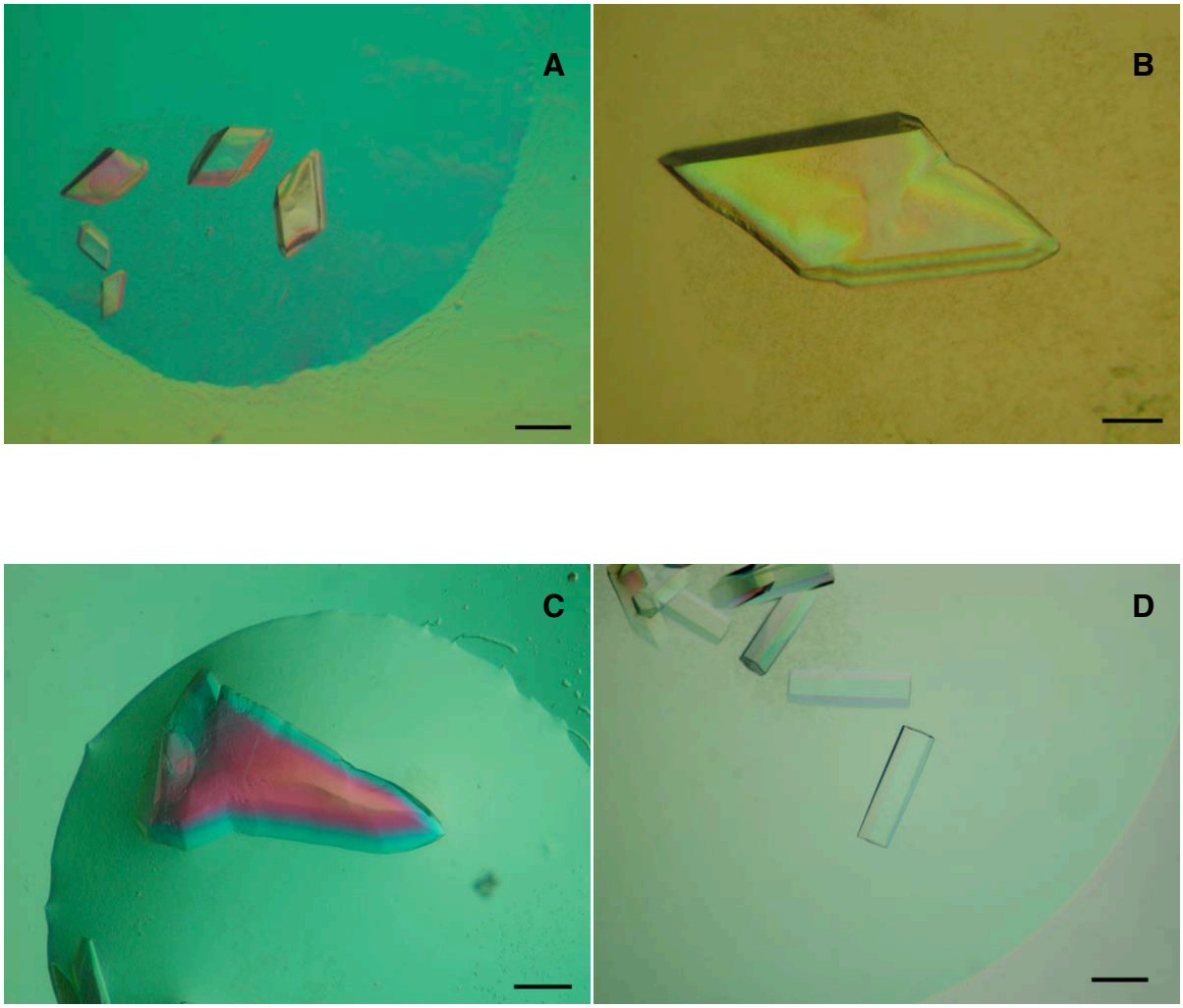

Figure 6.19: Different morphology of three-dimensional crystals of OmpG. All these crystals were obtained with LDAO as the detergent with different PEG's. The crystals in B and C grew large to reach a maximum size of 0.5 mm.
The scale bar is 100 □m.

Most of these crystals grew at high PEG concentrations and could be frozen directly in liquid nitrogen. When checked at the synchrotron the crystals diffracted to 5-6Å. Efforts to improve the crystal included the use of different detergents such as C_8E_5 or octyl glucoside, both with small micelles.

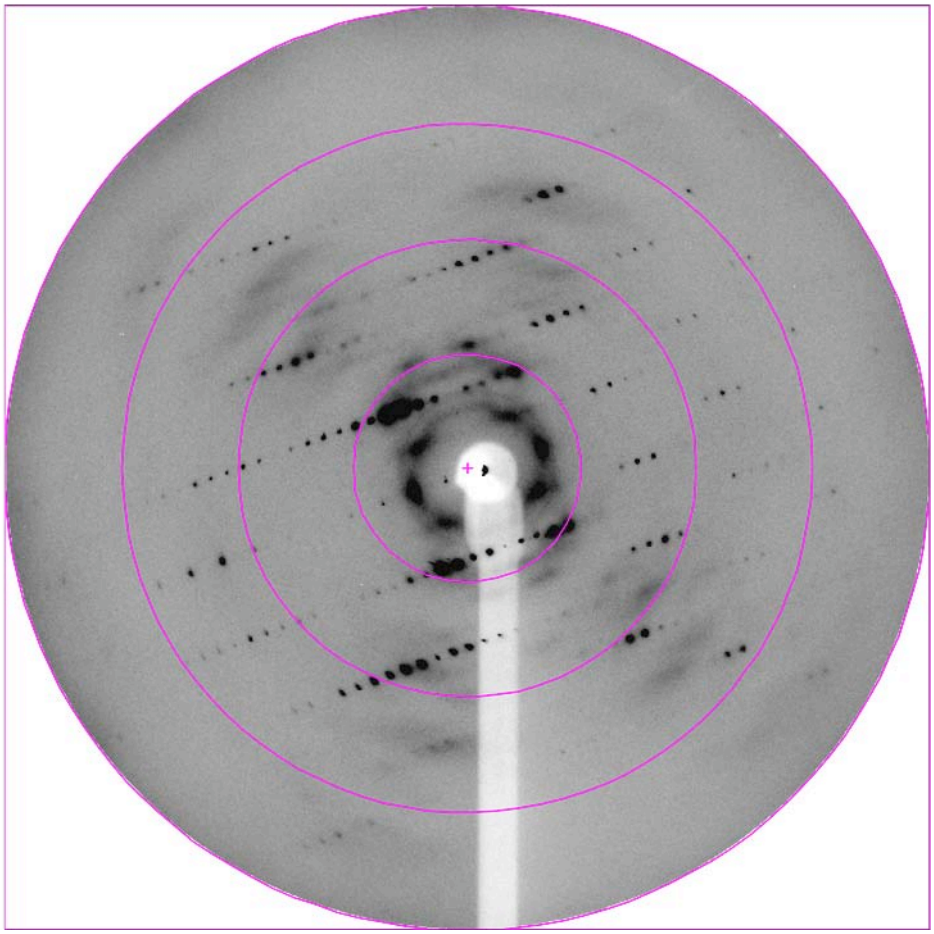

Figure 6.20: Diffraction pattern of a single crystal of OmpG. The rings correspond to 20,10,6.7 and 5Å. The spacing of the spots indicates a small unit cell (not determined).

6.2 DISCUSSION

6.2.1 WHY INCLUSION BODIES?

An essential pre-requisite for any crystallization project is the availability of homogenous protein both in terms of purity and conformation. To be able to screen many conditions and increase the probability of getting well diffracting crystals, one needs protein in milligram if not in gram quantities. Outer membrane proteins when expressed in *E.coli*, face the unique problem of crossing the inner membrane and then inserting into the outer membrane. A handful of outer membrane proteins have been expressed in outer membranes (Bannwarth and Schulz 2003) and yielded good quality crystals.

Alternatively, many of the outer membrane proteins have been expressed without the leader peptide and end up as non-functional cytoplasmic inclusion bodies (Buchanan 1999). This approach has produced 5-100 milligrams of protein per liter of culture. Subsequent in vitro refolding has yielded functional protein and in many cases crystals diffracting to high resolution (Dekker, Merck et al. 1995; Schmid, Kromer et al. 1996; Surrey, Schmid et al. 1996). Thus the choice of expressing the outer membrane protein either in their native state or inclusion bodies depends on the feasibility of the expression and the needs.

The expression of OmpG in inclusion bodies was favored over expressing in the membrane for the following reasons:

a) Native expression of OmpG from a multi-copy plasmid yields around a milligram per liter of culture and co-purifies with large amount of lipids (Fajarado et al 1998; Behlau et al 2001). The protein yield is insufficient for 3D crystallization and the presence of lipids could be a problem.

b) For solid state NMR measurements the protein needs to be labeled with isotopes, which means that the cells need to be grown in minimal media and it

would be difficult to get enough protein with specific labeling when expressed in the membrane.

My attempts to express OmpG inserted into the membrane resulted in a low yield. Most of the protein was either in the cytoplasm or stuck to the membrane presumably on its way to the outer membrane. The expression in inclusion bodies was by itself a purification step. A further step of purification of unfolded protein by ion exchange in presence of urea yielded very pure protein. The expression in inclusion bodies also allowed specific labeling with isotopes for MAS-NMR experiments (Hiller et al 2005 in press).

6.2.2 REFOLDING OF OmpG IN DETERGENT MICELLE

Refolding of proteins from solubilized inclusion bodies has been achieved either by dilution (Pautsch, Vogt et al. 1999), by dialysis (Surrey, Schmid et al. 1996) or folding on the column (Rogl, Kosemund et al. 1998). These processes have yielded functional protein in varying amounts (Buchanan 1999). With respect to OmpG, the dilution method is most efficient in terms of recovery of refolded product. Dialysis of protein against a detergent does result in refolding but due to removal of urea, the efficiency of refolding is low and aggregates are observed. On-column refolding is also possible but the yield is very low.

It is evident from previous studies that refolding of membrane proteins requires detergent micelles (Kleinschmidt, Wiener et al. 1999). This paper described a screen of detergents with different properties emphasizing that refolding is achieved only when the concentration is above the CMC of the detergent. I followed a similar approach to find the right detergent and its concentration for efficient refolding of OmpG. Phase behavior and assembled structures of detergents are markedly influenced by their unique physical and chemical properties but also by concentration, ionic conditions and presence of lipids and proteins. The CMC, a threshold monomer concentration above which the detergent tends to aggregate and form micelles, whereupon they are capable of solubilizing hydrophobic and amphipathic molecules is one

of the critical parameters in the use of detergent. Many small amphiphiles are known to affect the detergent micelle. Since refolding of OmpG involves urea, I thought it is essential to know the effect of urea on the CMC.

The CMC of detergents at different concentrations of urea is higher than the value obtained in water (Table 6.1 and Figure 6.4). Urea is known to disrupt the structure of water (Bennion and Daggett 2003) and this probably accounts for its effect on the CMC of the detergent. Among the detergents screened the glucosides and glucamides with carbon chain length of 6-9 are more efficient than other detergents. The pH of the buffer or the ionic strength has little effect, while the refolding is more efficient at higher temperature. The optimal condition for refolding is found with a final concentration of urea >3M, at 20°C incubated for 8 hours. Mass spectrometry revealed no degradation or modification of OmpG along the purification and refolding process (Figure 6.10). Similar results have been independently confirmed and published by another group (Conlan and Bayley 2003).

Gel filtration and blue native gel electrophoresis show a monomeric protein as expected from previous studies (Conlan, Zhang et al. 2000). Aggregates are rarely observed. The peak from the gel filtration when analyzed by SDS gel electrophoresis showed the presence of both the unfolded and folded forms. This can be explained as a completely folded and an intermediate form that is stuck to the detergent micelle.

In the presence of SDS, the intermediate product can be unfolded easily. It is well known that the □ barrel proteins can resist the action of SDS, hence the differential migration (Dornmair, Kiefer et al. 1990). This observation prompted me to use SDS in the gel filtration elution buffer for separating the two forms. The gel filtration yielded 2 peaks differing in retention volume (1.53 & 1.64ml). The peak at R_v of 1.64ml contained predominantly the folded form and the peak at R_v of 1.53ml contained the unfolded form. SDS is a difficult detergent to remove and hence this procedure of separating the folded and

unfolded forms was not pursued further.

After identifying the optimal conditions for refolding of OmpG, the procedure was scaled up. A second step of ion exchange was included to enrich the folded form. This additional step resulted in >95% of folded OmpG (Figure 6.12 & 6.13).

6.2.3 CRYSTALLIZATION IN THE LIPID BILAYER

Refolded OmpG yielded 2D crystals readily under similar conditions as described previously (Behlau et al. 2001). However, in contrast to native protein these crystals were small tubes and poorly ordered (Figure 6.14). Various parameters were screened to improve crystals. Crystallization at higher temperature yielded wider tubes and sheets that were multiple layers. These crystals were ordered to 6Å. The two crystals (narrow and wide tubes) differ slightly in their unit cell (Table 6.3). The small tubes have a longer b axis and this perhaps suggest that these crystals are more loosely packed. The higher temperature may influence the tighter packing by increasing the rate of detergent removal and promoting hydrophobic interactions, resulting in better ordered crystals. At the same time, it is worth mentioning that the higher temperature promotes the formation of stacked membranes (Figure 6.15).

The native OmpG co-purified with large amount of lipids, so it was necessary to remove them by phospholipase treatment and subsequent purification for crystallization (Behlau et al 2001). Since refolded OmpG does not contain any lipid one would expect it to form better crystals but it looks like some other parameter might have been critical that yielded better crystals of native OmpG. I tried different lipids but they did not improve the crystals much. Lipid such as phosphaditylcholine that is not a major *E.coli* lipid also yields small tubular crystals. Nevertheless, these crystals were good enough to collect untilted image by cryo-EM and are being used for MAS-NMR with greater success (Hiller et al 2005).

Having said that temperature promotes better ordering it is also worth mentioning the simultaneous observation of small tubes. This raises the question if there is an additional unidentified parameter that is needed to improve the crystals. This is a thought because crystals harvested and stored at 4°C, when checked after a period of months show only a single unit cell and well ordered irrespective of whether they are small tubes or sheets. The images from some of the multiple layered membranes were used for the processing since individual layers could be separated.

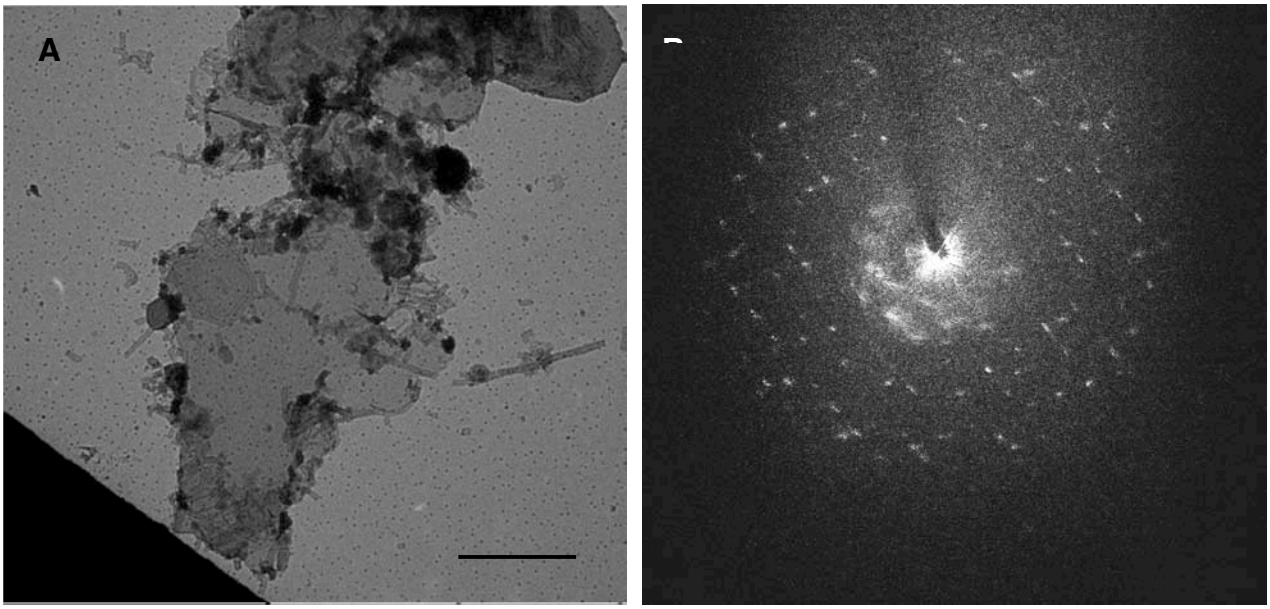

Figure 6.21: An example of multiply stacked membrane (A) and the diffraction pattern (B) (Scale bar – 2 □m). Due to the presence of more than one lattice the diffraction pattern looks confusing but they could be separated during indexing and processed. This image could be merged with single isolated tubes of similar unit cell with good agreement.

6.2.4 COMPARISON OF PROJECTION MAPS FROM NATIVE AND REFOLDED OmpG

Two crystal forms (centered and orthorhombic) were obtained for OmpG purified from native membranes that were ordered to 5Å (Behlau et al 2001). From the refolded OmpG only orthorhombic crystal type was observed. The unit cell and the projection map were comparable and a map calculated to 6Å showed features that were very similar to that of native OmpG. The phase statistics of both these data sets to 6Å were also similar. These observations confirmed that OmpG refolded by detergent dilution had attained its native structure.

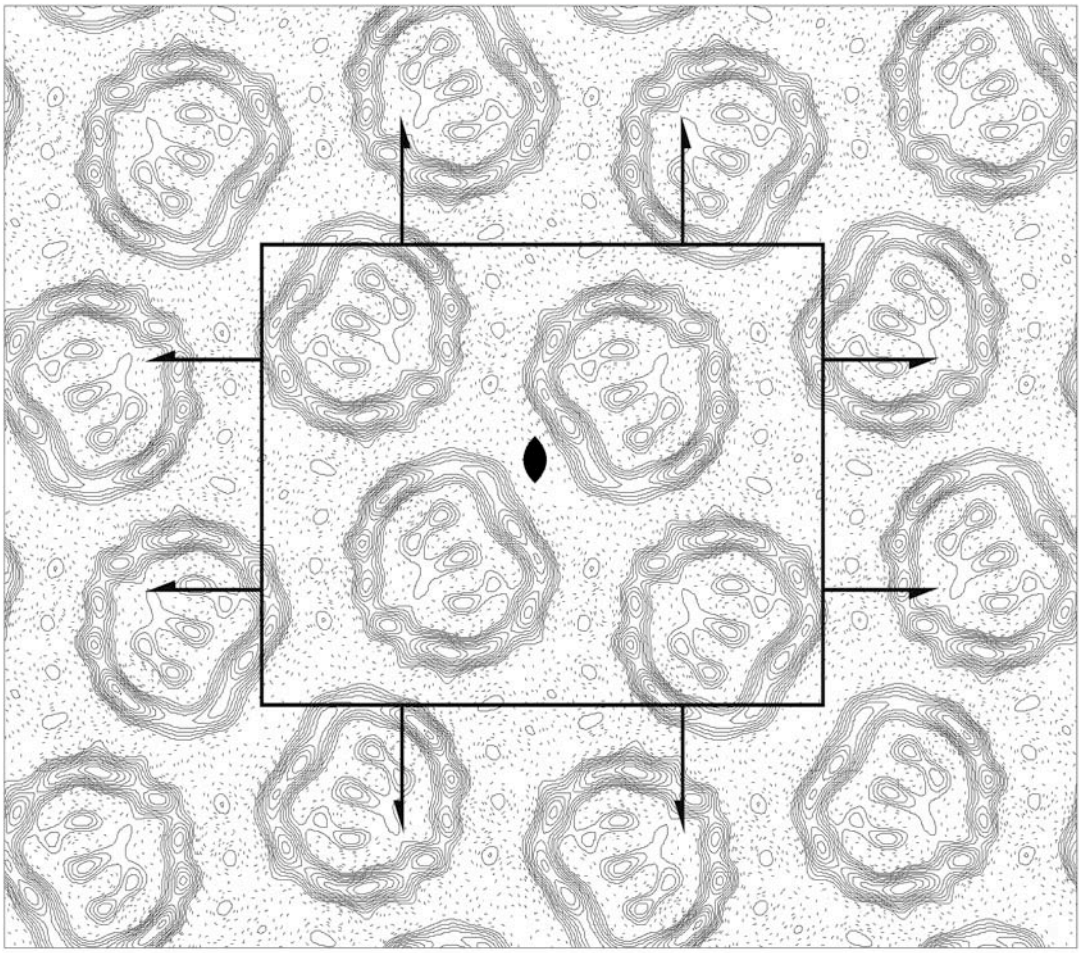

Figure 6.22: Projection of refolded OmpG at 6Å showing the internal loops. The map was calculated to a maximum density of 250 contoured in steps of 25 with a B factor of –300.

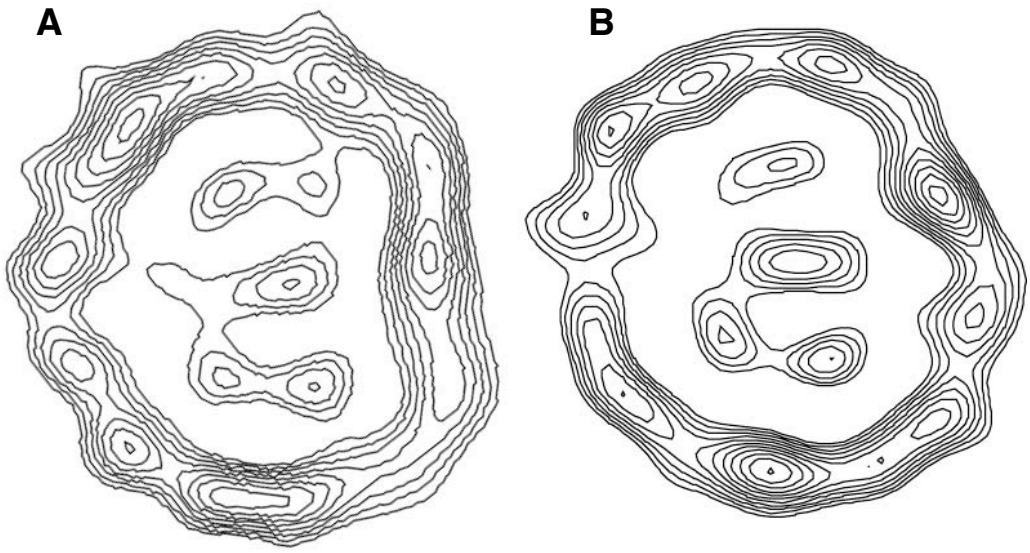

Figure 6.23: Comparison of refolded OmpG (A) and native OmpG (B) with only positive contours shown. The picture of native OmpG was taken from Behlau et al 2001. Both maps at 6Å but contoured differently.

The small size of the tubular crystals and the multiple layered crystalline sheets hampered my efforts to collect tilted images by cryo-EM and the construction of a 3D map. The fact that refolded OmpG looks essentially as the native protein and the high yield of protein prompted me to carry out 3D crystallization trials. Many different outer membrane porins have been successfully crystallized and their structure determined at high resolution, probably because of their stability and the large amount of protein obtained (Bannwarth and Schulz 2003). Hence it was easy to get the crystals of OmpG in different detergents. However, as is often the case with membrane proteins the resolution was low. Initial efforts to improve the crystals were not fruitful. Recently, Dr.Yildiz has obtained OmpG crystals diffracting to 2Å from a similar preparation and the structure will be solved in the near future.

Thus a multiple approach for structural solution of OmpG has resulted in 2D crystals suitable for MAS-NMR as well as electron microscopy (discussed in chapter 7). A projection map calculated from these 2D crystals shows essentially the same structure as the native protein. It will be interesting to compare the structures of OmpG obtained by x-ray crystallography and MAS-NMR once they are available.

7 GENERAL DISCUSSION

7.1 NOTES ON MEMBRANE PROTEIN EXPRESSION

One important aspect of success in structural biology lies in the ability to obtain sufficiently large amounts of protein to be able work on different aspects from function to structure. Not many membrane proteins are naturally abundant and for those that are, the structures have been solved (Section 1.10.1). This means that one has to look for systems that can produce a sufficient amount of protein to carry out crystallization trials and eventual structure determination as well as biophysical and functional studies. A wide range of expression systems have been developed in the past years (Tate 2001) that offer many different options. I have been working only with *E.coli* expression systems but working with different proteins yielded some observations that I thought might be interesting to discuss. Some parameters critical in obtaining good reproducible expression were:

1) Freshly streaked plates from glycerol stocks were essential to achieve reproducible and efficient expression of proteins. Occasionally, as an alternative approach freshly transformed cells were used. Use of fresh cells was important in particular when the antibiotic was ampicillin. Ampicillin is a weak antibiotic and even if a single cell finds a means to digest this drug then it could allow other satellite colonies to grow and eventually outnumber the cells that might have the vector and the gene of interest.

2) It was very important to follow the growth of the cells throughout the expression, in particular after induction. The behavior of cell growth described the ability of the cells to cope with expression.

I observed four different growth behaviors that depended on the protein and the cell strain. These include:

1) Cells start lysing after induction
2) Growth stops after induction
3) Growth slows after induction
4) No change in growth after induction

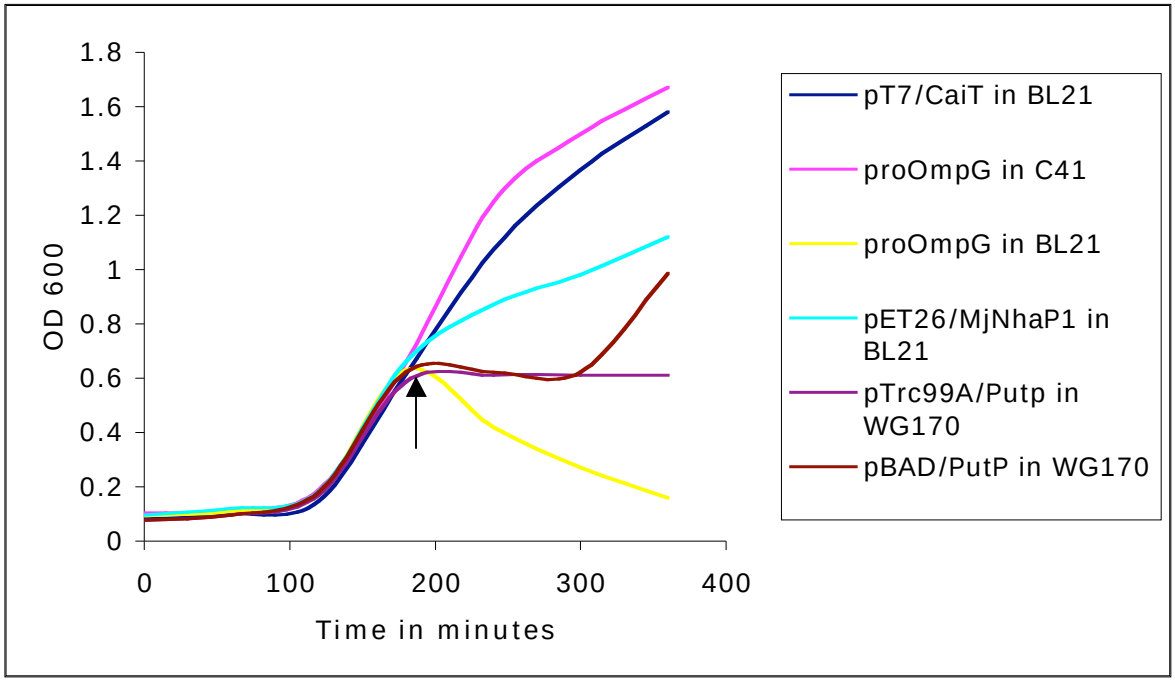

Figure 7.1: Growth curve of cells expressing different membrane proteins. The arrow indicates the time of induction either with 1mM IPTG or 0.2% arabinose.

Except for the expression of CaiT that showed a normal cell growth, all the other strains showed different behavior. My explanations for the above observation are as follows:

1) OmpG without its leader peptide was expressed as inclusion bodies in cytoplasm. Efficient expression was obtained only with strains C41 or C43, derived from BL21 that were generated by adaptation (Miroux and Walker 1996). Expression of proOmpG or OmpG without leader peptide in strain BL21 resulted in cell lysis after induction.

2) When PutP was expressed in strain WG170 with the Tac promoter, growth stopped after induction. The amount of cells obtained was low but this did not affect the amount of protein obtained. An interesting observation was made with cells expressing PutP with an arabinose promoter. The growth stopped after induction but after two hours or so the growth of cells started again. I think this is because the cell metabolizes arabinose while IPTG is a non-metabolizable substrate whose presence might tend to keep the growth retarded.

3) The only heterologous expression that has been described in this study is that of MjNhaP1 from the archaeon *Methanococcus jannaschii*. The expression of this protein slowed the cell growth after induction. Similar results were observed with another transporter (LacS) from *Archeaglobus fulgidus*. In both these cases the yield of protein was low as expected for a heterologous expression.

7.1.1 Why are different growth behaviors observed

It is becoming evident that most of the membrane proteins one way or the other use the protein secretion machinery for inserting into the membrane. It was thought that only the outer membrane proteins use the Sec translocon to by pass the inner membrane in order to reach the outer membrane but recent experimental evidence shows that even the inner membrane proteins tend to use coupled translation and insertion (de Gier, Mansournia et al. 1996; de Gier, Scotti et al. 1998).

Cells undergo a dual problem when over-expression is carried out. They have to maintain their cellular machinery for survival and at the same time produce enough protein to keep the experimenter happy. There are numerous cellular processes that are affected by the over-expression but I would like to focus on only the post-translational processes. Some important proteins that have been implicated in cell division are dependent on the translocon. So when the expression is induced, the ribosome and the protein secretion machinery are heavily worked and a failure of normal cellular proteins to reach their particular site results in either cell lysis or retardation of cell growth. Cell lysis has been observed with toxic soluble proteins from eukaryotic sources and even from *E.coli* [subunits of ATP synthase] (Kurland and Dong 1996; Miroux and Walker 1996). Outer membrane proteins when over-expressed with their leader peptide have shown to be very toxic resulting in cellular filamentation and lysis (Klose, Schwarz et al. 1988). This behavior can be explained by the jamming of the secretion machinery and subsequent block of cell division resulting in filamentation and cell lysis. Hence it was not

surprising that OmpG when expressed with leader peptide in BL21 strains resulted in cell lysis. However, the derivatives of the BL21 strains C41 and C43 (Walker strain) have shown to cope with the stress (Arechaga, Miroux et al. 2003) and could hold either OmpG or proOmpG better than their parent strains. The exact reason how these strains cope with the stress is not very clear.

A similar explanation would be valid for the observed growth profile of PutP in strain WG170. Involvement of ribosomes and the secretion machinery is further supported by the fact that when PutP expressed from an arabinose inducible promoter cells stop growing initially but once the stress is released they start growing again (Figure 7.1). All these facts stress the importance of using the right medium for expression. In my experience I find that LB or 2xYT media is optimal for growth but a rich medium such as terrific broth (TB) does not help to obtain more protein. When compared with LB, the purity of protein obtained after metal affinity chromatography from cells grown in TB is lower possibly due to higher cell density and non-specific binding of other abundant proteins. Alternatively, the cell growth could be slowed by a reduction in the growth temperature, thereby minimizing the load on the secretion machinery. However, the effect of temperature on the lipid composition of the membranes is dramatic and this can affect solubilization or protein quality, so any change in growth temperature should be used cautiously. I would like to emphasize that maintaining cell stocks and cell growth is important for efficient expression because these initial steps are most important to produce enough protein for large crystallization trails.

7.2 OLIGOMERIC STATE OF MEMBRANE PROTEINS

Oligomerization of membrane proteins provides a possible mechanism for stability and the specific regulation of proteins as well as the membrane structure. Experimental determination of the physiologically relevant oligomeric state of a protein is technically demanding and no single method can be said to be satisfactory. The oligomeric state of membrane proteins can

be analyzed either in detergent solution or in the membranes. A variety of techniques that have been used to analyze proteins in detergents include analytical ultracentrifugation, size-exclusion chromatography and blue native gel electrophoresis. In these techniques the determination of the amount of bound detergent/lipids, purity and the stability of the protein are critical (Heuberger et al 2002). It would be more realistic to study the oligomeric state in the membrane since it is the native environment. However it is more demanding than working with detergents. The dimensions and the oligomeric state in the membrane can be estimated from high-magnification electron-microscopic images, rotational mobility of the molecule, chemical cross-linking and genetic approaches (Gerchman, Rimon et al. 2001).

In my thesis I have used few of these techniques to analyze the oligomeric state of the membrane protein. Results from four different proteins is summarized in the following table:

Table 7.1:

Protein	Gel filtration Retention volume in ml	Blue native gel		2D crystals
		Observed mass (kDa)	Oligomeric state	
OmpG	1.64	65	monomer	monomer
PutP	1.51	75	monomer(?)	trimer
CaiT	1.42	240	trimer	trimer
MjNhaP1	1.62	134	dimer	dimer

Blue native gel electrophoresis has been used to study the oligomeric state of membrane proteins, including the SecYEG complex (Bessonneau, Besson et al. 2002), glutamate transporter (Gendreau, Voswinkel et al. 2004)

and lactose permease from *S.lactis* (Heuberger et al., 2002). Recently, the supercomplexes of the respiratory chain have been separated and purified from the blue native gels and subsequently used for structural studies (Schäfer E, personal communication). The advantage of the blue native gel system is the ability to analyze many different samples simultaneously and only a low amount of protein is required. Since the detergent is displaced by Coomassie (CBB) dye, the major drawback would be the solubility and stability of the protein and one would need to know the additional mass of bound CBB to able to calibrate the protein mass based on the known masses of soluble proteins.

During my work I used blue native gel electrophoresis extensively and this technique has helped in determining the oligomeric state of membrane proteins. I overcame the problem of measuring the bound CBB by using a ladder of oligomers generated by aggregation (Chapter 5, Figure 5.10). Except in the case of PutP (Figure 4.3) the oligomeric state of all other proteins could be determined accurately by blue native gel. However, many researchers are skeptical about the results obtained by blue native gel electrophoresis, since detergent is displaced by dye and this does not represent the native state. There are two experimental data in favor of the oligomeric state that I have determined by blue native gel electrophoresis.

1) The addition of SDS to the protein before loading on the BN gel results in dissociation of oligomers, if they are present. A comparison of this SDS dissociated and control protein without addition of SDS would indicate the oligomeric state (Figures 3.2, 5.4, 6.11). This is a simple and easy way to convince.

2) The biggest advantage I have had is the possibility to obtain 2D crystals of all these proteins. 2D crystals represent the native environment and indicate the structural unit of the proteins in lipid bilayer. The results I obtained by BN gel electrophoresis were in complete agreement with that of 2D crystals except in the case of PutP where the oligomeric state in detergent was

uncertain.

Since all these proteins have been studied in DDM on the same column (Superose 6), the retention volume in the gel filtration column could be used for comparison. I know from blue native gels and 2D crystals that OmpG is a monomer while MjNhaP1 is a dimer but the volume of these proteins in DDM are 1.64 and 1.62 ml respectively indicating that it would be difficult to determine the oligomeric state by the Stokes's radius alone. Since CaiT and PutP elute earlier than OmpG and MjNhaP1 this could indicate an oligomer greater than monomer. But the peak obtained with PutP is broad and could mislead in the assumption of oligomeric state. The amount of bound detergent and the shape of the protein-detergent micelle for each protein differ and for these reasons I have used gel filtration as a method to check the stability and for estimating the amount of aggregates, in complementation to blue native gel rather than to determine the oligomeric state.

7.3 STRATEGIES FOR SCREENING OF 2D CRYSTALS

2D crystals are produced by reconstitution of purified membrane protein into lipid bilayers and subsequent detergent removal. The advances in microscopy and experimental techniques have yielded highest resolution for a membrane protein by electron crystallography of 1.8Å (Gonen et al unpublished data; Fujiyoshi et al unpublished data). These results hold promise for 2D crystallization and electron crystallography. However screening is one of the limitations for 2D crystallization and cryo-EM, unlike 3D crystallization where one can screen a large number of conditions fast. A minimum of 10-15 minutes is required to screen one sample in the electron microscope and when unordered vesicles are observed, the need to check by freeze fracture EM requires a couple of more days. Approaches based on fluorescence light microscopy are still at an experimental stage and might be a solution in the future.

Membranes contain a large number of proteins and the advantage of 2D

crystallization is the minimal requirement of protein. If one could predict from the sequence a possible crystallization condition then that would speed up the procedure of crystallization with a focused approach. Based on my experience working with different proteins and from literature, I have tried to derive a possible strategy for initial crystallization and improving them, and in the end describing some common limitations that one faces with 2D crystallization and cryo-EM.

7.3.1 pH AND IONIC STRENGTH

In my experience, the most important parameter to obtain initial crystals is the pH of the buffer used for crystallization. The variation in the pH induces a change in the net charge of the protein, which will influence the interaction between the protein and hence crystallization. The approach I used for obtaining 2D crystals of different proteins was to start with a pH screen ranging from 4-9 with or without salt. The formation of vesicles and ordered arrays always required the presence of salt typically 0.1-0.25 M of monovalent ions. This screen yielded crystals pinpointing a narrow pH range for each protein. The crystals of PutP were obtained in pH range 5-5.5 and at pH7.5-9 for CaiT. In the case of MjNhaP1, acidic pH was obligatory for crystal formation, this I reasoned as a conformational lock at low pH as has been proposed for the homologous *E.coli* NhaA (Williams et al 1999).

As shown in tables 7.2 and 7.3, the optimal crystallization condition of membrane proteins has been found roughly two pH units from the theoretical pI, which holds good for most proteins. I have not done any experiment for determining the actual pI but using the information from the amino acid sequence it was possible to get an initial condition that was used as a platform. Although the theoretical pI could be used as a starting point this may also be deceiving as was the case with CaiT (Chapter 5). A more realistic way would be to determine isoelectric point of each protein experimentally and to compare this with the crystallization conditions reached. This way the system could be optimized and used as a platform in future.

There is a minimal ionic strength required for any protein to form crystals which can either be sodium or potassium salts. The influence of other salts or glycerol or additives depends on the particular system. The use of divalent ions such as magnesium or zinc in particular has been shown to be essential for formation of 2D crystals as I found with OmpG where crystals formed only in the presence of magnesium. Methyl-pentane-diol had been tried for NhaA initially (Williams et al 1999) and subsequently for MjNhaP1 (Vinothkumar, Smits et al. 2005).

7.3.2 LIPID

The choice of lipid for crystallization is critical. Use of mixture of lipids such as *E.coli* polar lipids provides a good starting point. Since this mixture has both charged and neutral lipids with different chain lengths and saturation, further screening with individual lipids could be derived from this mixture. If the crystals are poorly ordered, then one can screen for synthetic lipids such as the phosphatidylcholines, which was essential for obtaining better crystals of CaiT.

7.3.3 DETERGENT

One important parameter that is often overlooked in 2D crystallization is detergent. This is because of thinking that detergents are removed and why bother? However, experience shows that the quality and initial concentration of the detergent plays a major role in getting efficient reconstitution (Chapter 4 and 5). I have used always a second detergent to solubilize the lipids as has been reported for different proteins and generally one needs to find an optimal detergent by trial and error. My experience with OmpG shows that irrespective of detergents it formed similar tubes and therefore OmpG may not have been a good system to carry out such a study. I admit that I have not done a systemic study to describe the effect of a combination of detergents. In practice it is best to use a higher CMC detergent for solubilizing lipids against a low CMC detergent for the protein (Table 7.3).

7.3.4 METHOD

In my experience the most efficient method for obtaining 2D crystals was detergent removal by dialysis. This is also evident in the literature and highlighted in both tables. Except for proteins that are crystalline in vivo (such as bacteriorhodopsin), crystals of most other proteins have been obtained by dialysis, in particular the proteins that were over-expressed (Table 7.3). As described in chapter 4, use of biobeads is often not suitable due to the rapid rate of detergent removal. Even when crystals are obtained, they are generally poor (Mosser, Breyton et al. 1997).

7.3.5 TEMPERATURE

The effect of temperature on 2D crystallization is multiple. It affects the rate of detergent removal, fluidity of lipids and the hydrophobic interaction. Generally, detergent removal at room temperature or 37°C was found to be successful in the majority of cases and this was also observed with the proteins I worked on.

TABLE 7.2: 2D CRYSTALS OF PROTEINS DERIVED FROM NATURAL SOURCE

Proteins	Protein (mg/ml)	Lipids	Detergent Protein	Detergent Lipid	LPR (w/w)	Temp. (°C)	Theoretical pI	Optimal pH	Salt	Crystal type[a]	Resolution in Å[b]	Method	Ref.
BR	2.6	Native	OG	DTAC	-	20	6.28	5.2	-	sheets	3.4	Batch	1
LHCII	2.3	Native	NG	TX100	-	25↗37↘25	4.99	7	-	sheets	3.4/4.9	Batch	2
PSI_1	1.6	DMPC	DDM	OTG	0.25	25↗37↘25		7	Mg	3D		Dialysis	3
PSI_2	1	DMPC	OTG	OTG	0.8-1	26↗37↘26		6	NH_4^+	sheets		Dialysis	4
PSII_1	3.3	Native	DDM	HTG	-	19		6.5	Zn,Na,Ca	ves+2D		Biobeads	5
PSII_2	-	DMPC	OTG	-	0.1-1	6 ↗ 22		6	Na	tubes	8	Dilution	6
PSII_3	2	Native	HTG	-	-	20		6.5	Na,Zn	ves+2D		Biobeads	7
bc1	3.6	Mixture	TX100	-	1	4		8	Zn	tubes		Biobeads	8
b6f	0.5-1	PC & PG	HG	-	0.2	4,3x(-196),4		8	Ca	3D		Biobeads	9
Cytb0U0	1	PC & PE	TX100	-	0.29	37		9	-	tubes	6	Dialysis	10
PhoE	-	DMPC	-	-	0.25	-		-	-	-	3.5	-	11
MIP	1	E.coli	DM	OG	1	23↗37↘32		6	Na,Mg	ves+sheets	9	Dialysis	12
AQP0	0.5	E.coli	OG	-	0.5	25↗35↘25		6	Na	sheets	3/3.5	Dialysis	13
AQP1	1	DMPC	OG	-	-	RT		7.4	-	sheets	3.8/4.6	Dialysis	14
CaPump	-	Native	-	-	-	0		7.3	K,Mg	tubes	8	Induction	15
NaPump	1-2	Native	$C_{12}E_8$	-	0.25	20 ↘ 4		5.5	K	vesicles			16
H-ATPase	1	Native	DDM	-	-	4	5.03	6.8	NH_4^+	vesicles	8/22	Surface	17
b-rhodopsin	1	Native	LDAO	-	-	18	5.87	7	Na,Mg	tubes	5/13	Dialysis	18
f-rhodopssin	1	Native	Tween20	-	-	20	7.48	7.5	Na	tubes	6	Batch	19
Gap-junction	1	Native	Tween20	DHPC	-	27		7.5	K,Na	sheets	7/17	Batch	20
Acetylcholine Receptor	-	Native	-	-	-	-				tubes	4	in situ	21
Glutathione Transferase	0.5-1.75	Bovine PC	TX100	Cholate	3-5 (m/m)	21	7.67	7	K	sheets	6/12	Dialysis	22

Important parameters for obtaining are highlighted in red when known

[a] – ves denoted vesicles, [b] – resolution parallel/perpendicular to the membrane

1- Baldwin and Henderson 1988; 2 – Kühlbrandt and Wang 1991; 3 – Ford et al 1990; 4 – Karrash et al 1996; 5 – Hankammer et al 1999; 6 – Tsiotis et al 1996; 7 – Nakazato et al 1996; 8 – Akiba et al 1996; 9 – Mosser et al 1997; 10 – Gohlke et al 1997; 11 – Jap et al 1988; 12 -Hasler et al 1998 13 – Gonen et al 2004; 14 - Murata et al 2000; 15 – Toyoshima et al 1993; 16 – Mohraz 1999; 17 – Auer et al 1998; 18 – Krebs et al 1998; 19 – Schertler et al 1995; 20 – Unger et al 1997; 21 – Unwin 2003; 22 – Schmidt-krey et al 2000

Table 7.3: 2D CRYSTALS OF OVER-EXPRESSED PROTEINS

Proteins	Protein (mg/ml)	Lipids	Detergent Protein	Detergent Lipid	LPR (w/w)	Temp. (°C)	Theoretical pI	Optimal pH	Salt	Crystal type[a]	Resoltuion in Å[b]	Method	Ref
Nha A	0.5-0.8	E.coli	DDM	DM	0.2-0.5	37	9.28	4	K	tubes	7/14	Dialysis	1
MjNhaP1	0.5-1	E.coli	DDM	DM	0.4-0.5	37	5.46	4	Na	tubes	7	Dialysis	2
EriC	-	POPC	DDM	DM	0.4	-	8.38	7	Na/Mg	sheets	6.5	Dialysis	3
MelB	1	E.coli	DDM	DDM/OG	0.1	22	8.67	6	Na	tubes	8	Dialysis	4
OxlT		E.coli/POPC	DHPC	Cymal-7	0.15-0.4	37 ↘ RT	9.67	4.5	K	sheets/tubes	6.5/12	Dialysis	5,6
LacY[c]	-	DMPC&POPC	DDM	OG&DM	0.5-1.5	4↗13↗37↘13	-	7.4	Na,Mg	tubes,ves	25	Dialysis	7
BetP	1	E.coli	DDM	DM	0.15-0.25	20	5.51	7.5	Na	ves	7.5	Dialysis	8
CaiT	0.5-1.5	E.coli/POPC	DDM	DM	0.4-0.5	37	8.55	9	Na	ves/stacks	25	Dialysis	u
PutP	1	E.coli	DDM	DM	0.25-0.5	37	7.74	5[d]	Na	ves/stacks	20	Dialysis	u
GltPh	1	E.coli	DDM	DM	0.8-1.2	20	8.94	7.9	Na	ves	25	Dialysis	u
AmtB	0.5	DMPC	DDM	DM	0.4-1.4	-	6.26	8	Na	ves	12	Dialysis	9
EmrE	0.5-1	DMPC	DDM	CHAPS	0.1-0.4	-	7.72	7-7.5	Na/Mg	tubes	7/16	Dialysis	10
ATP carrier[e]	1.5	DOPC	DDM	DDM	0.2-0.45	8	9.82	6	Na	tubes	8	Dialysis	11
TetA	0.5-1	DMPC,POPC	DDM	DM	0.5-1.5	37	9.61	7.4	Na/Mg	tubes/ves	25	Dialysis	12
KcsA	1-2	DMPC	DDM	Cholate	-	RT	10.3	7.5	K	sheets	5	Dialysis	13
OmpG	0.5-2	E.coli	var	DM	0.1-0.75	37	4.6	7	Na/Mg	tubes/sheets	6	Dialysis	14
TolC	1	E.coli	C_8E_5	C_8E_5	-	35	5.46	7	Na/Mg	stacks	12	Dialysis	15
Kv1.2	0.8	DMPC/BPL	DDM	Chapso	0.4	37	-	6.8	K	ves	15	Dialysis	16
LTC4	1	DMPC	TX100	Cholate	1	RT	10.2	7.6	K	sheets	4	Dialysis	17
C-rings	1	POPC	OG	OG	0.5	20 ↗ 37	4.43	7.5	Na	tubes/ves	4/15	Dialysis	18
FhuA	1	E.coli	LDAO	OTG	0.5	RT	5.47	8	Na	ves+sheets	8	Dialysis	19
AqpZ	0.5	POPC/DMPC	DDM	OG	0.5	RT ↗ 37	6.96	6	Na,Mg	sheets	6	Dialysis	20
SecYEG	1	PE	$C_{12}E_9$	$C_{12}E_9$	0.2	23	-	8	Na	tubes	8/16	Dialysis	21

Important parameters for obtaining are highlighted in red where known

[a] ves denoted vesicles [b]– resolution parallel/perpendicular to the membrane, [c] – fusion protein with cytochromeC, [d] – crystals formed only with minidialyzer, [e] – crystals with inhibitor

1- Williams et al 2000; 2-Vinothkumar et al 2005; 3-Mindell et al 2001; 4-Heymann et al 2002 5-Heymann et al 2003; 6-Hirai et al 2002; 7-Zhuang et al 1999; 8-Ziegler et al 2004; 9- Conroy et al 2004; 10- Tate et al 2001; 11 – Kunji et al 2003; 12 – Yin et al 2000; 13 – Li et al 1998; 14 – Behlau et al 2002; 15 – Koronakis et al 1997; 16 – Parcej et al 2004; 17 – Schmidt krey et al 2004; 18 – Vonck et al 2002; 19 – Lambert et al 1999; 20 – Ringler et al 1999; 21 – Breyton et al 2002; u – unpublished observations

7.3.6 LIMITATIONS

2D crystals and projection map has been obtained for number of proteins but the three-dimensional map is available for only a handful of proteins (14 out of 43). The possible reasons are:

a) Formation of stacks of membranes or crystal growth in the third dimension, which I think is by far the most common problem for lack of 3D maps. A close look at the tables confirms this fact and indicates why people tend to go for 3D crystals (as in the case of TolC). Examples to overcome stacking are very scarce in literature but few approaches that have worked includes the temperature ramping and optimization of detergent concentration as in the case of LHCII (Kühlbrandt 1992) or use of high salt concentration (2M) as in the case of TolC (Koronakis, Li et al. 1997). My efforts to overcome the stacks in the cases of PutP and CaiT were not successful. This is one particular problem for which I don't have a very clear understanding and to solve it would require more work. Since surface charges play a possible role in formation of these stacks one approach would be to mutate residues on the loops to encourage the formation of single layered sheets.

b) The structure being solved by x-ray crystallography before a 3D map can be constructed is the second limitation. A handful of proteins have suffered such a fate, including the potassium channel (KcsA), ammonium channel (AmtB) and the chloride channel (EriC). In the case of the calcium pump the resolution obtained with 2D crystals was limited to 8Å (and were stacked), hence 3D crystallization was favored and has resulted in a series of high-resolution structures in different conformations. Once a well diffracting crystal is obtained then it is relatively easier to obtain atomic resolution by x-ray crystallography than electron microscopy, which is why 3D crystallization is favored.

In spite of the x-ray structures, there are things that can possibly be done only by 2D crystals as shown long ago by N.Unwin with connexins and acetylcholine receptor. The structure of bovine rhodopsin was solved by x-

ray crystallography in the ground state (Palczewski, Kumasaka et al. 2000; Okada, Fujiyoshi et al. 2002) but so far it has not been possible to obtain photoactivated state in 3D crystals. Freeze trapping of photointermediates has been possible for bacteriorhodopsin and a similar approach with rhodopsin yielded the 3D map of one of the intermediate (Ruprecht, Mielke et al. 2004). Also, I have illustrated in my work the use of 2D crystals to study effect of pH on the sodium/proton antiporter.

7.4 MAS-NMR AS A COMPLEMENTARY APPROACH

One important understanding that we have gained from electron microscopy and the MAS-NMR studies of OmpG is the need for crystalline samples to get a nice spectrum. For this OmpG was reconstituted at different LPR's that yielded tubular crystals as well as non-crystalline vesicles and analyzed subsequently by MAS-NMR.

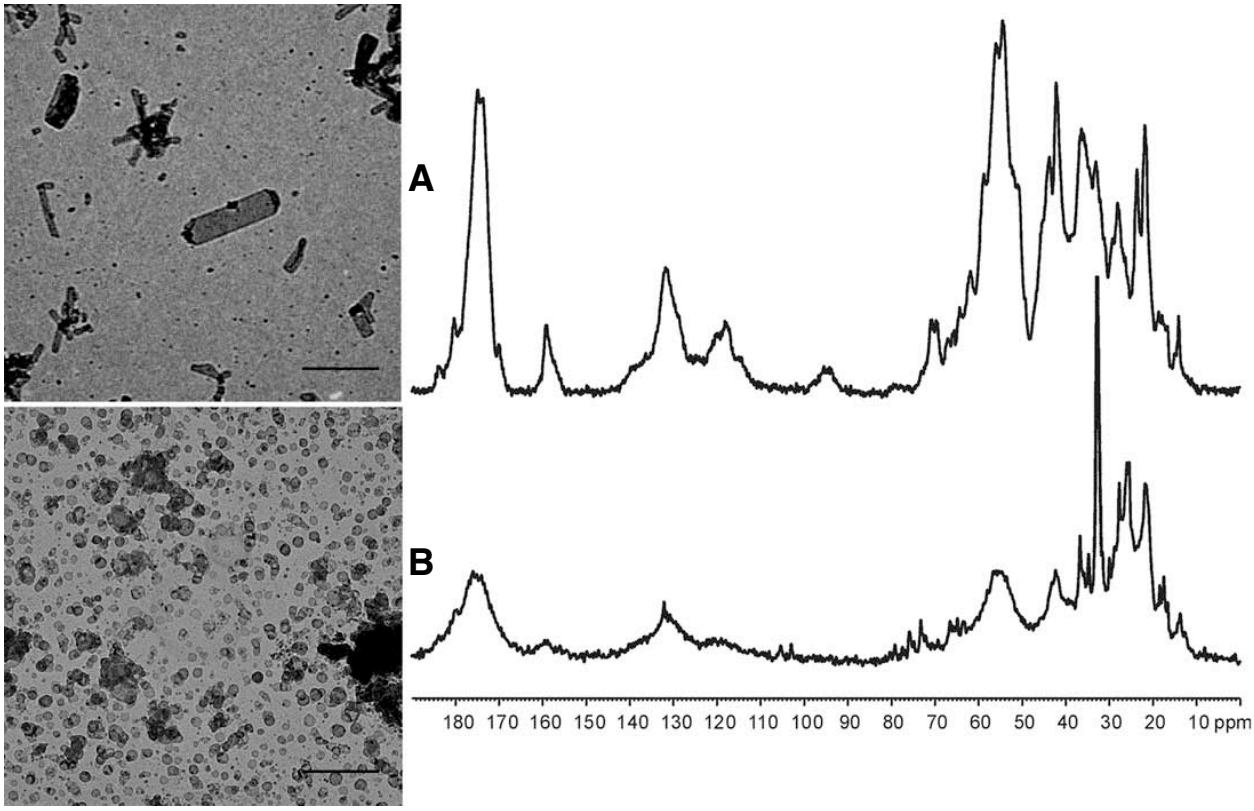

Figure 7.2: Electron micrographs and MAS-NMR spectrum of two different OmpG preparations.
A – The NMR spectrum shows peaks corresponding to the side chains of the protein. Spectra obtained from small crystalline tubes
B – The NMR spectrum shows only one sharp peak that probably corresponds to natural C^{13} lipid. Spectra obtained from non-crystalline vesicles.
(Figure reproduced from Hiller et al 2005).

The spectrum obtained with both these preparation differ remarkably and only when the sample is crystalline, sharp peaks are observed (Hiller et al 2005). In contrast non-crystalline vesicles show peak broadening and only one peak at around 30 ppm attributed to naturally abundant C^{13} in lipids (Figure 7.2B).

When 2D crystals are poorly ordered and not suitable for electron crystallography then MAS-NMR is a very good alternative. One important requirement would be to obtain large amount of labeled protein that might be the limiting factor in some cases. As described in the case of OmpG 2D crystals ordered to 8-10Å were sufficient to yield nice spectrum (Figure 7.2) that could be used to assign amino acids such as threonine and proline. These results indicate that long-range order is not required for MAS-NMR as in the case of diffraction techniques. MAS-NMR would be an alternative for example in the case of PutP where I could obtain 2D crystals but stacking makes it difficult to work with electron crystallography. If these crystals could be used for MAS-NMR then it will be interesting to see how the spectrum looks for a completely □-helical protein and the kind of structural information that could be obtained. Further, MAS-NMR could be used to study the dynamics of this transporter during substrate binding and translocation.

7.5 COMPARISON OF ION TRANSPORTERS

The formation of ion gradients across the membrane depends on two basic properties, primarily on the nature of the lipid bilayer as an impermeable ion barrier and secondly on the existence of ion transport proteins that can either be carriers, pumps or channels. The maintenance of these ion gradients is critical for many biological processes. Several secondary ion transporters along with the primary ion pumps act in concert to bring about ion homeostasis. The common pathways for ion flux in many different cells include the sodium/proton, potassium/proton and chloride/proton or bicarbonate exchange pathways.

As described in the introduction, depending on whether a cell undergoes

shrinkage or swelling due to the changes in osmolarity of the medium these ion transporters function respectively in transporting specific ions. Evidently little structural information has been obtained for ion transporters even though they are important physiologically. The structural information is available at different resolutions for ion transporters both by cryo-EM and x-ray crystallography. The x-ray structures include the high-resolution structures of a chloride antiporter (Dutzler et al 2002) and a sodium/proton antiporter (Hunte et al 2005) both from *E.coli*. Along with these, projection maps of two different sodium/proton antiporters, one anion exchanger and a chloride antiporter in the lipid bilayer are available. There is no significant sequence homology between these ion transporters but one common structural feature is shared by all of them this is their occurrence as a structural dimer in the membranes (Wang, Kühlbrandt et al. 1993; Williams 2000; Mindell, Maduke et al. 2001; Vinothkumar, Smits et al. 2005). The reason for this is not clear. From the structures there is no evidence that the dimer is important for function. But it has been proposed for Band 3 that a simultaneous mechanism, whereby two substrates are moved in opposite directions at the same time would be an advantage of having such an oligomeric arrangement in the membrane (Casey and Reithmeier 1991) and a possible co-operativity in regulation. All these proteins are antiporters transporting ions and a distinguishing feature is their ability to respond to pH that is well documented for Na^+/H^+ antiporter (Padan et al 2004; Hayashi et al 2002; Hellmer et al 2002) but unclear for the anion exchanger or the chloride transporter.

The projection structure of the membrane domain of the anion exchanger from erythrocytes was the first structural information obtained for an ion transporter showing a dimeric protein by negative stain EM at 20Å (Wang et al 1993) and subsequent 3D map revealed pore like features at the dimer interface as well within the monomer (Wang, Sarabia et al. 1994). At that time it was proposed that ion translocation pathway might be at the dimer interface. But today, we know from the x-ray structures (Dutzler et al 2002; Hunte et al 2005) as well as from two different conformations of MjNhaP1 that

each monomer has its own pathway for ion-translocation and both substrates use the same pathway. Whether this will also hold true for band3 needs to be verified. As shown in figure 7.3 it is quite interesting that in spite of the functional similarity (i.e., all are antiporters) these structures differ remarkably.

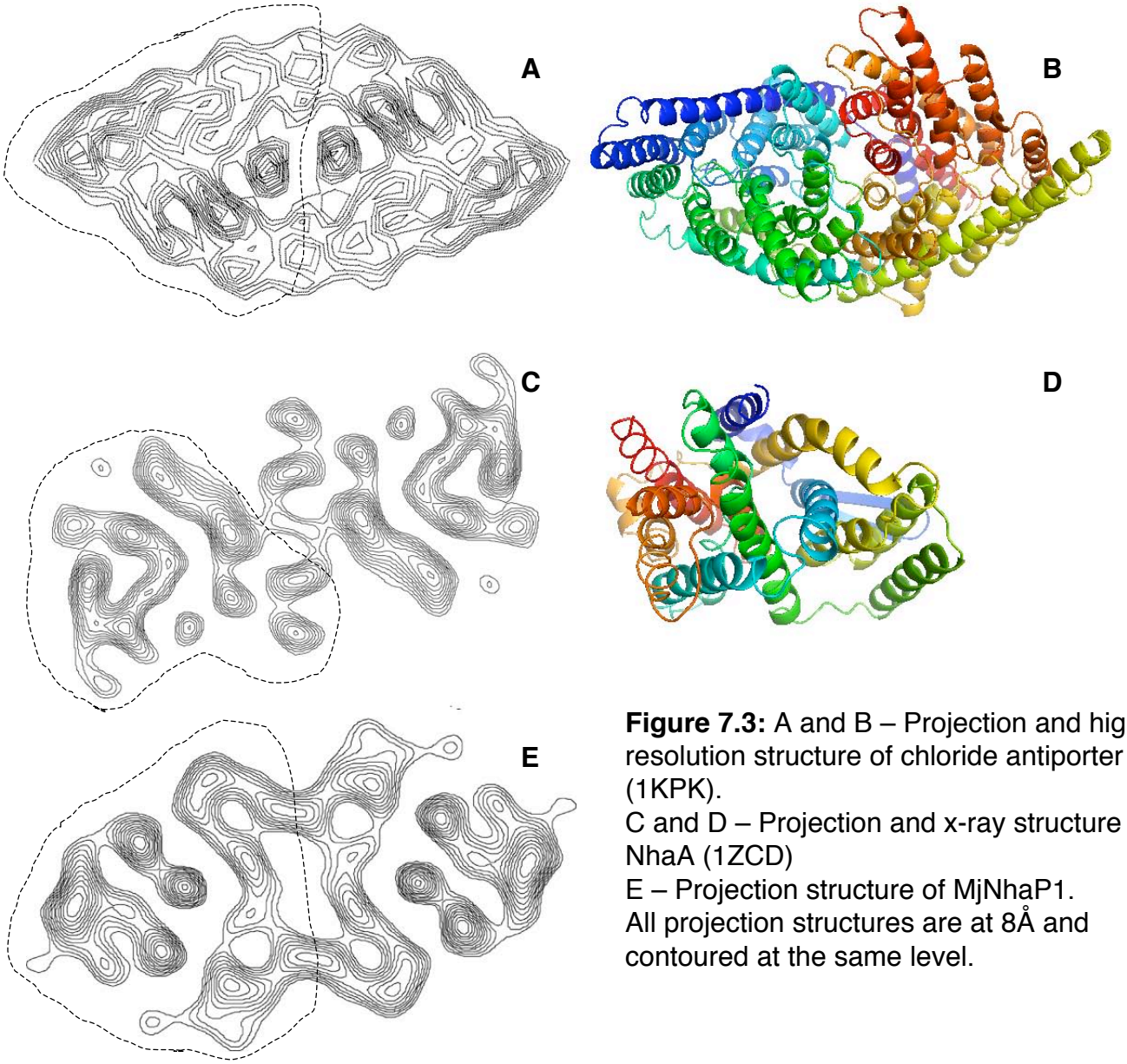

Figure 7.3: A and B – Projection and high-resolution structure of chloride antiporter (1KPK).
C and D – Projection and x-ray structure of NhaA (1ZCD)
E – Projection structure of MjNhaP1.
All projection structures are at 8Å and contoured at the same level.

The structure of chloride antiporter (Figure 7.3 B) show highly tilted □-helices, which are variable in length. Two halves in a monomer wrap around a

common centre such that the amino acids at the end of α-helices from different segments of polypeptide chain forms the selectivity filter within the membrane (Dutzler et al 2002). The N-terminus of helices from separate regions come together to form a positive end charge and point toward the binding site creating an electrostatically favorable environment for anion binding. The structure of NhaA shows two domains each of six helices essentially as visualized in the 3D map reconstructed from 2D crystals (Williams 2000; Hunte et al 2005). At the centre of the domain interface a funnel opens into the cytoplasm that is negatively charged suitable to attract cations. Thus these two antiporters use a common mechanism of helix-dipole to attract their respective ions. In the case of NhaA, deformation of regular α-helix of two TM domains (IV and XI) is unique and might play a role in the mechanism of substrate translocation.

The mechanism of transporters has been described based on an “alternating access” hypothesis (Jardetzky 1966). Two gates allow alternating access to the intra-membranous substrate-binding site from each side of the membrane. The x-ray structures shed light on the possible gates present in the antiporters. In the chloride antiporter, a glutamate residue on the periplasmic side has been postulated to act as one of the gates. This is supported from the mutation of glutamate that makes the protein transport only chloride (Dutzler et al 2003). But still the transporter doesn’t behave as a channel as one would expect (Accardi et al 2004) indicating the presence of an additional gate speculated to be a tyrosine on the cytoplasmic side. Similarly, deprotonation of aspartates has been proposed for activity of sodium/proton antiporters (Hunte et al 2005;Vinothkumar et al 2005).

7.5.1 MECHANISTIC DIFFERENCE BETWEEN SOLUTE AND ION TRANSPORTERS

From the structures of the solute transporters, the alternating access mechanism has been hypothesized to involve large movement of domains (Abramson et al 2003; Huang et al 2003; Yernool et al 2004; Pebay-Peyroula

et al 2003). These transporters have a low turnover between 4-40 per second (Table 7.4), which has been attributed to the extent of conformational change these transporters undergo. In contrast, the ion transporters have a rate in the range of 10^3-10^5 per second taking an intermediate position between the pumps and channels.

Table 7.4: RATE OF SECONDARY TRANSPORTERS

Transporters	Turnover number per second	Reference
Solute transporters		
LacY	10	Vitanen et al. 1984
GlpT	40	Auer et al. 2001
ATP/ADP carrier	13	Klingenberg 1981
MelB	4	Pourcher et al. 1990
Ion transporters		
EriC	10^5	Accardi et al 2004
Band 3	10^4	Wieth et al. 1982
NhaA	10^3-10^4	Dibrov et al. 1993

The higher rate implies that the ion transporters undergo small conformational changes such as rotation or tilt of individual helices or changes in sets of residues rather than movements of whole domains as observed for solute transporters of the major facilitator family or the calcium pump (Toyoshima et al 2004). The first instance of one such conformational change of an ion transporter related to its activity has been mapped in MjNhaP1 and the extent of change correlates well with the rapid dynamics needed for the faster rate of these transporters.

Ion transporters are at the heart of membrane transport. They are involved in maintaining the balance of ions and pH (Section 1.7 and 3.2.8) that are critical for cell survival. The higher transport rate correlates directly with the important function they carry out. These transporters use inward directed sodium or chloride gradient to maintain the intracellular pH. The

anion exchanger in the erythrocytes constitutes the major membrane protein which functions in removal of bicarbonate using the chloride gradient (Figure 7.4). Uncontrolled pH or the conversion of bicarbonate to carbon dioxide is undesirable for cells. This means that all these transporters have to act fast to a given response such as a change in pH and hence the higher rate. In fact the rate-limiting factor in removal of CO_2 from red blood cell is the number of band 3 molecules in the membrane and its turnover.

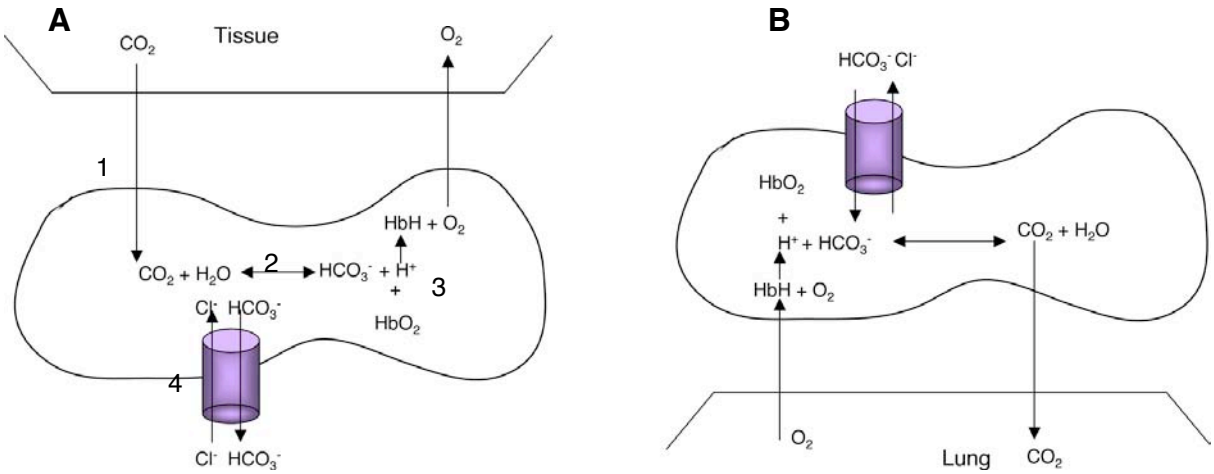

Figure 7.4: Schematic representation of partial processes involved in the transport of CO_2 as HCO_3^- in blood (redrawn from Weith 1982). This diagram indicates the importance of ion transporter (Band 3) in the removal of carbon dioxide.
A) Sequence of events in a tissue capillary
1 – Diffusion of CO_2 into the red cell
2 – Carbonic anhydrase catalyzed hydration of CO_2 to carbonic acid
3 – Buffering by hemoglobin (Hb)
4 – Exchange of intracellular HCO_3^- for extracellular chloride

B) Reverse sequence of events in lung capillaries

In the context of evolution, ion transporters bridge the gap between the channels and the pumps. I would like to add few words on the need to work on the eukaryotic homologues of the ion transporters. Recent evidences suggests that NHE1 and band 3 interact with each other indirectly via carbonic anhydrase (Li, Alvarez et al. 2002). The cytoplasmic C-terminal domain of both these transporters has been shown to interact with carbonic

anhydrase, a key enzyme catalyzing the reversible conversion of carbon dioxide to bicarbonate. This enzyme has high turnover number of 10^6 per second (Stein 1990) and the enzymatic activity of carbonic anhydrase produces protons as well as bicarbonate (Figure 7.4), an interaction with the ion transporters will increase the efficiency of removal of these ions (Sterling, Reithmeier et al. 2001). Such an assembly is termed as 'metabolon'. The presence of these carboxy terminal domains in the eukaryotic transporters and their importance in function and regulation implicate the need for obtaining high-resolution structures of these eukaryotic transporters.

The structural information obtained is the beginning in understanding of these dynamic transporters. In projection two of the sodium/proton antiporters differ significantly (Figure 7.3). I believe that residues and the architecture in the ion binding sites of sodium/proton antiporters will largely be similar (Appendix) and these transporters might differ in their response to pH and regulation. This highlights to need for determining the structure of transporters that might show some sequence homology but might differ structurally. 2D crystallization and electron microscopy will be suitable to carry out such an approach. If they differ significantly at low resolution then one could carry out efforts on high-resolution studies by x-ray crystallography as exemplified in the case of MjNhaP1. I personally feel it is wise to carry out multiple approaches in structural solution for membrane proteins.

ZUSAMMENFASSUNG

Alle lebenden Zellen werden von einer Membran umgeben, die als Barriere einen ungehinderten Stoffaustausch mit der Umgebung verhindert. Diese aus Lipiden bestehende Doppelschicht ermöglicht den Zellen die Aufrechterhaltung eines konstanten inneren Milieus. In die Membran eingebettete Proteine kontrollieren den notwendigen Stoffaustausch mit der Umgebung und verleihen den Zellen dynamische biochemische Anpassungsmöglichkeiten.

Der Transport von Substraten über die Membran kann mit Hilfe von Transportern oder Kanälen erfolgen. Letztere bezeichnen Proteine mit einer Pore, durch die das Substrat auf die andere Seite der Membran gelangt, ohne notwendigerweise an das Protein zu binden. Kanäle können daher ausschließlich entlang eines Konzentrationsgefälles transportieren. Im Gegensatz dazu haben Transporter eine definierte Bindungsstelle, die wechselseitig von den beiden Seiten der Membran zugänglich ist. Unter Energieverbrauch können Transporter auch Substrate entgegen einem Konzentrationsgefälle transportieren. Der eigentliche Transportvorgang erfolgt dabei entweder durch Diffusion des Proteins von einer Seite der Membran zur anderen, oder durch eine Konformationsänderung des Proteins, welche die Bindungsstelle von der anderen Seite der Membran aus zugänglich macht.

Primäre und sekundäre Transporter unterscheiden sich in der Energiequelle, die sie nutzen. Primäre Transporter nutzen ATP oder Lichtenergie für den Transport von Substraten entgegen dem Konzentrationsgefälle. Sekundäre Transporter nutzen den von den primären Transportern aufgebauten elektrochemischen Gradienten für den Transport. Primär- und Sekundärtransporter beeinflussen sich gegenseitig, da sie beide das über die Membran aufgebaute elektrochemische Potential verändern. Die Sekundärtransporter stellen eine der größten Familie innerhalb der

Membranproteine dar. Sie zeichnen sich durch zahlreiche, die Membran durchspannende Helices aus und können aufgrund ihrer Sequenz-Homologie und ihrer Funktion in verschiedene Familien eingeteilt werden. Der Transport des Substrates ist häufig an den Transport von H^+ und Na^+ gekoppelt und beruht in den meisten Fällen auf einer Konformationsänderung des Proteins, die den Zugriff auf die Substrate alternierend von den beiden Seiten der Membran ermöglicht. Für den Transport nahezu jeder niedermolekularen Substanz gibt es Sekundärtransporter, die nach diesem Prinzip den Transport ihrer Substrate über die Membran katalysieren (Sobczak und Lolkema 2005). Für ein Verständnis der Transportvorgänge auf der Ebene der Aminosäuren oder der beteiligten Atome fehlen strukturelle Informationen, insbesondere über die Unterschiede zwischen den verschiedenen Konformationen der Proteine. In den letzten Jahren sind die Strukturen von 7 verschiedenen Sekundärtransportern gelöst worden, die uns Momentaufnahmen der Architektur dieser dynamischen Proteine zeigen (Murakami et al. 2002; Dutzler et al. 2002; Abramson et al. 2003; Huang et al. 2003; Ma und Chang 2003; Yernool et al. 2004; Hunte et al. 2005). Trotz des grundlegenden gemeinsamen Mechanismus der Konformationsänderung unterscheiden sich die bisher gelösten Strukturen erheblich und haben eine Reihe von Fragen nicht ausreichend beantwortet

A) Gibt es auf struktureller Ebene ein gemeinsames Prinzip aller Sekundärtransporter oder handelt es sich um individuelle Lösungen?

B) Ist es möglich, die Änderung der Konformation zu studieren?

C) Ist es möglich, Transporter in unterschiedlichen Konformationen zu kristallisieren?

Ich habe daher in meiner Doktorarbeit Sekundärtransporter aus verschiedenen Familien untersucht. Im Mittelpunkt standen dabei Transporter, deren menschliche Homologe im Zusammenhang mit verschiedenen Erkrankungen stehen. Das Hauptaugenmerk der Arbeit lag neben der Expression und Aufreinigung der Proteine auf der 2D Kristallisation, die eine

strukturelle Untersuchung verschiedener Konformationen des Proteins durch Tieftemperatur-Elektronenmikroskopie (cryo-EM) erlaubt. Verschiedene 2D Kristalle zeigten eine Tendenz sich zu stapeln und dünne 3D Kristalle auszubilden. Dieses Verhalten habe ich als Ansatzpunkt für die Züchtung von 3D Kristallen genommen. Einige der Kristalle zeigten eine moderate Auflösung.

Ich habe im Folgenden die Hauptresultate zusammengefaßt, die ich für die verschiedenen bearbeiteten Proteine erreicht habe.

1) 2D Kristallisation von MjNhaP1 und pH induzierte Strukturveränderung: Na^+/H^+ Antiporter sind pH-abhängige Transporter, die für die Homeostase von H^+ und von Na^+ in lebenden Zellen verantwortlich sind. Der untersuchte Na^+/H^+ Antiporters (MjNhaP1) stammt aus *Methanococcus jannaschii*, einem hyperthermophilen Archaeon, das bei 85˚C optimal wächst. Das Protein wurde in *E.coli* heterolog exprimiert und aufgereinigt. Nach Rekonstitution des Proteins in Membranen bildeten sich 2D Kristalle bei einem pH-Wert von 4. Tieftemperatur Elektronenmikroskopie der Kristalle erbrachte eine Projektionskarte des Proteins in der Membran mit einer Auflösung von 8Å. Ähnlich wie der *E.coli* Antiporter NhaA (Williams et al. 1999), ist MjNhaP1 ein Dimer. Aber bereits in der Projektion unterscheiden sich die Strukturen der beiden Antiporter erheblich. Wir haben den Effekt einer Veränderung des pH-Wertes auf die Struktur von MjNhaP1 untersucht. Nach Erhöhung des pH Wertes auf pH 6 kam es innerhalb von Minuten zu einer Veränderung der Dichteverteilung innerhalb des Helixbündels und eine Verschiebung der Position des Bündels relativ zum Zentrum des Dimers. Die zwei Konformationen bei niedrigem und hohem pH repräsentieren wahrscheinlich den geschlossenen und geöffneten Zustand des Antiporters. Dies ist der erste Hinweis auf eine Konformationsänderung im Zusammenhang mit der Funktion eines Sekundärtransporters (Vinothkumar et al. 2005). Die dreidimensionale Untersuchung der pH-induzierten Konformationsänderung ist z.Zt. in Arbeit.

2) 2D Kristallisation des Prolintransporters:

Der Prolintransporter (PutP) von *E.coli* transportiert Natrium und Prolin im Verhältnis 1:1 und gehört damit in die Familie der Natrium-abhängigen Symporter, zu denen auch krankheitsrelevante Glukose- und Jodidtransporter beim Menschen gehören (Jung et al. 2001). Gereinigtes PutP wurde rekonstituiert und kristallisierte zu sechseckigen 2D Kristallen. Die Membranen zeigten eine ausgeprägte Tendenz sich zu Stapeln anzuordnen und somit dünne 3D Kristalle zu bilden. Ein Projektion der negativ kontrastierten 2D Kristalle von PutP zeigte eine trimere Anordnung des Proteins in der Membran. Im Gegensatz dazu ist für andere Mitglieder der Natrium Symporter Familie gezeigt worden, dass die Monomere aktiv sind (Eskandari et al. 2002). Mit Hilfe eines nativen Acrylamid-Gels konnte ich zeigen, dass das von mir gereinigte PutP in Lösung ebenfalls als Monomer vorliegt. Wahrscheinlich kann PutP als Monomer arbeiten, neigt aber bei höherer Konzentration und nach der Rekonstitution in die Membran dazu Trimere zu bilden. Die Bedeutung des Trimers für die Funktion des Proteins muss weiter untersucht werden.

3) Biochemische Charakterisierung und Kristallisation des Carnitintransporters von *E.coli*:

Der Carnitintransporter (CaiT) gehört der BCCT (Betain-, Carnitin- und Cholintransporter) Superfamilie der Sekundärtransporter an, die Moleküle mit quarternären Aminen wie Betain und Cholin transportieren. Er tauscht externes L-Carnitin gegen internes □-Butyrobetaine aus, wobei die Bedeutung dieses Transportes unbekannt ist. Die Sequenz von CaiT weist auf 12 Transmembranhelices hin. Im Gegensatz zu anderen Mitglieder dieser Transporterfamilie ist es nicht auf einen Ionengradienten angewiesen und reagiert nicht auf osmotischen Druck (Jung et al. 2002). Die Expression des Proteins liefert mehr als 2mg reines Protein pro Liter Kultur. Native Gelelektrophorese, Gelfiltration und Cross-Linking Experimente zeigen übereinstimmend, dass das Protein als Trimer isoliert wurde.

Elektronenmikroskopische Aufnahmen des isolierten Proteins zeigten eine dreieckige Struktur von drei Massen oder von zwei parallelen länglichen Dichten. Die länglichen Dichten stellen möglicherweise die Seitenansicht von 2 gestapelten Trimeren dar. Nach Rekonstitution von CaiT in Membranen formten sich 2D Kristalle, die in Projektion ebenfalls ein Trimer zeigten. Die große Stabilität des gereinigten Proteins legte es nahe eine 3D Kristallisation zu versuchen und ich habe Kristalle mit einer Auflösung von 6.5Å erhalten.

4) Äußeres Membran Protein G (OmpG):

Festkörper NMR ist eine alternative Möglichkeit die Struktur von Membranproteinen zu lösen, falls 2D oder 3D Kristalle nicht gut genug geordnet sind. Allerdings gibt es bisher noch keine Struktur eines Membranproteins, das durch NMR gelöst wurde. Gemeinsam mit Prof. Hartmut Oschkinat, Berlin wurde daher als Pilotprojekt die NMR Untersuchung des OmpG durchgeführt, einem Protein aus der äußeren Membran von *E.coli*. OmpG wurde ausgewählt aufgrund seiner geringen Größe von 33 kDa.

Nach Überexpression in *E.coli* konnten große Mengen an Isotopen-markiertem Protein aus Einschlusskörper gewonnen werden. Mehr als 90% des Proteins konnten in die native Form zurückgefaltet werden und kristallisierte sowohl nach Rekonstitution in Membranen als auch in Detergenzlösung. Die 2D Kristalle waren röhrenförmig und beugten bis zu einer Auflösung von 8Å. Die Struktur ist der des nativen Protein sehr ähnlich (Behlau et al. 2002). Der geringe Durchmesser der Röhrchen begrenzt allerdings die Auflösung der gekippten Aufnahmen und damit die Auflösung der dreidimensionalen Struktur. Die Kristalle können aber für Festkörper-NMR eingesetzt werden, wobei im Vergleich zu rekonstituiertem Protein ohne Ordnung die Halbwertsbreite der NMR Signale durch die 2D Kristalle deutlich verringert ist (Hiller et al. 2005). In der Zukunft bietet NMR daher die Möglichkeit, die Dynamik des Proteins zu studieren. 3D Kristalle von OmpG in Detergenz mit einer Auflösung von 5.5Å konnten ebenfalls erzeugt werden

und werden momentan verbessert.

Meine Untersuchungen unterstreichen die Bedeutung von unterschiedlichen Techniken für die strukturelle Untersuchung von Membranproteinen sowohl in Membranen als auch in Lösung. Im Post-Genome Zeitalter ist eine Annäherung an die Struktur der Membranproteine von verschiedenen Seiten notwendig.

APPENDIX

SEQUENCE ALIGNMENT OF TWO ANTIPORTERS FROM *M.jannaschii*

M.jannaschii encodes for two closely related sodium/proton antiproters and are designated as MjNhaP1 and MjNhaP2. Both proteins show for 48% identity and 75% similarity, indicating a gene duplication event during evolution.

A

```
  1 VNIVLFLGYLSILFAGGAIIAKIAKKIGIPDIPLLLIFGLILS.ILNVIP  49
    ::::: :|||:: :. |.::||||.|: |||||||||::|||:: :|.:||
  1 MELMMAIGYLGLALVLGSLVAKIAEKLKIPDIPLLLLLGLIIGPFLQIIP  50

 50 KNIVESSFDFIGNFGLIILLFIGSFEMEWNIMKRVLDVIIKLDILALLIV  99
    .: . . |:: | :|||::|: |.|.|  .::|||:..:::||.:.:||.
 51 SDSAMEIFEYAGPIGLIFILLGGAFTMRISLLKRVIKTVVRLDTITFLIT 100

100 WIISGIVFNFVFHLPILSLIGLLFGAIVSATDPATLIPIFSSMDIDPEVA 149
    ::|||::||:|::||. | :|.|||||..||||||||:||.: .:||||
101 LLISGFIFNMVLNLPYTSPVGYLFGAITAATDPATLIPVFSRVRTNPEVA 150

150 ITLEAESVFNDPLGIVVTLICLSALGLAKAENPILEFFSLAVGGIILGVI 199
    |||||||:|||||||| | :.|: :|| ...||::::.||.|:|::|::
151 ITLEAESIFNDPLGIVSTSVILGLFGLFSSSNPLIDLITLAGGAIVVGLL 200

200 AGKFYEIIISKIKFEDYIAPFTLGLAIAFWYFAEGIFPSITGYEISGFMA 249
    :|:|| || ...|.:|:||:.|| |: ::|.:::::|||.||::||:||
201 LAKIYEKIIIHCDFHEYVAPLVLGGAMLLLYVGDDLLPSICGYGFSGYMA 250

250 VAIMGLYIGNVIVHKKEHKKDMEKVAVFMDELSIFIRILIFVLLGASISI 299
    |||||||:|:.:.  :... | . :. | |:||:: |::|||:|||:|.:
251 VAIMGLYLGDALF..RADDIDYKYIVSFCDDLSLLARVFIFVFLGACIKL 298

300 PLLEKYALPAFLCALGSILLARPVGVLIATAIPPIRPLTERIYLALEGPR 349
    .:||.| :|::|.|||||:||||:||:::  |.. :.:.|::|:|||||
299 SMLENYFIPGLLVALGSIFLARPLGVFLG.LIGSKHSFKEKLYFALEGPR 347

350 GVVPATLAAMVYTEIMKHPNIVPKNIASLMPPTELAGTILVATFMTIIVS 399
    |||||.||. | .||:|::: :| .|...:.||::||||:::|||||::|
348 GVVPAALAVTVGIEILKNADKIPASITKYITPTDIAGTIIIGTFMTILLS 397

400 VVLEASWAKPLANILL...KRKTSTS... 422
    |:||||||  ||  ||   |.| ...
398 VILEASWAGMLALKLLGEYKPKYKEESHH 426
```

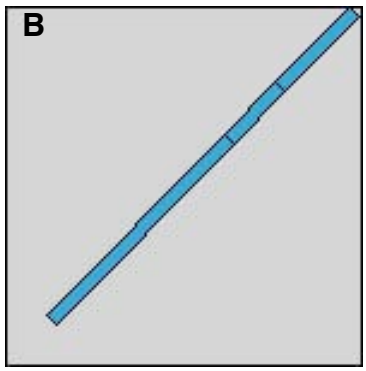

Figure A1:
A- Pairwise alignment of MjNhaP1 (red) and MjNhaP2 (black).

B – Graphical display showing the stretch of conserved regions in both proteins.

SEQUENCE ALIGNMENT OF NhaA and NhaP FAMILY

A multiple sequence alignment of two sub families of sodium/proton antiporters (NhaA & NhaP) shows three regions that are conserved in the transmembrane domains. These conserved residues are implicated in ion binding and transport (Padan et al 2004; Hunte et al 2005).

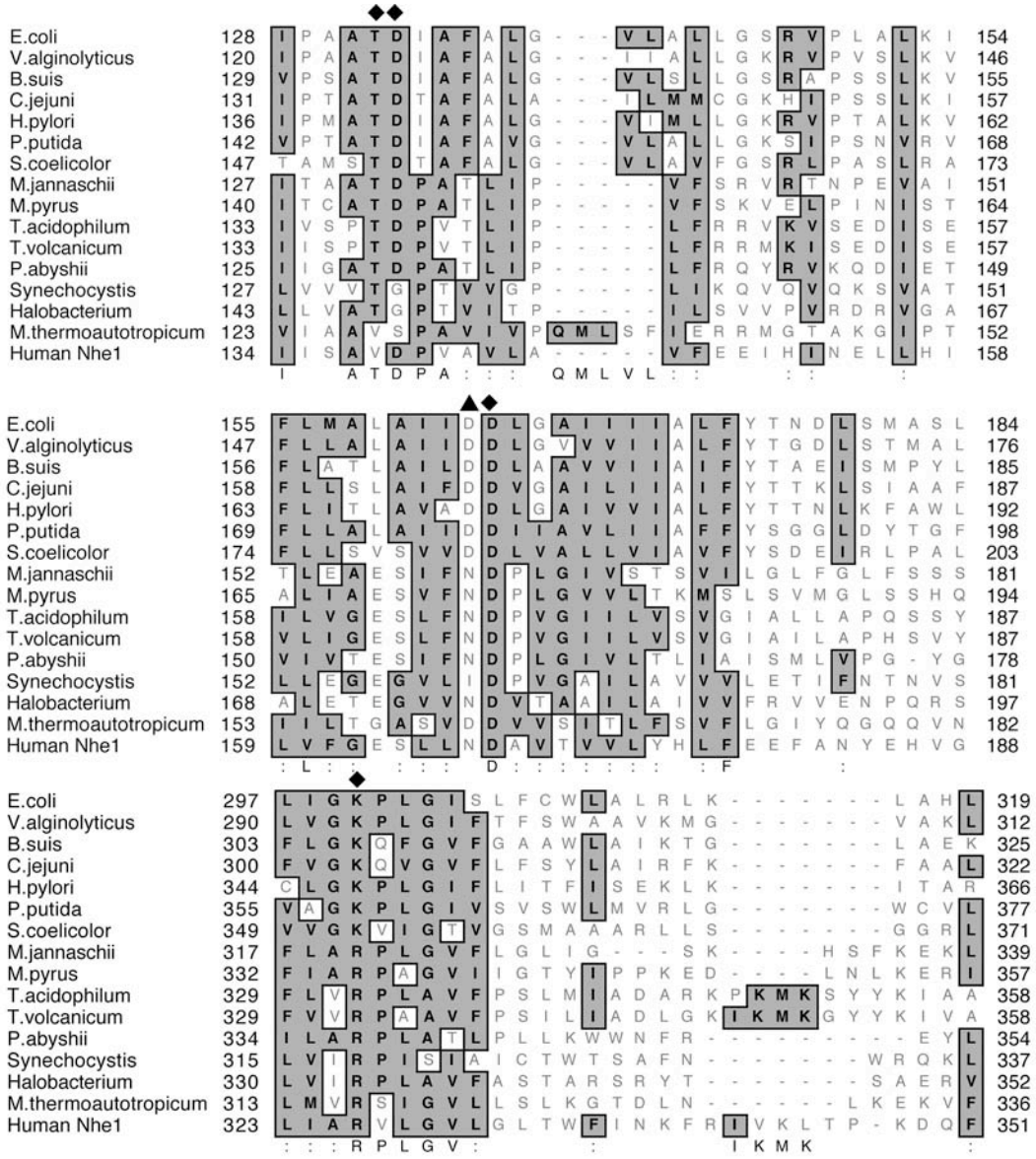

Figure A2: Multiple sequence alignment of NhaA and NhaP subfamilies. The residues marked with diamond are conserved in all the proteins and triangle denotes the residue that is conserved only in NhaA sub-family. The accession numbers are *Escherchia coli* (P13738), *Vibrio alginolyticus* (BAA04944), *Brucella suis* (AAN29343), *Camphylobacter jejuni* (CAB 73643), *Helicobacter pylori* (AAD 08592), *Pseudomonas putida* (NP 743293), *Streptomyces coelicolor* (CAC 03650) *Methanococcus jannaschii* (Q60362), *Methanopyrus kandleri* (NP_613837), *Thermoplasma acidophilum* (NP_394359), *Thermoplasma volcanicum* (NP_111535), *Halobacterium sp.*(NP_280739), *Pseudomonas aeruginosa* (NP_252428), *Pyrococus abyshii* (NP_126974), *Synechocystis sp.* (BAA10477) and Human NHE1

It is known from the biochemical studies that NhaA from *E.coli* is electrogenic with a H^+/Na^+ stoichiometry of 2:1 (Padan et al 2004), while human NHE1 is electroneutral with a stoichiometry of 1:1 (Aronson 1975). When I was aligning sequences from different proteins it struck me that the proteins belonging to the NhaA family all have a double aspartate in TM domain 5, while the NhaP family which includes the Nhe1 have a single aspartate along with an asparagine. In the x-ray structure of *E.coli* NhaA, 2:1 stoichiometry of protons and sodium has been explained based on the presence of two aspartates in the TM 5. It is proposed that the protons from the periplasmic side protonate these aspartates in exchange for a sodium or lithium (Hunte et al 2005). Both aspartates in *E.coli* NhaA are essential for activity. If this proposed mechanism of NhaA is right then it is also likely to explain the stoichiometry of the NhaP family since there is only one aspartate, which might account for the fact that they are electroneutral. The stoichiometry of the *E.coli* NhaA and human NHE1 have been determined experimentally, the stoichiometry of other proteins used in the sequence alignment need to be determined. Whether the mutation of asparagine to aspartate will change the electroneutrality of the NhaP family of transporters will be an interesting experiment to carry out.

ABBREVIATIONS

ACMA 9-amino-6-chloro-2-methoxyacridine

ANS 8-Anilino-1-naphthalenesulfonic acid

BSA Bovine Serum Albumin

□-ME 2-mercaptoethanol

BN Blue Native

BP blue Bromophenolblue

$C_{10}E_6$ Polyoxyethylene (6) decyl ether

$C_{12}E_8$ Polyoxyethylene (8) dodecyl ether

CBB Coomassie Brilliant Blue

CCD Charged Couple Device

CD Circular Dichroism

CHAPS [3-[(3-Cholamidopropyl)-dimethylammonio]-1-propane sulfonate

CHAPSO [3-[(3-Cholamidopropyl)dimethylammonio]-2-hydroxyl-
1- propanesulfonate

CMC Critical Micelle Concentration

Cryo-EM Cryo Electron microscopy

Cymal 6 n-Cyclohexyl-1-hexyl-□-D-maltoside

DM n-Decyl-□-D-maltoside

DDM n-Dodecyl-□-D-maltoside

DHPC 1,2-Diheptadecanoyl-sn-glycero-3-phosphocholine

DPPC 1,2-Dipalmitoyl-sn-glycero-3-phosphocholine

EM Electron microscopy

Hega 8 Octanoyl-N-hydroxyethylglucamide

Hega 9 Nonanoyl-N-hydroxyethylglucamide

IPTG Isopropyl-□-D-thiogalactopyranoside

LDAO n-Dodecyl-N,N-dimethylamine-N-oxide

LPR Lipid to protein ratio

MAS-NMR Magic-Angle Spinning-Nuclear Magnetic Resonance

Mega 8 Octanoyl-N-methylglucamide

Mega 9 Nonanoyl-N-methylglucamide

Mega 10 Decanoyl-N-methylglucamide

MME Monomethylether

MPD 2-Methyl-2-4-pentanediol

NG n-Nonyl-□-D-glucopyranoside

OG n-Octyl-□-D-glucopyranoside

PDB Protein Data Bank

PE Phosphatidylethanolamine

PG Phosphatidylglycerol

PEG Polyethylene glycol

POPC 1-Palmitoyl-2-oleoyl-sn-glycero-3-phosphocholine

SDS Sodium dodecyl sulfate

TM Transmembrane

TX-100 Triton X-100

Tris Tris -(hydroxymethyl-aminomethan)

ZW-3,12 n-dodecyl-N,N-dimethyl-3-amino-1-propanesulfonate

REFERENCES

Abrahams, J. P., A. G. Leslie, et al. (1994). "Structure at 2.8 Å resolution of F1-ATPase from bovine heart mitochondria." Nature **370**(6491): 621-8.

Abramson, J., I. Smirnova, et al. (2003). "The lactose permease of *Escherichia coli*: overall structure, the sugar-binding site and the alternating access model for transport." FEBS Lett **555**(1): 96-101.

Abramson, J., I. Smirnova, et al. (2003). "Structure and mechanism of the lactose permease of *Escherichia coli*." Science **301**(5633): 610-5.

Accardi, A. and C. Miller (2004). "Secondary active transport mediated by a prokaryotic homologue of ClC Cl^- channels." Nature **427**(6977): 803-7.

Akiba, T., C. Toyoshima, et al. (1996). "Three-dimensional structure of bovine cytochrome bc1 complex by electron cryomicroscopy and helical image reconstruction." Nat Struct Biol **3**(6): 553-61.

Ambudkar, S. V., C. O. Cardarelli, et al. (1997). "Relation between the turnover number for vinblastine transport and for vinblastine-stimulated ATP hydrolysis by human P-glycoprotein." J Biol Chem **272**(34): 21160-6.

Ambudkar, S. V., S. Dey, et al. (1999). "Biochemical, cellular, and pharmacological aspects of the multidrug transporter." Annu Rev Pharmacol Toxicol **39**: 361-98.

Arechaga, I., B. Miroux, et al. (2003). "Over-expression of *Escherichia coli* F_1F_0-ATPase subunit a is inhibited by instability of the uncB gene transcript." FEBS Lett **547**(1-3): 97-100.

Aronson, P. S. (1985). "Kinetic properties of the plasma membrane Na^+-H^+ exchanger." Annu Rev Physiol **47**: 545-60.

Arora, A., F. Abildgaard, et al. (2001). "Structure of outer membrane protein A transmembrane domain by NMR spectroscopy." Nat Struct Biol **8**(4): 334-8.

Artigas, P. and D. C. Gadsby (2002). "Ion channel-like properties of the Na^+/K^+ Pump." Ann N Y Acad Sci **976**: 31-40.

Auer, M., M. J. Kim, et al. (2001). "High-yield expression and functional analysis of *Escherichia coli* glycerol-3-phosphate transporter." Biochemistry **40**(22): 6628-35.

Auer, M., G. A. Scarborough, et al. (1998). "Three-dimensional map of the plasma membrane H^+-ATPase in the open conformation." Nature **392**(6678): 840-3.

Baldwin, J. M., R. Henderson, et al. (1988). "Images of purple membrane at 2.8 Å resolution obtained by cryo-electron microscopy." J Mol Biol **202**(3): 585-91.

Bannwarth, M. and G. E. Schulz (2003). "The expression of outer membrane proteins for crystallization." Biochim Biophys Acta **1610**(1): 37-45.

Bayley, H. and L. Jayasinghe (2004). "Functional engineered channels and pores (Review)." Mol Membr Biol **21**(4): 209-20.

Behlau, M., D. J. Mills, et al. (2001). "Projection structure of the monomeric porin OmpG at 6 Å resolution." Journal of Molecular Biology **305**(1): 71-7.

Bennion, B. J. and V. Daggett (2003). "The molecular basis for the chemical denaturation of proteins by urea." Proc Natl Acad Sci U S A **100**(9): 5142-7.

Bessonneau, P., V. Besson, et al. (2002). "The SecYEG preprotein translocation channel is a conformationally dynamic and dimeric structure." Embo J **21**(5): 995-1003.

Booth, I. R. (1985). "Regulation of cytoplasmic pH in bacteria." Microbiol Rev **49**(4): 359-78.

Bott, M. (1997). "Anaerobic citrate metabolism and its regulation in enterobacteria." Arch Microbiol **167**(2-3): 78-88.

Bradford, M. M. (1976). "A rapid and sensitive method for the quantitation of microgram quantities of protein utilizing the principle of protein-dye binding." Anal Biochem **72**: 248-54.

Breyton, C., W. Haase, et al. (2002). "Three-dimensional structure of the bacterial protein-translocation complex SecYEG." Nature **418**(6898): 662-5.

Buchanan, S. K. (1999). "Beta-barrel proteins from bacterial outer membranes: structure, function and refolding." Curr Opin Struct Biol **9**(4): 455-61.

Bult, C. J., O. White, et al. (1996). "Complete genome sequence of the methanogenic archaeon, *Methanococcus jannaschii*." Science **273**(5278): 1058-73.

Cadene, M. and B. T. Chait (2000). "A robust, detergent-friendly method for mass spectrometric analysis of integral membrane proteins." Anal Chem **72**(22): 5655-8.

Casey, J. R. and R. A. Reithmeier (1991). "Analysis of the oligomeric state of Band 3, the anion transport protein of the human erythrocyte membrane, by size exclusion high performance liquid chromatography. Oligomeric stability and origin of heterogeneity." J Biol Chem **266**(24): 15726-37.

Casey, J. R. and R. A. Reithmeier (1998). "Anion exchangers in the red cell and beyond." Biochem Cell Biol **76**(5): 709-13.

Chang, G. and C. B. Roth (2001). "Structure of MsbA from *E. coli*: a homolog of the multidrug resistance ATP binding cassette (ABC) transporters." Science **293**(5536): 1793-800.

Chang, G., R. H. Spencer, et al. (1998). "Structure of the MscL homolog from *Mycobacterium tuberculosis*: a gated mechanosensitive ion channel."

Science **282**(5397): 2220-6.

Christian, J. H. and J. A. Waltho (1962). "Solute concentrations within cells of halophilic and non-halophilic bacteria." Biochim Biophys Acta **65**: 506-8.

Conlan, S. and H. Bayley (2003). "Folding of a monomeric porin, OmpG, in detergent solution." Biochemistry **42**(31): 9453-65.

Conlan, S., Y. Zhang, et al. (2000). "Biochemical and biophysical characterization of OmpG: A monomeric porin." Biochemistry **39**(39): 11845-54.

Conroy, M. J., S. J. Jamieson, et al. (2004). "Electron and atomic force microscopy of the trimeric ammonium transporter AmtB." EMBO Rep **5**(12): 1153-8.

Crowther, R. A., R. Henderson, et al. (1996). "MRC image processing programs." J Struct Biol **116**(1): 9-16.

Csaky, T. Z. (1965). "Transport through Biological Membranes." Annu Rev Physiol **27**: 415-50.

Cuello, L. G., D. M. Cortes, et al. (2004). "Molecular architecture of the KvAP voltage-dependent K^+ channel in a lipid bilayer." Science **306**(5695): 491-5.

de Gier, J. W., P. Mansournia, et al. (1996). "Assembly of a cytoplasmic membrane protein in *Escherichia coli* is dependent on the signal recognition particle." FEBS Lett **399**(3): 307-9.

de Gier, J. W., P. A. Scotti, et al. (1998). "Differential use of the signal recognition particle translocase targeting pathway for inner membrane protein assembly in *Escherichia coli*." Proc Natl Acad Sci U S A **95**(25): 14646-51.

Deisenhofer, J., O. Epp, et al. (1984). "X-ray structure analysis of a membrane protein complex. Electron density map at 3 Å resolution and a model of the chromophores of the photosynthetic reaction center from Rhodopseudomonas viridis." J Mol Biol **180**(2): 385-98.

Dekker, N., K. Merck, et al. (1995). "In vitro folding of *Escherichia coli* outer-membrane phospholipase A." Eur J Biochem **232**(1): 214-9.

Dimroth, P. (1990). "Mechanisms of sodium transport in bacteria." Philos Trans R Soc Lond B Biol Sci **326**(1236): 465-77.

Dimroth, P. (1997). "Primary sodium ion translocating enzymes." Biochim Biophys Acta **1318**(1-2): 11-51.

Dohan, O. and N. Carrasco (2003). "Advances in Na^+/I- symporter (NIS) research in the thyroid and beyond." Mol Cell Endocrinol **213**(1): 59-70.

Dong, J., G. Yang, et al. (2005). "Structural basis of energy transduction in the transport cycle of MsbA." Science **308**(5724): 1023-8.

Dornmair, K., H. Kiefer, et al. (1990). "Refolding of an integral membrane

protein. OmpA of *Escherichia coli*." J Biol Chem **265**(31): 18907-11.

Doyle, D. A., J. Morais Cabral, et al. (1998). "The structure of the potassium channel: molecular basis of K^+ conduction and selectivity." Science **280**(5360): 69-77.

Dubyak, G. R. (2004). "Ion homeostasis, channels, and transporters: an update on cellular mechanisms." Adv Physiol Educ **28**(1-4): 143-54.

Dutzler, R., E. B. Campbell, et al. (2002). "X-ray structure of a ClC chloride channel at 3.0 Å reveals the molecular basis of anion selectivity." Nature **415**(6869): 287-94.

Dutzler, R., E. B. Campbell, et al. (2003). "Gating the selectivity filter in ClC chloride channels." Science **300**(5616): 108-12.

Eskandari, S., E. M. Wright, et al. (1998). "Structural analysis of cloned plasma membrane proteins by freeze-fracture electron microscopy." Proc Natl Acad Sci U S A **95**(19): 11235-40.

Facciotti, M. T., S. Rouhani-Manshadi, et al. (2004). "Energy transduction in transmembrane ion pumps." Trends Biochem Sci **29**(8): 445-51.

Fajardo, D. A., J. Cheung, et al. (1998). "Biochemistry and regulation of a novel *Escherichia coli* K-12 porin protein, OmpG, which produces unusually large channels." J Bacteriol **180**(17): 4452-9.

Fernandez, C., C. Hilty, et al. (2002). "Lipid-protein interactions in DHPC micelles containing the integral membrane protein OmpX investigated by NMR spectroscopy." Proc Natl Acad Sci U S A **99**(21): 13533-7.

Fernandez, C. and K. Wüthrich (2003). "NMR solution structure determination of membrane proteins reconstituted in detergent micelles." FEBS Lett **555**(1): 144-50.

Ford, R. C., A. Hefti, et al. (1990). "Ordered arrays of the photosystem I reaction centre after reconstitution: projections and surface reliefs of the complex at 2 nm resolution." Embo J **9**(10): 3067-75.

Frank, J., M. Radermacher, et al. (1996). "SPIDER and WEB: processing and visualization of images in 3D electron microscopy and related fields." J Struct Biol **116**(1): 190-9.

Fu, D., A. Libson, et al. (2000). "Structure of a glycerol-conducting channel and the basis for its selectivity." Science **290**(5491): 481-6.

Gadsby, D. C. (2004). "Ion transport: spot the difference." Nature **427**(6977): 795-7.

Gadsby, D. C. and A. C. Nairn (1999). "Regulation of CFTR Cl^- ion channels by phosphorylation and dephosphorylation." Adv Second Messenger Phosphoprotein Res **33**: 79-106.

Gendreau, S., S. Voswinkel, et al. (2004). "A trimeric quaternary structure is conserved in bacterial and human glutamate transporters." J Biol Chem **279**(38): 39505-12.

Gerchman, Y., A. Rimon, et al. (2001). "Oligomerization of NhaA, the Na^+/H^+ antiporter of *Escherichia coli* in the membrane and its functional and structural consequences." Biochemistry **40**(11): 3403-12.

Gohlke, U., A. Warne, et al. (1997). "Projection structure of the cytochrome bo ubiquinol oxidase from *Escherichia coli* at 6 Å resolution." Embo J **16**(6): 1181-8.

Gonen, T., P. Sliz, et al. (2004). "Aquaporin-0 membrane junctions reveal the structure of a closed water pore." Nature **429**(6988): 193-7.

Gottschalk, G. and R. K. Thauer (2001). "The Na^+-translocating methyltransferase complex from methanogenic archaea." Biochim Biophys Acta **1505**(1): 28-36.

Griffin, R. G. (1998). "Dipolar recoupling in MAS spectra of biological solids." Nat Struct Biol **5 Suppl**: 508-12.

Hacksell, I., J. L. Rigaud, et al. (2002). "Projection structure at 8 Å resolution of the melibiose permease, an Na-sugar co-transporter from *Escherichia coli*." Embo J **21**(14): 3569-74.

Hankamer, B., E. P. Morris, et al. (1999). "Revealing the structure of the oxygen-evolving core dimer of photosystem II by cryoelectron crystallography." Nat Struct Biol **6**(6): 560-4.

Harold, F. M. (1991). "Biochemical topology: from vectorial metabolism to morphogenesis." Biosci Rep **11**(6): 347-82; discussion 382-5.

Harries, W. E., D. Akhavan, et al. (2004). "The channel architecture of aquaporin 0 at a 2.2 Å resolution." Proc Natl Acad Sci U S A **101**(39): 14045-50.

Hasler, L., T. Walz, et al. (1998). "Purified lens major intrinsic protein (MIP) forms highly ordered tetragonal two-dimensional arrays by reconstitution." J Mol Biol **279**(4): 855-64.

Haupts, U., J. Tittor, et al. (1999). "Closing in on bacteriorhodopsin: progress in understanding the molecule." Annu Rev Biophys Biomol Struct **28**: 367-99.

Hayashi, H., K. Szaszi, et al. (2002). "A slow pH-dependent conformational transition underlies a novel mode of activation of the epithelial Na^+/H^+ exchanger-3 isoform." J Biol Chem **277**(13): 11090-6.

Hellmer, J., R. Patzold, et al. (2002). "Identification of a pH regulated $Na(^+)/H(^+)$ antiporter of *Methanococcus jannaschii*." FEBS Lett **527**(1-3): 245-9.

Hellmer, J., A. Teubner, et al. (2003). "Conserved arginine and aspartate residues are critical for function of MjNhaP1, a Na^+/H^+ antiporter of *M. jannaschii*." FEBS Lett **542**(1-3): 32-6.

Henderson, R. and P. N. Unwin (1975). "Three-dimensional model of purple membrane obtained by electron microscopy." Nature **257**(5521): 28-32.

Herz, K., S. Vimont, et al. (2003). "Roles of NhaA, NhaB, and NhaD Na^+/H^+

antiporters in survival of Vibrio cholerae in a saline environment." J Bacteriol **185**(4): 1236-44.

Heuberger, E. H., L. M. Veenhoff, et al. (2002). "Oligomeric state of membrane transport proteins analyzed with blue native electrophoresis and analytical ultracentrifugation." J Mol Biol **317**(4): 591-600.

Heymann, J. A., T. Hirai, et al. (2003). "Projection structure of the bacterial oxalate transporter OxlT at 3.4 Å resolution." J Struct Biol **144**(3): 320-6.

Higgins, C. F. and K. J. Linton (2004). "The ATP switch model for ABC transporters." Nat Struct Mol Biol **11**(10): 918-26.

Hilger, D., H. Jung, et al. (2005). "Assessing Oligomerization of Membrane Proteins by Four-Pulse DEER: pH-dependent Dimerization of NhaA Na^+/H^+ antiporter of E. coli." Biophys J. (in press).

Hiller, M., Krabben, et al. (2005). "Solid-State Magic-Angle Spinning NMR of Outer-Membrane Protein G from *Escherichia coli*." Chembiochem. (in press).

Hilpert, W. and P. Dimroth (1984). "Reconstitution of Na^+ transport from purified methylmalonyl-CoA decarboxylase and phospholipid vesicles." Eur J Biochem **138**(3): 579-83.

Hirai, T., J. A. Heymann, et al. (2002). "Three-dimensional structure of a bacterial oxalate transporter." Nat Struct Biol **9**(8): 597-600.

Howorka, S., S. Cheley, et al. (2001). "Sequence-specific detection of individual DNA strands using engineered nanopores." Nat Biotechnol **19**(7): 636-9.

Huang, Y., M. J. Lemieux, et al. (2003). "Structure and mechanism of the glycerol-3-phosphate transporter from *Escherichia coli*." Science **301**(5633): 616-20.

Hubbell, W. L., D. S. Cafiso, et al. (2000). "Identifying conformational changes with site-directed spin labeling." Nat Struct Biol **7**(9): 735-9.

Hunte, C. and H. Michel (2002). "Crystallisation of membrane proteins mediated by antibody fragments." Curr Opin Struct Biol **12**(4): 503-8.

Hunte, C., E. Screpanti, et al. (2005). "Structure of a $Na(^+)/H(^+)$ antiporter and insights into mechanism of action and regulation by pH." Nature **435**(7046): 1197-202.

Hwang, P. M., R. E. Bishop, et al. (2004). "The integral membrane enzyme PagP alternates between two dynamically distinct states." Proc Natl Acad Sci U S A **101**(26): 9618-23.

Iwata, S., C. Ostermeier, et al. (1995). "Structure at 2.8 Å resolution of cytochrome c oxidase from Paracoccus denitrificans." Nature **376**(6542): 660-9.

Iyer, R., T. M. Iverson, et al. (2002). "A biological role for prokaryotic ClC chloride channels." Nature **419**(6908): 715-8.

Jap, B. K. (1988). "High-resolution electron diffraction of reconstituted PhoE porin." J Mol Biol **199**(1): 229-31.

Jardetzky, O. (1966). "Simple allosteric model for membrane pumps." Nature **211**(52): 969-70.

Jiang, Y., A. Lee, et al. (2002). "Crystal structure and mechanism of a calcium-gated potassium channel." Nature **417**(6888): 515-22.

Jiang, Y., A. Lee, et al. (2003). "X-ray structure of a voltage-dependent K^+ channel." Nature **423**(6935): 33-41.

Jordan, P., P. Fromme, et al. (2001). "Three-dimensional structure of cyanobacterial photosystem I at 2.5 Å resolution." Nature **411**(6840): 909-17.

Jung, H. (1998). "Topology and function of the Na^+/proline transporter of *Escherichia coli*, a member of the Na^+/solute cotransporter family." Biochim Biophys Acta **1365**(1-2): 60-4.

Jung, H. (2001). "Towards the molecular mechanism of Na^+/solute symport in prokaryotes." Biochim Biophys Acta **1505**(1): 131-43.

Jung, H., M. Buchholz, et al. (2002). "CaiT of *Escherichia coli*, a new transporter catalyzing L-carnitine/gamma -butyrobetaine exchange." J Biol Chem **277**(42): 39251-8.

Jung, H., K. Jung, et al. (1990). "L-carnitine metabolization and osmotic stress response in *Escherichia coli*." J Basic Microbiol **30**(6): 409-13.

Jung, H., S. Tebbe, et al. (1998). "Unidirectional reconstitution and characterization of purified Na^+/proline transporter of *Escherichia coli*." Biochemistry **37**(31): 11083-8.

Kaback, H. R., M. Sahin-Toth, et al. (2001). "The kamikaze approach to membrane transport." Nat Rev Mol Cell Biol **2**(8): 610-20.

Kaim, G., F. Wehrle, et al. (1997). "Molecular basis for the coupling ion selectivity of F1F0 ATP synthases: probing the liganding groups for Na^+ and Li^+ in the c subunit of the ATP synthase from *Propionigenium modestum*." Biochemistry **36**(30): 9185-94.

Kapus, A., S. Grinstein, et al. (1994). "Functional characterization of three isoforms of the Na^+/H^+ exchanger stably expressed in Chinese hamster ovary cells. ATP dependence, osmotic sensitivity, and role in cell proliferation." J Biol Chem **269**(38): 23544-52.

Karrasch, S., D. Typke, et al. (1996). "Highly ordered two-dimensional crystals of photosystem I reaction center from *Synechococcus sp.*: functional and structural analyses." J Mol Biol **262**(3): 336-48.

Khademi, S., J. O'Connell, 3rd, et al. (2004). "Mechanism of ammonia transport by Amt/MEP/Rh: structure of AmtB at 1.35 Å." Science **305**(5690): 1587-94.

Kleinschmidt, J. H., M. C. Wiener, et al. (1999). "Outer membrane protein A of *E. coli* folds into detergent micelles, but not in the presence of

monomeric detergent." Protein Sci **8**(10): 2065-71.

Klingenberg, M. (1981). "Membrane protein oligomeric structure and transport function." Nature **290**(5806): 449-54.

Klose, M., H. Schwarz, et al. (1988). "Internal deletions in the gene for an *Escherichia coli* outer membrane protein define an area possibly important for recognition of the outer membrane by this polypeptide." J Biol Chem **263**(26): 13291-6.

Koronakis, V., J. Li, et al. (1997). "Structure of TolC, the outer membrane component of the bacterial type I efflux system, derived from two-dimensional crystals." Mol Microbiol **23**(3): 617-26.

Kramer, R. and S. Morbach (2004). "BetP of *Corynebacterium glutamicum*, a transporter with three different functions: betaine transport, osmosensing, and osmoregulation." Biochim Biophys Acta **1658**(1-2): 31-6.

Krebs, A., C. Villa, et al. (1998). "Characterisation of an improved two-dimensional $P22_12_1$ crystal from bovine rhodopsin." J Mol Biol **282**(5): 991-1003.

Krupka, R. M. (1999). "Limits on the tightness of coupling in active transport." J Membr Biol **167**(1): 35-41.

Kühlbrandt, W. (1992). "Two-dimensional crystallization of membrane proteins." Quarterly Reviews of Biophysics **25**(1): 1-49.

Kühlbrandt, W. and D. N. Wang (1991). "Three-dimensional structure of plant light-harvesting complex determined by electron crystallography.[see comment]." Nature **350**(6314): 130-4.

Kühlbrandt, W., D. N. Wang, et al. (1994). "Atomic model of plant light-harvesting complex by electron crystallography." Nature **367**(6464): 614-21.

Kunji, E. R. (2004). "The role and structure of mitochondrial carriers." FEBS Lett **564**(3): 239-44.

Kunji, E. R. and M. Harding (2003). "Projection structure of the atractyloside-inhibited mitochondrial ADP/ATP carrier of Saccharomyces cerevisiae." J Biol Chem **278**(39): 36985-8.

Kunji, E. R., E. N. Spudich, et al. (2001). "Electron crystallographic analysis of two-dimensional crystals of sensory rhodopsin II: a 6.9 Å projection structure." J Mol Biol **308**(2): 279-93.

Kuo, A., M. W. Bowler, et al. (2003). "Increasing the diffraction limit and internal order of a membrane protein crystal by dehydration." J Struct Biol **141**(2): 97-102.

Kuo, A., J. M. Gulbis, et al. (2003). "Crystal structure of the potassium channel KirBac1.1 in the closed state." Science **300**(5627): 1922-6.

Kurisu, G., H. Zhang, et al. (2003). "Structure of the cytochrome b_6f complex of oxygenic photosynthesis: tuning the cavity." Science **302**(5647):

1009-14.

Kurland, C. G. and H. Dong (1996). "Bacterial growth inhibition by overproduction of protein." Mol Microbiol **21**(1): 1-4.

Kuroda, T., N. Fujita, et al. (2004). "A major Li^+ extrusion system NhaB of *Pseudomonas aeruginosa* : comparison with the major Na^+ extrusion system NhaP." Microbiol Immunol **48**(4): 243-50.

Lancaster, C. R., A. Kroger, et al. (1999). "Structure of fumarate reductase from Wolinella succinogenes at 2.2 Å resolution." Nature **402**(6760): 377-85.

Landau, E. M. and J. P. Rosenbusch (1996). "Lipidic cubic phases: a novel concept for the crystallization of membrane proteins." Proc Natl Acad Sci U S A **93**(25): 14532-5.

Lemieux, M. J., R. A. Reithmeier, et al. (2002). "Importance of detergent and phospholipid in the crystallization of the human erythrocyte anion-exchanger membrane domain." J Struct Biol **137**(3): 322-32.

Lemieux, M. J., J. Song, et al. (2003). "Three-dimensional crystallization of the *Escherichia coli* glycerol-3-phosphate transporter: a member of the major facilitator superfamily." Protein Sci **12**(12): 2748-56.

Levy, D., A. Bluzat, et al. (1990). "A systematic study of liposome and proteoliposome reconstitution involving Bio-Bead-mediated Triton X-100 removal." Biochim Biophys Acta **1025**(2): 179-90.

Li, H. L., H. X. Sui, et al. (1998). "Two-dimensional crystallization and projection structure of KcsA potassium channel." J Mol Biol **282**(2): 211-6.

Li, X., B. Alvarez, et al. (2002). "Carbonic anhydrase II binds to and enhances activity of the Na^+/H^+ exchanger." J Biol Chem **277**(39): 36085-91.

Locher, K. P., A. T. Lee, et al. (2002). "The *E. coli* BtuCD structure: a framework for ABC transporter architecture and mechanism." Science **296**(5570): 1091-8.

Lolkema, J. S. and D. J. Slotboom (2003). "Classification of 29 families of secondary transport proteins into a single structural class using hydropathy profile analysis." J Mol Biol **327**(5): 901-9.

Lolkema, J. S., G. Speelmans, et al. (1994). "$Na^{(+)}$-coupled versus $H^{(+)}$-coupled energy transduction in bacteria." Biochim Biophys Acta **1187**(2): 211-5.

Luecke, H., B. Schobert, et al. (1999). "Structure of bacteriorhodopsin at 1.55 Å resolution." J Mol Biol **291**(4): 899-911.

Ma, C. and G. Chang (2004). "Structure of the multidrug resistance efflux transporter EmrE from *Escherichia coli*." Proc Natl Acad Sci U S A **101**(9): 2852-7.

MacKinnon, R. (2003). "Potassium channels." FEBS Lett **555**(1): 62-5.

Maloney, P. C. and T. H. Wilson (1993). "The evolution of membrane carriers." Soc Gen Physiol Ser **48**: 147-60.

Meier, T., P. Polzer, et al. (2005). "Structure of the rotor ring of F-Type Na^+ ATPase from *Ilyobacter tartaricus*." Science **308**(5722): 659-62.

Miller, S. L. and H. C. Urey (1959). "Organic compound synthesis on the primitive earth." Science **130**(3370): 245-51.

Mindell, J. A., M. Maduke, et al. (2001). "Projection structure of a ClC-type chloride channel at 6.5 Å resolution." Nature **409**(6817): 219-23.

Miroux, B. and J. E. Walker (1996). "Over-production of proteins in *Escherichia coli*: mutant hosts that allow synthesis of some membrane proteins and globular proteins at high levels." J Mol Biol **260**(3): 289-98.

Misra, R. and S. A. Benson (1989). "A novel mutation, cog, which results in production of a new porin protein (OmpG) of *Escherichia coli* K-12." J Bacteriol **171**(8): 4105-11.

Mitchell, P. (1966). "Chemiosmotic coupling in oxidative and photosynthetic phosphorylation." Biol Rev Camb Philos Soc **41**(3): 445-502.

Mitchell, P. (1967). "Proton-translocation phosphorylation in mitochondria, chloroplasts and bacteria: natural fuel cells and solar cells." Fed Proc **26**(5): 1370-9.

Mohraz, M. (1999). "Reconstitution of detergent-solubilized Na,K-ATPase and formation of two-dimensional crystals." J Struct Biol **125**(1): 76-85.

Mosser, G. (2001). "Two-dimensional crystallogenesis of transmembrane proteins." Micron **32**(5): 517-40.

Mosser, G., C. Breyton, et al. (1997). "Projection map of cytochrome b_6f complex at 8 Å resolution." J Biol Chem **272**(32): 20263-8.

Müller, V., M. Blaut, et al. (1988). "The transmembrane electrochemical gradient of Na^+ as driving force for methanol oxidation in *Methanosarcina barkeri*." Eur J Biochem **172**(3): 601-6.

Murakami, S., R. Nakashima, et al. (2002). "Crystal structure of bacterial multidrug efflux transporter AcrB." Nature **419**(6907): 587-93.

Murata, K., K. Mitsuoka, et al. (2000). "Structural determinants of water permeation through aquaporin-1." Nature **407**(6804): 599-605.

Murata, T., I. Yamato, et al. (2005). "Structure of the rotor of the V-Type Na^+-ATPase from *Enterococcus hirae*." Science **308**(5722): 654-9.

Nakazato, K., C. Toyoshima, et al. (1996). "Two-dimensional crystallization and cryo-electron microscopy of photosystem II." J Mol Biol **257**(2): 225-32.

Nelson, N., A. Sacher, et al. (2002). "The significance of molecular slips in transport systems." Nat Rev Mol Cell Biol **3**(11): 876-81.

Neutze, R., E. Pebay-Peyroula, et al. (2002). "Bacteriorhodopsin: a high-

resolution structural view of vectorial proton transport." Biochim Biophys Acta **1565**(2): 144-67.

Nogi, T., I. Fathir, et al. (2000). "Crystal structures of photosynthetic reaction center and high-potential iron-sulfur protein from *Thermochromatium tepidum*: thermostability and electron transfer." Proc Natl Acad Sci U S A **97**(25): 13561-6.

Okada, T., Y. Fujiyoshi, et al. (2002). "Functional role of internal water molecules in rhodopsin revealed by X-ray crystallography." Proc Natl Acad Sci U S A **99**(9): 5982-7.

Olsen, G. J. and C. R. Woese (1993). "Ribosomal RNA: a key to phylogeny." Faseb J **7**(1): 113-23.

Omote, H. and M. K. Al-Shawi (2002). "A novel electron paramagnetic resonance approach to determine the mechanism of drug transport by P-glycoprotein." J Biol Chem **277**(47): 45688-94.

Oomen, C. J., P. Van Ulsen, et al. (2004). "Structure of the translocator domain of a bacterial autotransporter." Embo J **23**(6): 1257-66.

Opella, S. J. (1997). "NMR and membrane proteins." Nat Struct Biol **4 Suppl**: 845-8.

Otzen, D. E. (2002). "Protein unfolding in detergents: effect of micelle structure, ionic strength, pH, and temperature." Biophys J **83**(4): 2219-30.

Padan, E., T. Tzubery, et al. (2004). "NhaA of *Escherichia coli*, as a model of a pH-regulated Na^+/H^+antiporter." Biochim Biophys Acta **1658**(1-2): 2-13.

Padan, E., M. Venturi, et al. (2001). "$Na(^+)/H(^+)$ antiporters." Biochim Biophys Acta **1505**(1): 144-57.

Palczewski, K., T. Kumasaka, et al. (2000). "Crystal structure of rhodopsin: A G protein-coupled receptor." Science **289**(5480): 739-45.

Palsdottir, H. and C. Hunte (2004). "Lipids in membrane protein structures." Biochim Biophys Acta **1666**(1-2): 2-18.

Parcej, D. N. and L. Eckhardt-Strelau (2003). "Structural characterisation of neuronal voltage-sensitive K^+ channels heterologously expressed in Pichia pastoris." J Mol Biol **333**(1): 103-16.

Paternostre, M. T., M. Roux, et al. (1988). "Mechanisms of membrane protein insertion into liposomes during reconstitution procedures involving the use of detergents. 1. Solubilization of large unilamellar liposomes (prepared by reverse-phase evaporation) by triton X-100, octyl glucoside, and sodium cholate." Biochemistry **27**(8): 2668-77.

Paulsen, I. T., M. K. Sliwinski, et al. (1998). "Microbial genome analyses: global comparisons of transport capabilities based on phylogenies, bioenergetics and substrate specificities." J Mol Biol **277**(3): 573-92.

Pautsch, A., J. Vogt, et al. (1999). "Strategy for membrane protein

crystallization exemplified with OmpA and OmpX." Proteins **34**(2): 167-72.

Pebay-Peyroula, E., C. Dahout-Gonzalez, et al. (2003). "Structure of mitochondrial ADP/ATP carrier in complex with carboxyatractyloside." Nature **426**(6962): 39-44.

Pedersen, P. L. and L. M. Amzel (1992). "F-type ATPases. Introduction." J Bioenerg Biomembr **24**(5): 427-8.

Perozo, E., D. M. Cortes, et al. (1998). "Three-dimensional architecture and gating mechanism of a K^+ channel studied by EPR spectroscopy." Nat Struct Biol **5**(6): 459-69.

Perozo, E., A. Kloda, et al. (2002). "Physical principles underlying the transduction of bilayer deformation forces during mechanosensitive channel gating." Nat Struct Biol **9**(9): 696-703.

Peterson, G. L. (1977). "A simplification of the protein assay method of Lowry et al. which is more generally applicable." Anal Biochem **83**(2): 346-56.

Pirch, T., S. Landmeier, et al. (2003). "Transmembrane domain II of the Na^+/proline transporter PutP of *Escherichia coli* forms part of a conformationally flexible, cytoplasmic exposed aqueous cavity within the membrane." J Biol Chem **278**(44): 42942-9.

Pirch, T., M. Quick, et al. (2002). "Sites important for Na^+ and substrate binding in the Na^+/proline transporter of *Escherichia coli*, a member of the Na^+/solute symporter family." J Biol Chem **277**(11): 8790-6.

Poolman, B. and W. N. Konings (1993). "Secondary solute transport in bacteria." Biochim Biophys Acta **1183**(1): 5-39.

Pourcher, T., M. Bassilana, et al. (1990). "The melibiose/Na^+ symporter of *Escherichia coli*: kinetic and molecular properties." Philos Trans R Soc Lond B Biol Sci **326**(1236): 411-23.

Rao, P. and T. N. Pattabiraman (1989). "Reevaluation of the phenol-sulfuric acid reaction for the estimation of hexoses and pentoses." Anal Biochem **181**(1): 18-22.

Reyes, C. L. and G. Chang (2005). "Structure of the ABC transporter MsbA in complex with ADP.vanadate and lipopolysaccharide." Science **308**(5724): 1028-31.

Rigaud, J. L., B. Pitard, et al. (1995). "Reconstitution of membrane proteins into liposomes: application to energy-transducing membrane proteins." Biochim Biophys Acta **1231**(3): 223-46.

Ringler, P., M. J. Borgnia, et al. (1999). "Structure of the water channel AqpZ from *Escherichia coli* revealed by electron crystallography." J Mol Biol **291**(5): 1181-90.

Rogl, H., K. Kosemund, et al. (1998). "Refolding of *Escherichia coli* produced membrane protein inclusion bodies immobilised by nickel chelating chromatography." FEBS Letters **432**(1-2): 21-6.

Rosenberg, M. F., R. Callaghan, et al. (2004). "3-D structure of P-glycoprotein: the transmembrane regions adopt an asymmetric configuration in the nucleotide-bound state." J Biol Chem.

Rosenberg, M. F., A. B. Kamis, et al. (2003). "Three-dimensional structures of the mammalian multidrug resistance P-glycoprotein demonstrate major conformational changes in the transmembrane domains upon nucleotide binding." J Biol Chem **278**(10): 8294-9.

Rosenbusch, J. P. (1974). "Characterization of the major envelope protein from *Escherichia coli*. Regular arrangement on the peptidoglycan and unusual dodecyl sulfate binding." J Biol Chem **249**(24): 8019-29.

Roux, B. (2005). "Ion conduction and selectivity in K($^{+}$) channels." Annu Rev Biophys Biomol Struct **34**: 153-71.

Rubenhagen, R., H. Ronsch, et al. (2000). "Osmosensor and osmoregulator properties of the betaine carrier BetP from *Corynebacterium glutamicum* in proteoliposomes." J Biol Chem **275**(2): 735-41.

Ruprecht, J. J., T. Mielke, et al. (2004). "Electron crystallography reveals the structure of metarhodopsin I." Embo J **23**(18): 3609-20.

Schäfer, G., M. Engelhard, et al. (1999). "Bioenergetics of the Archaea." Microbiol Mol Biol Rev **63**(3): 570-620.

Schertler, G. F. and P. A. Hargrave (1995). "Projection structure of frog rhodopsin in two crystal forms." Proc Natl Acad Sci U S A **92**(25): 11578-82.

Schmid, B., M. Kromer, et al. (1996). "Expression of porin from Rhodopseudomonas blastica in *Escherichia coli* inclusion bodies and folding into exact native structure." FEBS Lett **381**(1-2): 111-4.

Schmidt-Krey, I., Y. Kanaoka, et al. (2004). "Human leukotriene C_4 synthase at 4.5 Å resolution in projection." Structure (Camb) **12**(11): 2009-14.

Schmidt-Krey, I., G. Lundqvist, et al. (1998). "Parameters for the two-dimensional crystallization of the membrane protein microsomal glutathione transferase." J Struct Biol **123**(2): 87-96.

Schulz, G. E. (2002). "The structure of bacterial outer membrane proteins." Biochim Biophys Acta **1565**(2): 308-17.

Skou, J. C. and K. Zerahn (1959). "Investigations on the effect of some local anaesthetics and other amines on the active transport of sodium through the isolated short-circuited frog skin." Biochim Biophys Acta **35**: 324-33.

Skulachev, V. P. (1991). "Chemiosmotic systems in bioenergetics: H^{+} cycles and Na^{+} cycles." Biosci Rep **11**(6): 387-441; discussion 441-4.

Sobczak, I. and J. S. Lolkema (2005). "Structural and mechanistic diversity of secondary transporters." Curr Opin Microbiol **8**(2): 161-7.

Standfuss, J. and W. Kühlbrandt (2004). "The three isoforms of the light-harvesting complex II: spectroscopic features, trimer formation, and

functional roles." Journal of Biological Chemistry **279**(35): 36884-91.

Sterling, D., R. A. Reithmeier, et al. (2001). "Carbonic anhydrase: in the driver's seat for bicarbonate transport." Jop **2**(4 Suppl): 165-70.

Stillwell, W. (1980). "Facilitated diffusion as a method for selective accumulation of materials from the primordial oceans by a lipid-vesicle protocell." Orig Life **10**(3): 277-92.

Strange, K. (2004). "Cellular volume homeostasis." Adv Physiol Educ **28**(1-4): 155-9.

Subramaniam, S., M. Gerstein, et al. (1993). "Electron diffraction analysis of structural changes in the photocycle of bacteriorhodopsin." Embo J **12**(1): 1-8.

Subramaniam, S. and R. Henderson (1999). "Electron crystallography of bacteriorhodopsin with millisecond time resolution." J Struct Biol **128**(1): 19-25.

Surrey, T., A. Schmid, et al. (1996). "Folding and membrane insertion of the trimeric beta-barrel protein OmpF." Biochemistry **35**(7): 2283-8.

Taglicht, D., E. Padan, et al. (1993). "Proton-sodium stoichiometry of NhaA, an electrogenic antiporter from *Escherichia coli*." J Biol Chem **268**(8): 5382-7.

Tanford, C. (1978). "The hydrophobic effect and the organization of living matter." Science **200**(4345): 1012-8.

Tate, C. G. (2001). "Overexpression of mammalian integral membrane proteins for structural studies." FEBS Lett **504**(3): 94-8.

Tate, C. G., E. R. Kunji, et al. (2001). "The projection structure of EmrE, a proton-linked multidrug transporter from *Escherichia coli*, at 7 Å resolution." Embo J **20**(1-2): 77-81.

Tatulian, S. A. (2003). "Attenuated total reflection Fourier transform infrared spectroscopy: a method of choice for studying membrane proteins and lipids." Biochemistry **42**(41): 11898-907.

Tokuda, H. and T. Unemoto (1981). "A respiration-dependent primary sodium extrusion system functioning at alkaline pH in the marine bacterium Vibrio alginolyticus." Biochem Biophys Res Commun **102**(1): 265-71.

Tolner, B., B. Poolman, et al. (1997). "Adaptation of microorganisms and their transport systems to high temperatures." Comp Biochem Physiol A Physiol **118**(3): 423-8.

Toyoshima, C. and G. Inesi (2004). "Structural basis of ion pumping by Ca_2^+ ATPase of the sarcoplasmic reticulum." Annu Rev Biochem **73**: 269-92.

Toyoshima, C., H. Nomura, et al. (2003). "Crystal structures of Ca_2^+ ATPase in various physiological states." Ann N Y Acad Sci **986**: 1-8.

Toyoshima, C., H. Sasabe, et al. (1993). "Three-dimensional cryo-electron

microscopy of the calcium ion pump in the sarcoplasmic reticulum membrane." Nature **362**(6419): 467-71.

Tsiotis, G., T. Walz, et al. (1996). "Tubular crystals of a photosystem II core complex." J Mol Biol **259**(2): 241-8.

Turk, E., O. Kim, et al. (2000). "Molecular characterization of *Vibrio parahaemolyticus* vSGLT: a model for sodium-coupled sugar cotransporters." J Biol Chem **275**(33): 25711-6.

Ubarretxena-Belandia, I., J. M. Baldwin, et al. (2003). "Three-dimensional structure of the bacterial multidrug transporter EmrE shows it is an asymmetric homodimer." Embo J **22**(23): 6175-81.

Unger, V. M., N. M. Kumar, et al. (1997). "Projection structure of a gap junction membrane channel at 7 Å resolution." Nat Struct Biol **4**(1): 39-43.

Unwin, N. (1996). "Projection structure of the nicotinic acetylcholine receptor: distinct conformations of the alpha subunits." J Mol Biol **257**(3): 586-96.

Unwin, N. (2003). "Structure and action of the nicotinic acetylcholine receptor explored by electron microscopy." FEBS Lett **555**(1): 91-5.

Unwin, N., C. Toyoshima, et al. (1988). "Arrangement of the acetylcholine receptor subunits in the resting and desensitized states, determined by cryoelectron microscopy of crystallized Torpedo postsynaptic membranes." J Cell Biol **107**(3): 1123-38.

Vagin, A. and A. Teplyakov (2000). "An approach to multi-copy search in molecular replacement." Acta Crystallogr D Biol Crystallogr **56 Pt 12**: 1622-4.

Valiyaveetil, F. I., Y. Zhou, et al. (2002). "Lipids in the structure, folding, and function of the KcsA K^+ channel." Biochemistry **41**(35): 10771-7.

Valpuesta, J. M., J. L. Carrascosa, et al. (1994). "Analysis of electron microscope images and electron diffraction patterns of thin crystals of phi 29 connectors in ice." J Mol Biol **240**(4): 281-7.

Van den Berg, B., W. M. Clemons, Jr., et al. (2004). "X-ray structure of a protein-conducting channel." Nature **427**(6969): 36-44.

Viitanen, P., M. L. Garcia, et al. (1984). "Purified reconstituted lac carrier protein from *Escherichia coli* is fully functional." Proc Natl Acad Sci U S A **81**(6): 1629-33.

Vinothkumar, K. R., S. H. Smits, et al. (2005). "pH-induced structural change in a sodium/proton antiporter from *Methanococcus jannaschii*." Embo J. in press.

von Heijne, G. (1998). "Structural aspects of transmembrane alpha-helices." Acta Physiol Scand Suppl **643**: 17-9.

Vonck, J., T. K. von Nidda, et al. (2002). "Molecular architecture of the undecameric rotor of a bacterial Na^+-ATP synthase." J Mol Biol **321**(2): 307-16.

Wang, D. N., W. Kühlbrandt, et al. (1993). "Two-dimensional structure of the membrane domain of human band 3, the anion transport protein of the erythrocyte membrane." EMBO Journal **12**(6): 2233-9.

Wang, D. N., V. E. Sarabia, et al. (1994). "Three-dimensional map of the dimeric membrane domain of the human erythrocyte anion exchanger, Band 3." EMBO Journal **13**(14): 3230-5.

Warren, M. A., L. M. Kucharski, et al. (2004). "The CorA Mg_2^+ transporter is a homotetramer." J Bacteriol **186**(14): 4605-12.

Wegener, C., S. Tebbe, et al. (2000). "Spin labeling analysis of structure and dynamics of the Na(+)/proline transporter of *Escherichia coli*." Biochemistry **39**(16): 4831-7.

Weinglass, A. B., J. P. Whitelegge, et al. (2003). "Elucidation of substrate binding interactions in a membrane transport protein by mass spectrometry." Embo J **22**(7): 1467-77.

Wieth, J. O., O. S. Andersen, et al. (1982). "Chloride-bicarbonate exchange in red blood cells: physiology of transport and chemical modification of binding sites." Philos Trans R Soc Lond B Biol Sci **299**(1097): 383-99.

Williams, K. A. (2000). "Three-dimensional structure of the ion-coupled transport protein NhaA." Nature **403**(6765): 112-5.

Williams, K. A., U. Geldmacher-Kaufer, et al. (1999). "Projection structure of NhaA, a secondary transporter from *Escherichia coli*, at 4.0 Å resolution." EMBO Journal **18**(13): 3558-63.

Wright, E. M., D. D. Loo, et al. (2004). "Surprising versatility of Na^+-glucose cotransporters: SLC5." Physiology (Bethesda) **19**: 370-6.

Yernool, D., O. Boudker, et al. (2003). "Trimeric subunit stoichiometry of the glutamate transporters from *Bacillus caldotenax* and *Bacillus stearothermophilus*." Biochemistry **42**(44): 12981-8.

Yernool, D., O. Boudker, et al. (2004). "Structure of a glutamate transporter homologue from *Pyrococcus horikoshii*." Nature **431**(7010): 811-8.

Yin, C. C., M. L. Aldema-Ramos, et al. (2000). "The quarternary molecular architecture of TetA, a secondary tetracycline transporter from *Escherichia coli*." Mol Microbiol **38**(3): 482-92.

Zhang, H. and W. A. Cramer (2004). "Purification and crystallization of the cytochrome b_6f complex in oxygenic photosynthesis." Methods Mol Biol **274**: 67-78.

Zhuang, J., G. G. Prive, et al. (1999). "Two-dimensional crystallization of *Escherichia coli* lactose permease." J Struct Biol **125**(1): 63-75.

Ziegler, C., S. Morbach, et al. (2004). "Projection structure and oligomeric state of the osmoregulated sodium/glycine betaine symporter BetP of *Corynebacterium glutamicum*." J Mol Biol **337**(5): 1137-47.

BOOKS OF GENERAL REFERENCE

1) Introduction to Biological Membranes – M.K.Jain and R.C.Wagner, Wiley Publications 1980

2) Principles and models of biological transport – M.H.Friedman, Springer Publications 1986

3) The Hydrophobic effect Formation of micelles and biological membranes – Charles Tanford, Wiley Publications 1980

4) Membrane fluidity in biology (Volumes 1 & 2) – edited by R.Aloia, Academic Press 1983.

5) Channels,Carriers and Pumps: An introduction to membrane transport – Wilfred D. Stein A, Academic Press 1990.

6) Molecular cloning: A laboratory manual – Sambrook J., Fritsch E.F. & Maniatis T. Cold Spring Harbour Laboratory Press 1989.

CURRICULUM VITAE

Vinothkumar Kutti Ragunath

Born 15.03.1977 in Madurai, India

EDUCATION:

1994-1997	Bachelor of Science in Microbiology, Madurai Kamaraj University, Madurai, India
1997-1999	Master of Science in Biotechnology, Madurai Kamaraj University, Madurai, India
1999-2000	Research on differential expression of genes in melanocytes & pigmentation, in collaboration with Unilever (P) Limited
2001-2005	PhD student in the Department of Structural biology, Max-Planck Institute of Biophysics and Johann Wolfgang Goethe-Universität

PUBLICATIONS:

1) **Vinothkumar, K.R**., Smits, S., & Kühlbrandt, W. (2005). pH induced structural change in a sodium/proton antiporter from *Methanococcus jannaschii. EMBO J* (in press).

2) Hiller, M., Krappen, L., **Vinothkumar, K.R**., Castellini, F., van-Rossum B.J., Kühlbrandt, W., & Oschkinat, H. (2005). Solid-state Magic-Angle Spinning NMR of Outer-Membrane Protein G from *Escherichia coli ChemBiochem* 6 (in press).

3) **Vinothkumar, K.R.,** Raunser, S., Jung, H., & Kühlbrandt, W. Oligomeric structure of *E.coli* carnitine transporter (manuscript in preparation).

ACKNOWLEDGEMENTS

From among a large number of students, Prof. Werner Kühlbrandt somehow picked me up to work under him as a PHD student, I thank him and I feel glad for being his student. I hope that I have satisfied his selection. During the years of my PhD he has made me a better scientist and provided me with lot of freedom in work to carry out many different projects. This has allowed me to think independently which has given me immense confidence in designing and carrying out experiments. He has been patient in teaching me how to write good publications and presentation of results which are both essential to establish oneself in science. In the middle of his busy schedule he has always had time to discuss many of my funny questions that may not have been of scientific interest. We have had our differences on various topics but we put them aside when necessary. One area where he might not have been happy is my refusal to drink beer in these years in Germany. There are so many things I could write, may be some other time in future and for now I just want to say thanks for the endless support.

Prof.Heinrich Jung, initially at the University of Osnabrück and now at the LMU, Munich had taught me the basic techniques of handling membrane proteins, transferring the knowledge that he obtained from the lab of Ron Kaback and for being such a friendly collaborator and providing me place in his lab to carry out experiments. I acknowledge the help of Dr.Thorsten Prich and Monika Nietschke during my experiments in Osnabrück.

Prof. Bernd Ludwig for accepting me as PhD student for the JWG University. He has been very encouraging from the time of my interview and has remained till date. His interest in wanting to take me as his student gave me lot of confidence when I started here. He has always had very nice words for me and I believe this makes him the most sought person in a thesis defense.

If I know a little on electron microscopy it is because of Deryck Mills as my teacher, without him I would not have done most of the date collection. I have

learnt from him how to be patient in dealing variety of people and to be efficient in doing many different works at the same time. His initiatives in organizing social activities especially the “Bowling Club” which has brought members from different departments together leading to plenty of discussions. I should not forget to mention his ability to draw cartoons that were hilarious in the Christmas parties and praising the holy water from India for getting crystals.

If there is a person whom I know as a complete scientist then he is Dr.David Parcej who in my years at the department has been my impression for doing good science and in addition the only person whom I could speak about cricket apart from my Indian colleagues.

Dr.Janet Vonck for teaching me the basis of diffraction theory and image processing and answering a lot of silly questions that I kept asking about processing.

Dr.Inga Schmidt-krey, one of the nicest person I have met, who took her time in teaching me tricks about 2D crystallization, preparing cryo samples, image processing and many other stuffs related to post-doctoral research. She has provided me with good suggestions on many non-scientific problems and I am grateful for her advises in times of distress.

My sincere thanks to people in the “all-men” lab (L1.100), I hope Werner will change this in the near future to an equal proportion of gender. Matthias Appel for burning a lot of DVD’s for me, Johan Zeelan for his many insights in biochemistry and 3D crystallization, Goetz for lot of his funny and innovative approaches (and for translating a long abstract of my thesis into german, he must have been swearing at me when he did the translation), Carville for his discussions on lipids, detergent and advises in writing for fellowships, Stefan Raunser for sharing the office with me in the old institute and helping me out from lot of tight corners in a numerous parties with food.

Rana, for being tolerant to all my remarks for the past one year.

In the late stages of my PhD Dr.Anke TVS and Dr.Ötzkan have helped me understand better on the problems with crystallography and I would like to thank Anke on the initiative to conduct discussion groups which I think is a very tough job. Remco Wouts for being a wizard with computers and setting up the cluster home page that shares a lot of information.

Joerg and Ching-Ju Standtsai for being such a very nice neighbors who have provided me with lot of rides to and from institutes, lending me books and DVD's and listening to lot of my gossips.

I thank Dr.Christine Ziegler and Sander Smits for driving and accompanying me to numerous synchotron trips. Mirko and Sivaram for being in their own world and ignoring a lot of happenings around.

The new bloods in our department Panchali, Fuensanta, Tiago, Stefan and Preeti for keeping an energetic atmosphere and of course for a lot of noise they make.

Dr.Winfried Hasse for his help with freeze fracture electron microscopy and for his lessons in german. Ulrike Geldmacher Kaufer who has taken care of me like her son, providing me with lot of plants and one person who never forgot my birthday in these years. Heidi Betz, Luise and Friederike for their technical superiority and keeping things in order.

My sincere thanks to Franziska Langerheinrich, for her help during my initial years in Frankfurt and Monika Hobrack who succeeded her, has done a tremendous job for students. Rosemarie and Solveigh for their help in obtaining a lot of articles from nowhere and making the library a place to read.

I never thought I could share an apartment with a person but Gianni made it possible for more than four years. We complemented each other and had healthy discussions on scientific as well as non-scientific issues during the number of dinners we have had. He has set me a model how to enjoy life and

I hope I can follow him to certain level. I wish him a bright future in the years to come. Marco took over Gianni and he makes me think I must have had an Italian connection some where in the past.

Paolo Lastrico has helped me in making a lot of figures for articles and teaching me about graphics. Matteo, Luana, Hildur and Cinzia for their friendly approaches and lot of arguments that brought about healthy non-scientific discussions.

All the students from India who have made our country proud by being very efficient PhD students and I am not surprised to see that the number keeps increasing. I wish them all good luck for their PhD and more.

The advantage of traveling in the U-bahn has helped me observe and to gain few people from other departments working on different aspects of membrane proteins. Aihua Zhou for her insights into kinetics of transporters, Phil Wood on his thoughts on band 3 and permeases, Eva Lorenzi on her work with pumps and Cecile who made sure that I will not want to work on GPCR's.

I thank the Max-Planck society for their funding of the research school and providing us with such a nice infrastructure.

If my father was still there he would have been proud to see me stepping towards one of my goals and I believe he is there in me to feel so. I couldn't find enough words to say few things about my mom who has been instrumental in bringing me up this far and my sister even though younger has showed me how to be mature. I like my brother for being adamant and arrogant. Mr. Sivasubramaniam, who has shown me a new path in leading a peaceful life, I am following him and I hope I can gain his kind of charisma in the future.

… and miles to go miles to go

before I sleep